University of Southampton

Faculty of Environmental and Life Sciences

School of Biological Sciences

The Mechanism of Meiotic Drive in the Mouse Oocyte

Volume 1 of 1

by

Tianyu Wu

Thesis for the degree of Doctor of Philosophy

July 2019

University of Southampton

Abstract

Faculty of Environmental and Life Sciences

Biological Science

Thesis for the degree of Doctor of Philosophy

The Mechanism of Meiotic Drive in the Mouse Oocyte

Tianyu Wu

This thesis investigated the biased reorientation of asymmetrical bivalents and so the mechanism of meiotic drive. In the first meiotic division of oocytes, the cortically positioned spindle leads to bivalent segregation in which only the centre-facing homologues are retained. 'Selfish' chromosomes are known to exist, which bias their orientation in the spindle and hence retention in the egg, a process known as 'meiotic drive'. Here this phenomenon was investigated using oocytes from F_1 hybrid mice, in which parental strain differences in centromere and kinetochore sizes allowed distinction of the two homologous pairs that comprise a specific bivalent inside the F_1 oocyte. With this mouse model, it is shown that the homologue with smaller major satellite DNA region, larger minor satellite DNA region, and less of the kinetochore protein Spc24, is preferentially retained in the MII oocyte. The alignment process of this distinct bivalent was recorded by real-time imaging. The selfish retention of one homologue was found to depend on bivalent rotation during prometaphase, in a process dependent on AURKB/C activity. In addition to the asymmetries within the bivalents, I also found asymmetrical tubulin and microtubule organising centres intensity between the two halves of the spindle and cortically positioned homologues appeared to be under greater stretch than their centre-facing partners. These findings reveal a crucial model in which meiotic drive is explained by the relative impact of microtubule force asymmetry on homologues with different sized centromeres and kinetochores in meiosis I.

“Life is a game and every player is cheating.”

— Eva Stachniak, *The Winter Palace*.

Table of Contents

List of Tables

List of Figures

UNIVERSITY OF Southampton

Research Thesis:
Declaration of Authorship

Print name:	Tianyu Wu

Title of thesis:	The Mechanism of Meiotic Drive in the Mouse Oocyte

I declare that this thesis and the work presented in it is my own and has been generated by me as the result of my own original research.

I confirm that:

1. This work was done wholly or mainly while in candidature for a research degree at this University;

2. Where any part of this thesis has previously been submitted for a degree or any other qualification at this University or any other institution, this has been clearly stated;

3. Where I have consulted the published work of others, this is always clearly attributed;

4. Where I have quoted from the work of others, the source is always given. With the exception of such quotations, this thesis is entirely my own work;

5. I have acknowledged all main sources of help;

6. Where the thesis is based on work done by myself jointly with others, I have made clear exactly what was done by others and what I have contributed myself;

7. Parts of this work have been published as:

Wu, T., Lane, S. I., Morgan, S. L., & Jones, K. T. (2018). Spindle tubulin and MTOC asymmetries may explain meiotic drive in oocytes. Nat Commun. 9(1), 2952.

Signature:		Date:	

Acknowledgments

My sincere gratitude goes to Prof. Keith Jones for his supervision of my Ph.D. study. He gave me the precious opportunity to follow my research interests. His guidance helped me not only in scientific research but also my academic career.

I also would like to thank Dr. Simon Lane for his training of all my experimental skills and data analysis ability. I could not complete my project on time without his support.

Thank you to Dr. Stephanie Morgan who helped me with laboratory animal, reagent orders and culture media preparation throughout my time in the Ph.D. study.

Thanks to Dr. Karen Schindler, Dr. Melina Schuh, and Dr. Marie-Helene Verlhac for their generous plasmid constructs as gifts.

Finally, I also want to thank my family for the continuous love and help they have given.

Definitions and Abbreviations

aMTOC - Acentriolar MTOC

APC - Anaphase-promoting complex

AURKA - Aurora kinase A

AURKB - Aurora kinase B

AURKC - Aurora kinase C

CCAN - Constitutive centromere associated network

CDC42 - Cell division control protein 42

Cenp - Centromeric protein

Cep - Centrosomal protein

CM - Centrosomin motif

CPC - Chromosomal passenger complex

DSBs - Double-strand breaks

FRET - Fluorescence resonance energy transfer

FSH - Follicle stimulating hormone

GV - Germinal vesicle

GVBD - Germinal vesicle breakdown

ICA - Interchromatid axis

IF - Immunofluorescence

Incenp - Inner centromere protein

KIF11 - Kinesin family member 11

LH - Luteinizing hormone

LncRNA - Long non-coding RNA

MCAK - Mitotic centromere-associated kinesin

MI - Meiosis I

MII - Meiosis II

MPF - Maturation promoting factor

MTOC - Microtubule organising centre

OP18 - Oncoprotein 18

PCM - Pericentriolar material

PGC - Primordial germ cell

PMSG - Pregnant mare serum gonadotrophin

PVP - Polyvinylpyrrolidone

RA - Retinoic acid

RCC – Regulator of chromosome condensation

SAC - Spindle assembly checkpoint

SAF - Spindle assembly factor

SC - Synaptonemal complex

SCE - Sister chromatid exchange

SSC - Saline-sodium citrate

SN - Surrounded nucleolus

TALE - Transcription activator-like effectors

γ-TuRC – γ-tubulin ring complex

Chapter 1: Introduction

This thesis focuses on the mechanism of female meiotic drive in mouse oocytes. In the introduction, the initial observations and previous studies on meiotic drive are discussed. To show the rationality of the mechanism of meiotic drive, the process of spindle assembly is summarised to explain the asymmetrical microtubules distribution. In addition, an overview of female meiosis is also provided as the basic knowledge of female meiotic drive.

1.1 Female Meiosis

Female meiosis is a special cell division process which involves double chromosome segregations, meiosis I (MI) and meiosis II (MII). During oocyte maturation and fertilization, chromosomes are segregated twice with only one egg generated (Page and Hawley, 2003; Petronczki et al., 2003). As an important biological basis for female meiotic drive, the process of meiosis is necessary to be introduced in this chapter.

Before the initiation of female meiosis, primordial germ cells (PGCs) arise elsewhere in the embryo and migrate from the posterior primitive streak into developing genital ridges during embryonic development, after which they are ready to enter meiosis. In the first step of meiosis, the bivalent structure is assembled during homologous recombination and sister chromatids are tethered for sister chromatid exchange (SCE) (Nikolic et al., 2016). With the completion of meiotic recombination, oocytes arrest at prophase I for several months (mice) or years (humans). The first arrest is resumed by proper hormonal signals following puberty (Jaffe and Egbert, 2017).

To resume MI, germinal vesicle breakdown (GVBD) is induced by activated maturation promoting factor (MPF) and the chromatin condenses (Jaffe and Egbert, 2017). During MI, the meiotic spindle is assembled by microtubules and bivalents are attached and stretched by microtubules and aligned at the metaphase plate. The homologous chromosomes are segregated by microtubules at anaphase and the first polar body is generated after telophase (Holt and Jones, 2009; Mogessie et al., 2018). So far, the amount of genetic material of the oocyte is reduced by half.

Entry into MII is initiated immediately after polar body extrusion with no interphase. However, the MII oocyte then arrests at metaphase until it is activated by a sperm. After fertilization, the second polar body is extruded to reduce the amount of oocyte's genetic material by half again. With the addition of the genetic content of the sperm the fertilised egg now contains the correct number of chromosomes for full development.

1.1.1 Initiation of female meiosis I

Female meiosis is initiated from embryonic day 13.5 (E13.5d) of development in mice (Bowles and Koopman, 2007) and about week 10 in humans (De Felici and Barrios, 2013). In mice, the important role of retinoic acid (RA) in meiosis initiation was proposed and reported by two independent groups in 2006 (Bowles et al., 2006; Koubova et al., 2006). RA is produced by mesonephros (the primordial structure for the urinary system) and required for the expression of *Stra8* which is involved in both female and male meiosis initiation.

The expression of *Stra8* is necessary for female meiosis initiation because the chromosome condensation was prevented in *Stra8* knockout mice (Koubova et al., 2006). In addition, the synaptonemal complex (SC) formation is also stopped by *Stra8* knockout. However, meiosis is not initiated in male germ cells because RA is degraded by its specific enzyme CYP26B1 (Bowles and Koopman, 2007).

1.1.2 Chromosome recombination

With meiosis initiation, SC starts to form in leptotene stage, the first of five substages of prophase I in meiosis. SC is a protein structure that forms between homologous chromosomes during meiosis, which is responsible for chromosome pairing, synapsis and recombination. With the presence of SC, homologous chromosomes are aligned in pairs and tethered by cohesin during meiotic recombination (Handel and Schimenti, 2010). Recombination provides an opportunity for the exchange of genetic material and also is important for proper chromosome segregation (Handel and Schimenti, 2010; Wang et al., 2017).

With the homologous chromosomes paired, oocyte enters the zygotene stage of prophase. At this stage, the paired homologous chromosomes begin to synapse, and SC formation extends to the whole chromosomes. After the completion of SC formation

pachytene stage of prophase occurs. DNA interactions between homologous chromosomes are formed (physical linkage created) (Romanienko and Camerini-Otero, 2000). The homologous chromosomes are recombined at this stage and termed as 'bivalents'. Meanwhile, genetic variation is increased by recombination within a population. After the SC degrades and crossover formed, the oocyte enters the diplotene stage and remains arrested until meiosis resumption (Tripathi et al., 2010).

1.1.3 Germinal vesicle arrest and meiosis I resumption

Germinal vesicle (GV) arrest is sustained for a long time from recombination completion until the levels of cyclic AMP (cAMP) and cyclic GMP (cGMP) are decreased in the oocyte (Romanienko and Camerini-Otero, 2000). The level of these cyclic nucleotides is maintained by continuously activated G-proteins at the oocyte plasma membrane. The balance depends on phosphodiesterase 3A activity which is inhibited by the cGMP from granulosa cells at outside of oocyte (Jin et al., 2002; Masciarelli et al., 2004; Norris et al., 2009). As a result it is well known that follicular cells surrounding the oocyte are needed to maintain arrest. Meanwhile, the cAMP from granulosa cells activates protein kinase A (PKA) which inhibits CDK1 and inactivates the CDK1-cyclin B1 complex in oocyte (Mehlmann, 2005; Mehlmann et al., 2002). Therefore the oocyte is arrested at GV stage.

GV oocytes are arrested until the granulosa cells are stimulated by the surge of luteinizing hormone (LH) just before ovulation. Following the surge of LH, meiosis resumes immediately. LH can bind the receptor on the granulosa cells, closing the gap junctions, which inhibit the transportation of cGMP from granulosa cells to the oocyte. Loss of inhibition from cGMP causes phosphodiesterase 3A to become activated, in turn resulting in a decrease in the level of cAMP (Norris et al., 2009). After female meiosis is resumed, oocytes enter a process called 'maturation'.

In addition, LH also plays a key role in gonadal function. LH in synergy with follicle stimulating hormone (FSH) stimulates follicular growth and ovulation. FSH is crucial at an earlier stage of follicular development, perhaps earlier in the follicular phase, to induce the aromatase enzyme that converts androgen to estradiol (Raju et al., 2013). FSH can also stimulate multiple follicles growth in a single cycle, which is widely used in in vitro fertilization. Consequently, the experimental mouse ovaries were stimulated to

achieve superovulation and to collect more oocytes for my experiments (see Chapter 2.1.3). All these oocytes are as good as naturally produced oocytes for experiments.

1.1.4 Prometaphase

GVBD is the first morphological sign of re-entry into meiosis. After GVBD, chromosomes are released from nucleus envelope and start to interact with microtubules in early prometaphase (Figure 1.1). The bivalents are pushed out by microtubules onto the periphery of a microtubule ball in the first hour after GVBD. The rosette circular arrangement of bivalents is formed in the first two hours (Figure 1.1). After that, the bipolar spindle starts to form. However, in mouse oocytes, centrosomes are eliminated during oogenesis and the spindle is assembled by self-organised microtubule organising centres (MTOCs) (Figure 1.2) (see Chapter 1.4). The bipolar spindle is formed by around 4 hours after GVBD at the centre of oocyte (Figure 1.2) (Schuh and Ellenberg, 2007). In late prometaphase, microtubules start to search and capture kinetochores and align the bivalents.

1.1.5 Metaphase

Once the kinetochores are attached by microtubules, bivalents aligned in the middle of the spindle are stretched by the tension generated by the microtubules (Kitajima et al., 2011). Metaphase occurs when the bivalents are well aligned on the metaphase plate (Figure 1.1). To achieve appropriate kinetochore-microtubule (K-MT) attachments, the spindle assembly checkpoint (SAC) is essential, as it couples the chromosome capture to the cell cycle machinery. All the K-MT attachments are examined by SAC, and only the stable attachments can pass the examination (Hached et al., 2013; Jones and Lane, 2013). Only if the SAC is satisfied by proper K-MT attachments can the oocyte progress to anaphase.

The anaphase-promoting complex or cyclosome (APC/C) can be activated and 1-2 hours later is followed by anaphases initiation (Jones and Lane, 2012). Meanwhile, during metaphase, the spindle starts to migrate from the centre to the cortex to set up the oocyte for an asymmetrical cell division (Figure 1.2). To preserve most of the cytoplasm and maternal resources for further embryo development, oocytes undergo two highly asymmetrical cell division to eliminate the surplus chromosomes, whilst retaining the

cytoplasm (Brunet and Verlhac, 2011; Li et al., 2010; Schmerler and Wessel, 2011; Verlhac, 2011). Unlike in mitosis where spindles are always central, in oocytes the spindle is assembled in the cell centre but then migrates to the cortex for the first asymmetrical cell division (Verlhac, 2011) (Figure 1.2). Although in prometaphase of meiosis I the newly formed spindle is considered to be centrally located, it is always slightly off-centre. During spindle migration it is found to move along its long axis towards the nearest part of the plasma membrane (Figure 1.2) (Guillaud et al., 2002; Schuh and Ellenberg, 2008; Yi et al., 2013).

1.1.6 Anaphase

The degradation of cyclin B1 and securin occurs after APC activation, which releases active separase and cleaves the cohesion rings along chromosome arms. In anaphase I, only homologous chromosomes are separated (Figure 1.1), however, the sister chromatids are still held together by centromeric cohesion rings for later separation at meiosis II. Therefore, cohesin is an essential protein to avoid aneuploidy. The first polar body is extruded following chromosome segregation (Herbert et al., 2015; Holt and Jones, 2009; Jessberger, 2012).

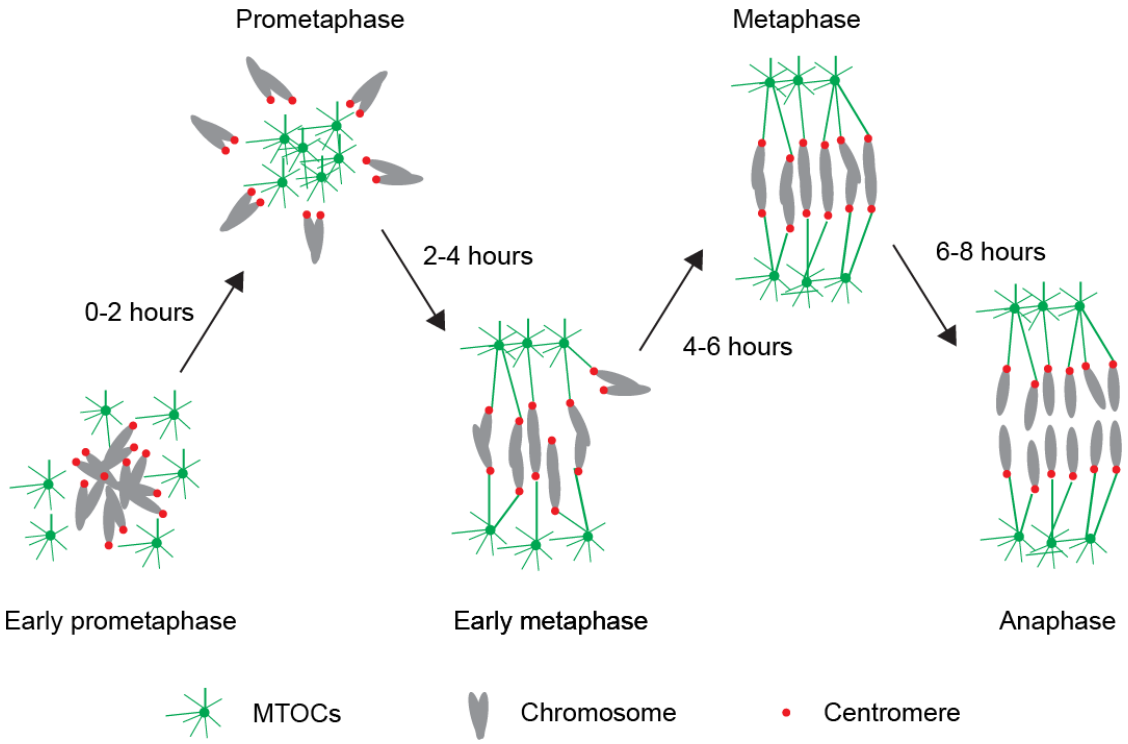

Figure 1.1 Schematic to show the process of chromosome alignment in meiosis I.

Chromosomes are individualized at prometaphase and then aligned at metaphase plate at metaphase. Bivalents are separated at anaphase. Green: MTOCs and microtubules; Grey: chromosomes; Red: centromeres. Time from GVBD.

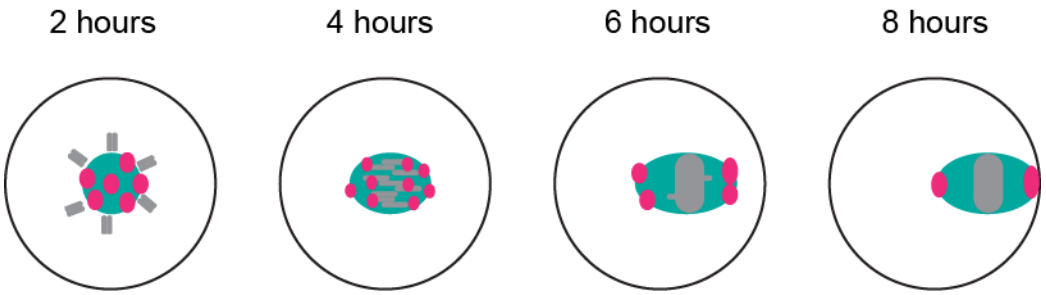

Figure 1.2 Schematic to show the process of spindle pole formation and spindle migration in meiosis I.

Spindle migration is initiated at 4-6 hours and arrived cortex at 7-8 hours after GVBD. Cyan: spindle; Grey: chromosomes; Magenta: MTOCs. Time from GVBD.

1.2 Structure of Centromere

The centromere is an important structure for proper chromosome separation to ensure that only one copy of each chromosome is transferred to each daughter cell during cell division. The centromere was initially observed in 1882 and termed in 1936, after that its crucial functions in cell division were widely investigated and understood (McKinley and Cheeseman, 2016). Structurally, the centromere is composed by both nucleic acid and proteins. The centromeric DNA provides a base for the centromeric proteins (Cenps) assembly (Gieni et al., 2008; Guenatri et al., 2004; Morris and Moazed, 2007). The interaction between the centromere and microtubules was initially observed by electron microscopy (Brinkley and Stubblefield, 1966; Jokelainen, 1967; Luykx, 1965). In this chapter, I would like to highlight the basic structure of mouse centromere as it is associated to my research throughout this thesis.

Basically, there are two sorts of tandemly repeated arrays, centromeric DNA and pericentromeric DNA, involved in mouse centromere architecture (Maison et al., 2011). Enriched satellite repeats were initially observed on chromosome stained by C-banding (McKay, 1973; Pardue and Gall, 1970). In *Mus musculus,* kinetochores are flanked closely by minor satellite repeats, then by more distally by the larger major satellite repeats (Figure 1.3) (Joseph et al., 1989).

1.2.1 Satellite DNA

In mouse, centromere localizes at the end of chromosome to form telocentric chromosomes (Garagna et al., 2001). The centromeric region is defined by repetitive centromeric DNA sequences, which are enriched in minor satellite repeats (600 kbp of 120 bp sequences) (Figure 1.3) (Guenatri et al., 2004). Minor satellite DNA is the major site for the centromeric proteins Cenp-A and Cenp-B assembly (Guenatri et al., 2004; Iwata-Otsubo et al., 2017). Cenp-A is a centromere-specific variant of histone H3, the most upstream factor in the centromere assembly, which is also critically important for the centromere identity and structure. However, Cenp-A may localise to DNA sequences that are not satellite repeats to form neocentromeres, because the identity of centromeres does not depend on the underlying DNA sequence (Earnshaw et al., 1989; Van Hooser et al., 2001; Palmer et al., 1987; Warburton et al., 1997). Cenp-B is a minor satellite DNA (centromeric DNA) binding protein. Despite the centromere sequence

variety across species, the Cenp-B box (17bp-long DNA) is highly conserved between rodents and primates (McKinley and Cheeseman, 2016).

The mouse pericentromeric region is composed of major satellite repeats (6 Mbp of 234 bp monomers) (Figure 1.3) (Guenatri et al., 2004), which is required for heterochromatin formation (Burton and Torres-Padilla, 2014). However, the role of major satellite DNA in cell division is still unclear.

1.2.2 Kinetochore Proteins

With the presence of Cenp-A, kinetochore components are recruited to the centromeres. The inner kinetochore is built by the constitutive centromere associated network (CCAN) consisting of various Cenps (Gascoigne and Cheeseman, 2011; Musacchio and Desai, 2017).

Based on CCAN, the outer kinetochore is assembled to bind microtubules directly and transduces the force required to move chromosomes during metaphase and anaphase. Its core is composed of three complexes, termed KMN (Knl1 complex, Mis12 complex, Ndc80 complex), which altogether comprise of 10 subunits (Cheeseman et al., 2004; Kline et al., 2006; Musacchio and Desai, 2017; Obuse et al., 2004).

The primary microtubule binding site, the Ndc80 complex, interacts with microtubules through its N-terminal regions (Ndc80 and Nuf2) and mediates kinetochore interactions with its C-terminal regions (Spc24 and Spc25), (Figure 1.4) (Ciferri et al., 2008; Tooley et al., 2011; Wei et al., 2005, 2007). The Mis12 complex act as an interaction hub to promote KMN assembly at the inner kinetochore, directly binding to Cenp-C and Cenp-T proteins. In addition, it can bind to both the Ndc80 complex and the Knl1 complex to connect them all together (Petrovic et al., 2010, 2014).

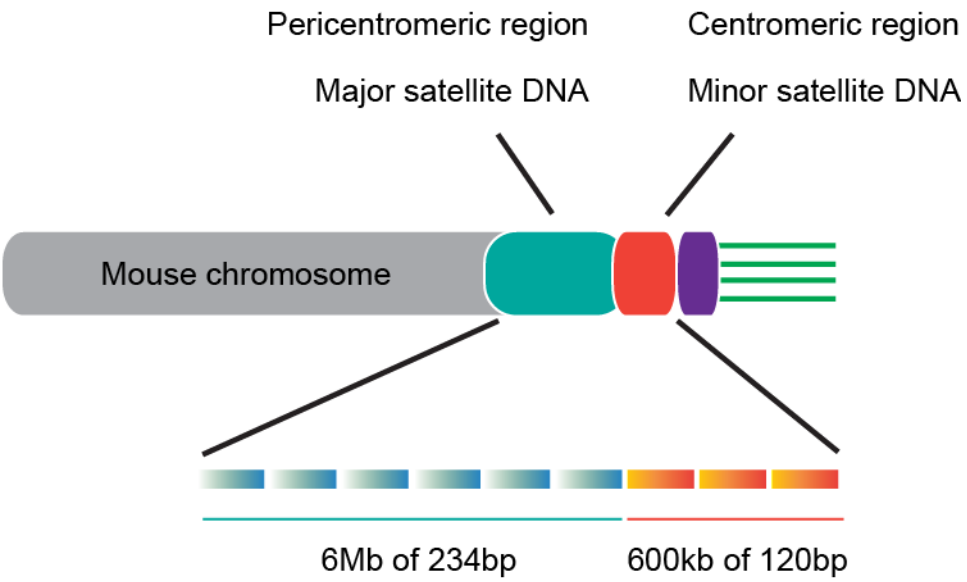

Figure 1.3 Schematic to show centromeric structure of mouse telocentric chromosomes.

Major satellite repeats localize at the pericentromeric region. Minor satellite repeats localize at the centromeric region. Rectangular gradient, shows the monomer for each satellite repeat. The kinetochore is mainly recruited to minor satellite DNA and attached by microtubules directly. Cyan: major satellite DNA; Orange: major satellite DNA; Purple: kinetochore; Green: microtubules; Grey: chromosome.

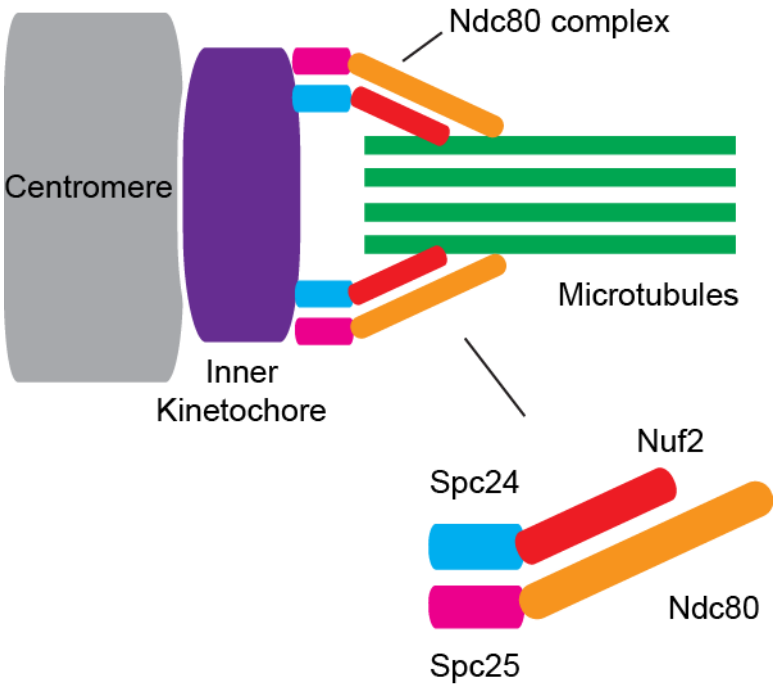

Figure 1.4 Schematic to show the structure of Ndc80 complex.

Ndc80 complex, as the main part of the outer kinetochore, binds the Inner kinetochore and microtubules together. Blue: Spc24; Red: Nuf2; Magenta: Spc25; Orange: Ndc80; Purple: inner kinetochore; Green: microtubules; Grey: centromere.

1.3 Mechanism of Meiotic Drive

Chromosome segregation during meiosis is considered as Mendelian, and as such it is generally accepted that each chromosome has an equal probability of transmission to the offspring. However, in mammalian female meiosis, only one of four meiotic products are transmitted to the offspring due to the highly asymmetrical cell division. This provides an opportunity for chromosomes to compete with each other to survive in the final gamete. Therefore, non-random segregation is feasible and is known as meiotic drive (also known as transmission ratio distortion, TRD).

The first example of a chromosome transmission ratio distortion was in female *Drosophila* reported in 1934 (Sturtevant, 1936, 1934). Biased chromosome transmission has been observed and described in different species since, and the mechanism of meiotic drive has proposed by different models in the past 85 years (Gabriel et al., 2014; Hewitt, 1976; Pardo-Manuel De Villena and Sapienza, 2001; Rhoades, 1942; Rosin and Mellone, 2017). The phenomenon was confirmed morphologically in 1942, when the biased transmission of the centromeric sequence was observed during maize female meiosis (Rhoades, 1942). A number of years later, the biased chromosome transmission was first termed as “meiotic drive” formally by Sandler and Novitski to emphasize the important role of the asymmetrical female meiosis (Sandler and Novitski, 1957).

The first evidence of meiotic drive was noticed and proved on Chromosome IV in female *Drosophila*. This study is based on the flies carrying two shorter chromosomes (IVs) as a duplication. These female flies were made heterozygous with the “normal” Chromosome IV. As expected, Chromosome IV segregation in Triplo-IV female meiosis resulted in two chromosomes moving to one pole and one to the other. However, the frequencies of the three potential segregation types show that transmission was not random (rate of shorter IVs passing to opposite poles, 95%) (Sturtevant, 1936, 1934). Later, evidence of meiotic drive was observed in maize (*Zea mays*) which has two Chromosome 10 variants. Therefore, a heterozygous maize model was produced to investigate chromosome transmission rate.

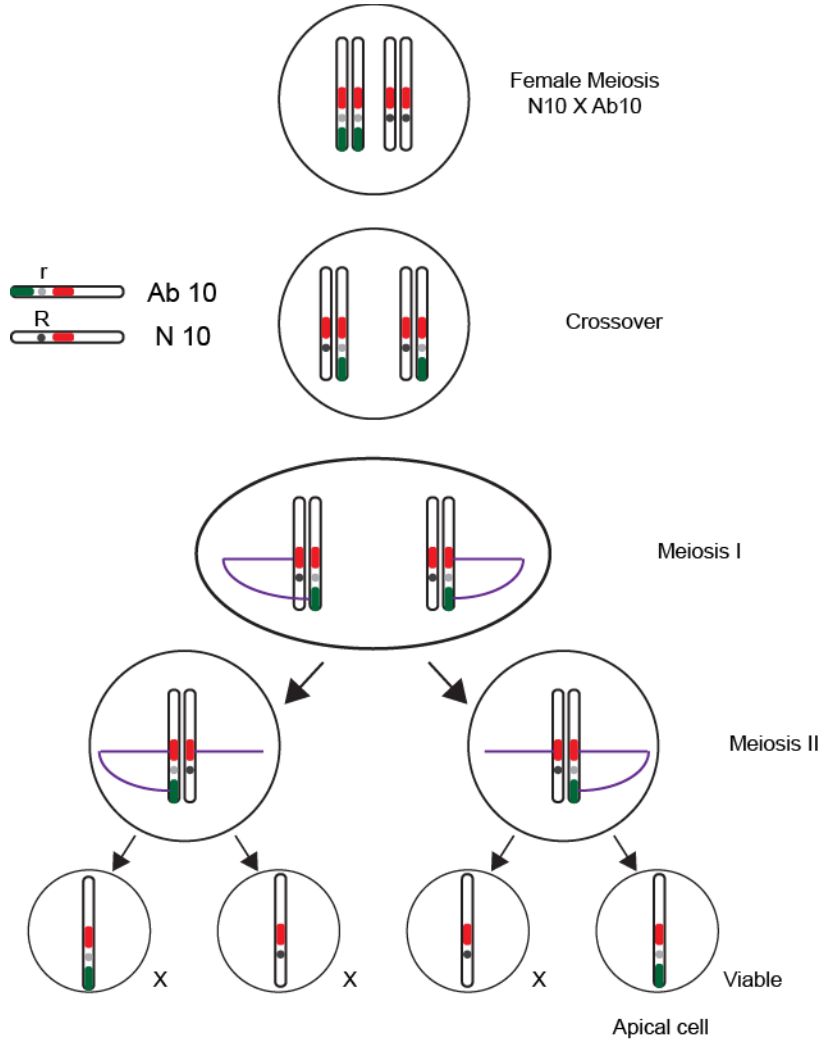

Figure 1.5 Biased chromosome transmission in Ab10/N10 heterozygotes maize.

Abnormal chromosome 10 (Ab10) with an extra knob (green) and r allele (light grey) is preferentially transmitted to the offspring. Centromeres are red, and spindle microtubules are purple. Ab10, abnormal chromosome 10; N10, normal chromosome 10. X: Non-viable

Normal Chromosome 10 (N10) with an R allele and its abnormal form (Ab10) with an r allele were combined as homologs in the heterozygous maize model. The genetic marker (r- allele) on Ab10 is responsible to code a dark anthocyanin pigment in maize seeds. To test the chromosome transmission ratio, heterozygotes (N10 X Ab10) were backcrossed and the seed colours of progenies was calculated to quantify the ratio. According to Mendel's first law, both variants (N10 and Ab10) of Chromosome 10 should be transmitted to the seeds with equal possibilities and the seeds colour was expected as 50% to 50%. However, in the seminal experiments, over 70% dark seeds (Ab10) were observed in the offspring, which is important evidence for female meiotic drive (Figure 1.5) (Rhoades, 1942).

Subsequently a mechanism has been proposed to explain the phenomenon, Ab10 has a distinct repetitive DNA sequence (knob) which can interact with microtubules as a neocentromere. Although the neocentromere could not assemble regular kinetochores on it (absence of assembly platform CENP-C), it can still lead to a non-random chromosome transmission rate, however its mechanistic details are still unknown (Muszynski et al., 2007; Yu and Dawe, 2000).

Although the centromere was assumed to be the selfish element (meiotic driver) in 2001 (Henikoff and Malik, 2002; Henikoff et al., 2001; Pardo-Manuel De Villena and Sapienza, 2001) and termed the mechanism a "centromere drive", which was not demonstrated in natural populations to explain meiotic drive until 2008 (Fishman and Saunders, 2008; Fishman and Willis, 2005).

To understand the role of the centromere in the meiotic drive, F_1 hybrid monkey flowers were generated by crossing *Mimulus nasutus* and *Mimulus guttatus*. The F_1 hybrids contain D locus on homologous chromosomes, which is thought to be the centromeric region. Chromosome transmission rate was examined in *Mimulus nasutus* (maternal; dd) x *Mimulus guttatus* (paternal; DD) F_2 hybrids. According to Mendel's first law, the expected ratio of D locus in F2 hybrids is Mendelian (1:2:1, dd: Dd: DD). Strikingly, there was such a strong transmission bias against the M. nasutus allele, the actual ratio is extremely non-Mendelian (0:2:2, dd: Dd: DD) (Fishman and Saunders, 2008). To prove the key role of D locus, F_2 hybrids were repeatedly backcrossed with homozygous *Mimulus nasutus*. Several generations later, it showed that despite most of the genome

was from *Mimulus nasutus*, the D locus from *Mimulus nasutus* was still observed in over 90% of the offspring (Figure 1.6). Therefore, the extremely biased transmission indicates that the D locus could play a key role in transmission ratio distortion (Fishman and Saunders, 2008; Fishman and Willis, 2005).

Apart from plants, the role of centromere in the meiotic drive was also demonstrated in a mouse model. The hybrid mouse model crossing CF1 and CHPO strains was created because their centromere strength was different. The strength of centromere was defined by Hec1 (Ndc80) immunofluorescence intensity which is higher in CF1 mice. In the F1 hybrid mouse, more Hec1 was recruited to one centromere when compared to the other. It seems that the biased Hec1 recruitment disturbed the random chromosome segregation in meiosis. The stronger centromeres (CF1) with higher HEC1 intensity were more likely retained in the MII eggs (60%) than weaker centromeres (CHPO). This investigation proposed that stronger centromeres could recruit more kinetochore protein and alter spindle microtubules attachments to stay in the egg (Gabriel et al., 2014).

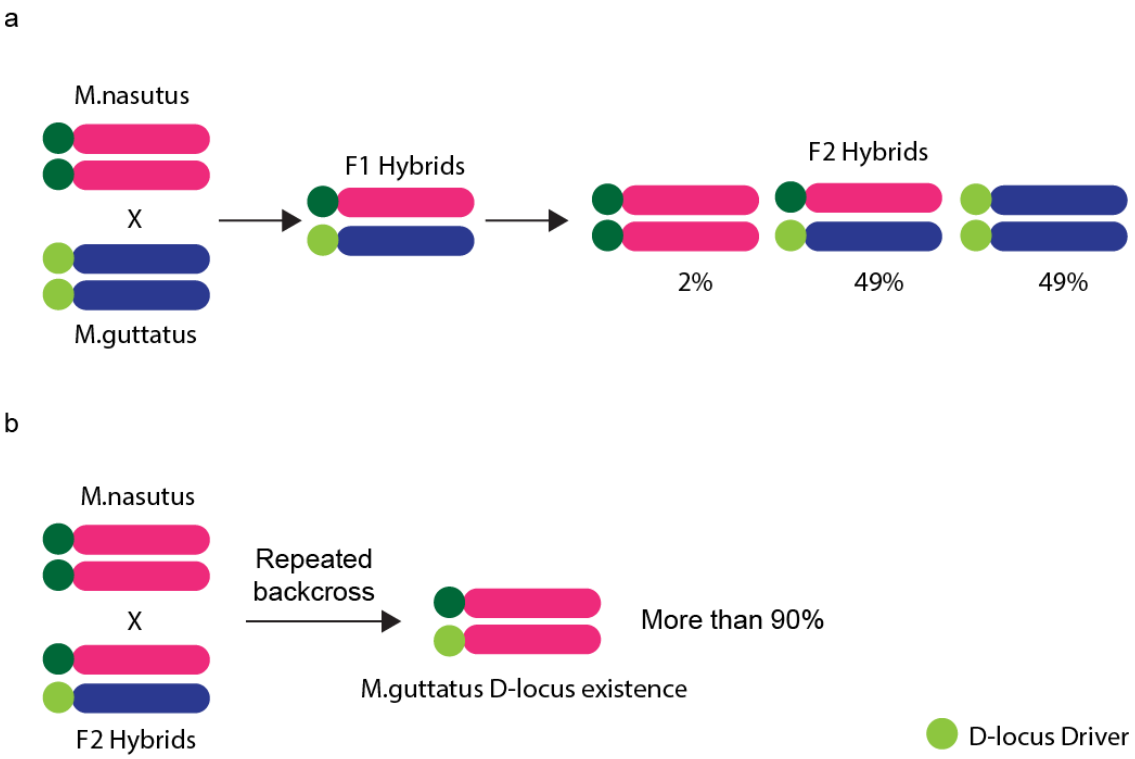

Figure 1.6 Biased chromosome transmission in hybrid Monkeyflowers.

(a) F_2 hybrid Monkeyflowers crossed by Mimulus nasutus (maternal; dd) and Mimulus guttatus (paternal; DD) were used to examine the chromosome transmission preference. The chromosome from M. guttatus with D-locus is preferentially transmitted to the next generation. **(b)** Female F_2 hybrids were repeated backcrossed by male M. nasutus and the genome was purified to homozygous for M. nasutus alleles after several recombinations. However, over 90% D-locus from M. guttatus remained in the offspring.

To understand why chromosomes with more Hec1 demonstrated meiotic drive, the centromeric proteins were examined in detail. The centromeric histone H3 variant Cenp-A is responsible for Hec1 localization. As the main centromeric structural platform, Cenp-A is mostly limited to minor satellite DNA and forms the main part of the centromere. In further research, Cenp-B recruitment was also observed to be limited by the size of minor satellite DNA. Finally, in the hybrid mouse model (CF1 x CHPO), the centromeres with more Hec1 were found to have expanded minor satellite repeats, could recruit more centromeric proteins and were preferentially retained in the egg (Iwata-Otsubo et al., 2017).

Although the biased allele inheritance was confirmed in different species, such as *Drosophila*, maize, monkey flower and mice, the mechanism of the meiotic drive is still unclear.

Putting all the previous observations together, a mechanical hypothesis was first summarized by Pardo-Manuel de Villena and Sapienza about 20 years ago to explain the mechanism of meiotic drive (Pardo-Manuel De Villena and Sapienza, 2001). Three basic requirements indicated by experimental results ware pointed out to explain meiotic drive. First of all, different cell fates (egg or polar body) are determined by the asymmetrical female meiosis. Only the chromosomes retained in the egg can be transmitted to the offspring. Second, heterozygous locus (centromere) of chromosomes can be identified by microtubules from the spindle. Thus, specific chromosomes can be preferentially selected for inheritance. Third, asymmetrical microtubules assembly on the meiotic spindle is also required to distinguish locus from homologous chromosomes. On the whole, all these requirements are necessary and sufficient to explain the phenomenon of the meiotic drive (Pardo-Manuel De Villena and Sapienza, 2001).

1.3.1 Asymmetrical cell division in female meiosis

Compared to mitosis, female meiosis is a specialised type of cell division which creates haploid gametes from diploid parental cells. Mammalian oogenesis is initiated from the primordial germ cell and transferred from mitosis to meiosis in the foetal ovary (McLaren, 2003). Oogenesis involves single chromosome duplication and two chromosome segregations (Page and Hawley, 2003; Petronczki et al., 2003). After oocyte maturation and fertilization, chromosomes are segregated twice with only one

egg generated (Figure 1.7). Meanwhile, with recombination in early meiosis I, each chromosome or chromatid is unique to others. After two asymmetrical cell divisions, there should be a 25% probability for each meiotic product to be segregated into the egg and transmitted to the offspring. The rest of the chromatids (75%) that were extruded into the polar bodies cannot be passed to the offspring (Figure 1.7) (Chaigne et al., 2017; MacLennan et al., 2015; Page and Hawley, 2003).

The asymmetrical cell division is thought to save loss of essential factors such as maternal RNAs and proteins needed for early embryonic development (Balboula et al., 2017). After meiosis resumption, the spindle is formed in the centre of the oocyte and then migrates to the cortex before anaphase I, permitting an asymmetrical cell division. After cell division, half of the homologous chromosomes are transferred into the first polar body with little cytoplasm. The polar body containing chromosomes will degenerate after a few hours (Schmerler and Wessel, 2011). Therefore, asymmetrical cell division in meiosis I is essential for female haploid gamete generation and chromosomal selections.

In terms of meiosis I, homologous chromosomes are paired and recombined with their partners, then separated away from each other at anaphase I. The random homologous chromosomes segregation in female meiosis is widely known as a physical basis of Mendelian inheritance which ensures the diversity of genome. Meanwhile, the different fates of meiotic products provide an opportunity for chromosomes to compete for survival (Henikoff and Malik, 2002; Pardo-Manuel De Villena and Sapienza, 2001). One more thing needs to be pointed out, it is not the whole chromosome though, because of recombination and exchange of genetic material, only the portion of the chromosome closest to the centromere is going to be selected.

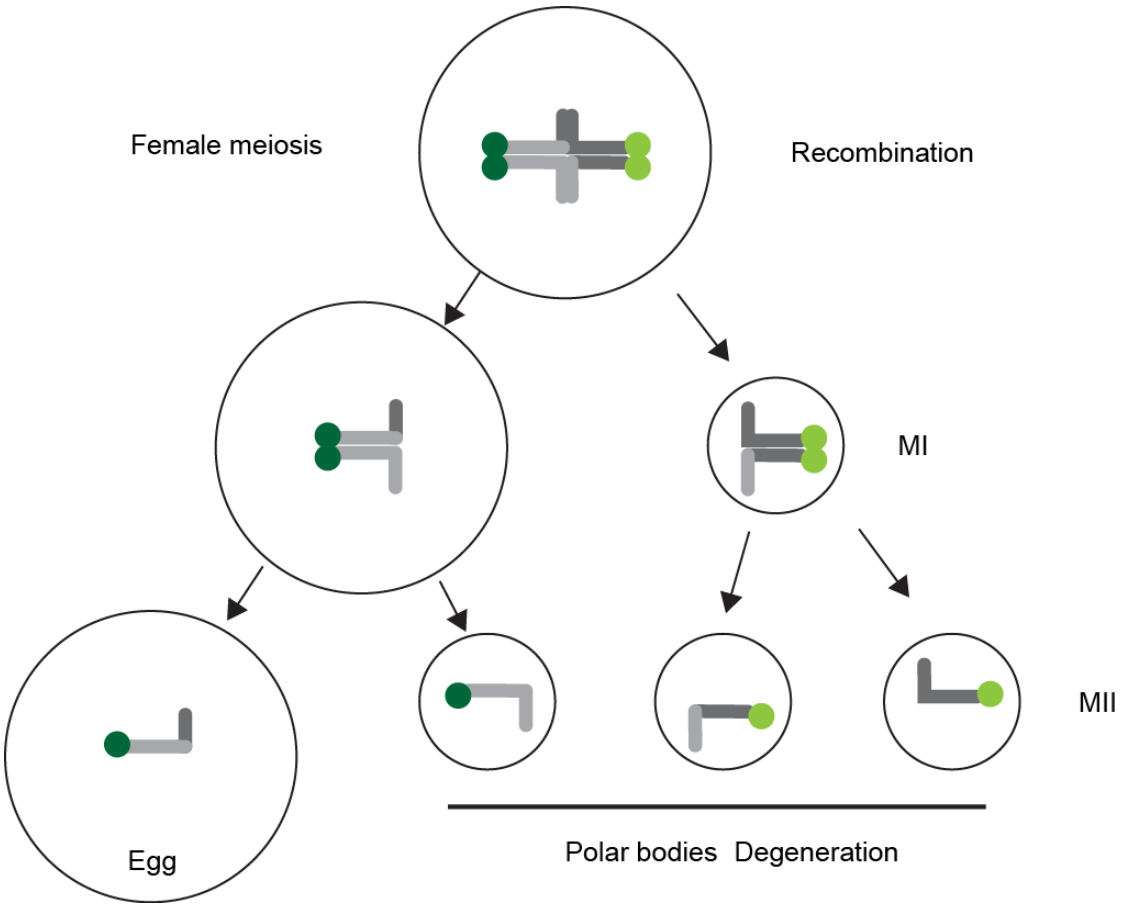

Figure 1.7 Female meiotic drive.

A schematic shows the asymmetrical female meiosis and biased chromosome transmission. The chromosome (grey) with driver element (dark green) is transmitted to the viable gamete (egg) whereas the other (non-driver element, light green) are degenerated in the polar bodies.

1.3.2 Asymmetrical centromeres on homologous chromosomes

Every eukaryotic chromosome has a centromere, which is essential to interact with microtubules for appropriate chromosome segregation in cell division. The function of the centromere is highly conserved across different species and was assumed to be the meiotic driver in previous research (Dawe and Cande, 2002; Peacock et al., 2006; Rhoades, 1942) because the orientation and movement of chromosomes are controlled by centromeres through attachments to microtubules. To create meiotic drive, asymmetrical centromeres are required for microtubule selection. Only the hybrid biological model with functional heterozygous centromeres and kinetochores would direct biased chromosome segregations.

The centromere is composed of centromeric DNA and centromeric proteins. In particular, the centromeric DNA is composed of minor satellite repeats (120 bp) in *Mus musculus*, or monomers termed α-satellite DNA (171 bp) in primates (Masumoto et al., 1989; Muro et al., 1992). The only conserved sequence in centromeric DNA from rodents to primates is the Cenp-B box, a 17bp DNA sequence for Cenp-B recruitment (Earnshaw and Rothfield, 1985). The centromeric DNA is also a primary position for Cenp-A nucleosome assembly (Iwata-Otsubo et al., 2017; McKinley and Cheeseman, 2016). Cenp-A is a fundamental centromeric protein component, which is mainly responsible for the localization of other centromere and kinetochore components, including Cenp-C and Hec1/Ndc80 complex (McKinley and Cheeseman, 2016). Outer kinetochore proteins (Hec1/Ndc80 complex) are attached by microtubules directly for chromosome bi-orientation and separation.

It seems possible that both centromeric proteins and kinetochore proteins will be involved in meiotic drive. In fact, although the role of the centromere in chromosome segregation is highly conserved for cell division, the centromeric DNA sequence and specific protein components have evolved rapidly. This phenomenon is observed and termed as the “centromere paradox” but its mechanism is still unclear (Henikoff and Malik, 2002).

The paradox indicates that a specific centromeric DNA sequence is not essential for centromere function. Therefore the centromere’s function can be maintained alongside rapid centromeric DNA evolution. However, a recent investigation discovered that Cenp-

A deposition is limited by the size of minor satellite DNA in mice (Iwata-Otsubo et al., 2017). This means the size of centromeric DNA could evolve, and could affect the level of centromeric and kinetochore proteins on the centromere. Therefore, the rapid evolution of centromeric DNA and proteins through genetic conflict was termed as centromere drive (Henikoff and Malik, 2002). This raises the possibility that the centromere can change in size through evolution of the underlying genetic elements.

Based on classic centromere drive, as a selfish element, centromeres are able to compete with each other in meiotic drive as a tug-of-war. In the competition, the stronger centromeres were observed with higher Hec1 intensity, which was preferentially retained in the egg after meiosis I (Figure 1.8) (Gabriel et al., 2014). The unequal evolution of homologous centromeric DNA creates not only the biased chromosome segregations in female meiosis, but also reduces male fertility by chromosome alignment distortion as a compromise (Lampson and Black, 2017). Interestingly, although the improper chromosome alignment was observed during the meiotic drive (Gabriel et al., 2014), the female fertility reduction was never reported.

Since the bivalents are oriented on the spindle through their interactions with microtubules it is thought that the microtubule binding apparatus (outer kinetochore) may be more important than the centromere/kinetochore as a whole. For example in human cells, each human kinetochore is attached by 12-24 microtubules (Wendell et al., 1993) or 13-22 microtubules (Yen et al., 2013). On average, each human kinetochore binds to about 17 microtubules and two-fold variability were observed among different chromosomes (Cherry and Johnston, 1987; Cherry et al., 1989; Drpic et al., 2018; Maraschio et al., 2004; Royle et al., 2017; Sanchez et al., 2011; Tomkiel et al., 1994). A recent investigation shows that the adaptive changes of kinetochore size and shape are important to chromosome orientation in human cells with a computational model (Magidson et al., 2015).

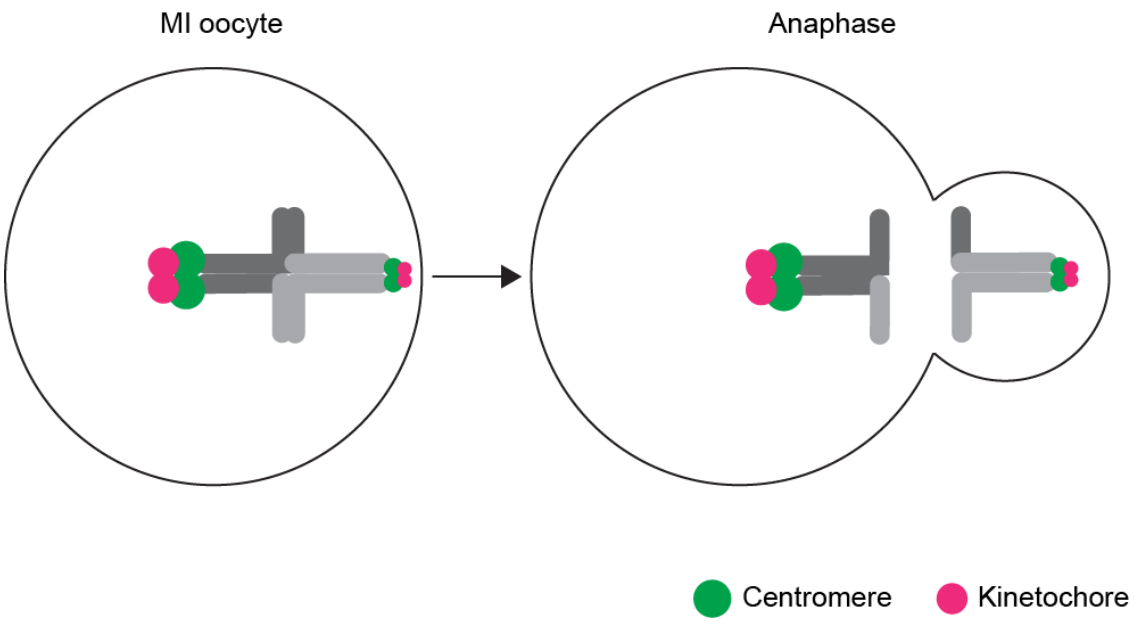

Figure 1.8 Centromere drive in female meiosis I.

Schematic presents the anaphase of meiosis I in mouse oocyte. The stronger centromere (larger size) with more kinetochore protein (Hec1) is preferentially maintained in oocyte after meiosis I, whereas the chromosome with weaker centromere is biased to extrude into the polar body.

Many observations relevant for the better understanding of meiotic drive were made while investigating mitosis. For example, it has been noticed that the size of the kinetochore is not consistent. The kinetochore size is not only variable in different chromosomes but also among different species (Comings and Okada, 1971; Koblížková et al., 2015; Moutinho-Pereira et al., 2006; Ribeiro et al., 2009). According to previous research, the size of a kinetochore is primarily determined by the size of centromeric DNA and centromeric proteins (Bodor et al., 2014; Fachinetti et al., 2015; Pedeutour et al., 2005; Sullivan et al., 2011). However, the exact relevance of centromere size and kinetochore size is still unclear.

Besides the length of the centromeric DNA, its transcripts are also responsible for kinetochore recruitment and stabilization. Therefore, I assume that the asymmetrical kinetochores on homologous chromosomes are generated by asymmetrical centromeric DNA transcripts deposition, because the centromere formation is promoted by centromeric transcripts locally (Bouzinba-Segard et al., 2006; McNulty et al., 2017; Perea-Resa and Blower, 2017). The centromeric transcripts were first discovered in mouse (Harel et al., 1968). The mouse minor satellite DNA transcripts are long non-coding RNAs (lncRNAs) which are suggested to be a fundamental part of the functional centromere (Perea-Resa and Blower, 2018). Apart from the core centromeric DNA, its flanking pericentromeric regions are also transcribed (Hall et al., 2002; Johnson et al., 2017; Maison et al., 2002; Swist-Rosowska et al., 2017; Volpe et al., 2002).

Compared to pericentromeric RNA, the generation and function of centromeric RNA are more important but more limited. In mouse cells, two RNA precursors (2000nt and 4000nt) are discovered to be spliced into several 120nt minor satellite RNAs, but the processing mechanism is still unclear (Bouzinba-Segard et al., 2006). In the mouse mitotic cell cycle, the level of minor satellite RNAs increases from G1 to G2/M (Ferri et al., 2009). In metaphase, Cenp-C is required for Cenp-A stabilization and some specific kinetochore proteins recruitment. Meanwhile, the investigators find the interaction between centromeric RNA and Cenp-C is essential for Cenp-C localization on centromere in different organisms (Figure 1.9) (Chen et al., 2015; Du et al., 2010; Rošić et al., 2014; Wong et al., 2007). It indicates that minor satellite RNAs may play a role in metaphase of the cell cycle. However, the mechanism of centromeric RNA related Cenp-C

stabilization needs further research. If the localization of Cenp-C requires centromeric RNAs in meiosis is currently unknown.

Apart from kinetochore proteins recruitment, the centromeric RNAs also have an essential role in the localization of chromosomal passenger complex (CPC) proteins which are important in kinetochore-microtubule attachment. It seems as another pathway to build meiotic drive. Aurora kinase B (AURKB), from the Aurora family of serine/threonine (S/T) kinases, is a crucial component of the CPC and plays a key role in chromosome segregation (Carmena et al., 2012). In mitosis, AURKB (AURKC in meiosis) localizes specifically at chromosomal arms and centromeres (Ndc80 complex) (Hengeveld et al., 2017), where it corrects kinetochore-microtubule attachment errors (Lampson and Cheeseman, 2011; Nguyen and Schindler, 2017). The interaction between AURKB and centromeric RNAs was initially confirmed in mouse somatic cells (Ferri et al., 2009), then also observed in a human cell line (Ideue et al., 2014). Indeed, Borealin (another CPC component) and AURKB provide the RNA binding sites for the interaction between the CPC and centromeric RNAs (Figure 1.9). The centromeric RNAs can not only localize AURKB, but are also required for its activation (Blower, 2016). For example, kinetochore-microtubule attachment errors are increased following centromere transcription block, because the R-loops (DNA : RNA hybrid structure) at centromeric regions is required to transmit the tension from microtubules to AURKB (Kabeche et al., 2018; Lampson et al., 2004; Perea-Resa and Blower, 2018; Petsalaki et al., 2011).

Collectively, according to their function and the specific localization on the centromere, centromeric RNAs are hypothesized as a potential effector to create asymmetrical kinetochores and promote centromere drive.

1.3.3 Asymmetrical microtubules on the meiotic spindle

For meiotic drive to exploit the asymmetrical centromeres, an asymmetrical spindle is also required. The homologous chromosomes attach by microtubules to opposite spindle poles have different fates. Only the chromosomes attached by pole at the oocyte centre can be transmitted to the offspring. The asymmetry within the spindle may arise as a consequence of differences between spindle poles. Asymmetry between the two meiotic spindle poles was observed about 20 years ago, however, its function and mechanism are unclear. Different shapes of opposite spindle poles were demonstrated in mouse oocytes (Carabatsos et al., 2000; Michaut et al., 2005), both O and C-shaped pericentrin (spindle pole protein, see section 1.4) clusters were observed at metaphase of meiosis I. However, in MII spindles, pericentrin is distributed symmetrically on opposite spindle poles (Carabatsos et al., 2000). It shows that the asymmetrical MTOCs recruitment is specific to meiosis I, not meiosis II.

Recently, a concept of the “reverse segregation” has been put forward and it suggests that sister chromatids of both homologs are separated at MI (normally at MII) due to chromosome recombination defects (Ottolini et al., 2015). The question arises how to reconcile this concept with meiotic drive.

Meiotic drive is active only in MI but not MII because in MII chromatids have the same sized centromeres and the spindle is parallel to oocyte membrane (the asymmetrical direction is disappeared). Therefore, in the reverse chromosome segregation pattern, meiotic drive might not happen anymore, because the MII spindle is parallel to oocyte membrane and cannot be directed and relocated as MI spindle. Therefore, the chromosome cannot be oriented to a specific direction and segregated asymmetrically.

The results from another group showed myristoylated alanine-rich C-kinase substrate (p-MARCKS) also localized asymmetrically at MI spindle poles. The opposing spindle poles were termed as the punctate-loci pole and the ring-shaped pole respectively, and the punctate-loci poles were observed preferentially rotated towards the cortex and extruded in polar bodies (Michaut et al., 2005).

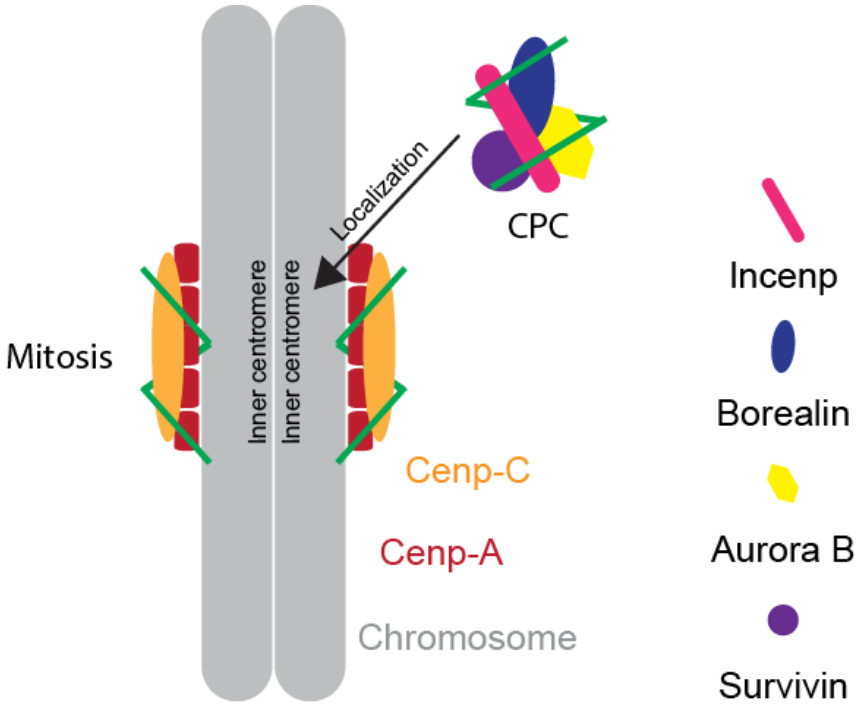

Figure 1.9 The function of centromeric RNAs in mitosis.

The schematic shows the role of centromeric RNA (green) in proper Cenp-C and CPC mitotic localization. In addition, centromeric RNA helps to assemble CPC and AURKB activation.

1.4 Microtubule Organizing Centres (MTOCs)

Microtubules are 25nm diameter tubes composed of alternating α/β-tubulin protein subunits and assembled by a special organizer. Although the structure for microtubule organizing had been described over several decades, it was finally termed microtubule organizing centres (MTOCs) by Pickett-Heaps in 1969. MTOCs were initially visualized and identified by electron microscopy, which provided the direction for the following research. The role of MTOCs for microtubule nucleation in meiosis is still unclear, therefore, their functions in mitosis are discussed here. In the past decades, microtubules assembly and regulation are well studied in mitosis, because they are important to cell division (Roostalu and Surrey, 2017). It is highly probable that many of these observations will apply to the mechanics and dynamicity of the meiotic spindle.

Classically, centrosome is a kind of MTOC in mammalian cell and composes of a pair of centrioles. Centrosomes are involved in microtubule growth, spindle assembly and chromosome segregation (Wittmann et al., 2001). Additionally, centrioles, a cylindrical organelle, can also work as basal bodies to create cilia and flagella, which are involved in cell polarity, signalling and intracellular trafficking (Strnad and Gönczy, 2008).

1.4.1 Centrosome guided spindle assembly in mitosis

In animal somatic cells, centrosomes are composed of two identical cylindrical structures termed centrioles, which are surrounded by pericentriolar material (PCM) components. The integrity of the centrosomal structure is maintained by centrioles, whilst the microtubules are nucleated and organized by the PCM (Nigg and Raff, 2009). During the G1 phase of the cell cycle there is only one centrosome in each normal somatic cell (Wittmann et al., 2001). Centrioles are duplicated during the G1 to S phase transition of the cell cycle because two identical centrosomes are required for proper chromosome segregation (Strnad and Gönczy, 2008). In metaphase of mitosis (M phase), the centrosome pairs are separated equally for bipolar spindle formation (Figure 1.10). To nucleate microtubules from two opposite spindle poles, earlier duplicated centrosomes are separated and moved to opposite sides of the nucleus before NEBD. In the beginning, centrosome separation is initiated by an increase of microtubule nucleation from centrosomes in prophase before NEBD. The nucleated microtubules interact with not only chromosomes but also with each other after NEBD. In the same

time, the astral microtubules growing towards the cortex and will encounter the cell membrane and be captured by cortical factors. The bipolar spindle assembly requires different types of microtubules as well as the associated proteins and motors which create the forces to push spindle poles apart from each other at metaphase (Tanenbaum and Medema, 2010).

Meanwhile, the sister chromatids are attached by microtubules from opposite spindle poles. In metaphase, chromosomes are aligned by microtubules at the metaphase plate in the middle of the spindle. At anaphase, sister chromatids are segregated and moved towards centrosomes, which are on the opposite spindle poles (Figure 1.11).

During cell division each daughter cell inherits just one centrosome (Figure 1.11) (Strnad and Gönczy, 2008). Nonetheless, some abnormal cells, e.g. cancer cells, have been observed to contain more than two centrosomes. Amplification of the centrosome induces multipolar spindle formation, which in turn influences the chromosome bi-orientation, thus increasing the aneuploidy rate after cell division (Saunders et al., 2002). However, most cells with multipolar spindle are still able to divide successfully because centrosomes, in these cells, are clustered into two groups to form bipolar spindles at metaphase (Franz et al., 2008). Remarkably, the clustered centrosomes are similar to the phenomenon of MTOCs clustering that is observed at prometaphase in mouse oocytes (Schuh and Ellenberg, 2007). Centrosome clustering was found to be dependent on both microtubule- and actin- associated proteins (Kwon et al., 2008), and this relationship has important implications for MTOCs clustering in mouse oocytes.

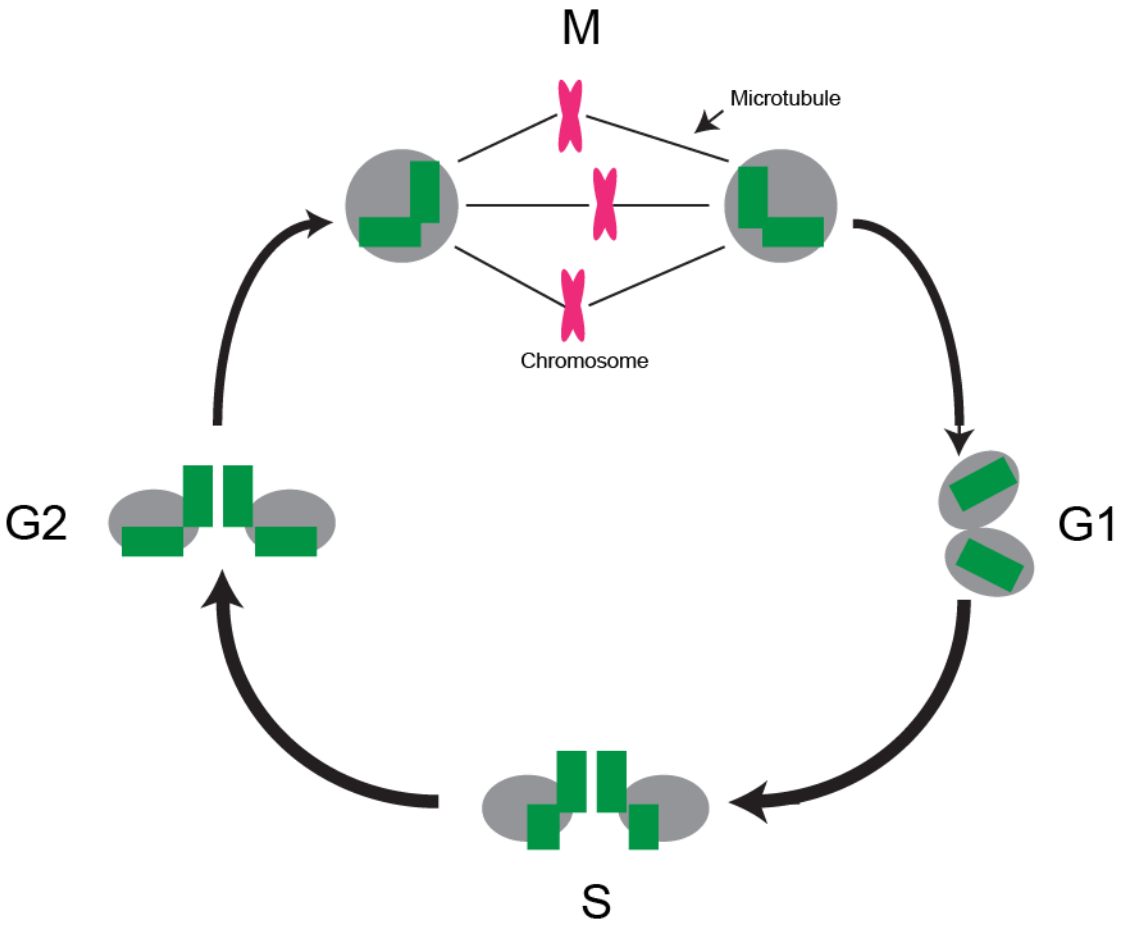

Figure 1.10 Centriole biogenesis.

The representative schematic of the centriole duplication during mitosis. Schematic shows centrioles (green) are surrounded by PCM (grey). Centrioles are duplicated at S phase and separated during the G2 to M phase.

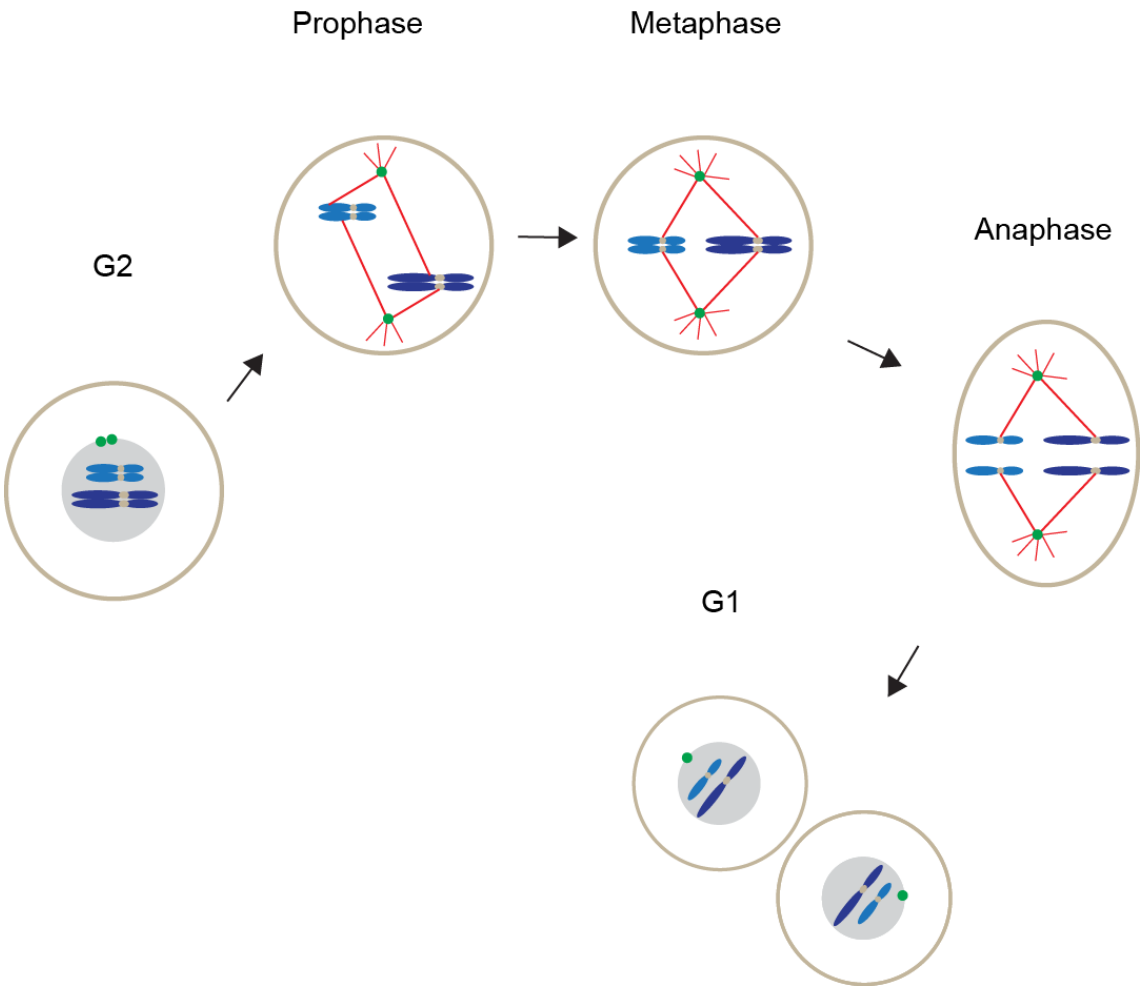

Figure 1.11 Process of mitosis.

The representative schematic of the mitosis shows different stages of cell division (chromosomes in blue; centrosomes in green and microtubules in red). It shows the spindle is assembled at metaphase and chromosomes are separated at anaphase.

1.4.2 Centrosome assembly

In mitosis, centrosomes are the most common structure of MTOCs and are responsible for microtubule nucleation in animal cells. As self-assembling structures, the components of centrosome, and their assembly process have been well investigated (Andersen et al., 2003; Müller et al., 2010).

To assemble the canonical centrosome, all the components of the PCM surround the mother centriole. The PCM core in mammalian cells is made of pericentrin, which is an elongated coiled-coil protein (Delaval and Doxsey, 2010). Pericentrin is recruited by the C-terminal PACT (pericentrin-AKAP450 centrosomal targeting) domain of coiled-coil protein AKAP450 , which is found in mammalian centrosomes (Gillingham &Munro 2000). However, the interaction between the centrosome and PACT is still unclear. Pericentrin is essential for centrosomal proteins (Cep) recruitment and organization. In mammalian cells, the recruitment of CEP215, CEP192, and its binding partner NEDD1 is pericentrin dependent (Figure 1.12)(Conduit et al., 2015; Mennella et al., 2014). On the contrary, another important conserved PCM component, Cep152, is not recruited by pericentrin (Chhun et al., 2012). Cep152 is dispensable for interphase PCM organization but initiates new centriole formation and is involved in mitotic PCM assembly (Dzhindzhev et al., 2010).

The recruitment of γ-tubulin ring complex (γTuRC) requires not only pericentrin but also multiple other centrosomal proteins. Pericentrin recruits the γTuRC through its N-terminal part, which is also responsible for CDK5 regulatory subunit–associated protein 2 (CDK5RAP2, termed as Cep215 in mammals) recruitment. CDK5RAP2 interacts with pericentrin by its C-terminal centrosomin motif 2 (CM2) (Wang et al., 2010) and binds to γTuRC through its N-terminal centrosomin motif 1 (CM1) (Choi et al., 2010; Sawin et al., 2004). Another protein associated with γTuRC recruitment in human cells is NEDD1 which provides γTuRC binding site for γTuRC recruitment but cannot initiate microtubule nucleation. In contrast, the γTuRC-binding site of CDK5RAP2 is involved in not only γ-TuRC recruitment but also γ-tubulin-mediated microtubule nucleation activation (Muroyama et al., 2016).

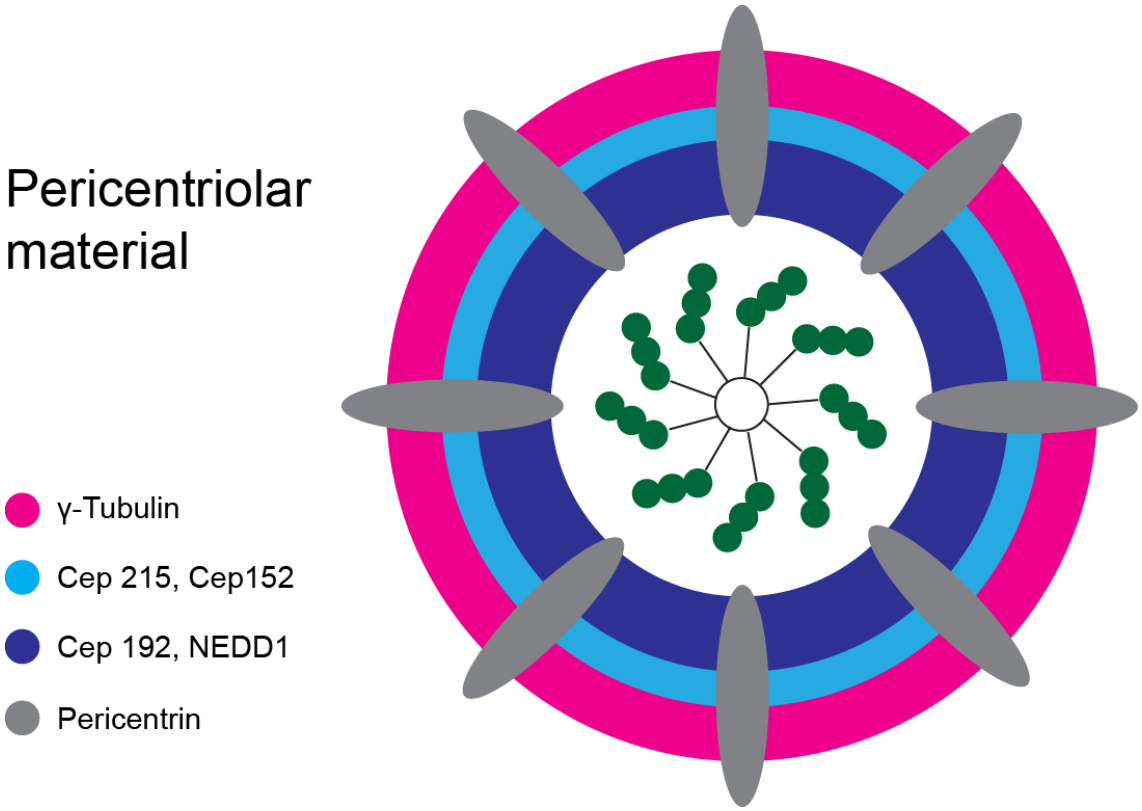

Figure 1.12 Localization of pericentriolar material (PCM) components.

Centriole (green) is surrounded by PCM components. Centrosomal proteins (Cep) recuitment requires pericentrin.

1.4.3 Nucleation of Microtubules

Microtubules are tubular protein filaments which are composed of α and β-tubulin heterodimers. In each microtubule, it is arranged in a head to tail style, with the minus end being nucleated and anchored by MTOCs and the plus being assembled at the opposite end (Figure 1.13). The plus end is thought to be the fast-growing end of the polar microtubule filament, with exposed β-tubulin at its terminus. In contrast, the minus end is the slow-growing end of the polar microtubule filament, with exposed α-tubulin at its terminus. Microtubules are involved in multiple processes of cell migration, cell shape determination and chromosome segregation (Kirschner and Mitchison, 1986; Sanchez and Feldman, 2017). Microtubules are extremely dynamic to form any desired architecture in a short time because of the high degree of plasticity and variable microtubule nucleation. With this feature, microtubules are quickly switched between growth and shrinkage phases, which is termed as dynamic instability (Figure 1.13). Although the regulation of microtubules is deeply investigated, the mechanism of nucleation is still unclear. It has been found that γTuRC is essential, but not sufficient for microtubule nucleation (Farache et al., 2018; Kollman et al., 2011a; Whittaker and Dean, 2017).

To understand the mechanism of microtubule nucleation, purified tubulin dimers were initially cultured in vitro. Microtubules were nucleated spontaneously with GTP and magnesium ions and the efficiency was highly restricted by an energy barrier and tubulin concentration (Kuchnir Fygenson et al., 1995; Voter and Erickson, 1984). It is difficult to form microtubule spontaneously due to its dynamic feature and complicated structures, which is formed by multiple parallel protofilaments array (13 in most cells, 10–16 in vitro) (McIntosh et al., 2009; Ray et al., 1993). However, the extension of an existing microtubule is more efficient and requires less energy (Voter and Erickson, 1984).

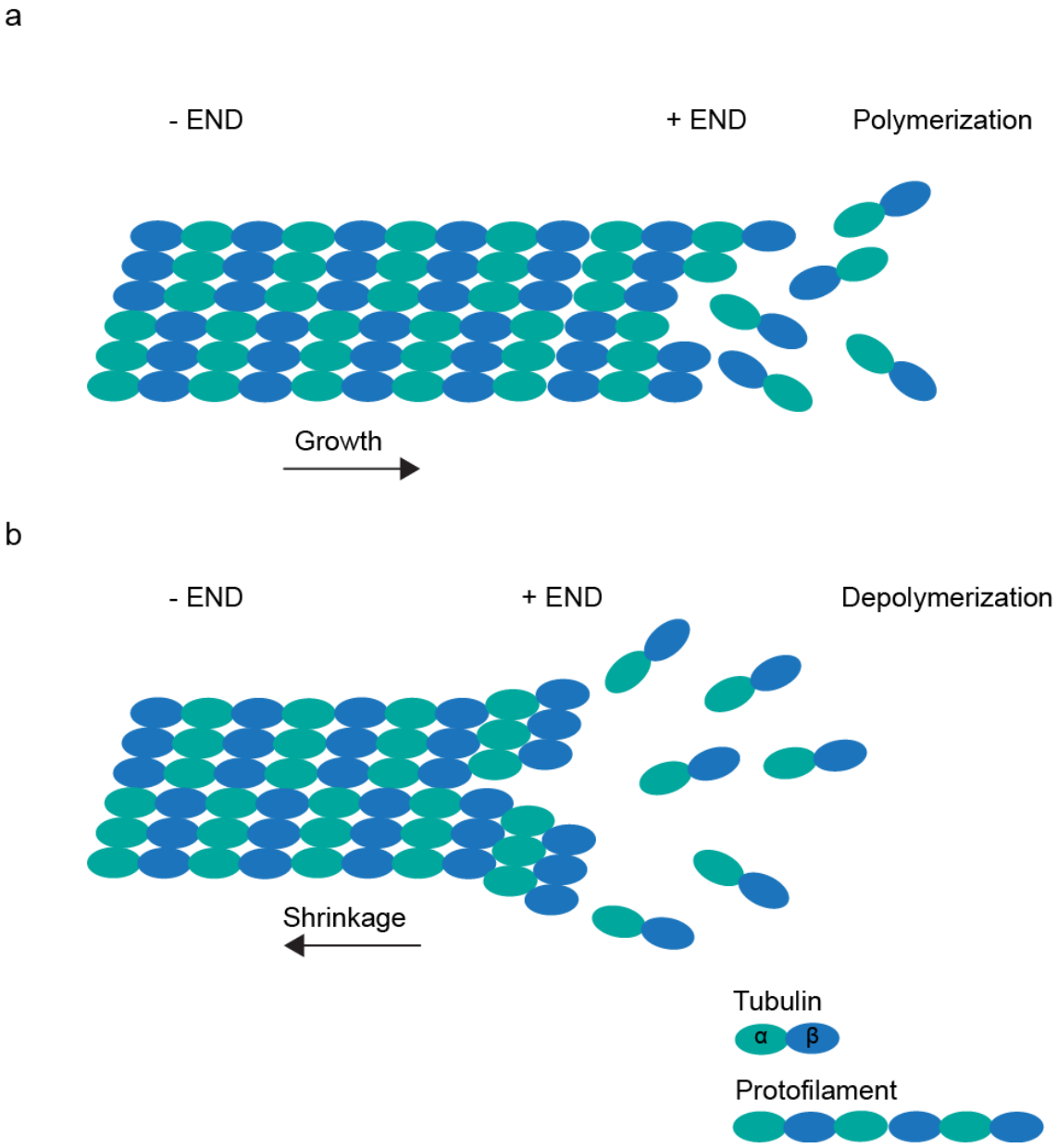

Figure 1.13 Microtubules growth and shrinkage.

(a) Tubulin dimers are recruited to the plus end of microtubules for growth. **(b)** In the dynamic process, Tubulin dimers are lost from the plus end of microtubules for shrinkage.

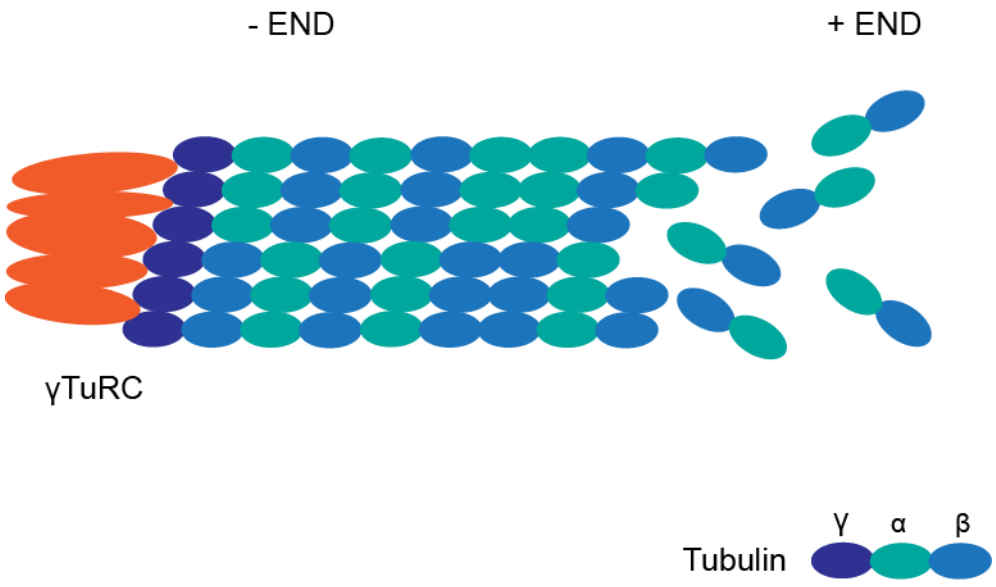

Figure 1.14 γ-TuRC nucleate microtubules as a template.

γ-TuRC subunit (orange) interact with γ-tubulin (purple) can nucleate microtubules. In the beginning, tubulin dimers are recruited to γ-tubulin to initiate the nucleation.

As the microtubule nucleation template, γTuRC is supposed to initiate the nucleation of microtubules in cells. To serve as a template, a stable conical cap composed by protein complex interacts with the microtubule minus end specifically (Figure 1.14) (Kollman et al., 2011b; Moritz et al., 2000; Stearns and Kirschner, 1994; Zheng et al., 1995). γTuRC is not only a microtubule nucleation template but it also can increase its efficiency of nucleation. Templated microtubule nucleation requires low tubulin concentration (> 6μM) which is much lower than the concentration needed for spontaneous nucleation (> 20μM) but higher than the concentration for existing microtubules extension (>1μM) (Voter and Erickson, 1984; Wieczorek et al., 2015).

Apart from γTuRC-mediated microtubule nucleation, newly generated microtubule ends were also observed as another template for microtubules nucleation in some specific cells, for example, mammalian neurons, plants, and nematodes (Baas and Ahmad, 1992; Srayko et al., 2006). The microtubule ends to serve as a platform for this distinct microtubules nucleation pathway, they are created by microtubule-severing enzymes which can cut pre-existing microtubules.

1.4.4 Acentriolar MTOC guided spindle assembly in mouse oocytes

In most animal species, oocytes complete two meiotic cell divisions (MI and MII) without the presence of classic centrosomes. Centrioles are eliminated during oogenesis in most species, including mice (Dumont and Desai, 2012; Szollosi et al., 1972), humans (Hertig, 2004), worms (Knott et al., 2012) and flies (Pimenta-Marques et al., 2016). Centrioles are observed in mouse oocytes until the pachytene stage of oogenesis (Szollosi et al., 1972) after which the regular centrioles are replaced by several small MTOCs (Mogessie et al., 2018; Schuh and Ellenberg, 2007). Centrioles first reappear at the preimplantation stage in the mouse embryo (Courtois et al., 2012). The advantage of centrioles elimination is still unclear. One possibility is to change the function of astral microtubules from centrosomes, which might prevent the cortical location of the spindle which is required for asymmetrical cell division (See Chapter 5). Another possibility is avoiding the multi-centrosomes in zygote after oocyte fertilized by sperm which contains a centrosome (Manandhar et al., 2004).

As in some other mammalian oocytes, the centrioles are eliminated from mouse oocytes during oogenesis and replaced by several smaller aMTOCs. The aMTOCs nucleate microtubules and organize the meiotic spindle as centrosomes do in somatic cells. However, the structure and composition of aMTOCs are still not clear (Bennabi et al., 2016). According to the available research, the aMTOCs are found with no centrioles, but contain several centrosome-associated proteins, such as γ-tubulin, Pericentrin, Nedd1, Cep192 and Cep215 (Baumann et al., 2017; Carabatsos et al., 2000; Clift and Schuh, 2015; Gueth-Hallonet et al., 1993; Ma et al., 2010).

The studies of meiotic spindle formation have been performed in mouse oocytes to understand how and where microtubules are nucleated and assembled without classical centrosomes (Clift and Schuh, 2015; Kitajima, 2018; Schuh and Ellenberg, 2007). An interesting experiment performed in Xenopus egg extracts indicates that microtubules are initially nucleated around the chromosomes (Blank et al., 2003). However, in mouse oocytes, the spindle formation appears to be initiated from aMTOCs instead of chromosomes (Szollosi et al., 1972). Different from conventional points of view, a very recent study presents the chromosome directed microtubule nucleation in early-stage

mouse embryo (Reichmann et al., 2018). Therefore, the mechanism of microtubule nucleation needs further research.

Without centrosomes, the bipolar spindle is assembled by antiparallel microtubules and associated microtubule motor proteins. In early prometaphase, an unorganized microtubule ball is initiated that later transforms into a bipolar spindle, supported by antiparallel microtubules growing in opposite directions (Blank et al., 2003). In mitosis, the spindle is formed quickly by two identical centrosomes whose positions define the long spindle axis, which typically forms within tens of minutes (Tanenbaum and Medema, 2010). In oocytes, spindle bipolarization takes much longer. Spindle formation takes about 12 minutes in C. elegans, 4h in mouse, and 6.5h in human atretic oocytes, taking approximately half of the time from NEBD to anaphase in these species (Dumont et al., 2007a; Holubcová et al., 2015; Schuh and Ellenberg, 2007). Therefore, the process of spindle assembly in oocytes is much more complicated.

In mouse oocytes, several large aMTOCs are maintained at the cortex during GV stage. Prior to NEBD, aMTOCs are recruited from the cortex to the periphery of nucleus (Wu et al., 2018). The aMTOCs are fragmented in three steps. First of all, the aMTOCs are decondensed by polo-like kinase (PLK1) which is involved in centrosome separation in mitosis. Second, aMTOCs are stretched along the nuclear envelope by dynein which is a nuclear envelope-associated motor protein. Third, aMTOCs are further fragmented into about 26 individual pieces by Polo-Like Kinase 1 (PLK1) and kinesin-like protein (KIF11) which is a plus-end-directed kinesin (Clift and Schuh, 2015). These aMTOCs around the chromosome assemble microtubules are then clustered to form the two blunt poles of the meiotic barrel-like spindle (Figure 1.15).

Therefore, without centrioles, their associated PCM (aMTOCs) is mainly responsible for the meiotic spindle formation in mouse oocytes. An important microtubule binding site on aMTOCs is nuclear mitotic apparatus protein (NuMA), which anchors microtubules minus end at spindle poles. In meiotic spindle formation, NuMA is involved in early spindle shaping and aMTOCs shaping at spindle poles. Conditional NuMA knockout female mice are sterile because of a high incidence of aneuploid eggs are produced during meiosis (Schatten and Sun, 2011; Silk et al., 2012).

Another important component of aMTOCs is γ-tubulin that is fundamental for microtubule nucleation in mouse oocytes. According to previous research, γ-tubulin is responsible for spindle formation and asymmetrical cytokinesis in mouse oocytes (Barrett and Albertini, 2007; Schatten and Sun, 2011; Sun et al., 2004). However, the mechanism of γ-tubulin action in mouse oocytes is still unclear

Pericentrin, an essential centrosome-associated scaffolding protein in mammalian somatic cells, is also an important component of aMTOCs in mouse oocytes. It binds to γ-tubulin and other components of PCM (Delaval and Doxsey, 2010). A study shows that pericentrin is important in mouse oocytes maturation. With pericentrin conditional knockdown, the fertility of female mice is significantly decreased. Meanwhile, the aMTOCs associated proteins, such as γ-tubulin and γ-tubulin ring complex (γTuRC) adaptor protein Nedd1, are distributed in the cytoplasm. In addition, the depletion of pericentrin increase the microtubule attachment errors and spindle assembly disruption. Taken together, all these problems in oocyte maturation could increase the aneuploidy rate of mouse eggs (Delaval and Doxsey, 2010).

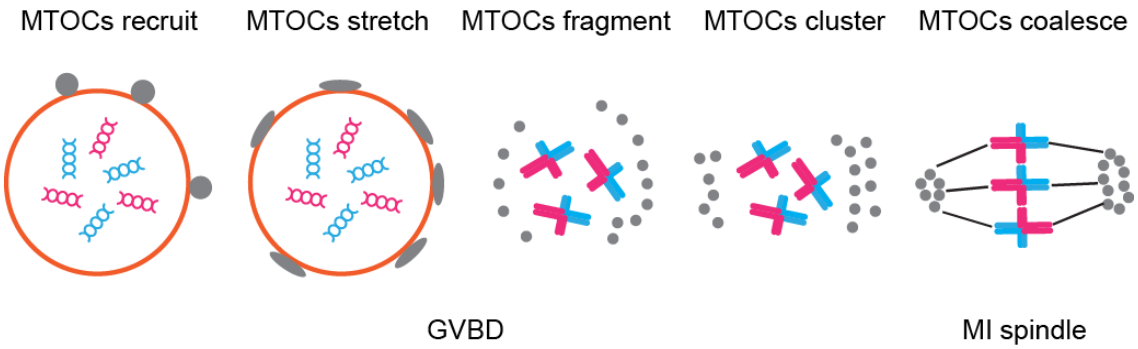

Figure 1.15 MTOCs transformation and migration.

MTOCs (grey) are recruited at nucleus envelope and well stretched before NEBD. After NEBD, MTOCs are fragmented to small pieces and migrated to spindle poles. Then the MTOCs are clustered to form spindle poles and nucleate microtubules to assemble spindle.

Centrosomal proteins are also involved in the PCM structure in mouse oocytes. For instance, Cep192 localized to aMTOCs at all stages of oocyte maturation, its depletion leads to aMTOC ablation, delayed spindle formation and non-aligned chromosomes. In terms of Cep152, it localizes on MTOCs until NEBD and then is involved in aMTOC fragmentation (Lee et al., 2018). In contrast to aMTOCs, 32 centrosomal proteins are found and investigated in centrosomes (Kumar et al., 2013). To understand the mechanism of aMTOCs formation and functions, the existence and function of centrosomal proteins on aMTOCs need to be investigated in greater depth.

Co-localized with γ-tubulin and pericentrin, NEDD1 is observed at aMTOCs in mouse oocytes. NEDD1 is a linker between pericentrin and γ-tubulin. Following Nedd1 RNA knockdown, most oocytes (65–70%) are arrested at MI. The MI arrest might be induced by abnormal spindle structure, low microtubule density and nonaligned bivalents. The activated SAC was detected in the arrested oocytes which indicates that the kinetochore-microtubule attachments were unstable. The depletion of Nedd1 affected the localization of γ-tubulin and increased chromosome non-disjunction errors. All these meiotic defects increased the aneuploidy rate of the oocytes that did progress to MII significantly (Ma et al., 2010).

1.4.5 RanGTP gradient Pathway in spindle assembly

Apart from MTOCs and PCM associated components, meiotic spindle formation is also chromosome dependent in mouse oocytes. The chromosome-generated Ras-related nuclear GTP (RanGTP) gradient is involved in spindle size restriction and spindle localization. The RanGTP gradient is initially visualized and observed in mouse oocytes by fluorescence resonance energy transfer (FRET)-based biosensor which is used to detect and quantify the interaction between proteins. With the same technique, chromatin-proximal increase in RanGTP gradient was found exactly around the chromatin during meiosis (Dumont et al., 2007a).

In terms of RanGTP formation, Ran guanosine exchange factor Regulator (Chromosome Condensation 1, RCC1) promotes the transformation from RanGDP to RanGTP at Ran protein. Chromosome binding of RCC1, means that chromosomes serve sites of RanGTP generation (Dumont et al., 2007a). Diffusion from the chromosomes creates a decreasing RanGTP gradient from the nucleus to the cell cortex (Figure 1.16) (Bischoff

and Ponstingl, 1991). Microtubules nucleation and stabilization are supported by RanGTP which activates critical spindle assembly factors (SAFs), such as TPX2 and NuMA, by releasing them from inhibitory Importin-α/β (Caudron et al., 2005; Gruss et al., 2001; Salmon et al., 2004; Wiese et al., 2001). In mitosis, 22 spindle assembly factors were regulated by RanGTP, however, the role of RanGTP in SAFs regulation is still unclear in meiosis. In the cytoplasm away from chromosomes, RanGTP is converted back to RanGDP by RanGTPase at the edge of RanGTP gradient. In such a dynamic system, the size of spindle is restricted strictly (Severance and Latham, 2018).

According to the experiments on mouse oocytes, the role of RanGTP gradient on MI and MII spindle formation is different. The MI spindle is elongated and late formed but not disrupted by RanGTP gradient depletion, which induces a larger polar body extrusion. The spindle is surrounded by RanGTP gradient along with the spindle migration, which indicates that RanGTP might be involved in this process. In contrast to MI spindle, RanGTP gradient is indispensable in MII spindle formation but does not affect its localization (Dumont et al., 2007a; Holubcová et al., 2015).

Compared to mouse oocytes, in human oocytes, inhibition of RanGTP gradient prevents microtubule nucleation and MI spindle formation (Holubcová et al., 2015). The function of the RanGTP gradient on MII spindle is still unknown. It is interesting to understand the function of RanGTP on human MII spindles because the roles of RanGTP on MI and MII spindles in mouse oocytes are different.

1.4.6 The CPC pathway in spindle assembly

As observed in former research, in mouse oocytes, the RanGTP gradient is helpful but not indispensable in MI spindle formation. The aMTOCs spindle assembly cannot be prevented by RanGTP inhibition (Bennabi et al., 2016; Dumont et al., 2007a). The CPC pathway was initially found in frog eggs, where it was shown to be required for aMTOCs spindle assembly (Ruchaud et al., 2007).

Chromosomal Passenger Complex is composed of Aurora kinase, inner centromere protein (Incenp) and the chromatin-targeting subunits Survivin and Borealin (Ruchaud et al., 2007). Basically, there are two downstream targets involved in the CPC pathway in Xenopus egg extracts. In the first pathway, AURKB phosphorylates and inactivates kinesin-13 that decreases the activity of mitotic centromere-associated kinesin (MCAK)

(Sampath et al., 2004). The downregulation of MCAK activity inhibits its microtubule depolymerase activity (Rivera et al., 2012). In the second pathway, Oncoprotein 18 (OP18) is phosphorylated by AURKB and this modification reduces its ability to prevent tubulin generation (Budde et al., 2001; Woo et al., 2007). Hence, a proper environment for microtubule polymerization is created (Niethammer et al., 2004). The CPC pathway in Xenopus egg extracts is relatively well studied, but far less is known in mammalian oocytes (Sampath et al., 2004; Tseng et al., 2010; Woo et al., 2007).

The latest results in mouse oocytes reveal that AURKB localizes to spindle microtubules and AURKC localizes to chromosome arms, centromeres and spindle poles until the onset of anaphase (Nguyen et al., 2018). Convincing evidence was found in mouse oocytes that AURKB/C inhibition affects the meiotic spindle formation (Lee et al., 2010; Ma et al., 2009; Na et al., 2010; Swain et al., 2008). Therefore, the CPC may have a role in microtubule nucleation and spindle formation in mouse oocytes, however, further investigation is required.

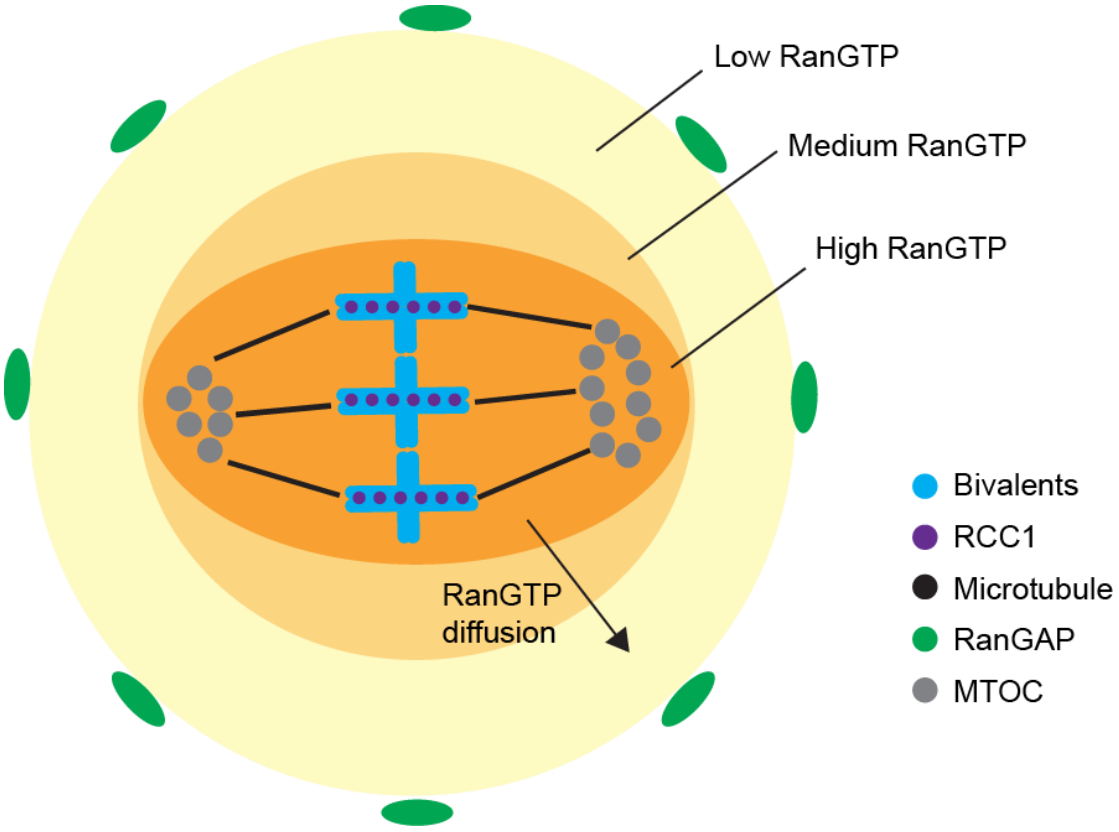

Figure 1.16 RanGTP gradient around MI spindle.

At the chromosomes, RCC1 converts RanGDP to RanGTP and diffusion of RanGTP forms the RanGTP gradient. In the cytoplasm, RanGAP converts RanGTP back to RanGDP, setting the boundary for the RanGTP gradient, and defining the region for spindle formation in the oocyte.

1.5 Conclusion

Although meiotic drive has been observed and investigated previously, the process of homologous chromosome selection remains elusive. The centromere evolution provides an opportunity for positive selection, the centromeres that are better at competing for retention in the oocyte can be transmitted more frequently to the offspring. Meanwhile, the asymmetrical MI spindles have the capacity to select specific centromeres, which provides the selection circumstance for meiotic drive.

1.6 Aims of the Thesis

The thesis describe two aspects of meiotic drive that have been investigated, centromere drive and spindle asymmetry. To this end I use time-lapse imaging to reveal how the asymmetrical bivalent is oriented and segregated preferentially during meiosis I. In addition, the assumption that there must be an asymmetrical spindle to provide directional context for the chromosomes is also addressed.

Chapter 2: Materials and Methods

2.1 Mouse Handling and Dissection

2.1.1 Ethics

All mice were used in accordance with local and UK government regulations on the use of animals in research. This work was approved by the University of Southampton Animal Welfare and Ethical Review Board. Personal licence number is ID7C47353, activated on 25 April 2016.

2.1.2 Mice

3-4 weeks old pure strain female mice (C57Bl/6) and F1 hybrid female mice (♀C57Bl/6 × ♂SJL) were used to perform experiments in this thesis (Charles River and Biomedical Research Facility Southampton University Hospital, UK).

2.1.3 Hormonal Priming

To harvest more fully grown germinal vesical (GV) stage oocytes and reduce the consumption of mice in experiments, 10IU Pregnant Mare Serum Gonadotrophin (PMSG-Intervet®, Centaur, UK) was injected into mice at 48 hours prior to oocytes collection. The injection site is in the animal's lower right quadrant of the abdomen to avoid damage to the organs and the PMSG (10IU, 0.2mL) was injected into the peritoneal cavity (Intraperitoneal injection) gently. The injected mice would be checked for general welfare 24 hours after injection.

2.1.4 Euthanasia, Dissection and Ovary Collection

The cervical dislocation euthanasia was performed to cull mice when they are needed for experiments. A secondary method, severing of the arteries of the neck, was used to ensure the permanent cessation of circulation in accordance with local guidelines. After culling, the abdominal cavity was exposed by scissors, and the ovaries were collected. The fresh ovaries were put into M2 media with 1μM milrinone (Sigma, UK) immediately for oocyte collection.

2.2 Oocyte Handling and Collection

2.2.1 Manufacture of Handling Pipettes

To collect oocytes, glass pipettes were heated in the flame of a small alcohol burner and pulled by hand. The glass pipettes were then broken around 3cm from the pipette shoulder, and only the pipettes with appropriate internal diameter were used to collect oocytes.

2.2.2 GV Oocyte Handling and Collection

GV oocytes were collected from ovaries on a stereomicroscope (SZ40, Olympus, Japan) with a heated stage at 37°C (MATS-U4020WF, Tokai Hit, Japan) in a dark room. Ovaries were punctured thoroughly by hypodermic needles (0.3mm×13mm) to release oocytes. The handling pipettes with a diameter 85-95μm were selected to strip cumulus cells from cumulus-oocyte complexes (COCs) and collect oocytes. The fresh oocytes were transferred into a fresh media droplet immediately after collection.

2.3 Oocyte Culture

In all experiments, the denuded oocytes were matured (In vitro maturation, IVM) in M2 media for 16 hours after milrinone wash out. The examination of maturation was confirmed by polar body extrusion observed under stereomicroscope at 60× magnification.

M2 media (Appendix B) was made fresh from stocks in the lab every two weeks and tested by oocyte maturation before experiment use, maturation rates of >80% were achieved. To prevent evaporation, M2 media was covered by mineral oil and pre-warmed to 37°C when it was used in oocytes handling and maturation. To keep the health of oocytes, all the process was performed on heat block in a dark room.

2.4 Agent Preparation and Treatment

2.4.1 Milrinone

Milrinone (Sigma, UK) was dissolved and diluted in 50% dimethylsulphoxide (DMSO) and 50% ethanol to 10mM for concentrated stock solution. Aliquots of 10 µL were stored at 4°C. The final working concentration was diluted to 1µM in M2 media. GV oocytes can be arrested in M2 with milrinone for several hours to allow time for microinjection and oocyte handling, and meiosis I resumes following milrinone wash out (Gilchrist et al., 2001).

2.4.2 Nocodazole

Powdered nocodazole (Sigma, UK) was dissolved and diluted in dimethylsulphoxide (DMSO) to 400µM for a concentrated stock solution (stored at -20℃). The final working concentration was diluted to 400nM in M2 media. Oocytes were treated with nocodazole for an hour at 4 hours after NEBD for microtubule depolymerization experiments.

2.4.3 Cytochalasin

Cytochalasin B was used to depolymerise actin filaments. Powdered cytochalasin B (Sigma, UK) was dissolved and diluted in DMSO to 1mM for a concentrated stock solution stored at -20°C. The final working concentration was diluted to 1µM in M2 media. Oocytes were treated with cytochalasin B for 1 hour at 6 hours after NEBD to depolymerize actin.

2.4.4 Monastrol

Monastrol is a selective inhibitor of mitotic kinesin Eg5. Powdered monastrol (Sigma, UK) was dissolved and diluted in DMSO to 1mM for a concentrated stock solution (stored at -20℃). The final working concentration was diluted to 1µM in M2 media. Oocytes were treated with Monastrol for an hour at 4 hours after NEBD to inhibit Eg5 and break the bipolar meiotic spindle structure.

2.4.5 ZM447439

ZM447439 is a selective and ATP-competitive Aurora kinase inhibitor. All three isoforms of Aurora kinase family (AURKA/B/C) are potentially inhibited by ZM447439. Both Aurora A and B can be inhibited by ZM447439, because they have similar half maximal inhibitory concentration (IC50, Aurora A: 110nM vs Aurora B: 130nM) (Ditchfield et al., 2003). Powdered ZM447439 (Tocris Bioscience, USA) was dissolved and diluted in DMSO to 10mM for a concentrated stock solution (stored at -20°C). The final working concentration was diluted to 10µM in M2 media. Oocytes were treated with ZM447439 at 2 hours after NEBD.

2.4.6 Timeline of Agent Treatment

Oocytes were treated with previously mentioned agents at different time points during in vitro maturation according to the purposes of investigations described in Chapter 4 and 5.

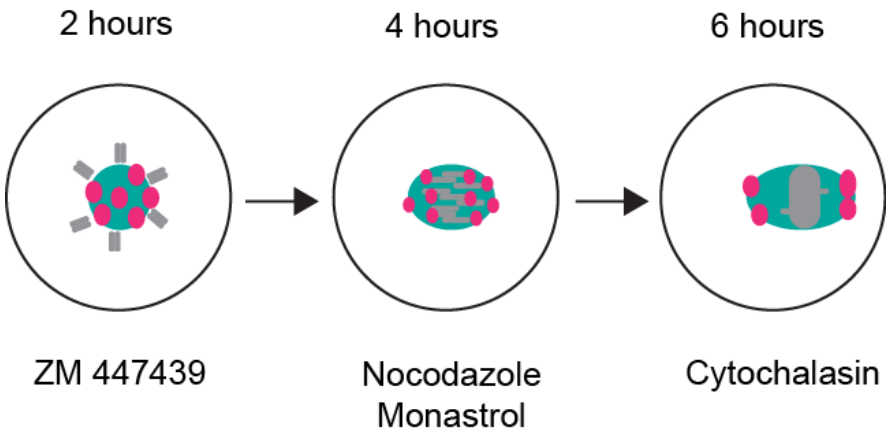

Figure 2.1 Schematic to show the time point of agent treatment according to the progress of meiosis I.

Spindle relocation is observed between 6 to 7 hours after NEBD, after which the spindle can be separated as cortical or central halves. Cyan: spindle; Grey: chromosomes; Magenta: MTOCs. Time from NEBD.

2.5 Oocyte Fixation

Oocytes were washed briefly and fixed for 30 minutes in fixing solution (PBS containing 2% formaldehyde and 0.05% Triton-X), and were then treated in permeabilization solution (PBS containing 1% PVP and 0.05% Triton-X) for 15 minutes. Fixing and permeabilising was performed at room temperature and oocytes were extensively washed with PBS-PVP solution between stages. The fixed oocytes were washed 3 times in PBS-PVP solution and finally preserved in PBS-PVP solution at 4°C for two weeks.

In this thesis, MI oocytes were fixed at 7 hours after NEBD for MTOCs comparison experiments, because by that time the spindle has been relocated already so that the cortical and central MTOCs can be distinguished (Figure 2.1).

2.6 Immunofluorescence

2.6.1 Immunofluorescence Procedure

Immunofluorescence (IF) is a widely used laboratory technique in cell biology. The specific antibodies with chemically conjugated fluorophore can detect the proteins of interest. To label the proteins specifically, two kinds of antibodies are required. The target protein is recognized by a primary antibody which is subsequently bound by the secondary antibody with a conjugated fluorophore (Figure 2.1). Then the fluorescence can be visualized by fluorescence microscopy.

For immunofluorescence, the fixed oocytes (see section 2.5) were transferred between wells on a 96-well plate. To prevent non-specific binding and decrease the florescence background, oocytes were incubated in blocking solution (Table 2.1) at 4°C overnight. After washed 3 times in washing solution, the oocytes were incubated with the primary antibody that was diluted in blocking solution for 1 hour at 37°C. After 3 times wash in washing solution (Table 2.2), oocytes were incubated with secondary antibody in a dark environment for an hour at 37°C. Following with 3 times wash in the washing solution, oocytes were counterstained with Hoechst (20µg/mL; Sigma, UK) which are diluted in PBS for 10 minutes. Brief wash was performed prior to imaging.

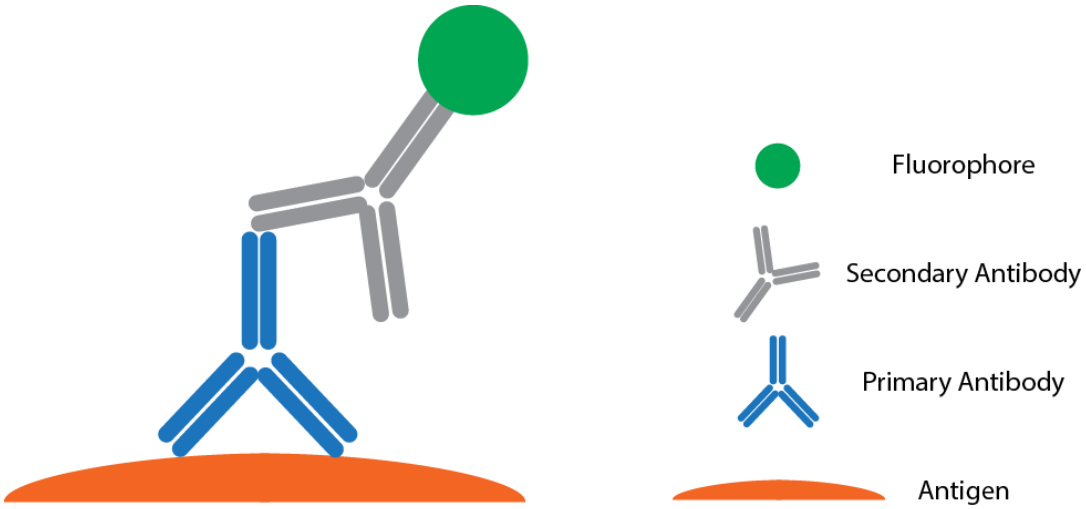

Figure 2.2 The protein of interest is labelled by IF.

The antigen (orange) is recognised by the primary antibody (blue). Then the secondary antibody (grey) with a fluorophore (green) binds to the primary antibody to provide fluorescence.

Table 2.1 The composition for blocking solution

Component	Concentration
PBS	92.5%
Goat serum	7%
Tween-20	0.5%

Table 2.2 The composition for washing solution

Component	Concentration
PBS	99.995%
BSA	5g/L
Tween-20	0.005%

2.6.2 Antibodies

All the antibodies used in experiments were purchased commercially. To visualize MTOCs, an antibody was used to label pericentrin. The primary antibody used was mouse anti-pericentrin (1:500; BD Biosciences 611815, USA). The secondary antibody used was goat anti-mouse Alexa-488 (1:500; Life Technologies #a-21070, UK).

2.7 DNA Fluorescence in Situ Hybridization (FISH)

2.7.1 Zona Pellucida Removal

GV oocytes were matured to 6 hours after NEBD (bivalents are fully individualized, Figure 2.1) and collected for zona pellucida removal. MI oocytes were transferred into acid Tyrode's solution (Table 2.3) (Nicolson et al., 1975) with minimum M2 media. The zona pellucida was dissolved in 2 minutes, following which the oocyte was immediately transferred to fresh M2 media. Acid Tyrode's solution was washed out in fresh M2 media. Zona-free oocytes were collected for chromosome spreading.

Table 2.3 The composition of acid Tyrode's solution (pH: 7.4)

Component	Concentration
NaCl	137mM
KCl	2.7mM
$CaCl2 \cdot 2H_2O$	1.8mM
$MgCl_2 \cdot 6H_2O$	0.5mM
D-glucose	5.5mM
PVP (Polyvinylpyrrolidone)	0.09mM

2.7.2 Chromosome Spreading

A drop of chromosome spread solution (Table 2.4, made with ultrapure water) (Hodges and Hunt, 2002) was placed on a clean 8-well printed slide at room temperature. Less than 5 zona-free oocytes were transferred into the chromosome spread solution drop each time. Oocytes were dissolved in the drop for 10 seconds. The slides were then dried at room temperature for staining.

Table 2.4 The composition of chromosome spread solution (pH 9.2)

Component	Concentration
Paraformaldehyde	1%
Triton X100	0.15%
DTT	3mM

2.7.3 FISH Procedure

FISH probe (10µL) was placed on the well containing dissolved oocytes and covered by coverslip (10×10mm^2, trimmed manually). To prevent evaporation, the coverslip was sealed by rubber cement. The experiment proceeds as follows.

The oocytes were put on the slide and denatured on a heat block at 75°C for two minutes. After 12 hours incubation at 37°C (keep humidified), slides were washed in 0.4 × Saline-Sodium Citrate (SSC) buffer at 72°C for two minutes. Slides were washed again in 2 × SSC (Table 2.5, made with ultrapure water) containing 0.05% Tween-20 at 25°C for 30 seconds, and then washed in ultrapure water to avoid crystal formation. In the end, oocytes were covered with 10µL Hoechst for 10 minutes to counterstain chromatin. After all these process, the slides were stored at -20°C or processed with confocal microscopy.

2.7.4 FISH Probes

The mouse chromosome 17 FISH probe (Zeiss Ltd, UK; cat no 0528-878) was used in asymmetrical chromosome identification.

Table 2.5 The composition of 2×Saline-Sodium Citrate (SSC) buffer

Component	Concentration
NaCl	0.3M
sodium citrate-dihydrate	30mM

2.8 cRNA manufacture

2.8.1 Plasmid

The plasmid of Maj.Sat.-mClover and Min.Sat.-mRuby were gifts from Maria-Elena Torres-Padilla (Addgene plasmid #47878 and #47880, respectively) (Miyanari et al., 2013). They are designed to label major or minor satellite DNA, which they bind specifically by the means of transcription activator-like effectors (TALEs) (Figure 2.2). The construct of Cep192-GFP was a gift from Melina Schuh (Clift and Schuh, 2015). The construct of α-Tubulin-GFP was a gift from Marie-Helene Verlhac (Dumont et al., 2007a). The construct of Spc24-mCherry was made by PCR from testis cDNA and restriction enzyme cloned into a pRN3 derivative plasmid with C-terminal mCherry. Dominant negative Aurora Kinase C was a gift from Karen Schindler (Balboula and Schindler, 2014).

Plasmids that were delivered on filter paper were extracted prior to transformation. The marked plasmid area was cut from filter paper using clean scissors and placed into a small tube (0.6mL) with a small hole at the bottom. The filter paper was covered by 100µL nuclease free water in the small tube. Later, a small tube was put into a larger tube (1.5mL) and the plasmid recovered in the larger tube by centrifugation at maximum speed for one minute.

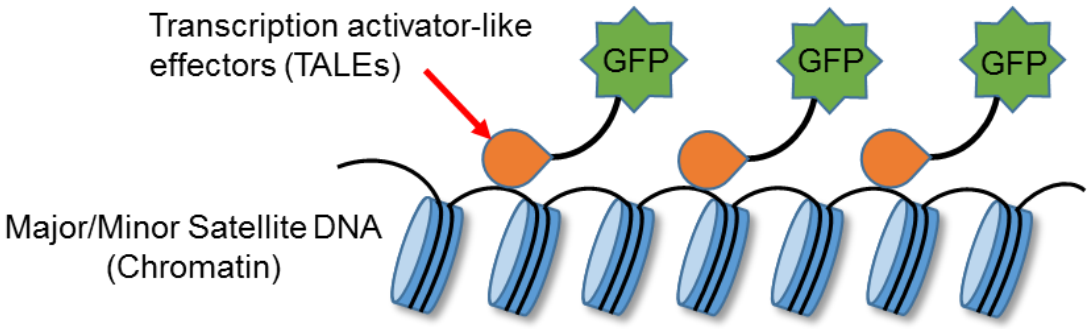

Figure 2.3 The major and minor satellite DNA is recognised by TALEs.

TALEs (orange circle) can be engineered to bind to any desired DNA sequence, so when it is combined with GFP, the DNA sequence can be recognised by fluorescence.

2.8.2 Transformation

To transfer plasmid of interest into Competent E. coli cells (NEB, UK), the following steps (from the manufacturer's protocol) were performed.

For transformation of bacteria, 50ng of plasmid DNA was added to the competent E. coli cells, which were thawed on ice for 10 minutes. The mixture was placed on ice for 30 minutes and then in water bath (heat shock, 42°C) for exactly 30 seconds. The mixture was then placed on ice for another 5 minutes before 950µl of room temperature SOC Outgrowth Medium addition. After vigorous shaking (250rpm) at 37°C for 60 minutes, the cells were placed onto a selection plate and incubated overnight at 37°C.

The selection plate contained either 0.1mg/mL ampicillin or 0.1mg/mL kanamycin, according to the resistance gene present in the plasmid. Following 15 hours incubation, a bacterial colony was selected and transferred to 3mL of LB media containing the same antibiotic and was cultured overnight (250rpm, 37°C, 15 hours).

2.8.3 Plasmid DNA Collection

To collect purified plasmid for cRNA transcription, PureYield™ Plasmid Miniprep System (Promega, UK) was used in the experiments. The collection consists of the following steps according to the manufacturer's protocol:

The bacterial culture (600µL) grown in LB medium was transferred into a 1.5mL centrifuge tube, with addition of 100µL of Cell Lysis Buffer. After mixture, Neutralization Solution (350µL, 4–8°C) was added and mix thoroughly by inverting the tube. The tube was then centrifuged at maximum speed for 3 minutes, after which the supernatant (about 900µL) was transferred to a PureYield™ minicolumn. The minicolumn was placed into a PureYield™ collection tube and centrifuged for 15 seconds at maximum speed to collect plasmid in the minicolumn. The Endotoxin Removal Wash solution (200µL) was then added to the minicolumn and centrifuged for 15 seconds at maximum speed to remove endotoxin from the sample. Finally, the Column Wash solution (400µL) was added to the minicolumn and centrifuged for 30 seconds at maximum speed to wash plasmid. To collect purified plasmid, nuclease-free water (30µL) was directly added to the minicolumn matrix. The minicolumn was then centrifuged for plasmid DNA collection.

2.8.4 Plasmid DNA Linearization

A restriction enzyme digestion was performed in a volume of 20µl with 0.5–1.5µg of substrate DNA and a two to tenfold excess of the enzyme (Table 2.6). The following components (Table 2.7) were assembled in a PCR tube and incubated at the enzyme's optimum temperature for 3 hours in a PCR machine. The efficiency of linearization was examined by gel analysis.

Table 2.6 The restriction enzymes

Enzyme	Temperature	Company
SfiI	50°C	Takara
NedI	37°C	Promega
NotI	37°C	Promega

Table 2.7 The system of plasmid DNA linearization

Component	Volume
Restriction Enzyme 10X Buffer	2µL
Acetylated BSA, 1µg/µL	2µL
DNA,1µg/µL	1µL
Restriction Enzyme	0.5µL
Nuclease-free Water	To 20µL

2.8.5 Phenol/Chloroform Extraction

The nuclease-free water was added to increase the reaction volume up to 200µL. Then, 200µL Phenol-chloroform-isoamyl alcohol mixture (Sigma, UK) was added to the tube inside a fume cupboard and vortexed for 15 seconds. The tube was centrifuged at maximum speed for 10 minutes. The aqueous phase was removed to a new tube containing an equal volume of chloroform. Vortex and spin for another two minutes and remove the aqueous phase to a new tube.

2.8.6 Precipitation of DNA Sample

The linearized DNA sample was purified by ethanol precipitation by following the steps:

Pellet Paint Co-Precipitant (1µL, Novagen) and 3M Na Acetate (0.1 × volume, Novagen) were added to the linearized DNA samples. Then with 2 x volume 100% ethanol addition, the mixture was vortexed briefly and incubated in a tube at room temperature for 2 minutes. The mixture was centrifuged at maximum speed for 5 minutes and checked for the painted pellet at the bottom of the tube. The supernatant was removed and the painted pellet was rinsed with 70% ethanol to purify the sample. Finally, the pellet was suspended in 20µL nuclease-free water and its concentration measured by comparison against a DNA standard run on a 1% agarose gel. The remaining DNA was stored at -20°C in freezer.

2.8.7 In Vitro Transcription

The cRNA was transcribed in vitro from purified linear double strand DNA templates. mMessage T3 and T7 RNA kits (Thermo Fisher Scientific, US) were used for the in vitro transcription. The following components (Table 2.8) was assembled in a centrifuge tube and incubated at the 37°C for 2 hours in a PCR machine.

To stop the reaction, 30µL Nuclease-free water and 30µL Lithium Chloride (LiCl) precipitation solution were added into the reaction. The system was mixed thoroughly and chilled at -20°C overnight. The following steps were taken in order to recover the cRNA.

The mixture was centrifuged at 4°C for 15 minutes at maximum speed to pellet the cRNA. To get purified cRNA, the supernatant was removed and the pellet was washed with 0.5mL 70% ethanol, then re-centrifuge to maximize the removal of unincorporated nucleotides. After ethanol removal, the cRNA was suspended in 10µL nuclease-free water. The cRNA concentration was determined by nanodrop and diluted down to 3000ng/µL. The cRNA was aliquoted and stored at -20°C for microinjection.

Table 2.8 The system of in vitro transcription

Component	Volume
Enzyme Mix	2µL
2X NTP/CAP	10µL
10X Reaction Buffer	2µL
linear template DNA	1µg
Nuclease-free water	To 20µL

2.9 Microinjection

2.9.1 Injection Pipette Manufacture

Microinjection pipettes were produced from borosilicate glass pipettes (0.84mm inner diameter and 1.5mm outer diameter). The glass pipettes were pulled by a Flaming-Brown micropipette puller (Model P97; Sutter Instrument Co, USA). To generate a fine tip for microinjection, the pipette puller was calibrated to produce appropriate pipette (about 7mm taper and 0.5µm tip) for mouse oocytes. The tip of microinjection pipette was broken by a gentle touch on the surface of the tissue (KimTech, Kimberly Clark Professional, USA). Following that, the broken pipettes were examined and selected with a 40x compound microscope. Only the microinjection pipettes with proper size were stored for microinjection experiments.

2.9.2 Loading Syringe Preparation

The cRNA was loaded into microinjection pipettes by loading syringes, which are produced by 1mL plastic syringes (BD Plastipak, UK). The syringe was melted by ethanol burner flame and pulled by hand to generate a long thin tip for cRNA loading. The tip of loading syringes was cut to 4-7cm which is appropriate for cRNA loading.

2.9.3 Microinjection

The microinjection was performed on TE300 inverted microscope (Nikon, Japan). A metal chamber with sealed glass bottom (22mm cover slip) was created for microinjecting. The M2 media with milrinone was placed in the chamber and covered by mineral oil. The media was warmed to 37°C by a heater (Intracel, UK).

The holding pipette was placed into the chamber until its tip touched the surface of the glass bottom. With the holding pipette set up, injection pipette can be prepared. The diluted cRNA (0.4µL; 500-600ng/µL) was loaded into the injection pipette and the pipette was stood for about 5-10 minutes to remove air bubbles in the tip. If the air bubbles were not removed completely, gentle flicking or centrifuge could be performed to get rid of bubbles. After air bubbles removal, the injection pipette was set into the

chamber by mounting on three-axis micromanipulators (Narashige, Japan). Some remaining air bubbles in the tip were finally squeezed out by short time consistent high pressure (80 psi). The injection pressure was decreased to 30 psi and the injection time was adjust to 100ms. All these settings were performed on Pneumatic PicoPump (World Precision Instruments, UK) to create proper injecting volume for mouse oocytes. The injection pressure and time were adjusted in each experiment to get consistent injection volumes in different experiments.

The denuded oocytes were transferred to the chamber for microinjection. To observe the injection clearly, a 20× objective lens was used in microinjection. For microinjection, 20-30 oocytes were placed into the chamber and the each oocyte was held by holding pipette for every microinjection. The tip of the injection pipette was placed on the top of oocytes and lowered slowly. The injection site should be away from the nucleus area. With the injection pipette getting lower, the zona pellucida was broken through. With the oocyte penetrated by the tip, the cRNA was released immediately by gentle pressure. The microinjection pipette was removed out of the oocytes as soon as possible after injection so that any harm from microinjection was minimized.

The injected oocytes were transferred to M2 media containing milrinone and arrested for two hours on a heat block at 37°C in a dark environment to allow time for protein expression following cRNA injection.

2.10 Confocal Microscopy

2.10.1 General Principles

In this thesis, all the imaging experiments were performed on a confocal microscope (Leica SP8). The technology of protein fluorescence in confocal microscopy is the same as traditional florescence microscope. The laser light with a specific wavelength can be absorbed by the sample, which then emits another specific light with a longer wavelength.

The difference in wavelength between excitation light and emission light provides an opportunity for fluorescence detection. To capture the light emitted from a florescent component specifically, a dichroic mirror is used to transmit only longer wavelength light (emission light) and reflect lower wavelength light (excitation light). Therefore, only the light emitted by the fluorescent component is detected by the detector.

Compared to the use of dichroic mirrors in a traditional confocal microscope, acousto-optical beam splitting (AOBS) technique is used to separate excitation and emission light in a Leica SP8 confocal. To diffract the light by different wavelength, the refractive index of a TeO_2 crystal is changed by a mechanical radio-frequency wave which can affect its periodic density (Figure 2.3). Therefore, the excitation and emission light with different wavelength are separated.

2.10.2 Detector

The light from the specimen is focused onto a pinhole which prevents unfocused light passing through to photomultiplier (PMT) which is a classic light detector. The detector on Leica SP8 confocal is more sensitive than a classical PMT. Combined PMT with the highly sensitive avalanche photodiodes (APDs), the hybrid detector (HyD) is able to provide a high definition image. This results in super-sensitivity and large dynamic range combined with rapid detection speed and low dark noise, making them an ideal detector for all samples.

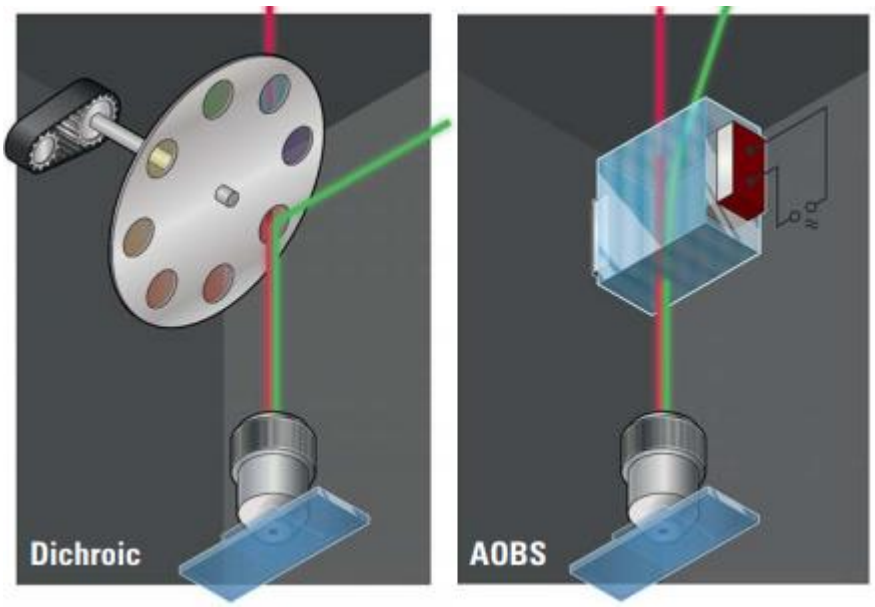

Figure 2.3 Comparison between a dichroic mirror and an acousto-optical beam splitter.

All conceivable dichroic and multichroic mirrors are replaced by AOBS, which is a single programmable optical element for visible range laser scanning microscopy (Image from Leica AOBS-Brochure).

2.11 Imaging

2.11.1 Fluorescent Proteins, Spectra and Settings

Fluorescent proteins and dyes are widely used to visualize specific proteins or structures in a biological sample. Multiple fluorescence can be visualized together when they have different excitation and emission wavelengths. The following table presents all the fluorescent dyes and proteins used in this thesis (Table 2.9).

Table 2.9 The excitation wavelengths for use with different fluorescent dyes and proteins.

Fluorescent Dye/Protein	Excitation maximum (nm)	Emission maximum (nm)	Laser wavelength for Fluorophore
Hoechst	352	461	405
Alexa fluor-488	495	519	488
mCherry	587	610	594
GFP	484	507	488
mClover	506	518	488
mRuby	558	605	561

2.11.2 Chromosome Tracking Time-lapse Imaging

All the time-lapse imaging was performed with a Leica SP8 fitted with HyDs. To record the process of oocyte maturation, the temperature (37°C) was maintained by an environmental chamber. The oocytes were imaged individually by a ×40/1.3NA plan apochromat oil immersion lens. Meanwhile, an overview image (~ 15 oocytes/per image) was taken to visualize the position of spindles. Images were taken at 10 minutes intervals for 15 hours to cover the whole process of meiosis I.

To track chromosomes and get high-quality images, in-lab software written in Python language was used to image multiple stage regions. The weighted intensity centre of H2B-mCherry signal was used to ensure bivalents remained in the centre of a ~32 × 32 × 32μm imaging volume. In each experiment, no more than 30 oocytes were imaged.

2.12 Image Analysis

All the images were taken by Leica SP8 and analysed by ImageJ software (NIH, USA) with the plugins and homemade macros described below.

2.12.1 Intensity of Foci Analysis

The integrated intensity of centromeric DNA and kinetochore proteins were measured by Foci_Picker3D plugin (Version 1.0, CAS, China). To get accurate results, only the intensity in a small volume (1.6, 1.6, 2.7μm) was measured.

To distinguish the chromosome with asymmetrical major satellite DNA (Chromosome 17), the intensity of each major satellite DNA was measured with the same threshold and compared with each other. The 3D position of each major satellite DNA was logged by an in-house macro.

To compare the integrated intensity of minor satellite DNA and Spc24, the intensity of paired major satellite DNA was treated as a marker. Each focus was measured individually by an ImageJ macro (Appendix C) and the same threshold was applied to paired foci.

2.12.2 Chromosome 17 Tracking

Chromosome 17 from F_1 hybrid mice (section 2.1) was tracked in time-lapse imaging to show its reorientation. All the time-lapse images were recorded for 15 hours from NEBD. Z-stacks of the entire bivalent region were imaged with a z-step of 1.2µm. Chromosome 17 was distinguished from the other bivalents by the extreme asymmetry between its two major satellite DNA signals. Chromosome 17 could be followed through the time-lapse because its movement between frames (interval was set to 10 minutes) was not too great (<0.15 microns).

2.12.3 Chromosome Migration Displacement

Oocytes expressing H2B-mCherry were matured from NEBD. In maturation, the chromosome migration was imaged by time-lapse imaging with z-stacks. Oocytes were imaged for 15 hours from NEBD and time interval is 10 minutes. The weighted intensity centre of H2B-mCherry signal was treated as the centre of chromosomes. The displacement of chromosomes was analysed in 3D from NEBD by a homemade ImageJ macro (Appendix C). The position of chromosomes was measured and recorded by the macro in each frame. All the displacements are relative to the position of chromosomes at NEBD.

2.12.4 C-Kt Separation Comparison

Oocytes expressing Spc24-mCherry and Maj.Sat.-mClover were matured in M2 media to 4 or 7 hours relative to NEBD, because the spindle is relocated to cortex at 5-6 hours after NEBD (Figure 2.1). After counter-staining with Hoechst (20µg/mL), confocal image stacks were taken with a z- separation of 300nm and X and Y pixel size of 36nm. To get more accurate results, centromere–kinetochore separations were only measured in the oocytes whose long axis of the spindle were parallel with the x–y plane. The position of major satellite DNA and Spc24 were determined by the weighted intensity centre of the foci. Positions were measured by an in-house macro (Appendix C) utilising the Foci_Picker3D Plugin (Version 1.0, CAS, China). The distance (separation) between major satellite DNA and Spc24 weighted intensity centres were calculated in Excel (Microsoft, USA) using 3D Pythagoras.

2.12.5 Cortical and Central Half Spindle Comparison

Oocytes expressing α-Tubulin-GFP and H2B-mCherry were matured to 4 hours and 7 hours after NEBD. To quantify the intensity of α-Tubulin-GFP, spindle images were captured with a 40× objective (xy pixel size: 0.1μm and a z-resolution: 1μm). Spindles were only measured in the oocytes whose long axis of the spindle were parallel with the x–y plane.

Image J software was used to measure the α-Tubulin-GFP intensity on the spindle, using the 'plot profile' plugin to capture the α-tubulin and H2B intensity along the long axis of the spindle. The background intensity was defined by the area without tubulin. The edge of the spindle was determined by a threshold which is set as background intensity.

Data were analysed in Microsoft Excel, with background values subtraction, the exact tubulin intensity values were calculated. The centre of the bivalents was also calculated from the H2B-mCherry signal and used to define the mid-line of the spindle to divide it into two halves. The sum of the tubulin intensity values within 10μm (7h after NEBD) or 7μm (4h after NEBD) away from mid-point at each side of the spindle was calculated, normalised and compared.

2.12.6 MTOCs Tracking and Analysis

MTOC intensities were tracked and imaged by time-lapse imaging. Oocytes expressing Cep192-GFP and H2B-mCherry were imaged from NEBD. To compare the spindle poles, z-stacks of the entire spindle region (~40 × 40 × 37.5μm, z-resolution 1.5μm) were imaged with a 63× objective (NA 1.4). Cortical and central spindle poles were distinguished by an overview image. The integrated intensity of all MTOCs was measured by an in-house macro utilising the ImageJ plugin Foci_Picker3D. The background spindle poles were subtracted. The same threshold was selected for paired spindle poles of each meiotic spindle.

2.13 Statistical Analysis

All of the data was analysed with Prism software (GraphPad Software, Inc). The analysis of categorical data was performed with Fisher's Exact test. The normality of continuous data was assessed prior to analysis using the 'Column Statistics' tool. Only if all groups of data passed the normality test, Analysis of Variance (ANOVA) with Tukey's post hoc analysis or student t-test were used.

Chapter 3: Establishment of a Mouse Model to Examine Meiotic Drive

3.1 Introduction

To investigate meiotic drive in mammalian oocytes it was necessary to establish a model containing asymmetrically sized centromeres on a homologous chromosome pair. Laboratory mice are small mammals, easily bred and used for biological research. They are therefore the preferred animal to study this process in mammals. The F_1 hybrid mice, created by crossing two pure inbred mouse strains with different centromere sizes offer the opportunity to establish such a model. Indeed, Yoshida and Kodama (1983) showed that specific chromosomes in different mouse strains have different sized centromere bands (C-bands). As such they offer the potential to create paired homologue pairs with asymmetrical centromeres in F_1 hybrid mice (Table 3.1).

Table 3.1 Characteristics of C-bands in 3 mouse strains

Strain	Chromosome																			
	1	2	3	4	5	6	7	8	9	10	11	12	13	14	15	16	17	18	19	X
C57Bl/6	s	n	n	n	n	n	n	l	n	n	n	n	n	n	n	l	n	l	n	n
BALB/c	s	n	n	n	n	n	s	n	l	n	n	n	l	l	n	l	n	n	n	n
SJL	s	n	l	s	n	n	n	n	l	n	n	l	l	n	n	n	o	n	n	n

Size of C-bands: l = large; n = normal; s = small; o = little or invisible. Data taken from Yoshida and Kodama (1983).

According to the size of centromere on each chromosome, three mouse strains (C57Bl/6, BALB/c, SJL) are suitable for F_1 hybrid mouse model establishment (Yoshida and Kodama, 1983). The C57BL/6 inbred mouse model is a widely used strain, which are black coated and good breeders (Seong et al., 2004). The BALB/c is a popular inbred mouse strain and is used in many different research disciplines, such as cardiovascular, aging and pharmacological studies (Pummerer et al., 1996; Roberts et al., 2005). The SJL inbred model with a white coat was developed in 1955 from Swiss Webster outbred mice of three origins (Plum et al., 2002).

In this Chapter, I generated two independent F_1 hybrid mouse models ($B6CF_1$ and $B6SJLF_1$) which have asymmetrical centromeres on specific homologue pairs. Once the mouse model was established, I tested the transmission rate of asymmetrical centromeres on a homologous pair and demonstrated larger centromeres were preferentially retained in the oocytes of B6SJL hybrid mice.

3.2 Results

3.2.1 Establishment of $B6CF_1$ hybrid mouse model to study meiotic drive

To create bivalents recombined by two homologue pairs from different mouse strains, a hybrid mouse model ($B6CF_1$) was generated by crossing female C57BL/6 and male BALB/c mice. Major satellite DNA was labelled with transcription activator-like effectors to show the pericentromeric region and so aid in recognising the asymmetrical bivalents. Satellite DNA is visualized by transcription activator like effectors that are combined with a fluorescent probe. Major satellite-mClover and H2B-mCherry cRNA were microinjected into oocytes at the GV stage to visualize major satellite DNA and chromatin respectively. After labelling, oocytes were matured for 6 hours from NEBD and imaged for major satellite DNA intensity three dimensionally (Figure 3.1a).

Bivalents with asymmetrical major satellite DNA were found in the $B6CF_1$ oocytes (Figure 3.1b) and the intensity ratios of paired major satellite DNA were measured to test the asymmetry within each bivalent (12 oocytes combined from two independent experiments) (Figure 3.1c). In terms of paired major satellite, intensity ratios were measured by dimmer major satellite DNA divided by brighter major satellite DNA. Intensity ratios were tested individually, however, the differences between paired major satellite DNA were not obvious enough to be recognised in different oocytes and tracked in Z-stack time-lapse imaging (Figure 3.1b). Meanwhile, it was also difficult to identify the same bivalent from different oocytes by the specific ratio of major satellite DNA.

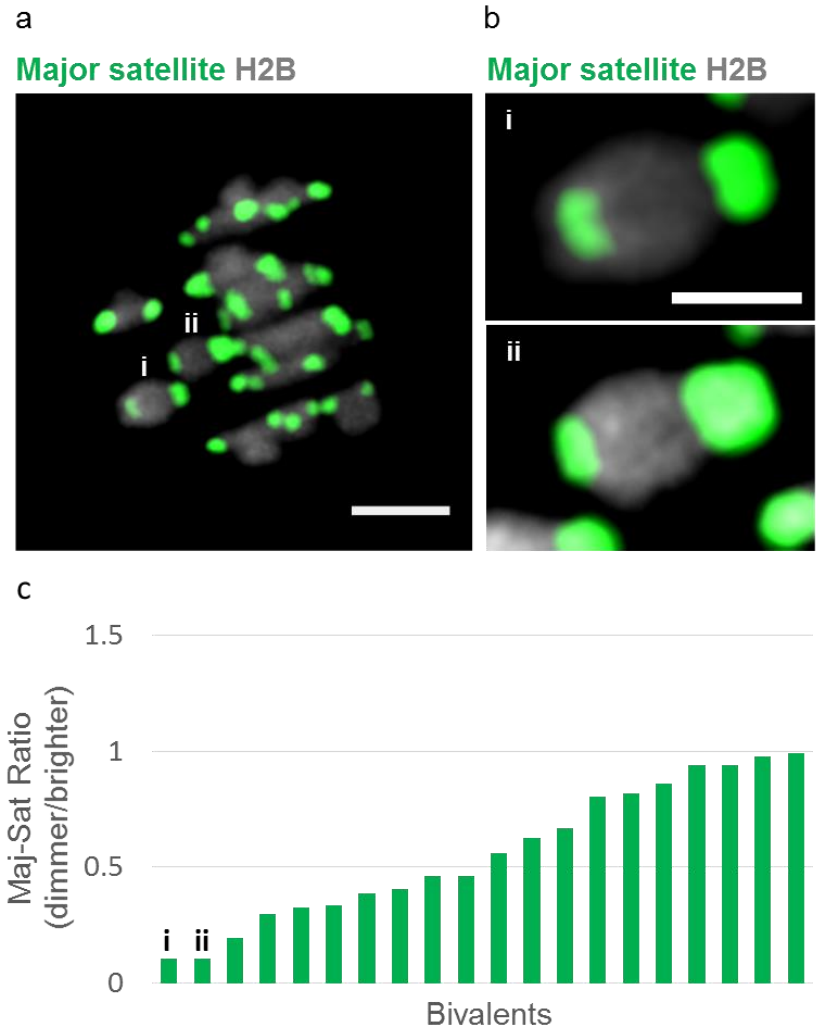

Figure 3.1 Bivalents with asymmetrical major satellite DNA in C57BL/6 x BALB/c F_1 hybrid mouse oocytes.

(a) Bivalents alignment in $B6CF_1$ hybrid mouse oocyte at metaphase of meiosis I. chromosomes with asymmetrical major satellite DNA. Scale bar: 5µm. **(b)** Enlarged asymmetrical bivalents. Scale bar: 2µm. Green: Major satellite-mClover. Grey: Histone H2B-mCherry (chromosomes). **(c)** Intensity ratios of major satellite DNA in 20 paired chromosomes in a single oocyte. (12 oocytes were tested in two independent experiments).

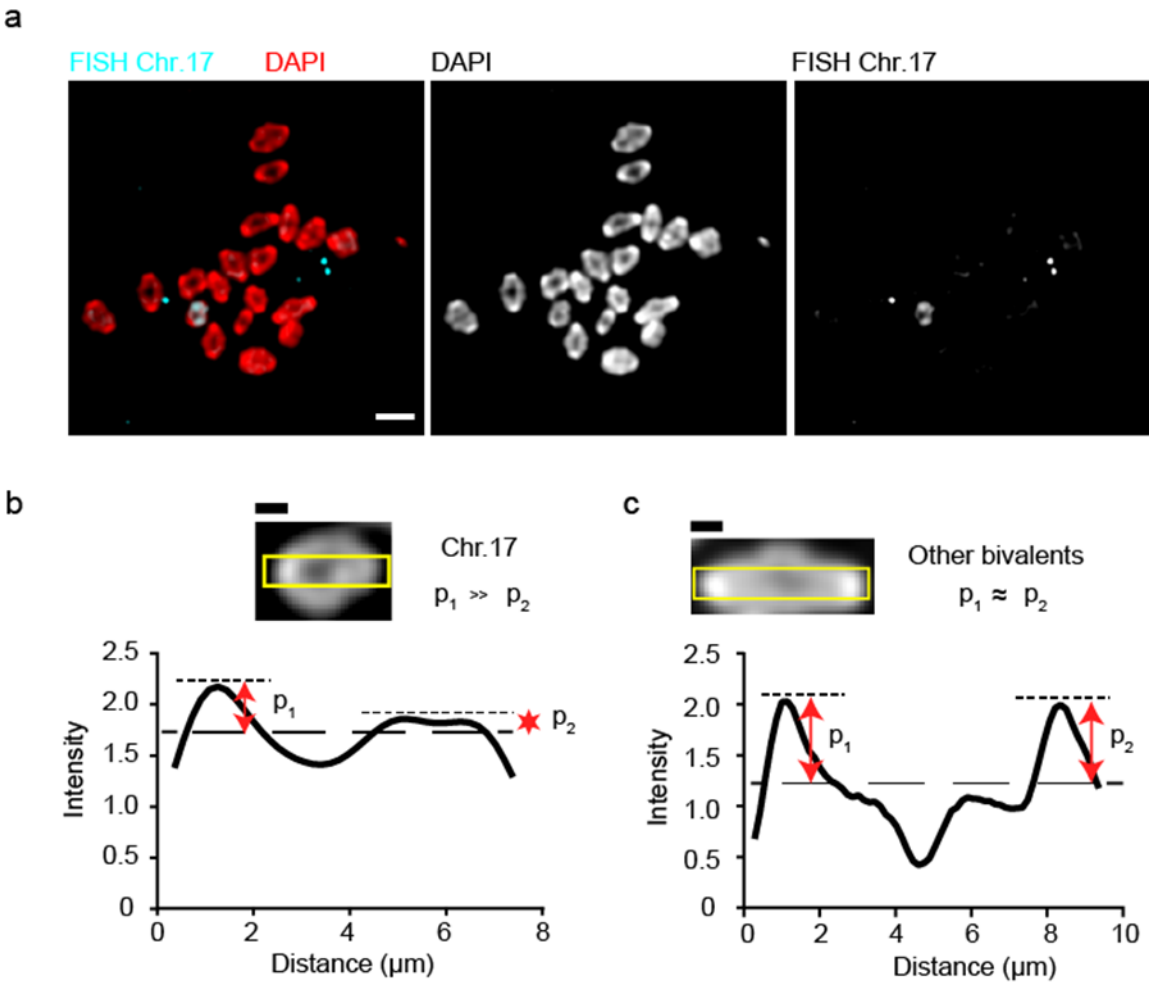

Figure 3.2 Chromosome 17 with asymmetrical major satellite DNA in C57BL/6 x SJL hybrid mouse oocytes.

(a) Chromosome 17(cyan) was labelled by FISH probe and counterstained with DAPI (red) after chromosome spreading at metaphase of meiosis I. Scale bar: 10 μm. **(b,c)** Peak intensity at centromeric regions labelled by DAPI are shown as P_1 and P_2 (red arrows). Dash line shows the average intensity of chromatin. Scale bar: 2μm. **(b)** Representative image of Chromosome 17 with asymmetrical intensity on centromeric regions ($P_1 >> P_2$). Low intensity was shown at P_2 (asterisk). **(c)** Representative image of a random chromosome with identical intensity on centromeric regions ($P_1 = P_2$). Yellow boxes show area for intensity measurements. Dashed lines show the average intensity in the yellow boxes.

3.2.2 Establishment of B6SJLF$_1$ hybrid mouse model to study meiotic drive

In order to be able to track a bivalent with asymmetrical major satellite DNA, it was necessary to choose mouse strains with more extreme differences in their reported C-banding. The SJL strain was selected to make a hybrid mouse model because it has a small C-band on Chromosome 4 and the smallest C-band on Chromosome 17 (Table 3.1). Therefore, a new hybrid mouse model, B6SJLF$_1$, was generated by mating female C57BL/6 and male SJL mice.

Yoshida and Kodama (1983) reported that Chromosome 17 has a normal C-band from C57BL/6 mice and a very small/non-existent C-band in SJL mice. To confirm such asymmetry for this chromosome, oocytes were matured for 6 hours from NEBD and then fixed for chromosome spreading. Here chromosomes were spread on the surface of coverslips, an approach different from the so called "in vivo chromosome spreading", where chromosomes are spread in the oocyte by the means of spindle structure disruption. After spreading, all bivalents were in the same focal plane and stained easily by probes. Bivalents were labelled with DAPI and Chromosome 17 specifically labelled with its chromosome-specific FISH probe (2 oocytes, Figure 3.2a). DAPI could be used to identify major satellite DNA because they are composed of heterochromatin, which is stained more intensely than euchromatin (Silva and Guerra, 2010). Chromosome 17, identified by the Chromosome 17 FISH probe, showed asymmetrical heterochromatin at its pericentromeric region with one half of the bivalent containing no detectable DAPI fluorescence (Figure 3.2b), a finding consistent with the reported C-banding and not observed in other bivalents (Fig 3.2c). During imaging, as the cytoplasm is washed away, bivalents were imaged with low background, which was better for chromosome identification.

Chromosome 4 is also reported to be asymmetrical for C-banding, with only a small amount of C-banding in the SJL strain (Table 3.1). However, I failed to identify Chromosome 4 with Chromosome 4 specific FISH probe.

After confirming the extreme DAPI heterochromatin asymmetry on Chromosome 17, Major satellite-mClover and H2B-mcherry cRNA were microinjected into oocytes at the GV stage to visualize major satellite DNA and chromatin. This was needed as a procedure for live oocytes imaging during maturation using real-time probes for major satellite and

chromatin respectively. DAPI was not a useful probe in live oocytes because the concentration of DAPI for live cell staining is too high to keep oocytes healthy, and for fluorescence microscopy, DAPI is excited with ultraviolet light that is also phototoxic.

Oocytes were imaged at metaphase of meiosis I, and I observed two bivalents per oocyte with severe asymmetrical major satellite repeat intensity between the homologs. These throughout the rest of the thesis were assumed to be Chromosome 4 and 17, and are referred to in this way. They could be individually identified by their major satellite DNA in each imaged oocyte, especially so for Chromosome 17. In the observation of 15 oocytes (combined from three independent experiments), I could consistently distinguish two bivalents from their major satellite repeat fluorescence respectively (Figure 3.3a, b).

In Chromosome 4, the homologue pair from C57BL/6 mice has normal sized major satellite DNA, however, the homologue pair from SJL mice has small major satellite DNA (interpreted from Table 3.1). In Chromosome 17, the homologue pair from C57BL/6 mice has normal major satellite DNA but the homologue pairs from SJL mice has the smallest major satellite repeat (interpreted from Table 3.1) (Seong et al., 2004). Such extreme asymmetries in paired major satellite DNA were not reported in other chromosomes (Table 3.1). While it remains extremely likely that Chromosome 17 has been correctly identified (through a FISH probe, its DAPI staining characteristics, and its major satellite fluorescence), it must be noted that Chromosome 4 has not. However, given the ability to detect just two bivalents per oocyte with these major satellite asymmetries and the reported C-banding characteristics agreeing with this, there can be a certain amount of confidence that these two chromosomes have been correctly identified.

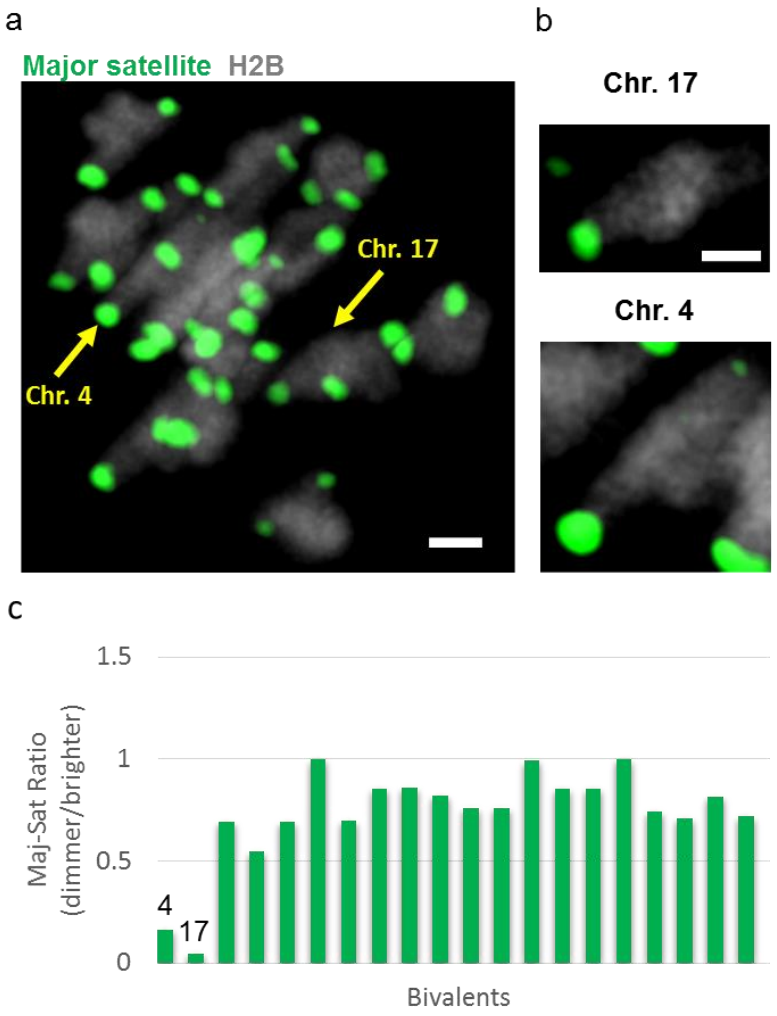

Figure 3.3 Chromosomes with asymmetrical major satellite DNA in C57Bl/6J x SJL hybrid mouse oocytes.

(a) Chromosomes alignment in B6SJLF$_1$ hybrid mouse oocytes at metaphase of meiosis I. Yellow arrows show Chromosome 4 and 17 with asymmetrical major satellite DNA. Scale bar: 5µm. **(b)** An enlarged image of asymmetrical major satellite DNA in Chromosome 4 and 17. Scale bar: 2µm. Green: Major satellite-mClover. Grey: H2B-mCherry (chromatin). **(c)** Intensity ratios of major satellite DNA in 20 paired chromosomes in a single oocyte. Ratios of Chromosome 4 and 17 are labelled with numbers. (15 oocytes were tested in 3 independent experiments)

3.2.3 Homologue pair with the larger major satellite repeat is preferentially extruded into polar body

To test the transmission rate of the two asymmetrical chromosomes (Chr 4 and 17), chromosome segregations were captured at anaphase of meiosis I in B6SJLF$_1$ hybrid oocytes. The oocytes were microinjected with major satellite-mClover and H2B-mCherry cRNA at GV stage to label major satellite DNA and bivalents respectively. Time-lapse imaging was performed to record bivalents separation at anaphase of meiosis I during maturation.

In the time-lapse images, Chromosome 17 could be identified at anaphase with relative ease by its extreme asymmetrical major satellite repeat (Figure 3.4). Therefore the fate of each homologue pair could be defined by polar body extrusion direction (Figure 3.5a, b, c). In terms of Chromosome 17, the homologue pair with larger major satellite DNA was found preferentially extruded into the polar body (35/45 oocytes, 77.7%; data combined from 6 independent experiments; chi-square test, $p< 0.01$) (Figure 3.5d).

In order to confirm if the larger major satellite repeat of the other asymmetrical bivalents were also preferentially extruded into polar bodies, Chromosome 4 was analysed in the same time-lapse images. Although the difference of major satellite DNA intensity between two homologue pairs in Chromosome 4 was slightly smaller, its position could nonetheless be identified with accuracy enough to determine its transmission rate into the polar body. As for Chromosome 17, the larger major satellite repeat in Chromosome 4 was preferentially extruded into the polar body and smaller major satellite DNA were preferentially retained in the oocytes (26/34 oocytes, 76.5%; data combined with 4 independent experiments; chi-square test, $p< 0.05$) (Figure 3.6).

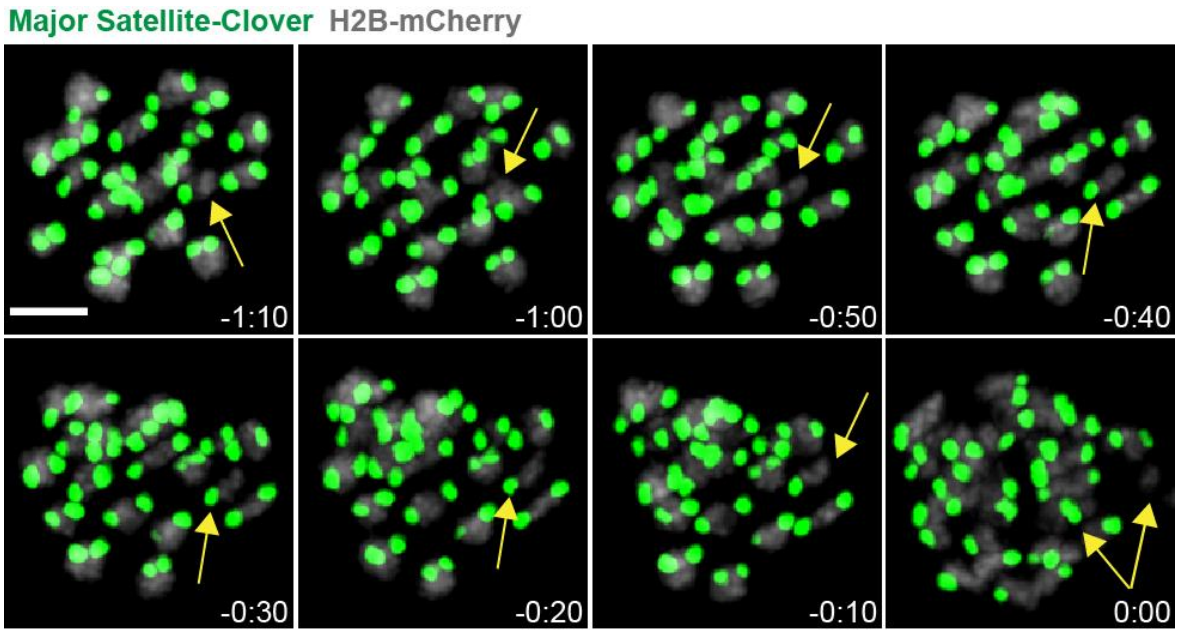

Figure 3.4 Chromosome 17 can be tracked in B6SJLF1 hybrid mouse oocytes.

Representative time-lapse images for chromosome segregations before anaphase. Yellow arrow shows Chromosome 17 with asymmetrical Major satellite DNA were tracked before and in separation. Green: Major satellite-mClover. Grey: Histone H2B-mCherry (Chromosomes). Scale bar: 5μm. Time point relative to anaphase.

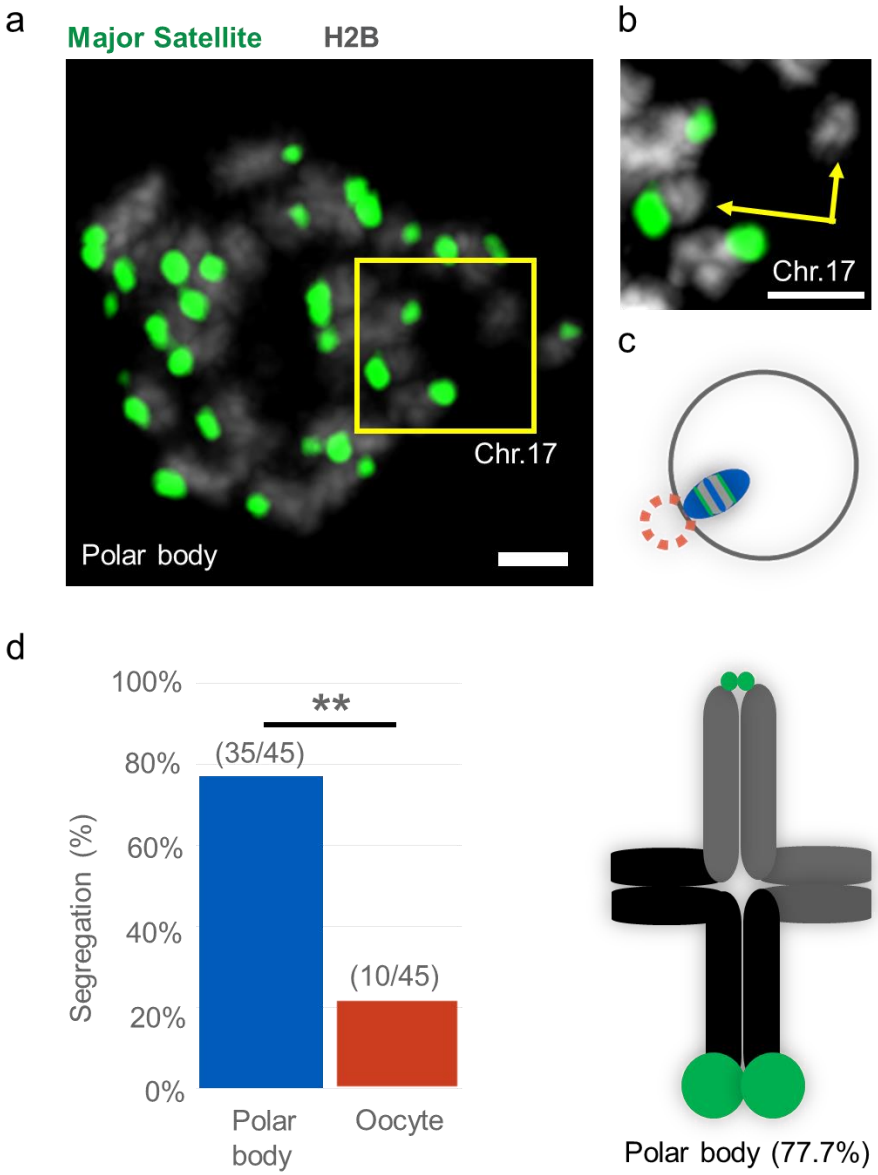

Figure 3.5 Biased Chromosome transmission rate of Chromosome 17 in B6SJLF1 hybrid mouse oocytes.

(a) Chromosomes segregation at anaphase by oocyte meiosis time-lapse. Yellow box shows Chromosome 17 with asymmetrical major satellite DNA in separation. Scale bar: 5 µm. **(b)** An enlarged image of asymmetrical Major satellite DNA of Chromosome 17. Green: Major satellite DNA. Grey: Histone 2B (Chromatin). Scale bar: 5 µm. **(c)** A schematic of anaphase in meiosis I shows the polar body extrusion direction (Green: Major satellite-mClover, Grey: H2B-mCherry, Blue: Spindle, Orange: Polar body). **(d)** Segregation rate of larger Major satellite DNA in Chromosome 17. Schematic shows asymmetrical major satellite DNA (Chi-square test, ** $p<0.01$).

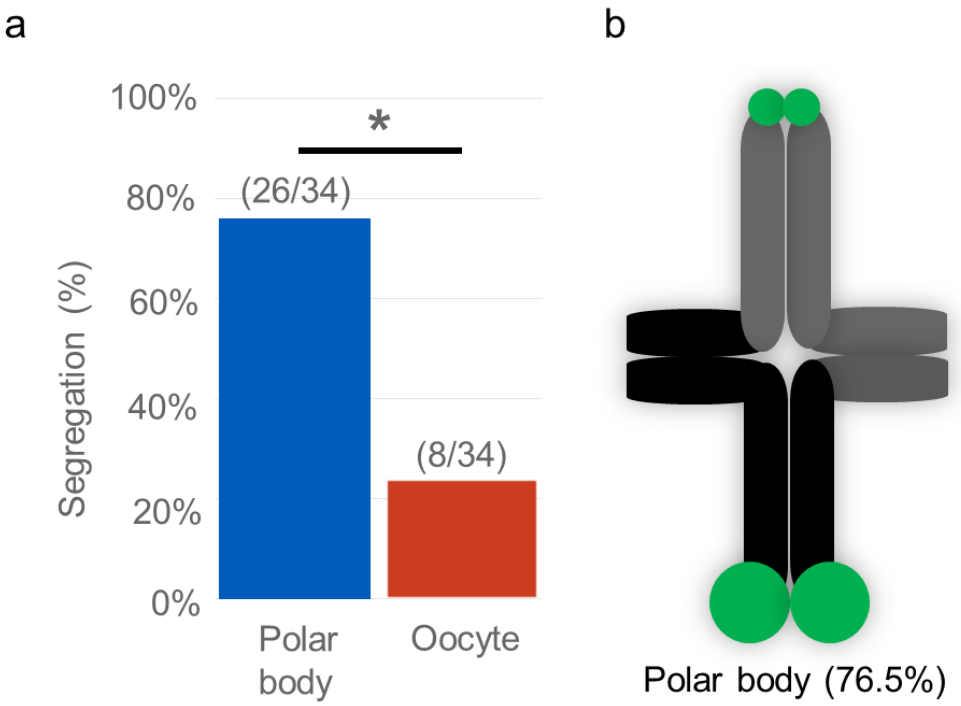

Figure 3.6 Biased chromosome transmission rate of Chromosome 4 in B6SJLF1 hybrid mouse oocytes.

(a) Segregation rate of larger major satellite DNA in Chromosome 17. (Blue: extruded into polar body; Orange: retained in the oocyte, Chi-square test, * $p<0.05$). **(b)** Schematic shows asymmetrical major satellite DNA. (Green: Major satellite DNA. Grey: Bivalents).

3.2.4 Larger major satellite DNA correlate with smaller minor satellite DNA on Chromosomes 4 and 17

According to previous research, the sizes of both centromeres and kinetochores are factors involved in meiotic drive (Chapter 1.3) (Chmátal et al., 2014). This led me to focus on the details of centromere size in the hybrid mouse model. In mouse oocytes, major satellite DNA is at the pericentromeric region (Jagannathan et al., 2018) and minor satellite DNA at the centromeric region (Bouzinba-Segard et al., 2006) (Chapter 1.2). Since meiotic drive correlated strongly with the size of the major satellite repeat on Chromosomes 4 and 17 of the C57/SJL hybrid mice I next looked to see if the minor satellite DNA size was also associated with non-random segregation at meiosis I.

Major satellite-mClover and Minor satellite-mRuby cRNA were microinjected into GV oocytes to visualize major and minor satellite DNA respectively. F_1 hybrid mouse oocytes were matured for 6 hours from NEBD and chromosomes 4 and 17 were identified by the major satellite DNA ratio between paired homologue pairs using 3D imaging (Figure 3.7a).

In both Chromosome 4 and 17 of B6SJLF_1 hybrid mice, more intense major satellite DNA but less intense minor satellite DNA were observed on the same homologue pair (Figure 3.6a, b). The asymmetrical intensity levels of major satellite DNA and minor satellite DNA were tested in Chromosomes 4 and 17. In terms of major satellite DNA, obvious asymmetries were found in Chromosome 4 and extreme asymmetries were found in Chromosome 17. I tested the ratio of paired major satellite florescence and paired minor satellite florescence on the Chromosomes 4 and 17 (15 oocytes for major satellite DNA, 13 oocytes for minor satellite DNA; 3 independent experiments). The homologue pairs from C57BL/6 mice contains larger major satellite DNA with smaller minor satellite DNA in them, on the contrary, the homologue pairs from SJL mice contains smaller major satellite DNA with larger minor satellite DNA on them (Figure 3.7 b, c).

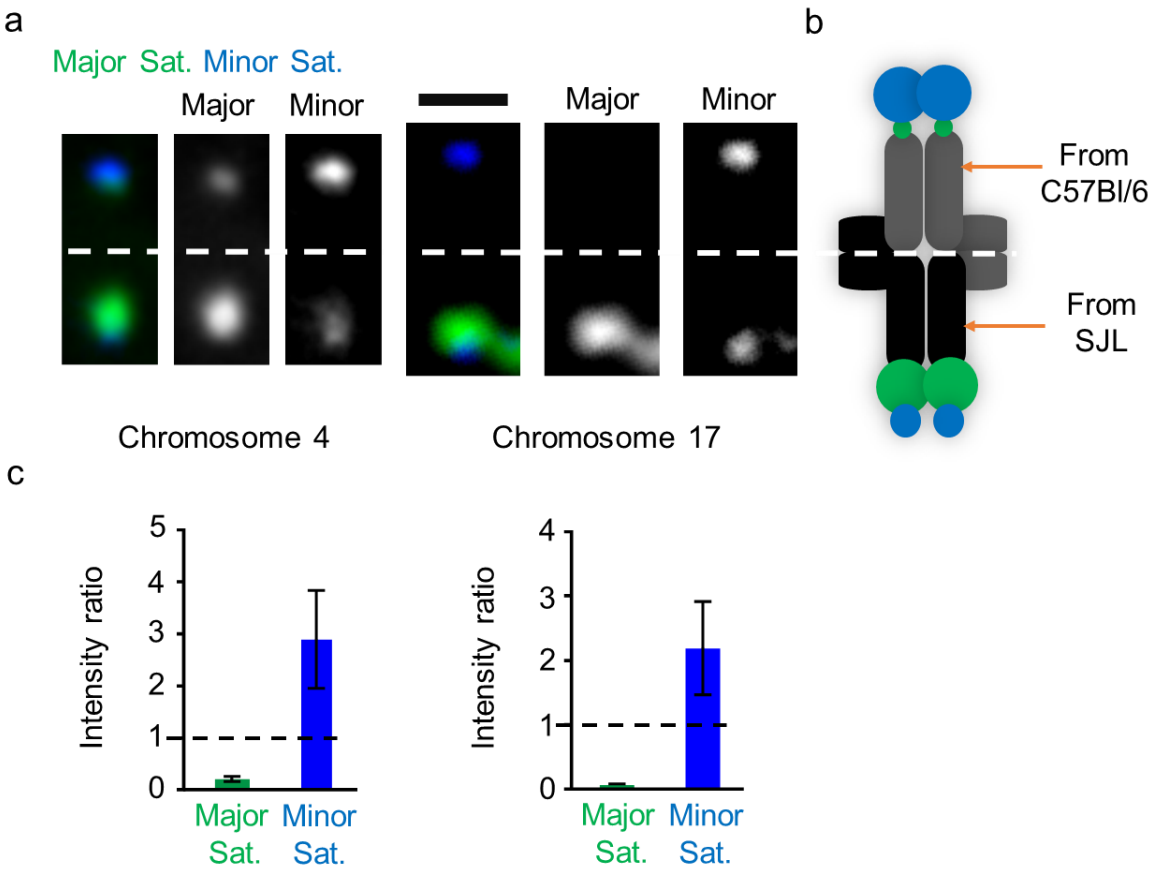

Figure 3.7 Reciprocal relationship between major and minor satellite DNA intensity for Chromosome 4 and 17.

(a) Representative images show the fluorescence of the major satellite repeat and minor satellite repeat on Chromosome 4 and 17. Scale bar: 2 µm. **(b)** Major satellite DNA intensity ratio is calculated with Major satellite DNA from SJL mice divided by major satellite DNA from C57BL/6 mice (15 oocytes from three independent experiments). Minor satellite DNA intensity ratio is calculated with Minor satellite DNA from SJL mice divided by minor satellite DNA from C57BL/6 mice (13 oocytes from three independent experiments). Error bars are 95% confidence intervals. **(c)** Schematic shows position and relationship between major satellite DNA and minor satellite DNA in Chromosome 4 and 17. (Green: Major satellite-mClover; Blue: Minor satellite-mRuby; Grey and black: Chromosomes). The sizes are represented from measurements made in (a). The homologue pairs are assigned to mouse strain inferred by their known C-banding.

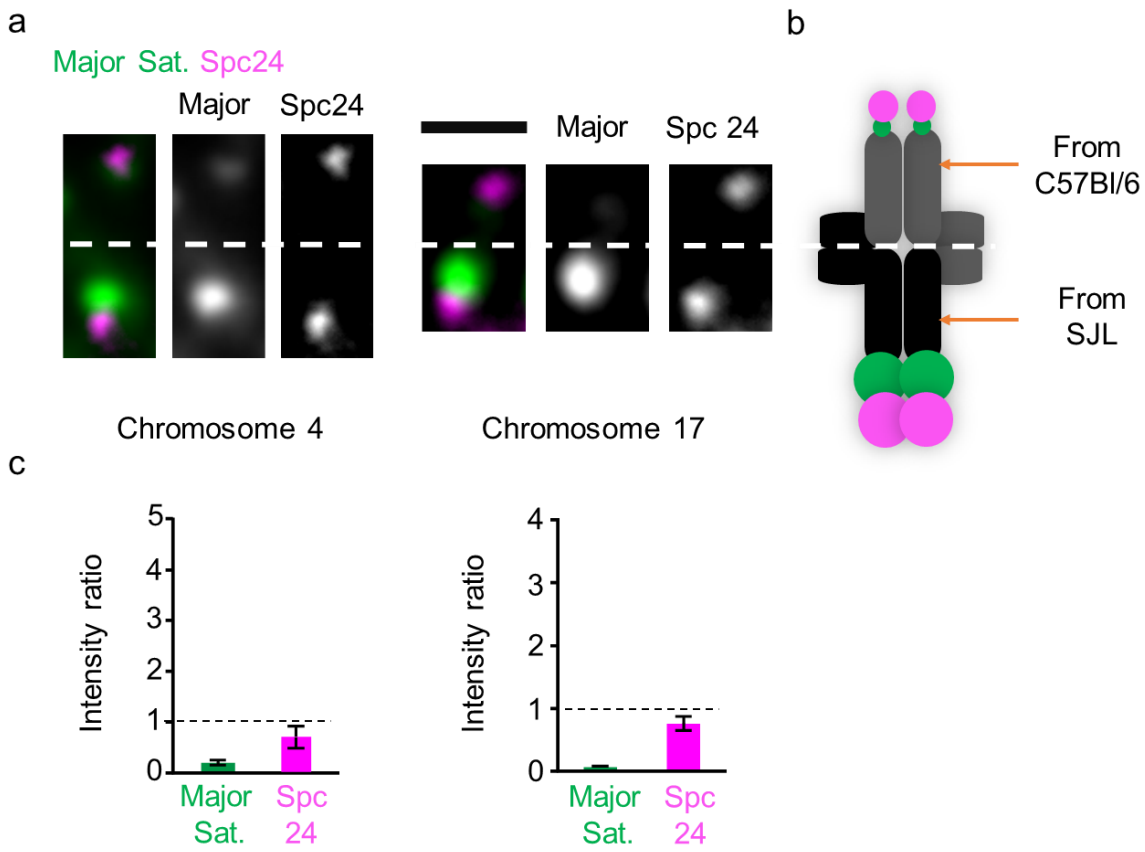

Figure 3.8 Reciprocal relationship between major satellite DNA and Spc24 intensity for Chromosome 4 and 17.

(a) Representative images show the fluorescence of Major satellite DNA and Spc24 in Chromosome 4 and 17. Scale bar: 2µm. **(b)** Schematic shows position and relationship between major satellite DNA and Spc24 in Chromosome 4 and 17. (Green: Major satellite-mClover; Pink: Spc24-mCherry; Grey and black: Bivalents). **(c)** Major satellite DNA intensity ratio is the same as Figure 3.7. Spc24 intensity ratio is calculated with Spc24 from SJL mice divided by Spc24 from C57BL/6 mice (12 oocytes from three independent experiments). Error bars are 95% confidence intervals.

3.2.5 Larger major satellite correlate with larger Spc24 on Chromosome 4 and 17

Although the asymmetrical major and minor satellite DNA were observed and analysed, the mechanism of biased homologue selection is still unclear because the satellite DNA (DNA) is not able to be attached to microtubules and be selected for retention by meiotic drive directly. In meiosis, microtubules attach to kinetochores directly which are recruited by Cenps on minor satellite DNA. Since microtubule-kinetochore attachment is essential for chromosome segregation, I next tested the size of kinetochores in B6SJLF$_1$ hybrid mice. Spc24 is a kinetochore protein, a component of the Ndc80 complex that binds to the microtubules directly. Spc24-mCherry cRNA was microinjected into GV oocytes to visualize Spc24, which is a part of NDC80 complex. After 6 hours maturation, the fluorescence of Spc24 was imaged and the intensity was measured for Chromosome 4 and 17.

For both Chromosome 4 and 17, the homologue pairs from C57BL/6 mice with larger major satellite DNA recruited more Spc24 than the homologue pair from SJL (Figure 3.8 a, b). This raised the possibility that there might be more microtubules bound to the kinetochores and centromeres on the homologue pairs from C57BL/6 mice. When the relative size of the major satellite DNA and Spc24 foci were calculated as a ratio (homologue pairs of SJL / homologue pairs of C57Bl/6; 12 oocytes from 3 independent experiments; Figure 3.8 c), it was noted that the large homolog with the larger major satellite DNA also had a significantly greater Spc24 signal (95% confidence interval).

3.3 Discussion

In this chapter, I generated a B6SJLF$_1$ hybrid mouse model which contains two asymmetrical bivalents in oocytes. The two asymmetrical bivalents are Chromosome 4 and 17 with asymmetrical major satellite DNA, minor satellite DNA and outer kinetochores (as measured by Spc24-mCherry intensity). In terms of Chromosome 4 and 17, the homologue pairs with larger Major satellite DNA were preferentially extruded into polar bodies in meiosis I. The homologue pairs from C57BL/6 mice with larger major satellite and smaller minor satellite DNA could recruit more Spc24, and on the contrary, the homologue pairs from SJL mice with smaller major satellite and larger minor satellite DNA could recruit less Spc24. These asymmetries in the centromere and kinetochore

correlated with a biased chromosome transmission rate. Although meiotic drive was observed in meiosis I of hybrid mouse oocytes, a few questions still need to be answered.

3.3.1 Some mouse strains with different sized major and minor satellite DNA

Meiotic drive is related to asymmetrical centromeres on the same homologue pairs from hybrid mice crossed by two different mouse strains which contain different sized centromeres (minor satellite DNA) (Chmátal et al., 2014). In the result 3.2.2, homologue pairs of Chromosome 4 and 17 from C57BL/6 and SJL mice have different sized major and minor satellite DNA which helped to identify the bivalents and observe the biased homologue pairs transmission rate at anaphase of meiosis I.

In Chromosome 4 and 17, homologue pairs from SJL mice possess larger centromeres than C57BL/6 mice. Although the reason for variable centromeric DNA in different mouse strains is still unclear, the phenomenon has been observed widely (Henikoff et al., 2001; Malik and Henikoff, 2009). Based on the natural variation of centromeres, some mouse strains have small centromeres and some other mouse strains have large centromeres, consistent with divergent centromere evolution. Rapid centromere evolution was hypothesized as a competition between paired centromeres of the same bivalents. In the hybrid mice, only stronger centromeres, which win the competition, are retained in the egg and then transmitted to offspring. Selected by evolution, only the stronger centromeres are retained in the species. Meanwhile, the size of centromere is limited by its function in chromosome segregations. If the centromere is too strong to provide proper function, they could induce wrong chromosome segregation and be abandoned during development. Therefore, with long term of hybridization and evolution, a range of different sized centromeres are formed and stabilized.

Regardless of the rapid evolution of minor satellite DNA at centromeric regions, major satellite DNA at pericentromeric regions are also variable in different mouse strains (Plohl, 2002). In the house mouse (Mus musculus, such as C57BL/6, BALB/c and SJL), major satellite DNA is much larger than minor satellite DNA, and therefore more easily detected. Taking advantage of this feature, unique asymmetrical major satellite DNA ratios were used as a marker of Chromosome 4 and 17 and the origin of homologue pairs could be distinguished by different sizes of major satellite DNA.

3.3.2 Minor satellite DNA was supposed as the driver of meiotic drive

As seen in this Chapter, smaller major satellite DNA with larger minor satellite DNA of Chromosome 4 and 17 tended to remain in the oocyte and so not be extruded into the polar body. The role of major and minor satellite DNA in meiotic drive therefore needs to be understood.

According to recent research, meiotic drive requires asymmetrical minor satellite DNA on the same bivalents because Cenp-A specifies the sites of kinetochore assembly and mainly localizes at minor satellite DNA. Apart from this, the minor satellite transcripts are also important in the localization of Cenp-C and chromosomal passenger complex (CPC) (Talbert and Henikoff, 2018). Compared with minor satellite DNA, major satellite DNA at pericentromeric regions can localize much less centromeric proteins and kinetochores on to it (Iwata-Otsubo et al., 2017). Meanwhile meiotic drive was observed in the bivalents who have asymmetrical minor satellite DNA but symmetric major satellite DNA (Iwata-Otsubo et al., 2017). It shows minor satellite DNA plays a more important role than major satellite DNA in meiotic drive.

The role of minor satellite DNA in meiotic drive were only investigated in the M. musculus subspecies in which the kinetochore is mainly limited to the minor satellite DNA region. However, the absence of minor satellite DNA in M. caroli would seem to argue against a direct correlated organization between minor satellite and kinetochore (West et al., 1978; Wong et al., 1990).

Although minor satellite DNA was supposed as the main base for centromeric proteins and kinetochore which attach to microtubules, it does not mean meiotic drive is major satellite DNA independent. Major satellite transcripts are indispensable for proper chromosome alignment and segregation and therefore likely have a role in chromosome attachment to the spindle (Ideue et al., 2014). It is therefore possible that some property of the major satellite repeats plays a role in meiotic drive. Indeed, major satellite repeat transcripts recruit heterochromatin factors that maintain the modifications of heterochromatic histone, such as H3K9me2, H3K9me3, H3K27me2, and H3K27me3 (Hall et al., 2012).

3.3.3 B6SJLF$_1$ hybrid mouse model is appropriate for meiotic drive research

Meiotic drive was observed in F_1 hybrid mouse oocytes in which all the bivalents with asymmetrical centromeres (minor satellite DNA) were tested together (Iwata-Otsubo et al., 2017). However, to investigate bivalent reorientation in MI oocytes, specific bivalent tracking is very important because bivalents are reoriented three times on average during meiosis I, which disturbs transmission rate measurements (Kitajima et al., 2011). Without specific bivalent tracking, it is difficult to uncover the mechanism that how the bivalents transmission rate affected by asymmetrical centromeres.

Asymmetrical centromeres were generated on specific bivalents in B6SJLF$_1$ hybrid mouse model, specifically bivalents (Chr 4 and 17) with asymmetrical centromeres are able to be identified respectively and tracked in z-stack time-lapse imaging. However, in B6CF$_1$ hybrid mouse model, the bivalents with asymmetrical centromeres cannot be identified and tracked because the asymmetrical intensity ratios of these paired major satellite DNA are too similar to be distinguished in z-stack time-lapse imaging. This is likely because the parent strains, C57BL/6 and BALB/c, were derived originally from a single female of the subspecies *Mus musculus domesticus* (Ferris et al., 1982). The lineage of the SJL is from three outbred Swiss mice, and when compared to BALB/c likely diverged from the last common ancestor of C57BL/6 by significantly greater period of time.

Apart from the influence from the centromere, to understand the mechanism of biased chromosome transmission rate, the stage in meiosis and process of bivalent re-orientation need to be investigated further. Although the bivalents change of direction has been reported briefly, the process of a specific bivalent re-orientation is still necessary to be record and analysed.

Chapter 4: Driving Bivalents can Re-orientate during Prometaphase

4.1 Introduction

In meiosis, live mouse oocytes imaging shows that bivalents are stretched and aligned on the meiosis I spindle in the centre of oocyte before spindle migration (Kitajima et al., 2011; Li et al., 2008; Schuh and Ellenberg, 2007). The process of spindle formation and bivalents alignment is complicated and lengthy; it takes about 6 hours from NEBD to metaphase. Initially, bivalents are individualized on the surface of a microtubule ball. Then, a prometaphase belt is formed by circled bivalents around microtubule ball. Finally, a metaphase plate is formed by bivalents with their inward invasion into the spindle (Can et al., 2003; Kitajima et al., 2011; Luksza et al., 2013; Mattson and Albertini, 1990; Messinger and Albertini, 1991; Mogessie et al., 2018; Schuh and Ellenberg, 2007).

To investigate the mechanism of meiotic drive in mouse oocytes it is necessary to record the behaviour of driving bivalents meticulously during the period of chromosome biorientation and migration, to see if the process of bivalent biorientation provides an opportunity for biased homologue pair extrusion.

After NEBD, clustered chromosomes and kinetochores are moved slightly by NEBD, and chromosome-microtubule interactions increase as early spindle formation begins (Figure 4.1a) (Kitajima et al., 2011; Schuh and Ellenberg, 2007). By two hours after NEBD, three types of kinetochore-microtubule attachments are observed: lateral attachment (a kinetochore is attached by the sides of microtubules), merotelic attachment (a kinetochore is attached by the ends of microtubules from opposite poles), and amphitelic attachment (a kinetochore is attached by the ends of microtubules from one pole) (Kitajima et al., 2011; Lampson and Grishchuk, 2017; Nicklas, 1997). Once these microtubule- kinetochore interactions start the process of bi-orientation is initiated. Bivalents biorientation is widely explained as the classic “search and capture” model, in which paired kinetochores are captured and stretched by microtubules (Figure 4.1). The stable bivalents biorientation can be formed only with paired kinetochores attached correctly by microtubules emanating from opposite spindle poles (amphitelic

attachment) (Barisic et al., 2015; Kapoor et al., 2006; Magidson et al., 2011; Mihajlović and FitzHarris, 2018).

In the process of biorientation, Aurora kinases have key roles to regulate bivalents alignment, SAC activation and kinetochore-microtubule attachment (K–MT attachment) correction (Carmena and Earnshaw, 2003; Nguyen and Schindler, 2017). Aurora kinases are a highly conserved family proteins with three isoforms: Aurora A, B and C. AURKA and AURKB are expressed in all mammalian cell lineages, however, AURKC is primarily restricted to expression in mammalian meiosis, i.e. gametes (Gopalan et al., 1997; Tseng et al., 1998; Yanai et al., 1997). All the three isoforms are required in mammalian cell division (Nguyen and Schindler, 2017). AURKA is recruited by spindle poles for spindle organisation in metaphase (Saskova et al., 2008; Yao et al., 2004). AURKB, localizing to spindle microtubules in mitosis, is responsible for bivalent alignment and erroneous K-MT attachments detection (Kelly and Funabiki, 2009; Santaguida et al., 2011). Although the functions of AURKB are well known in mitosis, its role in meiosis still remains elusive (Nguyen et al., 2018). Compared with AURKB, AURKC has a similar sequence (75% in the kinase domain) (Quartuccio and Schindler, 2015) but plays dominant role as a subunit of chromosomal passenger complex (CPC) in mouse oocytes. In meiosis, AURKC is much more stable than AURKB, which has destruction motifs in the N-terminus (Schindler et al., 2012). AURKC was found to localize to spindle poles, centromeres and the interchromatid axis (ICA) in oocytes and works on MTOC clustering, chromosome alignment, chromosome condensation and K–MT attachment correction (Nguyen and Schindler, 2017).

Central to AURKB/C function is the correction of erroneous kinetochore-microtubule attachments. If a kinetochore is not attached by microtubules properly, for example attached to both spindle poles (Figure 4.1b, left kinetochore), it can be corrected by Aurora B/C kinase which is responsible for detaching wrong microtubules attachments that are detected by tension (Lampson and Grishchuk, 2017; Monda and Cheeseman, 2018; Nguyen et al., 2018). The attachments not under tension can be detected and corrected. AURKB/C localize close to K-MT attachments and destabilize incorrect microtubule attachments by phosphorylating their substrates at kinetochores, such as the Ndc80 complex, to reduce microtubule binding affinity. After bivalents bi-oriented and correct K-MT attachments formed, the Ndc80 complex are dephosphorylated and

K-MT attachments are stabilized at the same time (Davydenko et al., 2013; Holt and Jones, 2009; Kitajima, 2018; Watanabe, 2012; Yoshida et al., 2015). The correction of erroneous K-MT attachments is essential in meiosis I, however is often incomplete as most aneuploidy in eggs is induced by incorrect K-MT attachments that remain until chromosome segregation in MI oocyte (Lane et al., 2012).

During attachment correction events, bivalents are likely rotated by unbalanced pulling force from microtubules (See Chapter 4.3.2). During the rotation of bivalents, an appropriate opportunity for homologue pair selection and bivalents reorientation is provided.

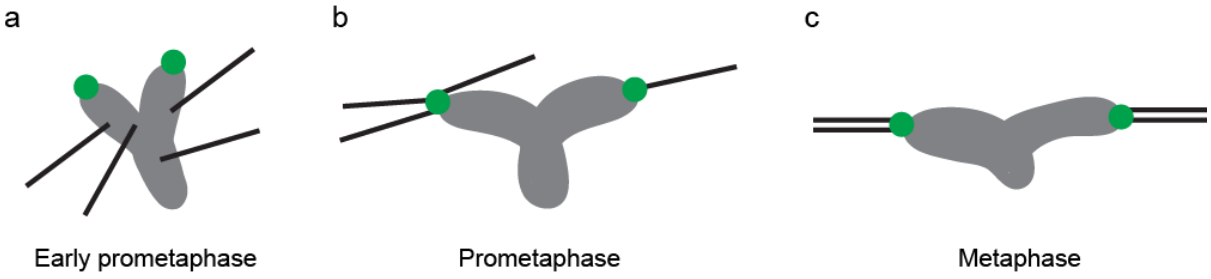

Figure 4.1 Representative schematic for bivalent biorientation.

(a) Schematic of Chromosome Arm-Microtubule interaction at early prometaphase. **(b)** Schematic shows merotelic K-MT attachment (unstable). **(c)** Schematic shows amphitelic K-MT attachment (stable). Green: Kinetochore; Grey: Chromosome; Black: Microtubule.

Specifically during meiosis I in oocytes bivalents reorientation becomes non-arbitrary, as during this division chromosomes facing towards each end of the spindle have different destinies (Akera et al., 2017). In meiosis I, spindles are formed in the centre and migrate to the cortex during meiosis I. The spindle pole close to cortex, termed as the 'cortical' spindle pole, is extruded into the polar body, on the contrary, the other spindle pole close to centre, termed as the 'central' spindle pole, is retained in the egg

(Almonacid et al., 2014; Chaigne et al., 2012; Li et al., 2008; Mogessie et al., 2018; Schuh and Ellenberg, 2008). Therefore, the homologue pair will be retained in the egg only if it is attached to the central spindle pole before chromosome segregation, otherwise, it would be lost in polar body, and cannot be passed on to future generations, creating a strong selection pressure. It occurs only in female meiosis because the asymmetrical cell division is only takes place in oocytes but not in sperms (Can et al., 2003; Mihajlović and FitzHarris, 2018).

To investigate the role of Aurora kinase in meiotic drive, throughout this chapter, the inhibitor ZM447439 was used to inhibit Aurora kinases (Lane et al., 2010; Nguyen and Schindler, 2017). All three isoforms of Aurora kinase family are potentially inhibited by ZM447439. Both Aurora A and B can be inhibited by ZM447439, because they have similar half maximal inhibitory concentration (IC50, Aurora A: 110nM vs Aurora B: 130nM) (Ditchfield et al., 2003). Cells treated with ZM447439 presented a distinct phenotype (Lane et al., 2010; Macůrek et al., 2008; Seki et al., 2008). AURKC is also likely to be inhibited, given its high sequence homology to AURKB (Tseng et al., 1998).

To avoid the influence from AURKA, dominant-negative versions of AURKC were used to decrease the activity of AURKB/C. The strategy of this dominant-negative mutant is straight forward, the overexpressed inhibitory variant outcompetes the wild-type proteins (AURKB/C) for the common binding partner (INCENP) (Figure 4.2). The inhibitory variant lacks kinase activity because of two threonine's mutations in the activation loop (Balboula and Schindler, 2014), so there is no active Aurora kinase recruited to the centromeric region (Figure 4.2b). (Herskowitz Ira, 1987; Schindler et al., 2012).

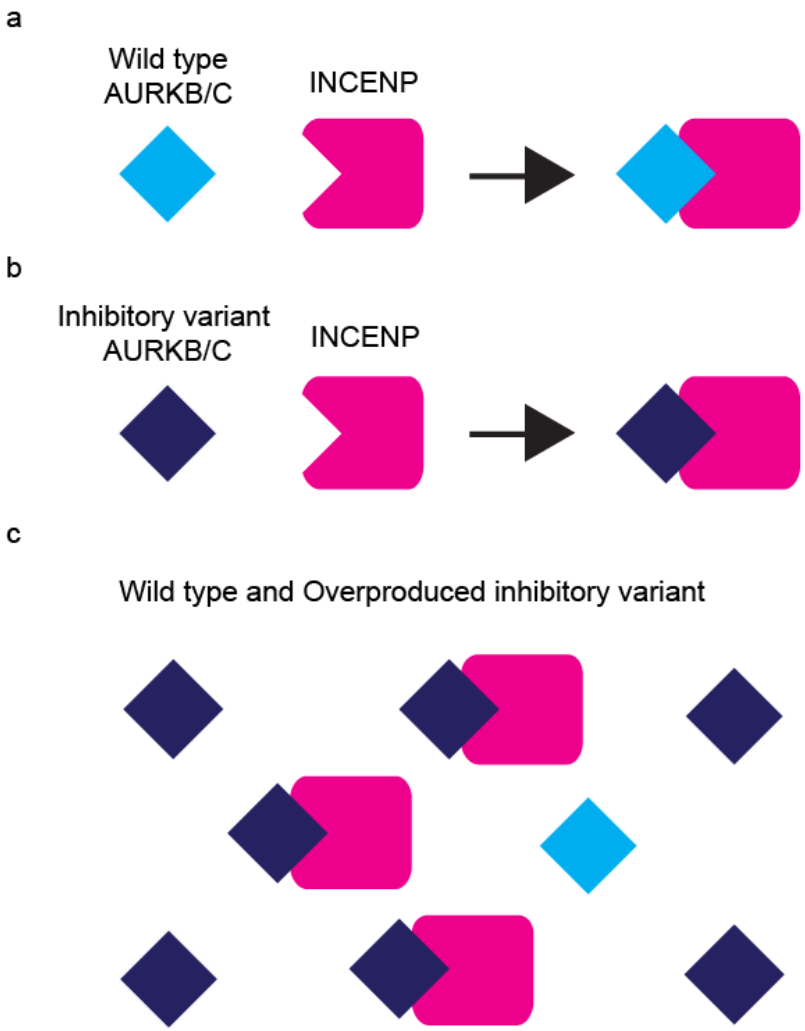

Figure 4.2 Schematic for mechanism of dominant-negative AURKB/C.

(a) Schematic of wild type AURKB/C (functional) is recruited by INCENP. **(b)** Schematic shows dominant-negative AURKB/C (with no function) localize at the same binding site as wild type. **(c)** Schematic shows overproduced inhibitory varient compete binding sites with wild-type AURKB/C. Blue: wild-type AURKB/C; Purple: Dominant-negative variant of AURKB/C; Magenta: INCENP (Binding partner of AURKB/C).

4.2 Results

4.2.1 The initial orientation of larger major satellite DNA is formed randomly

Having previously demonstrated that Chromosome 17 of B6CF1 mice experienced meiotic drive, I next sought to investigate when during meiosis I the orientation of Chromosome 17 became biased. In B6CF1 mice, Chromosome 17 was therefore tracked in live oocytes and its orientation recorded using time-lapse confocal microscopy during maturation. Oocytes were microinjected with Major satellite-mClover and H2B-mCherry cRNA at GV stage to visualize major satellite DNA and bivalents respectively. After microinjection, oocytes were arrested at GV stage for two hours for cRNA expression. Bivalents aligned normally in microinjected oocytes during imaging and anaphase I occurred with normal timing (5.8h ± 0.6h; Figure 4.3).

To track bivalents, oocytes were imaged every ten minutes with three-dimensional microscopy from NEBD to anaphase (8.30 ± 1.30h, mean ± std. dev., 29 oocytes). In B6CF1 mice, Chromosome 17 can be recognised at most time points during meiosis I because of the almost invisible major satellite DNA from SJL mice and the direction of larger major satellite DNA can be defined only after bivalents individualization at about 2 hours after NEBD (Schuh and Ellenberg, 2007) (Figure 4.3). Chromosome 17 could be recognised in Z-stack images easily (Figure 4.4a) and could be distinguished from Chromosome 4, which also has a weak major-satellite signal (Figure 4.4b).

The location of the oocyte cortex was defined by using a low magnification overview image that combined transmitted light and the H2B-mCherry fluorescence channel (Chapter 5). After knowing the relative position of the chromosomes and the nearest part of the oocyte cortex it is possible to define the orientation of chromosome 17 at almost all time points (>90% of time points). Data was collected at prometaphase stage, just after chromosome individualization (2-3hours after NEBD), at that time point the bivalents have formed their initial attachments to the spindle and so their direction can be determined (Figure 4.5a). The larger satellite repeat (from the C57 parent) of Chromosome 17 was observed in both cortical and central directions (Maj.Sat. Cortex and Maj.Sat. Centre).

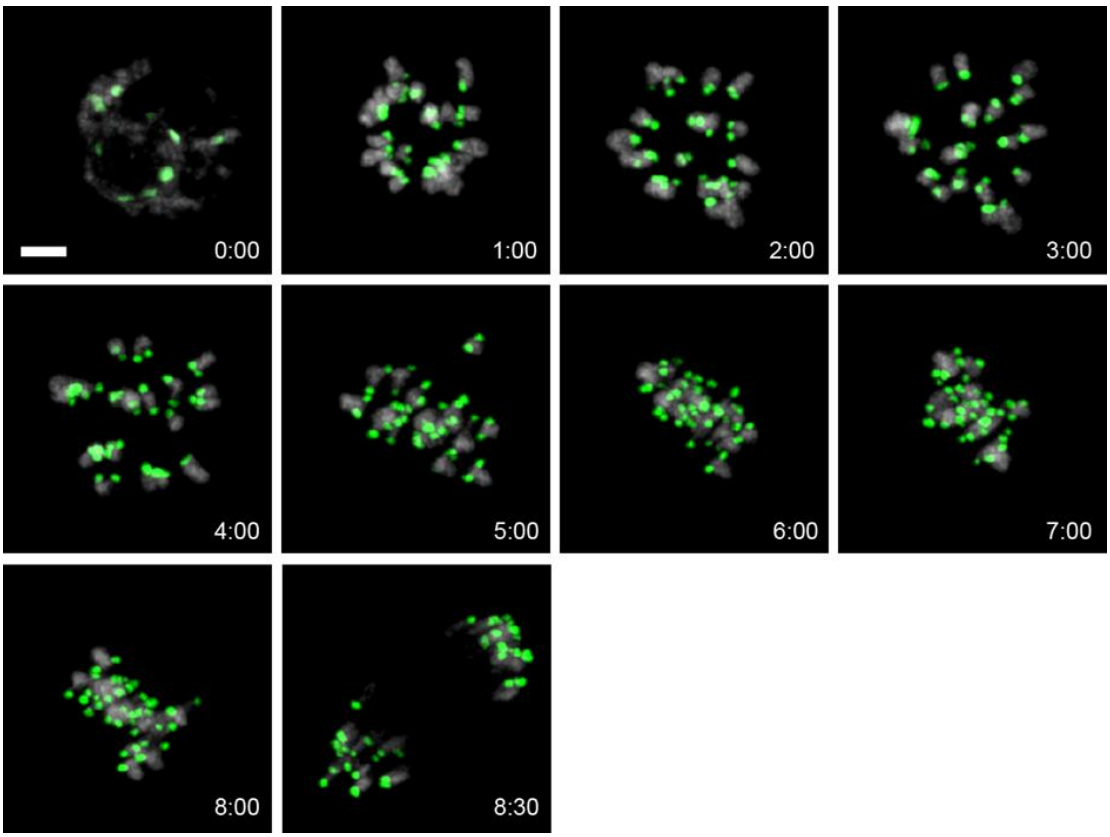

Figure 4.3 Bivalents alignment and segregations are not affected by major satellite-mClover and H2B-mCherry microinjection.

Time-lapse imaging for bivalents alignment and segregations in meiosis I. Time from NEBD. Green: Major satellite-mClover. Grey: H2B-mCherry (Chromosomes). Scale bar: 5µm.

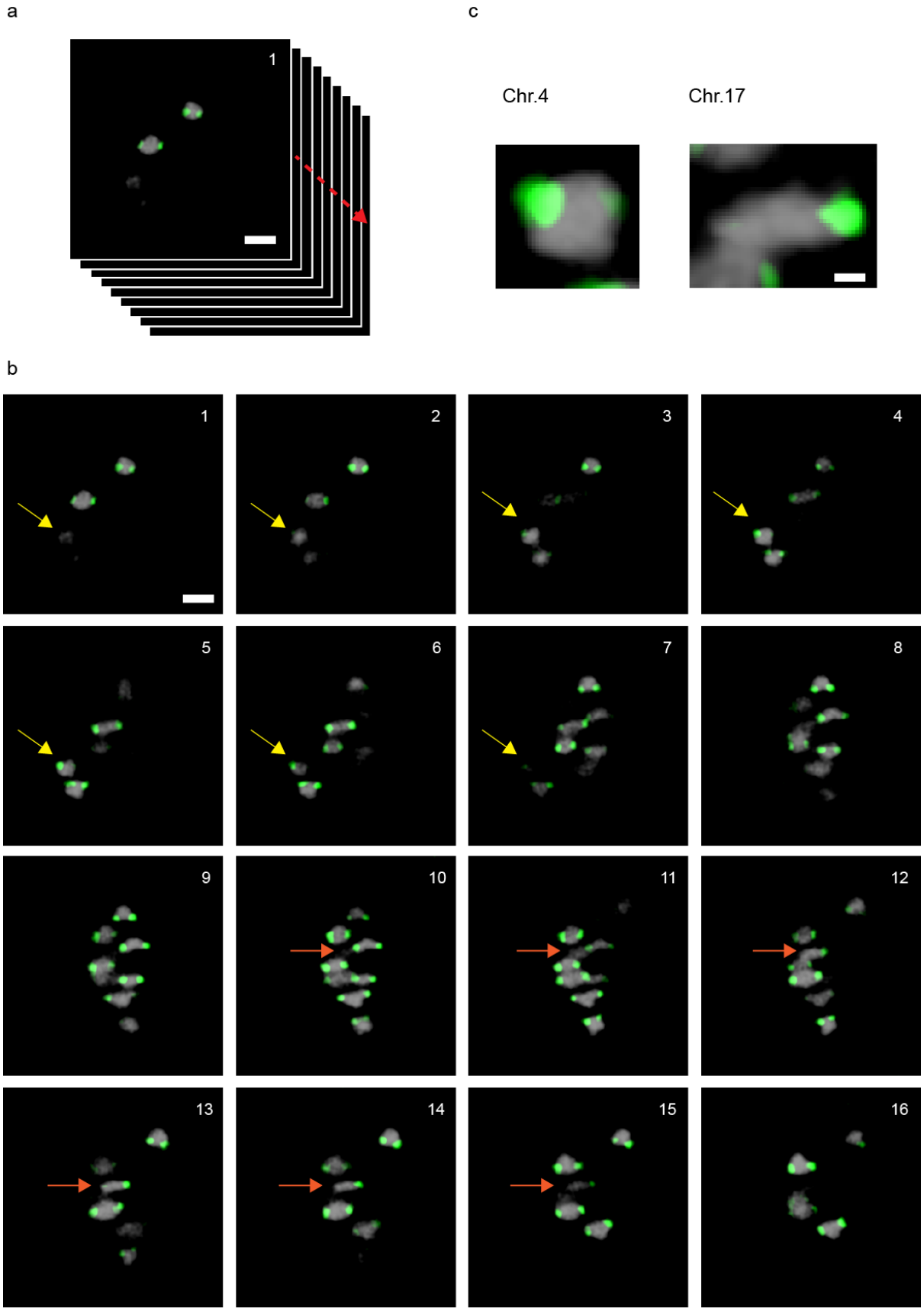
a
1
c
Chr.4
Chr.17
b
1
2
3
4
5
6
7
8
9
10
11
12
13
14
15
16

Figure 4.4 Chromosome 4 (assumed) and 17 are recognised and captured in Z-stack imaging.

(a) Three-Dimensional spatial bivalents biorientation was record by Z-stack time lapse imaging (interval=1.25μm). Scale bar: 5μm. Red arrow: Order of Z-stack scan. **(b)** Chromosme 4 (assumed) and 17 are recognised individually in Z-stack imaging during bivalents alignment. Green: Major satellite-mClover. Grey: H2B-mCherry (Bivalents). Yellow arrow: Chromosome 4 (assumed); Orange arrow: Chromosome 17. Scale bar: 5μm. Number: Order of Z-stack scan. **(c)** The different asymmetry of Chromosme 4 (assumed) and 17. Green: Major satellite-mClover. Grey: H2B-mCherry (Chromosomes). Scale bar: 2μm.

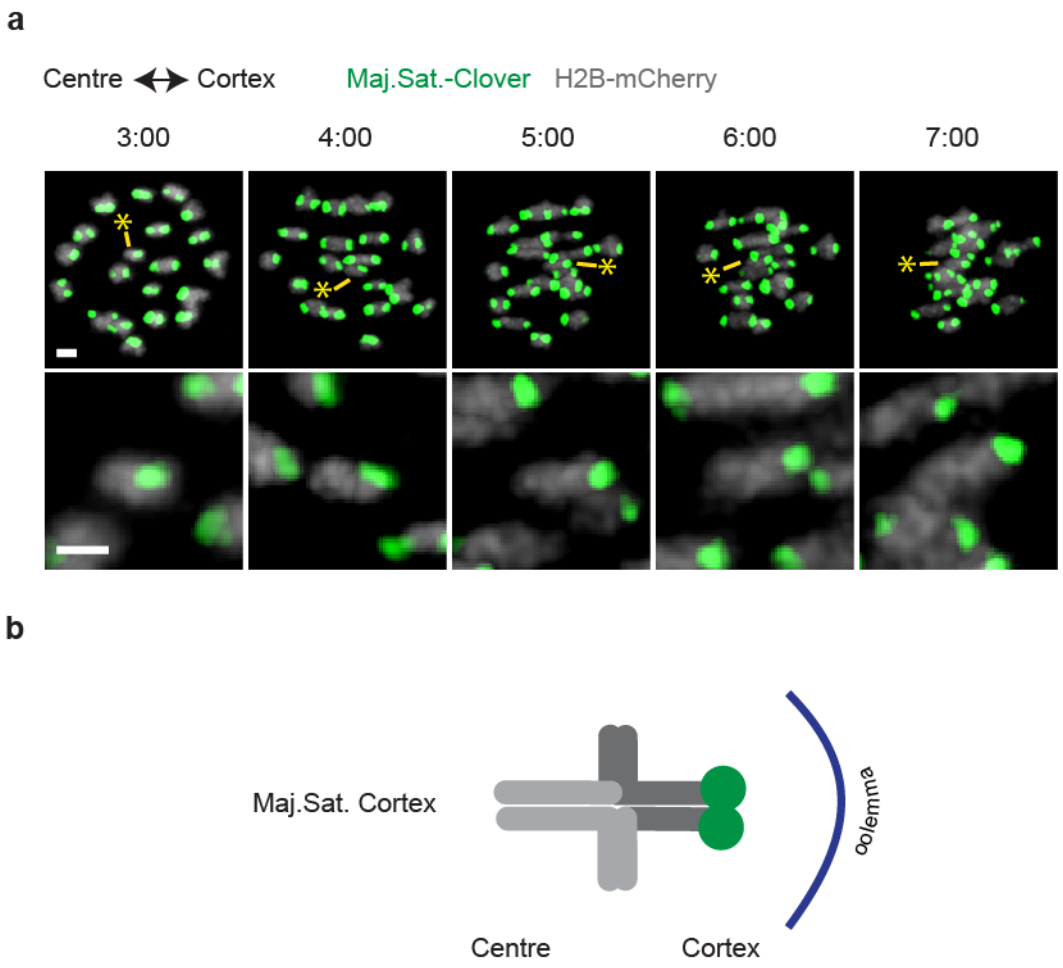

Figure 4.5 Larger major satellite DNA towards cortex initially can keep initial direction.

(a) Representative images show Chromosome 17 was tracked by time-lapse imaging during meiosis I. The large Major satellite DNA shows consistent cortical direction (Maj.Sat Cortex). Overview images show the position of Chromosome 17 (yellow asterisk, top). Enlarged images show the consistent direction of bivalent (bottom). Scale bar: 2 µm. Time from NEBD. **(b)** Schematic shows Maj.Sat Cortex direction. Green: Major satellite-mClover. Grey: H2B-mCherry (Chromosomes).

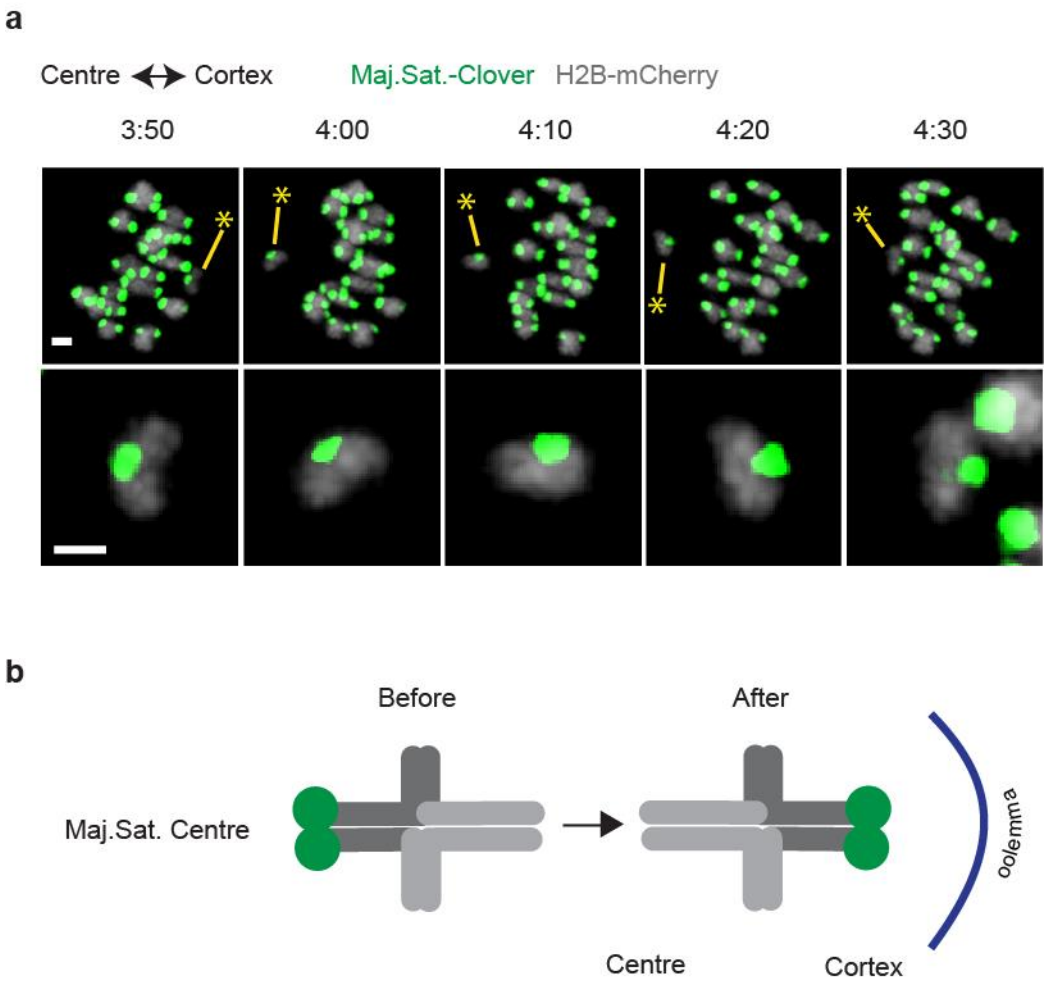

Figure 4.6 Larger major satellite DNA towards centre initially can be reoriented.

(a) Representative images show Chromosome 17 was tracked by time-lapse imaging at prometaphase. The large Major satellite DNA with Maj.Sat Cortex direction initially was changed to Maj.Sat Centre. Overview images show the position of Chromosome 17 (yellow asterisk, top). Enlarged images show the process of bivalent rotation (bottom). Scale bar: 2µm. Time from NEBD. **(b)** Schematics shows Maj.Sat Centre direction was reoriented to Maj.Sat Cortex during bivalents biorientation at prometaphase. Green: Major satellite-mClover. Grey: H2B-mCherry (Chromosomes).

The orientation appeared to be random as it did not differ significantly from the expected 50:50 ratio during this time window. Analysed in early prometaphase, larger major satellite DNA towards the cortex was observed in 41% of oocytes (n = 12/29) and the larger major satellite DNA towards centre was found in the rest 59% of oocytes (n = 17/29). Basically, according to the experiments, the initial directions of larger major satellite DNA were randomly formed (Figure 4.7a).

4.2.2 Maj.Sat. Cortex direction is favoured by Chromosome 17 in prometaphase

To understand when is the biased Maj.Sat. direction formed, behaviours of Chromosome 17 were recorded by time lapse-imaging. Directions of the larger major satellite were initially able to be defined at about two hours after NEBD because bivalents start to interact with the nascent spindle at this time. However, directions were then checked just before spindle migration initiation at 6 hours after NEBD. At this time only 24.1% of oocytes (n = 7/29) had the larger major satellite DNA orientated towards the centre whereas the other 75.9% (22 oocytes) were found to have a cortical direction (Figure 4.7b). This demonstrated that the biased Maj.Sat. direction was formed between 2 and 6 hours after NEBD, after nascent spindle formation, but before spindle migration.

I next focused on the behaviour of Chromosome 17 in the above established time-frame of biased orientation. The individual chromosome investigation by time-lapse imaging revealed some interesting behaviours in live oocytes.

Chromosome 17 with larger major satellite DNA initially facing towards the cortex (Maj.Sat. Cortex, Figure 4.5b) maintains its direction from the beginning to the end of meiosis I (Figure 4.5a, 4.7a). Even though the average bivalent re-orientates around three times during meiosis I (Kitajima et al., 2011), the direction of Chromosome 17 remained consistent with its initial direction.

When those chromosomes with the alternative initial Maj.Sat. Cortex direction were considered (Maj.Sat. Centre, Figure 4.6b left) the situation was different. Of the 17 examples of initial central orientation only 7 maintained their direction during meiosis I. The other 10 oocytes (58.8%) with an initial Maj.Sat. Centre direction were re-oriented to a Maj.Sat. Cortex direction during prometaphase (Figure 4.6, 4.7). This shows the

Maj.Sat. Cortex direction is preferentially chosen during prometaphase of meiosis I. Interestingly, in all 10 oocytes where this occurred, I found that this bivalent was reoriented between 2-6 hours after NEBD, which is before spindle migration (Reorientation duration: 54 ± 34.705 min) (Figure 4.7a).

4.2.3 Meiotic drive is dependent on Aurora Kinase activity

Comparison of initial and final orientation shows bivalent reorientation taking place during meiosis I. As discussed in the Introduction, bivalent reorientation happens because of K-MT attachment correction. Before all the bivalents are aligned properly, the kinetochore can be attached and released by microtubules until stable Kinetochore–Microtubule attachments formed. Kinetochore–Microtubule attachments correction in mouse oocytes is known to be Aurora Kinase B/C activity dependent (Kitajima et al., 2011; Schindler et al., 2012). I therefore hypothesised Aurora kinase might have a role in biased bivalents reorientation during K-MT attachment correction.

To examine whether the reorientation of Chromosome 17 depends on AURKB/C, the activity of AURKB/C was inhibited in mouse oocytes maturation. Oocytes were cultured with Aurora Kinase inhibitor ZM447439 at 2.5 hours after NEBD to decrease the activity of AURKB/C (Yun et al., 2014). Bivalents biorientation and alignment were recorded from 2.5 hours after NEBD and the direction of larger major satellite DNA in Chromosome 17 was tracked and examined.

Interestingly, with ZM447439 treatment, the reorientation of Chromosome 17 was blocked and most of their orientations (87.5%, 21/24 oocytes) were constant from beginning to the end of meiosis I (up to 9 hours from NEBD, Figure 4.9a). With larger major satellite DNA direction analysis, the ratios of initial and final Maj.Sat. Cortex direction were almost the same (41.7% vs 45.8%, Figure 9c). Meanwhile, anaphase was much earlier than in the control group consistent with Aurora Kinase inhibition (Chapter 4.3.2) bypassing the SAC, as which has been reported previously (Lane et al., 2010).

However, a pharmacological approach such as that adopted with ZM447439 is subject to off-target effects. To determine if the same observations on bivalents could be reached by a non-pharmacological method a dominant negative mutant of AURKC was used to decrease the activity of AURKB/C specifically on the centromere (Nguyen and

Schindler, 2017; Schindler et al., 2012). The efficiency of the AURKC dominant negative construct was also tested by its ability to shorten oocyte maturation. The AURKC Dominant Negative construct accelerated the time of maturation, by virtue of SAC inhibition, providing an early anaphase I compared with control group (Control 8.5 ± 0.1h, 12 oocytes; AURKC DN 6.8 ± 0.1h, 18 oocytes; ****: P<0.0001).

GV oocytes were microinjected with AURKC dominant negative mutant and then arrested for two hours before maturation. The orientation of Chromosome 17 was tracked from NEBD to anaphase of meiosis I. The directions of larger major satellite DNA were initially observed and defined at about two hours after NEBD and the directions were completely constant with initial directions from NEBD maintained throughout meiosis I, to anaphase (30/30, Figure 4.9b). The direction of larger major satellite DNA was analysed, to compare the ratios of initial and final Maj.Sat. Cortex direction. These ratios were not changed at all during meiosis I (43.3% vs 43.3%, Figure 4.9c). These data support the conclusion that AURKB/C is essential for Chromosome 17 reorientation by correcting the Kinetochore - Microtubule attachments.

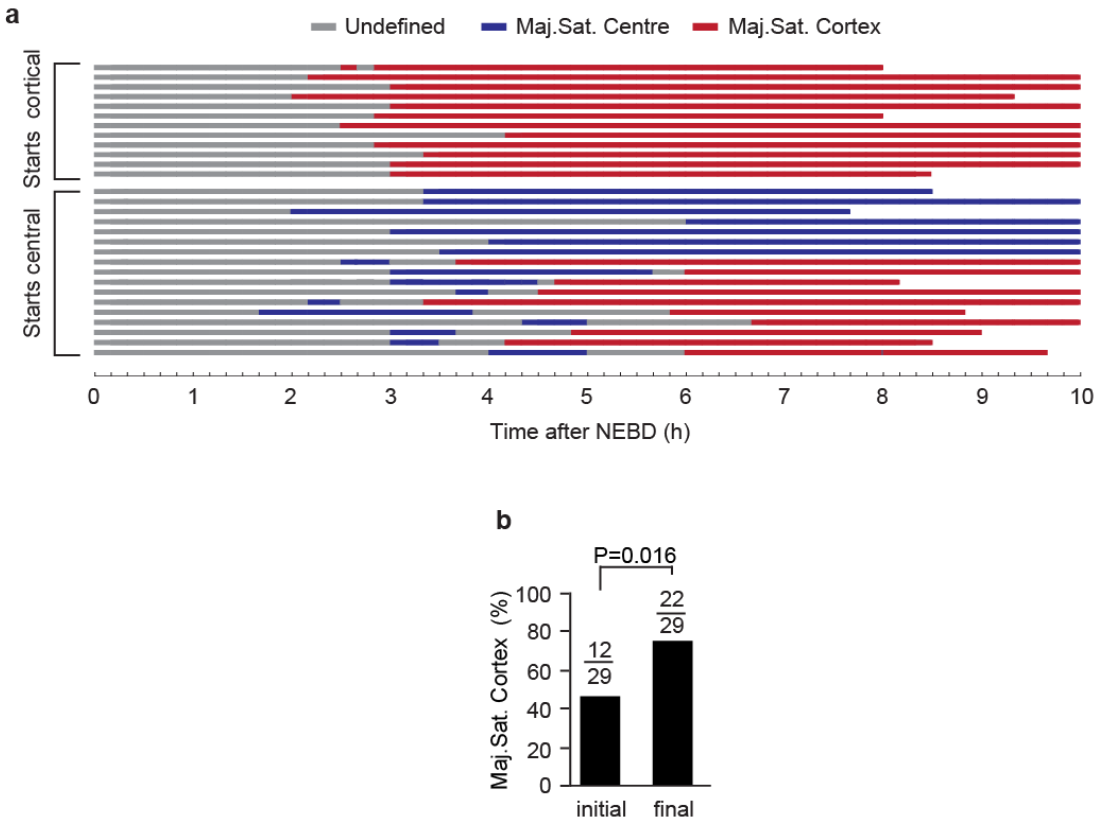

Figure 4.7 Larger major satellite DNA was preferentially reoriented to cortex.

(a) Time course of Chromosome 17 bivalent orientation (Maj.Sat. Cortex, red; Maj.Sat. Centre, blue; undefined, grey) from NEBD to anaphase or 10 h after NEBD in 29 oocytes. **(b)** Orientations of initial and final bivalent were measured at the time point of first bi-orientation (initial) and the frame immediately before anaphase (final) in 29 oocytes (P values from Fisher's exact test).

a

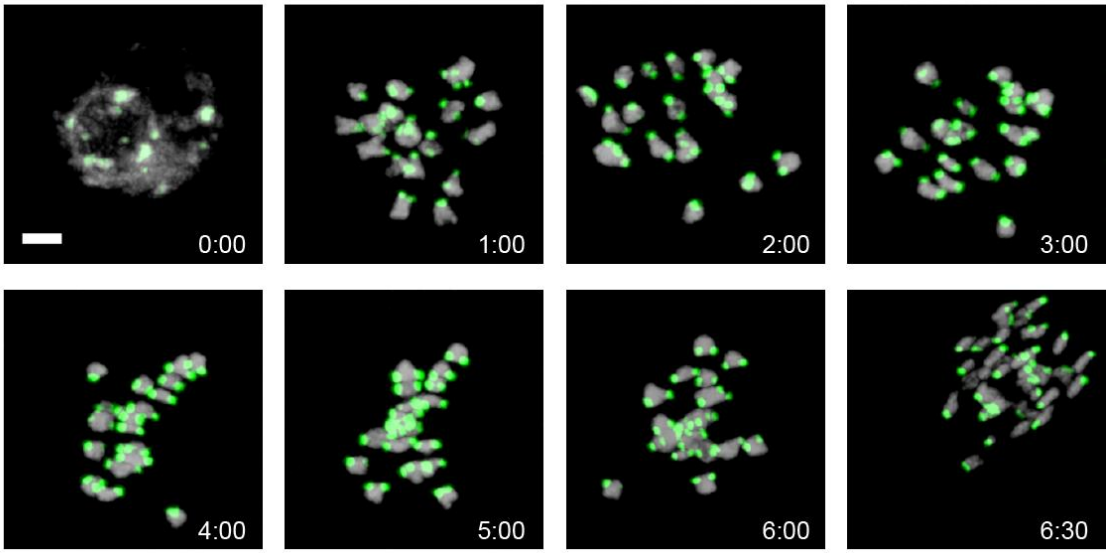

b

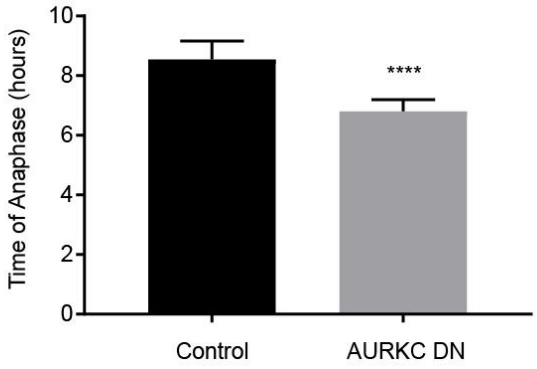

Figure 4.8 Early anaphase I is caused by AURKC DN.

(a) Non-alignment bivalents and early anaphase are shown in meiosis I by the time lapse imaging. Time from NEBD. Green: Major satellite-mClover. Grey: H2B-mCherry (Bivalents). Scale bar: 5μm. **(b)** Timepoint of anaphase is compared between contorl and AURKC DN group. (Control 8.5 ± 0.1h, 12 oocytes; Aurora B/C DN 6.8 ± 0.1h, 18 oocytes), ****: P<0.0001.

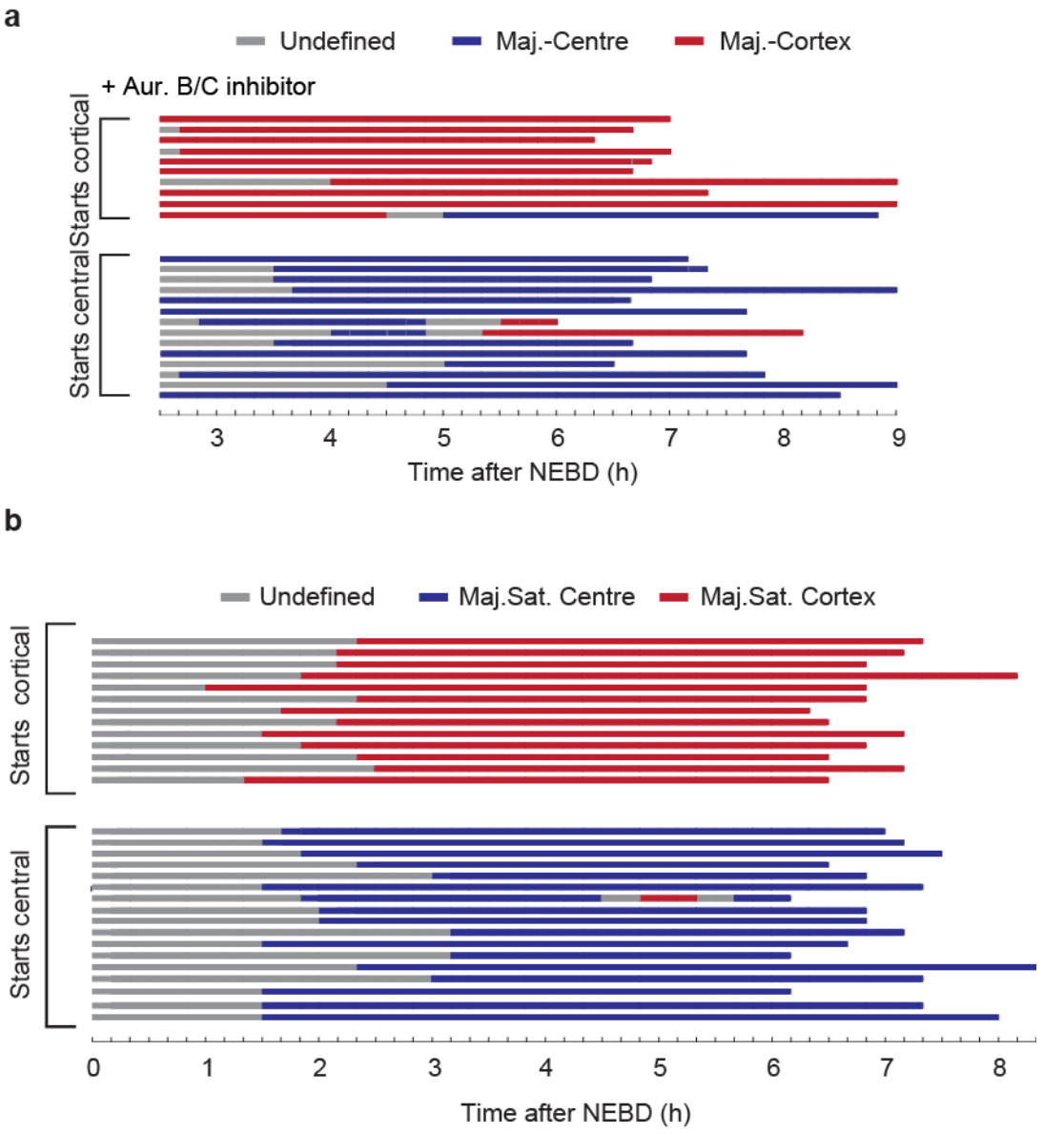
a
Undefined
Maj.-Centre
Maj.-Cortex
+ Aur. B/C inhibitor
Starts cortical
Starts central
3
4
5
6
7
8
9
Time after NEBD (h)
b
Undefined
Maj.Sat. Centre
Maj.Sat. Cortex
Starts cortical
Starts central
0
1
2
3
4
5
6
7
8
Time after NEBD (h)

c

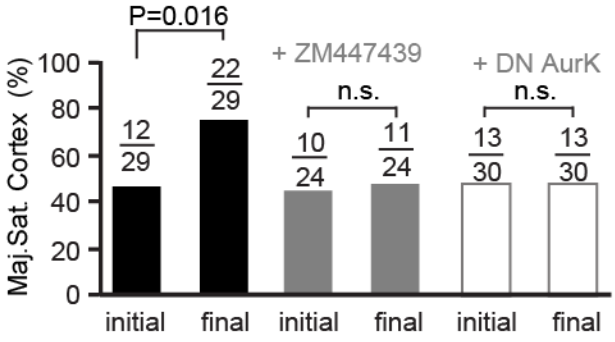
P=0.016
+ ZM447439
n.s.
+ DN AurK
n.s.
Maj.Sat. Cortex (%)
100
80
60
40
20
0
12/29
22/29
10/24
11/24
13/30
13/30
initial
final
initial
final
initial
final

Figure 4.9 Larger major satellite DNA reorientation requires Aurora kinase activity.

(a, b) Time course of Chromosome 17 bivalent orientation from NEBD to anaphase or 9 h after NEBD in oocytes treated with Aurora Kinase inhibitor **(a)** or DN-aurora kinase C construct **(b)**. Group separated by initial direction of larger major satellite DNA (Maj.Sat. Cortex, red; Maj.Sat. Centre, blue; undefined, grey). **(c)** Initial and final bivalent orientation, measured at the time of first bi-orientation (initial), and the frame immediately before anaphase (final) in untreated group and other groups treated with ZM447439 or DN-aurora kinase C construct (P values from Fisher's exact test).

4.3 Discussion

In this chapter, I examined the preferred direction of asymmetrical bivalents (Chromosome 17) and observed that Maj.Sat. Cortex direction is favoured. The Maj.Sat. Cortex direction was Aurora kinase dependent and formed at prometaphase at meiosis I. Here, I initially proposed the key role of Aurora kinase in meiotic drive. The individual bivalent time-lapse imaging recorded the process of chromosome reorientation for the first time. And then, I would like to discuss the principle of bivalents rotation and the function of Aurora kinase in it.

4.3.1 Bivalents rotation occurs frequently in prometaphase of meiosis I

In mitosis, the stable K-MT attachments are formed within a short time (several minutes) of spindle formation (Godek et al., 2015; Lampson and Cheeseman, 2011). Compared with mitosis, it takes much longer time to form stable K-MT attachments in meiosis I (6-12 h in mice, 15-20 h in humans) (Kitajima, 2018). In meiosis I, stable K-MT attachments are formed gradually and slowly through prometaphase and metaphase (Brunet et al., 1999; Davydenko et al., 2013; Gui and Homer, 2012; Lane et al., 2012). The delayed stable K-MT attachments formation is caused by gradually increased Cdk1 activity during prometaphase and metaphase I in oocytes (Choi et al., 1991; Davydenko et al., 2013; Gavin et al., 1994).

Interestingly, the experimental data shows biased chromosome transmission was determined by selective bivalent-reorientation in prometaphase of meiosis I. Previously studies have shown, with the attempts of biorientation, bivalents are likely rotated by K-MT attachment correction (Kitajima et al., 2011). Therefore, bivalent reorientation was investigated at prometaphase which is the main stage for bivalents biorientation and Kinetochore-Microtubule attachments correction.

Importantly, in B6CF1 mice, Chromosome 17 with an asymmetrical centromere and kinetochore (Chapter 3) is able to be reoriented by microtubules during K-MT attachments correction in prometaphase. Kinetochore from most organisms binds a bundle of microtubules (about 17 in mitosis for human) which are termed as kinetochore fibre (k-fibre) (Chen and Zhang, 2004; Salmon and Begg, 1980; Yen et al., 2013). Size of kinetochore and centromere were supposed to determine the binding

sites for k-fibres, larger kinetochore is assumed to provide more k-fibre binding sites (Iwata-Otsubo et al., 2017). The asymmetrical kinetochores of Chromosome 17 could therefore be providing asymmetrical microtubules' binding sites which may in turn provide differential force generation. During attachment correction, the bivalents could be rotated by such unbalanced microtubules attachments. After the wrong attachments corrected, bivalents with stable attachments are bi-oriented and the orientation of bivalents are selected and fixed (Figure 4.10). I predict from my data that there must also be an asymmetry in the spindle that allows preferential orientation of the bivalent (See chapter 5).

4.3.2 Anaphase is accelerated by Aurora Kinase activity decrease

AURKB/C activity can be decreased by AURKC Dominant Negative mutations which is competes with AURKB/C, which bind to INCENP (Ciferri et al., 2005), but not AURKA, which binds to Bora aurora kinase A activator (BORA) (Balboula and Schindler, 2014; Schindler et al., 2012). In my experiments, the oocytes microinjected with AURKC Dominant Negative mutations show much more non-aligned bivalents and earlier polar body extrusion (Figure 4.8). These special phonotypes revealed that AURKB/C activity decreased in oocytes by competitive inhibition as ZM447439 inhibition induced the same phenomenon (Lane et al., 2010) (Figure 4.9a). Interestingly, in my experiments with ZM447439 addition after NEBD, a few polar bodies were retracted by oocytes after polar body extrusion (Figure 4.11).

The acceleration of polar body extrusion suggests the SAC point was abrogated by AURKB/C activity decreasing. Without AURKB/C, some wrong Kinetochore-Microtubule attachments are able to evade the SAC causing the early chromosome segregation (Schuh and Ellenberg, 2007). Definitely, the shortened meiosis I came with non-alignment bivalents and lagging chromosomes, both of which suggest both an override of the SAC and the function of AURKs in correcting unstable K-MT attachments (Mihajlović and FitzHarris, 2018).

Interestingly, although the competitive inhibition by dominant negative mutations occurs before NEBD, polar body extrusion was still not prevented. However, ZM447439 stopped polar body extrusion by early treatment during oocytes maturation (before

NEBD) (Lane et al., 2010). This difference might be because AURKA is inhibited by ZM447439 treatment as well as AURKB/C.

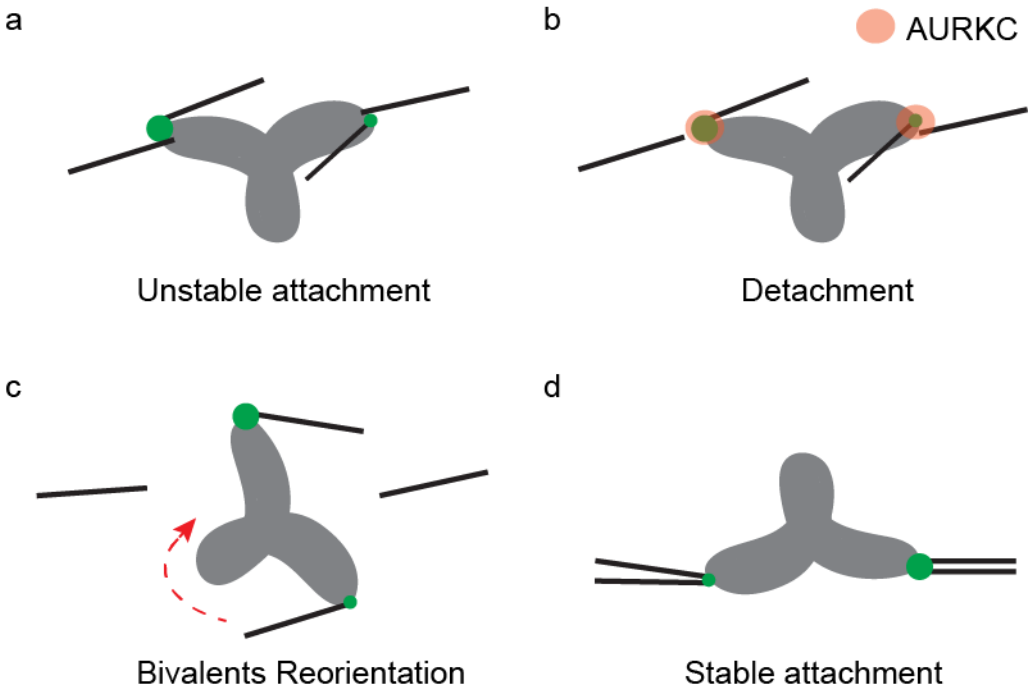

Figure 4.10 Representative schematic for bivalents reorientation.

(a) Schematic of unstable attachments at early prometaphase. **(b)** Schematic shows attachments are detached by AURKC. **(c)** Bivalents under unbalanced tension are rotated. **(d)** Bivalents orientation are fixed by stable attachments. Green: Kinetochore; Grey: Chromosome; Black: Microtubule.

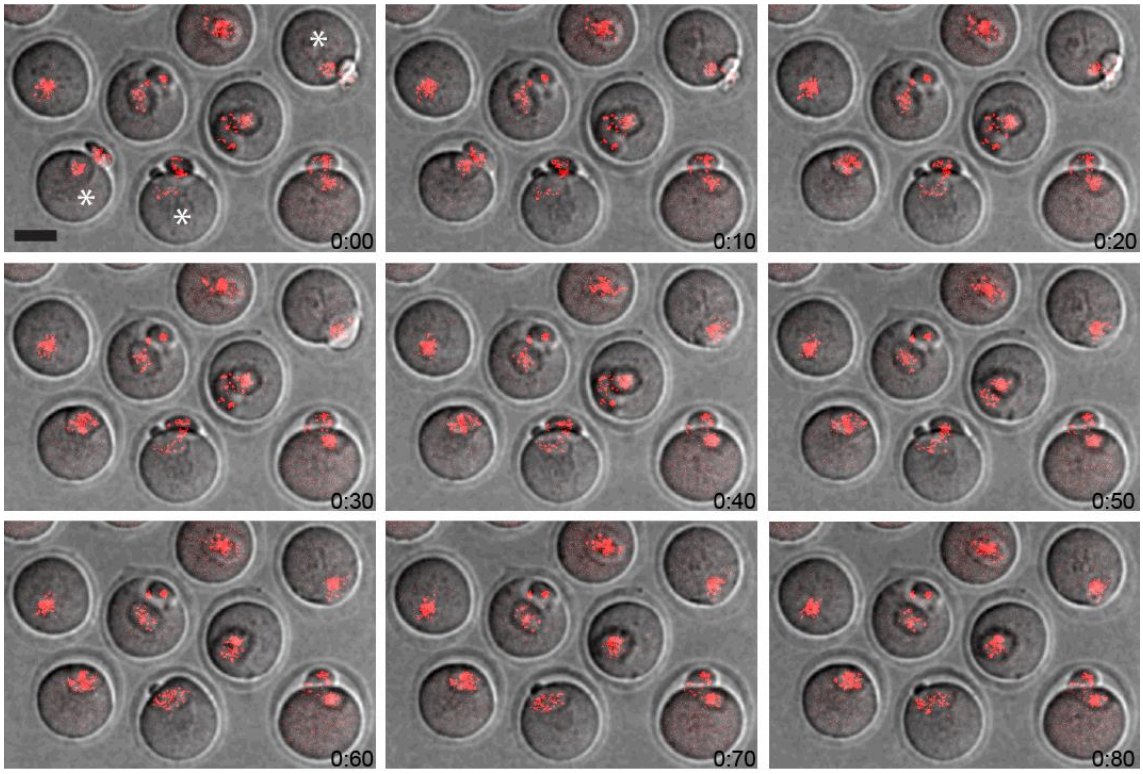

Figure 4.11 DN AURKC induced the polar body retraction.

Polar bodies were retracted after extruded by the oocytes with Aurora kinase activity decrease. Time from beginning of record. Green asterisk: Polar body retraction. Red: H2B-mCherry (Bivalents). Scale bar: 40µm.

Chapter 5: Examination of Kinetochore Tension on Homologous Chromosome Pairs during Meiosis I

5.1 Introduction

In chapter 4, I found that bivalents orientated in a non-random fashion on the MI spindle. To investigate the mechanism behind this biased bivalent reorientation, Kinetochore-Microtubule attachment (K-MT attachment) was investigated. K-MT attachment is critical to chromosomes alignment and segregation on the spindle. I was also interested to know if meiotic drive depended on the position of the spindle inside the oocyte, as spindle migration (from the centre to the cortex) is a prominent feature of meiosis I. As the spindle migrates away from the oocyte centre towards the cortex K-MT attachments can be distinguished by their directions: either cortical or central facing. Throughout this chapter, I investigated the asymmetrical K-MT attachments to explain the mechanism of biased bivalent reorientation. The tension on central and cortical facing kinetochores were compared to reveal the asymmetrical tension caused by microtubules. Tension is represented by kinetochore and centromere separations because outer kinetochores are stretched by microtubules.

5.1.1 Kinetochores are stretched by microtubules in K-MT attachments

The structure of K-MT attachment is very important to its function. Kinetochore proteins are recruited by a specific region of chromatin on the chromosomes. The inner kinetochore contains some highly conservative centromeric proteins, such as Cenp-A which is a variant of histone H3 and forms a centromere-specific nucleosome (Vafa and Sullivan, 2004). As a core component, it is involved in many centromeric proteins localization, particularly Cenp-I, Cenp-H, and Cenp-C (Trazzi et al., 2002). Cenp-C is another core component of the inner kinetochore/centromere and localized to it via two distinct domains the central and C-terminal regions (Przewloka et al., 2011). Meanwhile, the N-terminus is responsible for recruiting KMN proteins (KNL1/Spc105, Mis12 complex, and Ndc80/Hec1 complex) (Sanders and Jones, 2018). The Ndc80 complex is composed of four proteins (Ndc80, Nuf2, Spc25 and Spc24) which are localized at outer kinetochore.

Ndc80 interacts with microtubules and Spc25-Spc24 sub-complex binds the inner kinetochore (Ciferri et al., 2007).

Apart from the structure of K-MT attachment, timing is also important for tension measurements. To bi-orientate and align the bivalents on the equator of the spindle, outer kinetochores are stretched by microtubules until anaphase I. Before anaphase, kinetochores are attached and stretched in a stretching phase (2-4 hours after NEBD) and a stabilization phase (4-7 hours after NEBD) (Yoshida et al., 2015). Time during meiosis I for K-MT attachment stabilization is also provided by the SAC. In early prometaphase, Mad2 as a member of SAC is recruited to unattached kinetochores (Vallot et al., 2018). In late prometaphase (4 hours after NEBD), most Mad2 is removed from kinetochores after stable attachments formed (Hached et al., 2011; Wassmann et al., 2003). With stable K-MT attachments, bivalents are stretched by microtubules, and kinetochores are under tension. Therefore, the attachments are stable at 4-7 hours after NEBD, which provides a window for tension measurements.

5.1.2 The spindle is formed in the centre of oocyte and migrates to cortex in MI

To understand if the tension on K-MT attachments can be affected by spindle relocation, in this chapter I performed some examination of it in relation to spindle migration. Previous research has suggested that chromosomes can move to the cortex without the spindle structure (Guillaud et al., 2002; Li and Albertini, 2013; Longo and Chen, 1985). This research has demonstrated that chromosome migration is not microtubule cytoskeleton dependent but is instead actin dependent. Meanwhile, an asymmetrical force on the spindle structure is supposed to be the reason for spindle migration during oocyte maturation (Li and Albertini, 2013). Previous research has demonstrated the importance of actin in spindle migration (Van Blerkom and Bell, 1986; Longo and Chen, 1985), with Formin-2, a filamentous actin (F-actin) nucleating protein, being key. Formin-2 belongs to the Formin protein family (Dumont et al., 2007b; Leader et al., 2002). F-actin only functions during the initiation of spindle migration and then such movement depends on cytoplasmic streaming, which is orchestrated by the ARP2/3 complex (Yi et al., 2013). In mouse oocytes, cytoplasmic streaming is initiated when the chromosomes are moved close to cortex (about 20μm) (Yi et al., 2013).

This chapter has used a number of pharmacological approaches to study the spindle. To test if the tension on kinetochores is affected by spindle position, cytochalasin was used to prevent spindle migration. Cytochalasin is widely used to depolymerize F-actin, which provides the pulling or pushing force to move the spindle in oocytes (Li and Albertini, 2013; Schuh, 2011). Cytochalasin B inhibits the actin filaments interaction and the actin polymerization rate (MacLean-Fletcher, 2004). Actin monomer assembly is inhibited at the filaments barbed ends, which decreases the polymerization rate (MacLean-Fletcher, 2004). Interestingly, inhibition with cytochalasin is reversible when oocytes are washed out and re-cultured in fresh media. For example, in oocytes, spindle migration can be stopped by cytochalasin and rescued by washing out the inhibitor (Azoury et al., 2009; Guillaud et al., 2002; Longo and Chen, 1985).

To confirm the tension on kinetochores is created by microtubules, nocodazole was used to depolymerize microtubules. Nocodazole is widely used as an inhibitor of microtubule polymerization. It shows little effect on the synthesis of DNA, RNA or protein, however, it is observed to interfere the process of microtubules polymerization and spindle structure maintenance. Therefore, nocodazole provides a reversible inhibition for cell cycle research (Brunet et al., 1999; Guillaud et al., 2002; Vasquez et al., 2013; Winston et al., 1995; Zieve et al., 1980). To investigate the role of microtubules in chromosome migration, nocodazole was added during oocyte maturation. Chromosomes can still move to the cortex without the spindle structure, which shows chromosome migration is microtubule independent (Chaigne et al., 2012; Li et al., 2008).

To understand if the tension on kinetochores is spindle structure dependent, monastrol was used to break the normal spindle structure and stop bivalent stretching. As a specific Eg5 inhibitor, monastrol inhibits microtubule-stimulated ADP release from Eg5 (Maliga et al., 2002), a Kinesin-5 family member, which is also termed as Kinesin family member 11 (KIF11). Without this microtubule motor protein, spindle formation and maintenance are disrupted (Sawin et al., 1992; Slangy et al., 2004). In the spindle, the interpolar antiparallel microtubules are connected by KIF11 through crosslinking and sliding overlapping (Kapitein et al., 2005). As a reversible inhibitor, the spindle cannot only be collapsed onto a single pole by its treatment but also rebuilt after inhibitor removal (Cochran et al., 2005; Huber et al., 2003; Maliga et al., 2002; Mayer et al., 1999; Wojcik et al., 2004).

Throughout this chapter, I examine the displacement of chromosomes relative to the time after NEBD in meiosis I. The role of microtubules and actin in chromosome migration were investigated and discussed.

5.2 Results

5.2.1 Meiotic spindle is accelerated to migrate to cortex 6 hours after NEBD

To understand the details of spindle migration, chromosome displacement was recorded by 3D time-lapse imaging. Chromatin and tubulin in mouse oocytes were visualized by expression of H2B-mCherry and α-Tubulin-GFP. Oocytes were arrested for 2 hours after microinjecting to express the fluorescent proteins. Then, chromosome migration was tracked by confocal microscopy.

To investigate the chromosome migration at the beginning of meiosis I, chromosome displacement was analysed from 0-3 hours after NEBD (Fig 5.1a). Chromosomes and microtubules were labelled, and overview imaged from the beginning of meiosis I. During this time period the nascent spindle was formed, consistent with prior observations (Schuh and Ellenberg, 2008) (Fig 5.1a). In order to track chromosome position with time, the fluorescent images were processed using an ImageJ macro to determine their centre of brightness over the time-lapse. Chromosome gravity centre migration was measured, but only random movement (less than 5 μm, average from 6 oocytes) was recorded immediately after NEBD (Fig 5.1b).

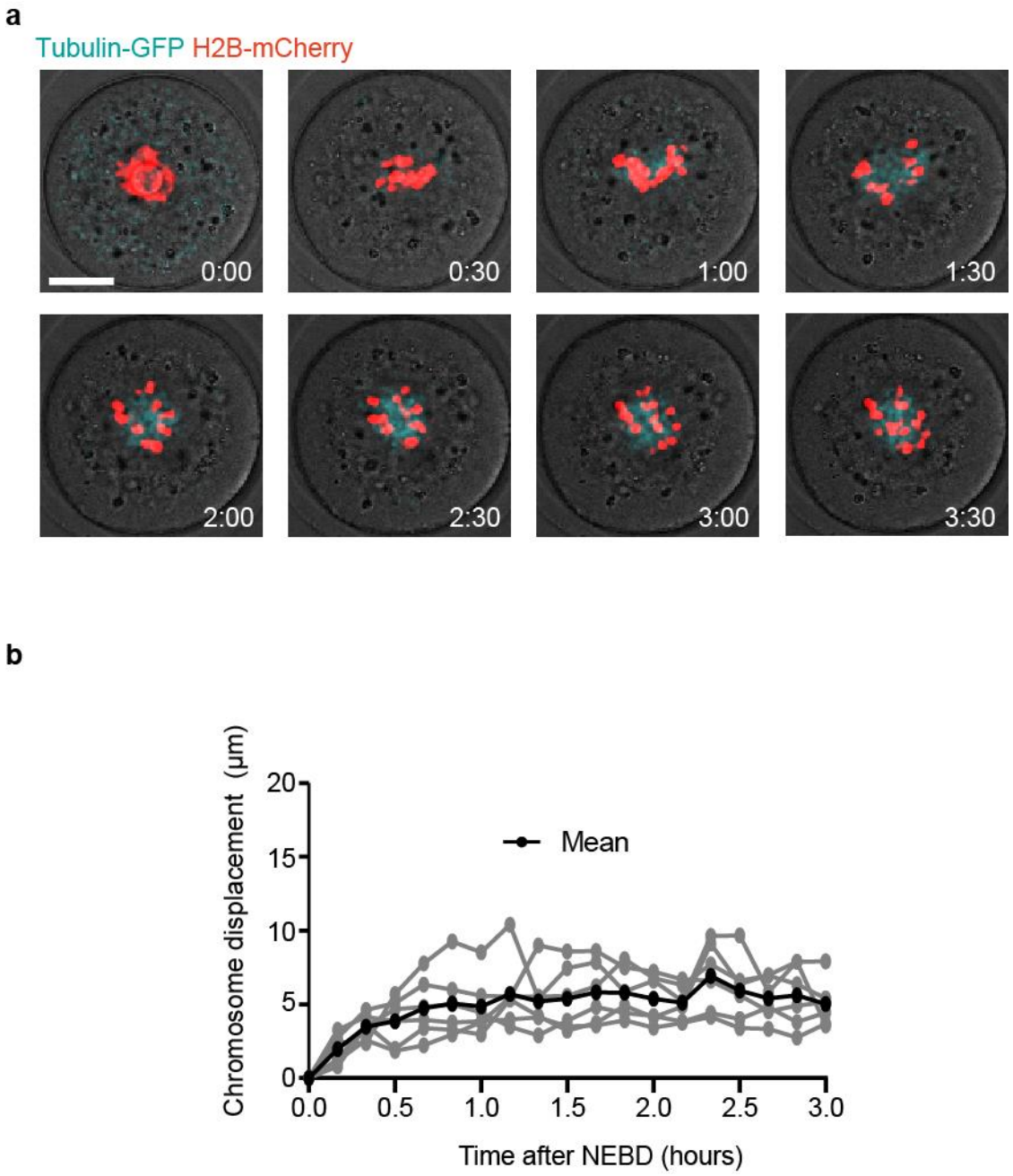

Figure 5.1 Chromosomes displacement in the first 3 hours after NEBD.

(a) Representative time-lapse images show that the spindle is assembled at the centre of oocyte in the first 3.5 hours after NEBD (H2B-mCherry, red; α-Tubulin-GFP, cyan). Times (h:mm) are relative to NEBD. Scale bar is 20µm. **(b)** Displacement of chromosomes in the first 3 hours after NEBD (grey, n=6 oocytes). Displacement is relative to the chromosome position at NEBD. The mean chromosome displacement shows little movement chromosomes in the first 3 hours after NEBD (black line). Times are relative to NEBD.

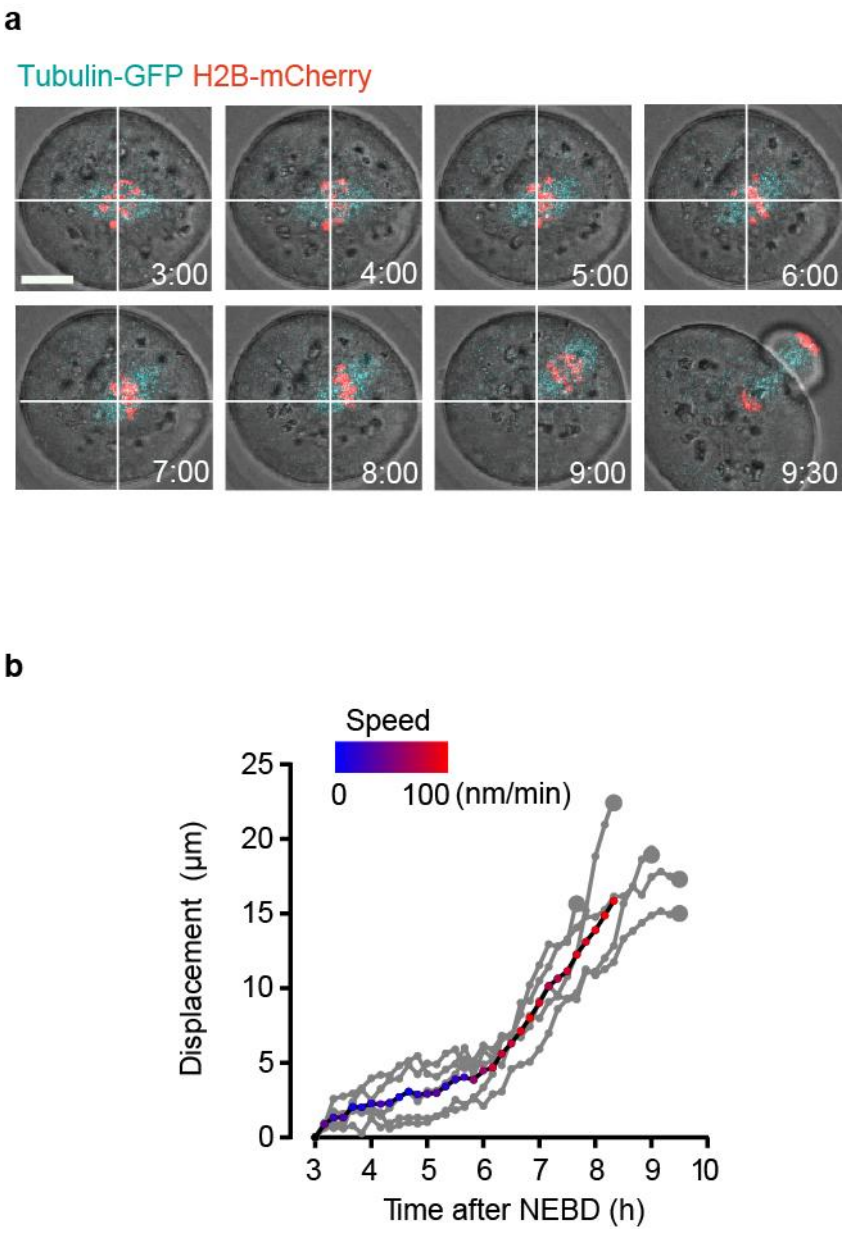

Figure 5.2 Chromosome displacement after 3 hours from NEBD.

(a) Representative time-lapse images show that the spindle migrates from the centre to the cortex of oocyte after 3 hours of NEBD (H2B-mCherry, red; α-Tubulin-GFP, cyan). Times (h:mm) are relative to NEBD. White cross shows chromosome centre of mass at 3:00. Scale bar is 20µm. **(b)** Displacement of chromosomes from 3 hours after NEBD to anaphase (grey, n=5 oocytes). Displacement is relative to the starting image. The red/blue line represents the mean displacement of chromosomes, with speed colour coded as indicated (blue=0nm min^{-1}, red=100nm min^{-1}). Times are relative to NEBD.

The spindle was assembled in the centre of oocytes at about 3 hours after NEBD when the bivalents were not aligned. Chromosome centre of gravity was measured and analysed from 3 hours after NEBD to anaphase, relative to its initial position. Chromosomes migrated by a small amount and with low speed (0–3nm/min, blue) between 3 hours to 6 hours after NEBD (Fig 5.2a, b). In this period, chromosomes migrated only 2-7μm in five individual oocytes. From 6 hours after NEBD, chromosome migration was accelerated and moved progressively towards the cortex (migration distance: 10–20μm, n=5) at higher speed (7–100nm/min, red) (Fig 5.2a, b). These measurements and observations are consistent with previous published work (Li et al., 2008).

5.2.2 Proper chromosome migration requires both actin and microtubules

To confirm the role of F-actin in spindle migration, cytochalasin B was added as an actin inhibitor before oocyte maturation. Chromatin and tubulin in mouse oocytes were visualized by H2B-mCherry and α-Tubulin-GFP expression. Chromosome migration was recorded by 3-D time-lapse imaging from NEBD to anaphase I (Fig 5.3a). The average chromosome displacement (Black; Fig 5.3b) is less than 5 μm (1.3-4.5μm) from NEBD and the direction of movement is random (Fig 5.3). It shows that chromosome migration is actin dependent, which is consistent with earlier research (Guillaud et al., 2002).

Previous research has found that microtubules are not involved in migration of the meiosis I spindle (Guillaud et al., 2002). To confirm this, nocodazole (1μM) was used as a microtubule inhibitor and was added 10 minutes before oocytes in vitro maturation. Chromosome migration was recorded by 3-D time-lapse imaging. The spindle was not able to form with nocodazole treatment and chromosomes were gathered without microtubules attaching after NEBD.

Compared with a slow central spindle formation in control oocytes (Fig 5.2), following nocodazole addition chromosomes started migration immediately after NEBD (0 hour from NEBD) and moved to cortex at much higher speeds (Figure 5.4, Average speed : 0.2 μm/min, $P<0.001$, t-test, 9 oocytes). As a consequence of this earlier and speedier migration, chromosomes arrived at the cortex at about 2 hours after NEBD (Figure 5.4), which is much earlier than the untreated control group (Fig 5.2, more than 7.5 hours) ($P<0.001$, t-test, 9 oocytes). Polar body extrusion was blocked by nocodazole treatment,

because chromosomes failed to separate without microtubules (n=0/9 oocytes extruded a polar body). Therefore, the chromosome migration is initiated much earlier and the speed is accelerated by microtubule disruption.

To investigate the function of microtubules in spindle migration, a low dose of nocodazole (25 nM) was used to treat oocytes throughout maturation. This low dose of nocodazole was not enough to disrupt all microtubules but was able to affect regular chromosome alignment (Lane and Jones, 2017). To find the influence of this dose of nocodazole on chromosome migration, chromosomes were labelled with H2B-mCherry and imaged by time-lapse imaging (Fig. 5.5a). With 25nM nocodazole treatment, chromosomes moved to cortex in two hours with an average speed of 0.18 μm/min (Fig. 5.5b, 12 oocytes), which is similar to 1μM nocodazole treatment. The average displacement of chromosome relative to their initial position at NEBD was 21.3μm (Fig. 5.5b, 12 oocytes). The polar body extrusion rate in 25nM nocodazole treatment was 30% (6 in 20 oocytes), which was much higher than 1μM nocodazole treatment (0%, 0 in 24 oocytes) ($P< 0.05$, Fisher's exact test).

To confirm the function of microtubules in chromosome migration, oocytes at 6 hours after NEBD were also treated with 25nM nocodazole. I found the chromosomes moved from the centre to cortex in 20 minutes (4 oocytes) after nocodazole treatment (Fig 5.6 a, b). However, in the untreated oocytes, it took 2 hours for chromosome migration (5 oocytes) from 6 hours after NEBD (Fig 5.6 c). Therefore these observations suggest both actin and microtubules are required for the proper spindle migration.

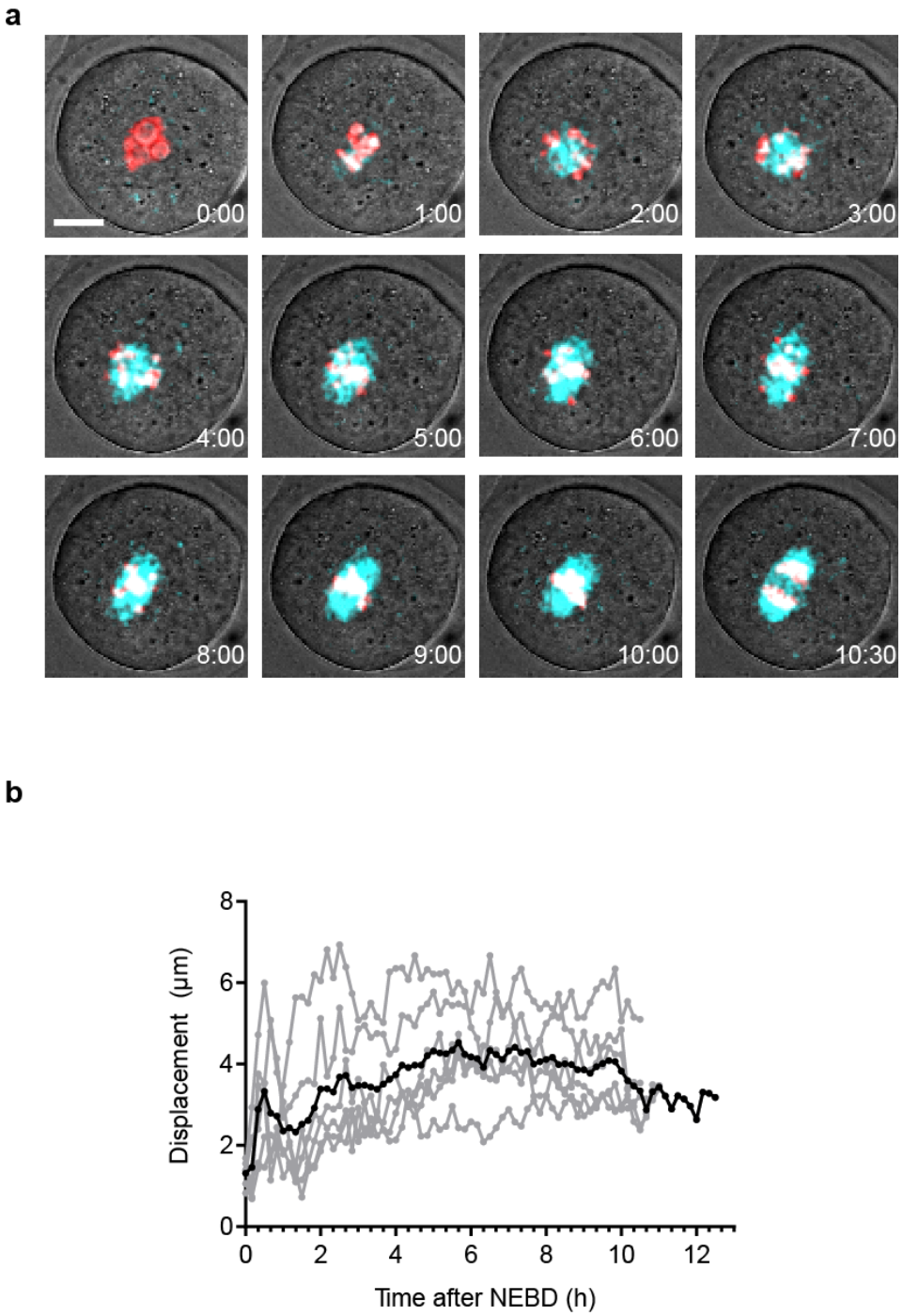

Figure 5.3 Chromosome displacement from NEBD with cytochalasin B treatment.

(a) Representative time-lapse images show that the chromosomes displacement from NEBD to anaphase (H2B-mCherry, red; α-Tubulin-GFP, cyan). Times (h:mm) are relative to NEBD. Scale bar is 20µm. **(b)** Displacement of chromosomes from NEBD to anaphase with cytochalasin B treatment (grey, n=6 oocytes). The black line represents the mean displacement of chromosomes. Times are relative to NEBD.

a

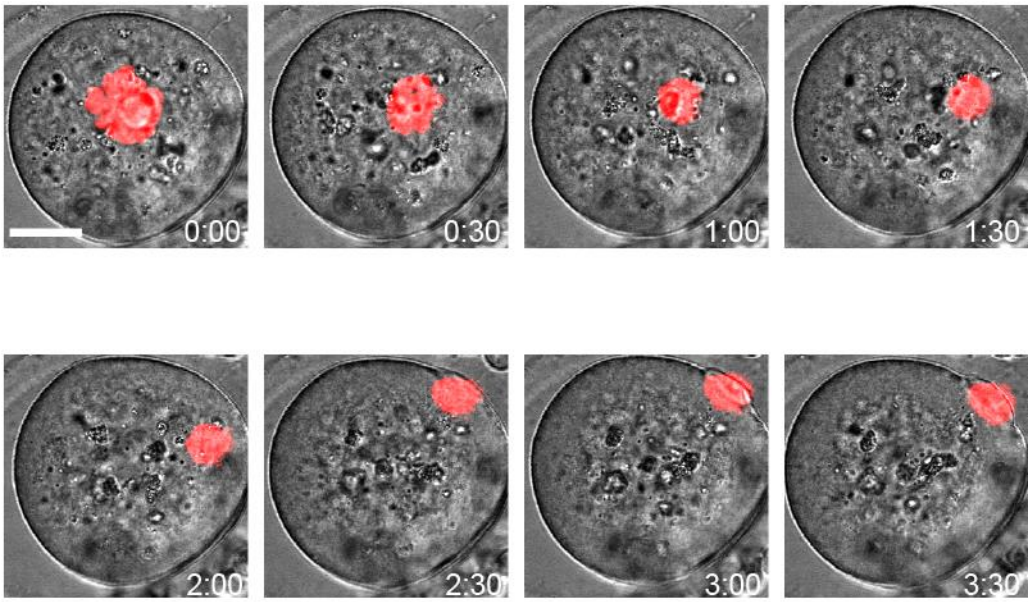

b

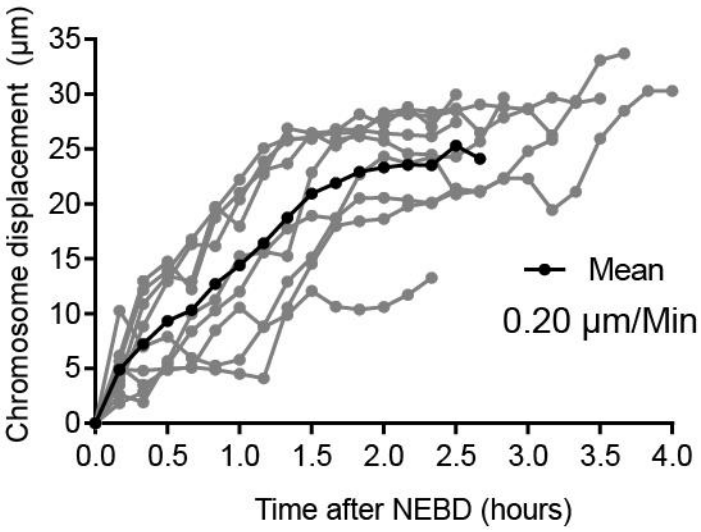

Figure 5.4 Chromosome displacement from NEBD with 1µM nocodazole treatment.

(a) Representative time-lapse images show the chromosome displacement from NEBD (H2B-mCherry, red). Times (h:mm) are relative to NEBD. Scale bar is 20µm. **(b)** Displacement of chromosomes within 4 hours from NEBD with nocodazole treatment (grey, n=9 oocytes). The black line represents the mean displacement of chromosomes. The average speed is 0.20µm/min. Times are relative to NEBD.

a

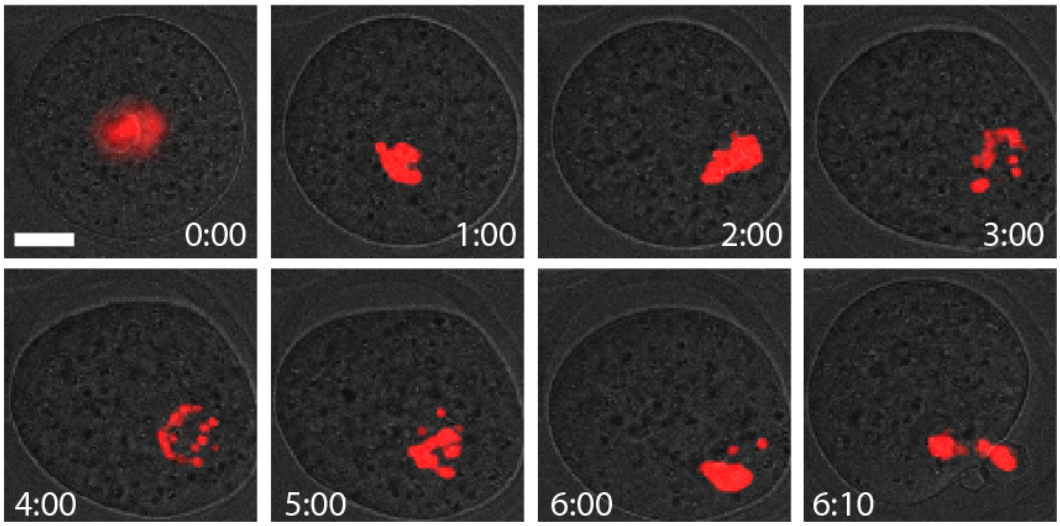

b

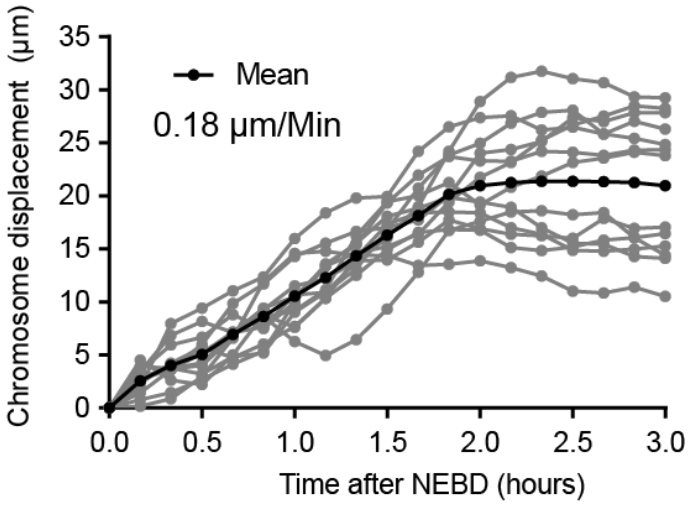

Figure 5.5 Chromosome displacement from NEBD with 25nM nocodazole treatment.

(a) Representative time-lapse images show the chromosome displacement from NEBD to anaphase (H2B-mCherry, red). Times (h:mm) are relative to NEBD. Scale bar is 20µm. **(b)** Displacement of chromosomes within 3 hours from NEBD with 25nM nocodazole treatment (grey, n=12 oocytes). The black line represents the mean displacement of chromosomes. The average speed is 0.18µm/min. Times are relative to NEBD.

5.2.3 Separation between centromere and kinetochore is created by microtubules

To reveal if the homologue paired kinetochores are under asymmetrical tensions, I developed a new method to measure and compare the tensions at a kinetochore. Theoretically, the outer kinetochore is attached and dragged away from its centromere by microtubules. Therefore, under the tension from microtubules, kinetochores might be separated from centromeres. I tested this hypothesis by measuring the separation between centromere and outer kinetochore in live oocytes.

To visualize kinetochore and centromere in live mouse oocytes, Spc24-mCherry and Major satellite-mClover were used to label the outer kinetochore and centromere respectively (Fig 5.7). GV oocytes were microinjected with cRNA of Spc24-mCherry and Major satellite-mClover, then matured for 4 hours after NEBD until kinetochore-microtubule attachment was established (Chapter 4). I assumed that the tension on the kinetochore can be taken as the centromere and kinetochore separation (C-Kt separation), such that larger distances are created by greater tension from microtubules (Fig 5.7a).

At 4 hours after NEBD, chromosomes were all in the centre of oocyte and 460 C-Kt separations were imaged by 3D confocal microscopy and measured individually (Fig 5.7). The separations were measured as the distance between the gravity centre of Spc24 and major satellite signals. C-Kt separations were also measured in nocodazole and monastrol treatment groups as a means of dissipating tension. Compared with untreated oocytes, the C-Kt separations were decreased by microtubule disruption significantly (Fig 5.8, $p < 0.0001$, one-way ANOVA with Tukey's post-hoc test, bivalent numbers are 242 in nocodazole treatment and 128 in monastrol treatment respectively), and the C-Kt separations were consistent in each oocyte with same treatment (Fig 5.8 b, c). It suggests the tension on kinetochore creates the C-Kt separations, which is microtubule dependent.

a

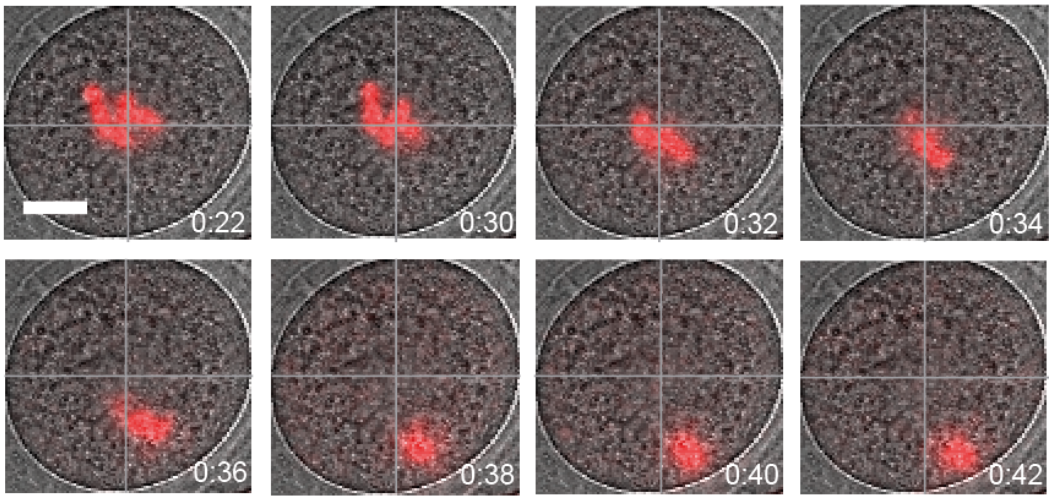
0:22
0:30
0:32
0:34
0:36
0:38
0:40
0:42

b

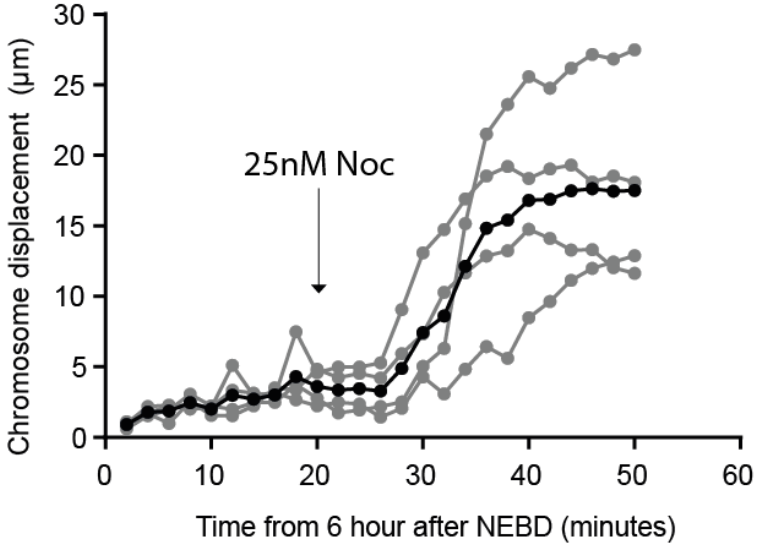
Chromosome displacement (µm)
25nM Noc
Time from 6 hour after NEBD (minutes)

c

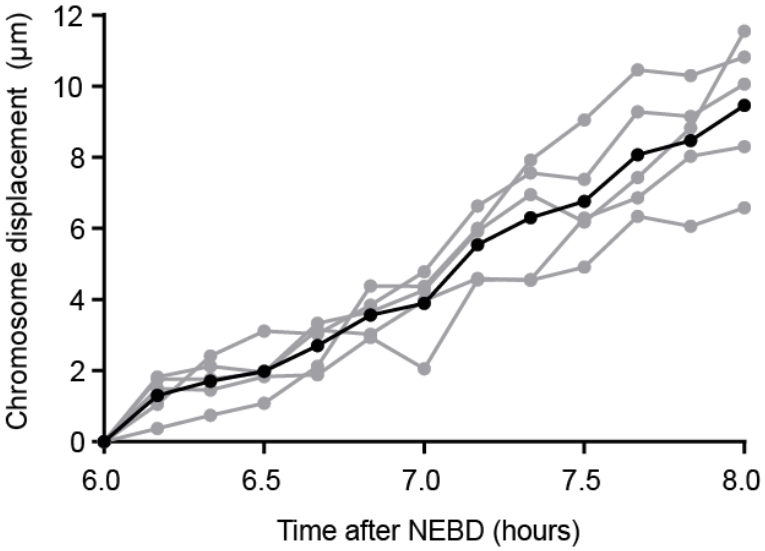
Chromosome displacement (µm)
Time after NEBD (hours)

Figure 5.6 Chromosome displacement from 6 hours after NEBD with 25nM nocodazole treatment.

(a) Representative time-lapse images show the chromosome displacement after 25nM nocodazole treatment at 6 hours after NEBD (H2B-mCherry, red). Treatment was performed at 0:20, times (h:mm) are relative to the start of imaging. Scale bar is 20μm. **(b)** Displacement of chromosomes within one hour from nocodazole treatment (grey, n=4 oocytes). The black line represents the mean displacement of chromosomes. Times are relative to the start of imaging. Treatment was performed at 20 minutes from imaging. **(c)** Displacement of chromosomes of untreated oocytes from 6 hours to 8 hours after NEBD (grey, n=5 oocytes). The black line represents the mean displacement of chromosomes. Times are relative to the NEBD.

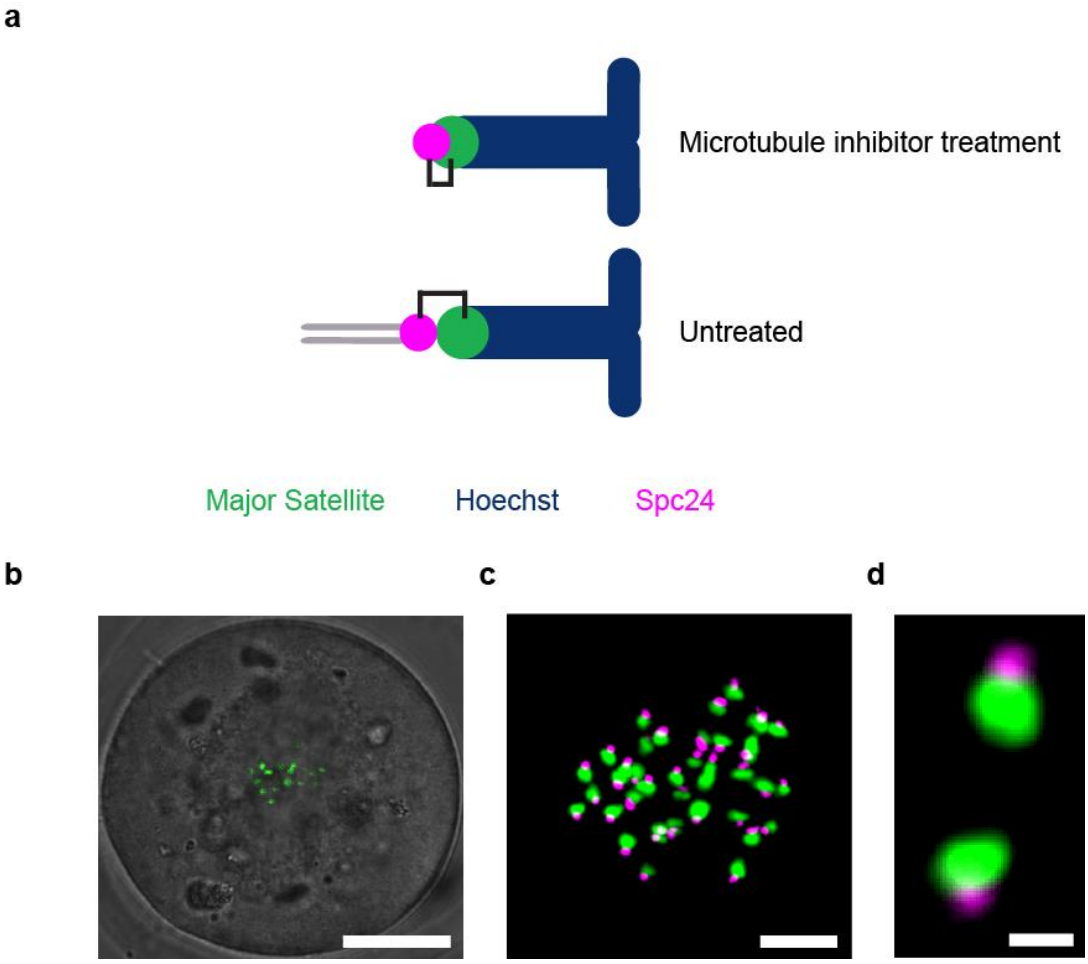

Figure 5.7 C-Kt separation measured at 4 hours after NEBD.

(a) Schematic of Centromere-Kinetochore separation at 4 hours after NEBD. Kinetochore is released by microtubules following inhibitor treatment (top); Kinetochore is attached by microtubules (bottom) **(b)** Representative overview image shows the localization of chromosome at 4 hours after NEBD. Green: Major satellite-mClover Scale bar is 20µm. **(c)** Paired centromeres show stretched Bivalents by microtubules at 4 hours after NEBD. Scale bar is 5µm. (d) Enlarged representative paired centromere and kinetochore. Scale bar is 1µm. (c, d: Green: Major satellite-mClover, Magenta: Spc24-mCherry).

5.2.4 Cortical kinetochores are under greater tension than central kinetochores.

Since oocytes have extremely asymmetrical divisions it seemed prudent to investigate if the tension on kinetochores differed from one side of the spindle to the other. Therefore, the homologue C-Kt separations on each side of the spindle were compared at 4 hours after NEBD for each bivalent (Fig 5.7d). I compared the C-Kt separations on one side of spindle with the other side in each oocyte and found significant greater C-Kt separations from one spindle side in 6 of 12 oocytes (Fig 5.9, 6 oocytes, Paired t-test, $P<0.05$). The spindle halves were not able to be defined as being central or cortical facing because at this time they were still in the centre of the oocytes (Fig 5.7b).

To compare the C-Kt separations on cortical and central kinetochore, oocytes labelled with Spc24-mCherry and Major satellite-mClover (Figure 5.10a) were imaged by 3-D confocal microscopy at 7 hours after NEBD when spindle migration occurs (Figure 5.10b). Homologue C-Kt separations were measured and compared (Figure 5.10). The C-Kt separation close to the oocyte plasma membrane were defined as cortical C-Kt separations, and the separations close to the centre of the oocyte were defined as central C-Kt separations (Figure 5.10).

At 7 hours after NEBD, C-Kt separations were measured individually in each oocyte, the cortical C-Kt separations were significant larger than central C-Kt separations in most oocytes (Fig.5.11a, paired t-test, 13 of 14 oocytes). The difference between cortical and central C-Kt separations was more significant when I pooled all 14 oocytes (cortex: 0.70 µm, centre: 0.46µm, $P < 0.0001$, ANOVA with Tukey's post-hoc test; Fig. 5.12). It suggests that cortical kinetochores are under greater tension than are central kinetochores.

To determine if the asymmetrical tension was created by spindle migration, oocytes were treated with cytochalasin B at 6 hours after NEBD before spindle migration and imaged by 3-D confocal microscopy at 7 hours after NEBD. The difference between cortical and central C-Kt separations also persisted when actin depolymerised by cytochalasin B (cortical: 0.68µm, central: 0.51µm, $P < 0.0001$, ANOVA with Tukey's post-hoc test; Fig. 5.12). The cortical C-Kt separations were larger than central separations in every tested oocytes (Fig.5.11b, paired t-test, 7 of 7 oocytes). It shows that it is the position of the spindle, and not its movement during migration that seems to cause the asymmetry.

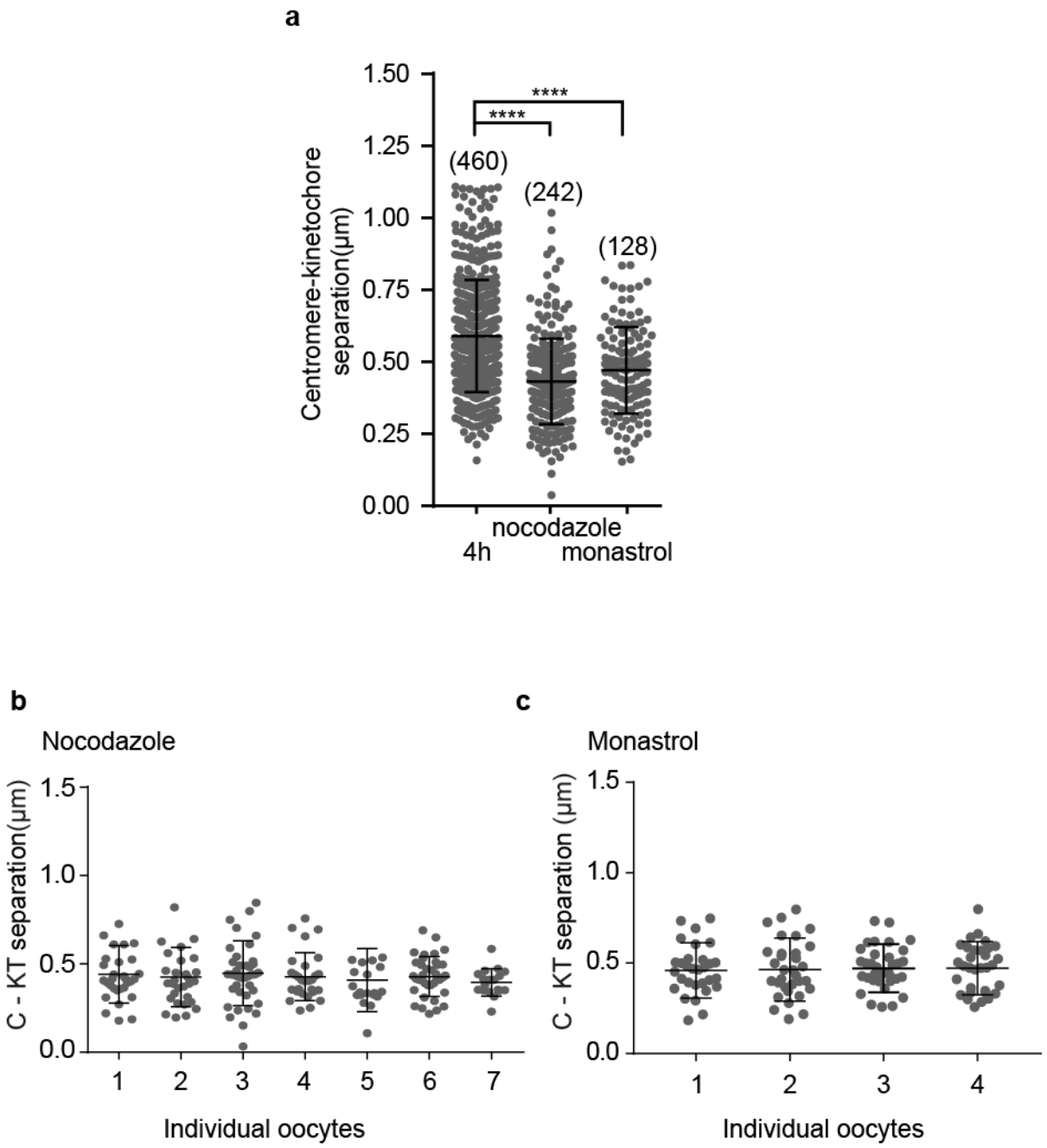

Figure 5.8 C-Kt separation is decreased by microtubule inhibitor treatment at 4h after NEBD.

(a) All C-Kt separations are plotted at 4 h after NEBD following the indicated drug additions (****P < 0.0001, one-way ANOVA with Tukey's post-hoc test, bivalent numbers are indicated. Measurements were made on 12, 7 and 4 oocytes, for untreated, nocodazole and monastrol groups, respectively). (b) C-Kt separations from each oocyte with nocodazole addition are plotted. (c) C-Kt separations from each oocyte with monastrol addition are plotted. Horizontal lines for each condition represent means and the error bars are s.d.

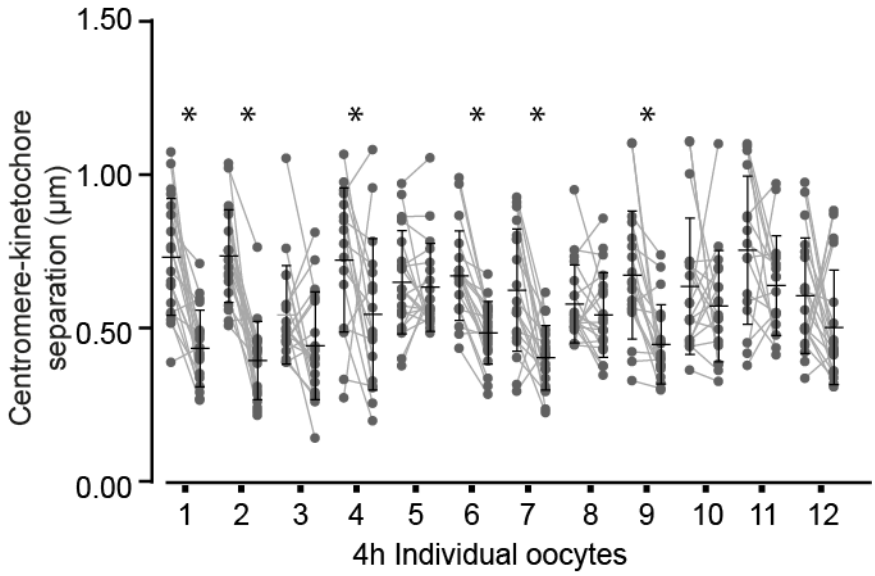

Figure 5.9 Bivalents experience different C-Kt separations between two sides of the spindle at 4 hours after NEBD.

C–Kt separations from individual oocyte at 4 h after NEBD are plotted (*P < 0.05, paired t-test, 12 oocytes are analysed, significant difference shows in 6 oocytes). Horizontal lines for each condition represent means and the error bars are s.d.

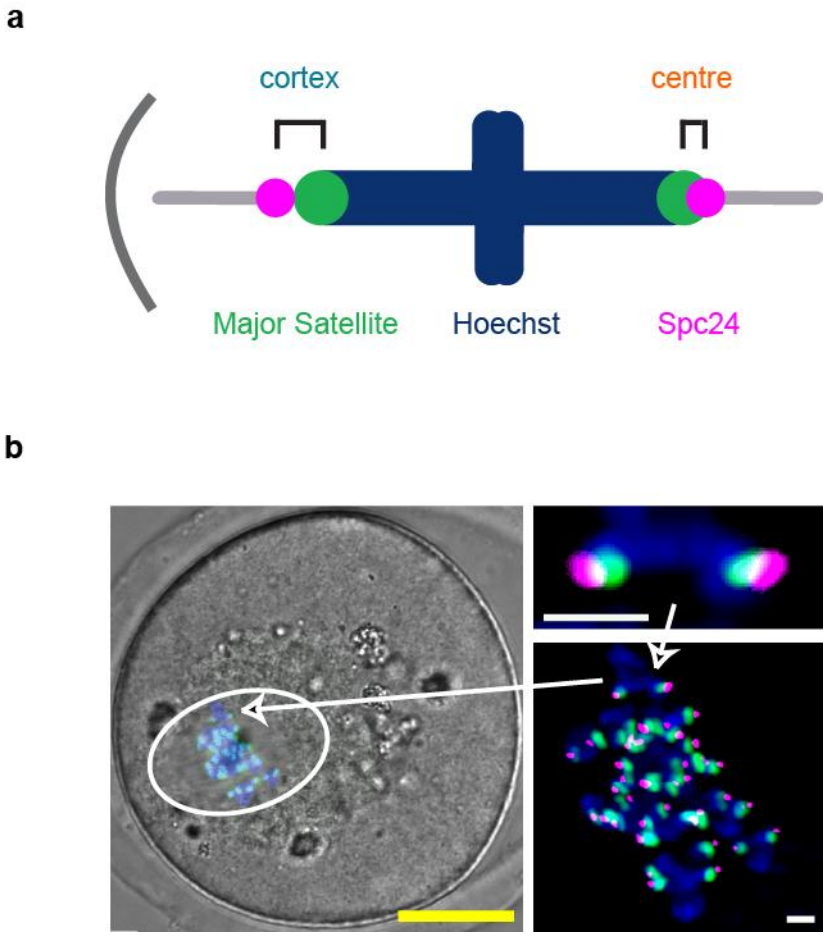

Figure 5.10 Cortical and central C–Kt separations are measured at 7h after NEBD.

(a) Schematic to show the location of the probes used and the measurement of central and cortical centromere–kinetochore (C-Kt) separation. **(b)** A representative image to show centromeres (Major satellite-mClover, green), kinetochores (Spc24-mCherry, magenta), and chromatin (Hoechst, blue) in oocytes. Arrow shows the same bivalent at different magnifications. Scale bars; yellow, 20 µm; white, 2µm.

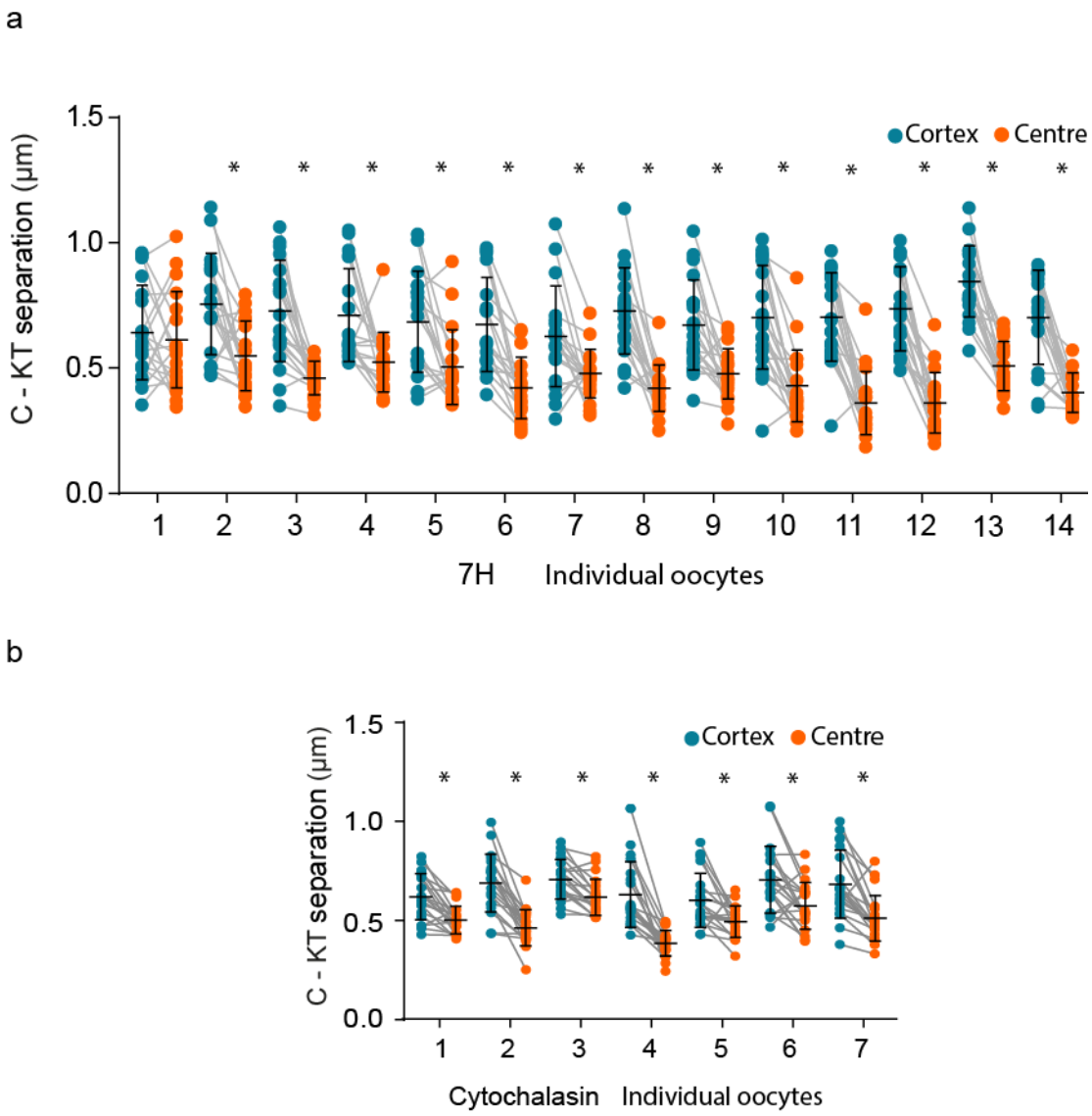

Figure 5.11 Cortical C–Kt separations are larger than central at 7 hours after NEBD.

(a) C–Kt separations from individual oocyte at 7 hours after NEBD are plotted (*P < 0.05, paired t-test, 14 oocytes are analysed, significant difference shows in 13 oocytes). **(b)** C–Kt separations from individual oocyte with cytochalasin treatment are plotted (*P < 0.05, paired t-test, 7 oocytes are analysed, significant difference shows in 7 oocytes). Horizontal lines for each condition represent means and the error bars are s.d.

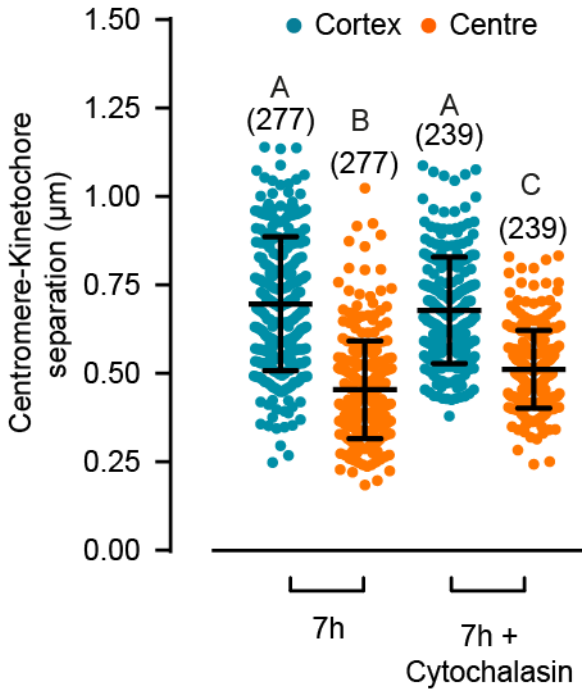

Figure 5.12 Bivalents experience greater C–Kt separation on the cortical side of the spindle.

Cortical (blue) and central (orange) C–Kt separations for oocytes at 7 h after NEBD, with or without prior treatment with cytochalasin B (for 1 h). Bivalent numbers are indicated, with measurements made on 12 oocytes with cytochalasin and 14 without. Differences between each group were tested using one-way ANOVA with Tukey's post-hoc test; different letters denote significant difference ($P<0.05$). Horizontal lines for each condition represent means and the error bars are s.d.

5.3 Discussion

In this chapter, I found proper spindle migration required both actin and microtubules in mouse oocyte meiosis I. I also found that very minor spindle migration occurred prior to 6 hours after NEBD, and a far more rapid and large movement taking place after 6 hours. The timing of this spindle migration could be brought forward, and the rate of migration increased by addition of low levels of nocodazole. It was also clear that asymmetrical tension exists between homologous kinetochores at 7 hours after NEBD, during spindle migration, and possibly also at 4 hours, before spindle migration. The cortical kinetochore was under greater tension than the central kinetochore, and this imbalance was actin independent. Therefore further investigation is required as to why the cortical kinetochore is under greater tension.

5.3.1 Meiotic spindle migration is accelerated at 6 hours after NEBD

Actin related spindle migration has been reported previously, but the mechanism of migrating initiation and acceleration were still unclear (Van Blerkom and Bell, 1986; Longo and Chen, 1985). In my research, the meiotic spindle was found formed in the centre of the oocyte (0-6 hours after NEBD) and moved to a subcortical location at high speed (6-9 hours after NEBD), which is consistent with previous results (Li et al., 2008).

Basically, a related study revealed two phase of spindle migration including the slow and random movement in the beginning followed by fast and directed movement (Yi et al., 2013). The random migration requires that the spindle be surrounded by actin which generates random directed force on chromosomes. Under the force from a random direction, the spindle moves randomly until it reaches a threshold distance close enough to the cortex. The ARP2/3 complex at the cortex is activated only when the spindle is close enough to the cortex, which initiates cytoplasm-streaming for accelerated migration (Li and Albertini, 2013).

In my experiments, spindle migration was initiated regularly at 5-6 hours after NEBD and then moved to cortex within a further 2 hours. In further research, it would be interesting to investigate why the spindle takes such a long time to active ARP2/3 complex at the cortex and initiate cytoplasm-streaming.

5.3.2 Proper spindle migration is also microtubule dependent

Movement of chromosomes from the oocyte centre to cortex is the most important step for cortical polarity establishment. According to previous research, spindle migration is supposed to rely only on actin but not microtubules (Guillaud et al., 2002; Li and Albertini, 2013; Li et al., 2008; Schuh and Ellenberg, 2008; Verlhac, 2011). Although the fact that chromosomes without microtubules are able to move to the cortex either together or in several clusters in meiosis I has been demonstrated (Guillaud et al., 2002; Longo and Chen, 1985), further research is still necessary to be performed in order to understand the details of this process.

However, in my research, I found that normal spindle migration is not only actin dependent but also influenced by microtubules. The chromosome migration in live oocyte was initiated and arrived much earlier and moved much faster when microtubules were depolymerised by nocodazole.

A simple explanation for this high-speed movement is that chromosomes without a spindle structure are getting smaller and are able to be much more easily pushed by F-actin. Without the spindle, bivalents are not stretched by microtubules but instead squeezed into a chromatin ball making them smaller (Guillaud et al., 2002; Li et al., 2008). The chromatin ball with smaller volume and less surface area may face less resistance which allows more rapid movement. In this condition, the acceleration is a result of spindle collapse. However, this simple model cannot explain the early initiation of chromosome migration (Figure 5.4, 5.5).

Another possible explanation for the high-speed movement is that chromosome movement is limited by microtubule interactions. In mouse oocytes, the meiotic spindle is assembled by acentriolar MTOCs which are localized at spindle poles. There are about 80 MTOCs with variable size in mouse oocytes at GV stage (Schuh and Ellenberg, 2007) and they are moved from the cortex to the perinuclear region by attracting each other through direct MTOC-MTOC contacts only prior to NEBD (Van Blerkom, 2006). After NEBD, MTOCs work as main microtubules nucleation and anchoring sites (Clift and Schuh, 2015) so that the MTOCs are connected with each other by microtubules which form the microtubule network (Schuh and Ellenberg, 2007). Therefore, the microtubules network may play a role in maintaining the spindle forming at the centre of the oocyte

and so delaying spindle migration. Microtubule-chromosome interaction is built immediately after NEBD, and able to keep chromosome in the centre. With depolymerised microtubules, chromosomes may lose this inhibitory control and so moved by F-actin immediately after NEBD.

Therefore, microtubules are not only essential for chromosome separation but also proper timing of spindle migration. With the results on the time points of spindle migration in this chapter, I will go on to focus on spindle assembly to investigate the asymmetry of microtubule distribution according to spindle migration.

Chapter 6: Greater MTOCs at Cortex May Create More Microtubules during Meiosis I

6.1 Introduction

In this chapter, I try to find out the origin of asymmetrical tensions (see Chapter 5) and then explain the mechanism of biased bivalents reorientation. An asymmetrical meiotic spindle was purported to be an important element to provide opportunities for centromere drive (see Chapter 1).

In most of mammalian somatic cells, the centrosomes are responsible for organising microtubules and forming the bipolar spindle (See Chapter 1.4). To assemble the bipolar spindle in newly generated cells, the centrosome is duplicated at S-phase and one copy transmitted to each new daughter cell during mitosis (Prosser and Pelletier, 2017; Vertii et al., 2016). To assemble the spindle for chromosome separation, microtubules are nucleated and emanated from the separated centrosomes, which are located at opposite spindle poles respectively (Tanenbaum and Medema, 2010). To perform the symmetric cell division, the symmetric mitotic spindle is formed by two identical centrosomes which are responsible for microtubule assembly (Tanenbaum and Medema, 2010).

However, compared with somatic cells, mammalian oocytes (e.g. mouse and human) have no canonical centriole-containing centrosomes and the mechanism of centrosome elimination is still unclear (Prosser and Pelletier, 2017; Vertii et al., 2016). In the mouse oocyte, acentriolar microtubule-organizing centres (aMTOCs), instead of centrosomes, assemble a meiotic spindle (Clift and Schuh, 2015; Mogessie et al., 2018; Schuh and Ellenberg, 2007). Without centrioles, the aMTOCs contain many pericentriolar material components, however, the mechanism of bipolar meiotic spindle assembly by multiple aMTOCs remains unclear. Although the function of MTOCs have been examined by previous research, the exact composition of MTOCs is still unclear. Only some basic components of centrosomes were observed, such as γ-tubulin and pericentrin (Carabatsos et al., 2000; Gueth-Hallonet et al., 1993).

In mouse oocytes, the fragmented aMTOCs are separated and clustered during bipolar spindle formation, without identical centrosomes, and the spindle poles are formed potentially unequal. I hypothesised that asymmetrical aMTOCs separation and clustering is important for asymmetrical tension because the aMTOCs are also involved in microtubule nucleation. Therefore, asymmetrical microtubules assembly on the meiotic spindle was a possibility to explain asymmetrical tension on paired centromeres (see Chapter 5).

In mouse oocytes, aMTOCs play a key role in meiotic spindle formation and maintenance. Meiotic spindle assembly requires aMTOCs proper organization to ensure bipolarization. Before NEBD, Polo-like kinase 1 (PLK1) decondense aMTOCs which are stretched and spread along the nuclear envelope. This process requires not only microtubules but also dynein to create forces on aMTOCs. After NEBD, aMTOCs are fragmented into multiple smaller structures by Kinesin-5 (Eg5) (Clift and Schuh, 2015; Luksza et al., 2013). Later the fragmented MTOCs are coalesced into two dominant clusters which go on to form two distinct spindle poles (analogous to the role of centrosomes in mitosis) before 3 hours post-NEBD (Schuh and Ellenberg, 2007). After the bipolar spindle forms, the clustered aMTOCs are responsible for maintaining the integrity of spindle poles (Kolano et al., 2012). Therefore, the aMTOCs are highly involved in meiotic spindle assembly.

According to the process of spindle poles formation, I proposed a hypothesis to explain the asymmetrical cell division. The migration of aMTOCs to spindle poles is a dynamic process which is random and self-organised. Therefore, aMTOCs are likely distributed asymmetrically on opposite poles (differ to mitosis with identical spindle poles) and this could generate imbalanced forces on bivalents. This phenomenon has been observed in cancer cells, where unbalanced centrosomes induce chromosome mis-segregation (Kwon et al., 2008).

In this chapter, to find out the reason for asymmetrical tensions on paired centromeres, the density of microtubules was compared between central and cortical spindle halves. The aMTOCs distribution was examined on both spindle poles during the whole of meiosis I, and the process of aMTOCs recruitment was analysed to investigate the origin of asymmetrical spindle poles. The asymmetrical aMTOCs distribution was supposed to be an explanation for asymmetrical microtubules assembly.

6.2 Results

6.2.1 Asymmetrical tubulin across the meiotic spindle in meiosis I

In Chapter 5, I observed asymmetrical stretch across the bivalents both when they were at the oocyte centre and off- centre (e.g. Fig 5.9-5.12). My hypothesis was that the asymmetry was generated by the meiotic spindle imparting unequal force on the chromosomes via their k-fibre attachments. I therefore first compared the spindle microtubules on the central and cortical sides of the spindle.

GV oocytes were microinjected with α-tubulin-GFP and H2B-mCherry and arrested for two hours to allow for fluorescent protein expression, α-tubulin-GFP tubulin intensity was then measured after spindle formation. The meiotic spindle was fully assembled within 4-5 hours of NEBD (See Chapter 5). Therefore, in my experiments, α- tubulin intensity was measured at 7 h after NEBD whilst the centre-weighted intensity of the H2B-mCherry signal was used to define the middle of the spindle. As the spindle had migrated towards the cortex at this time, it was possible to define the two spindle halves as being either 'cortical' (i.e. closest to the oocyte cortex) or 'central' (i.e. closest to the oocyte centre). The tubulin density of cortical half spindle was greater than the central half, which was consistent with the C–Kt distance asymmetry (Tubulin density ratio cortex/centre: 1.274, 95% CI: 1.217–1.332, n= 10 oocytes; Fig. 6.1b, c). The asymmetrical spindle suggests that the cortical half spindle assembles more microtubules (greater tubulin density), which may exert greater force to stretch kinetochores.

6.2.2 Asymmetrical MTOCs may organize the asymmetrical microtubules in meiosis I

To find the origin of asymmetrical microtubules density in meiotic spindle, I focused on the acentriolar MTOCs which are involved in microtubule nucleation in mouse oocytes. Cep192 was used as a marker for acentriolar MTOCs because this protein can provide a lower background than pericentrin during imaging (Clift and Schuh, 2015).

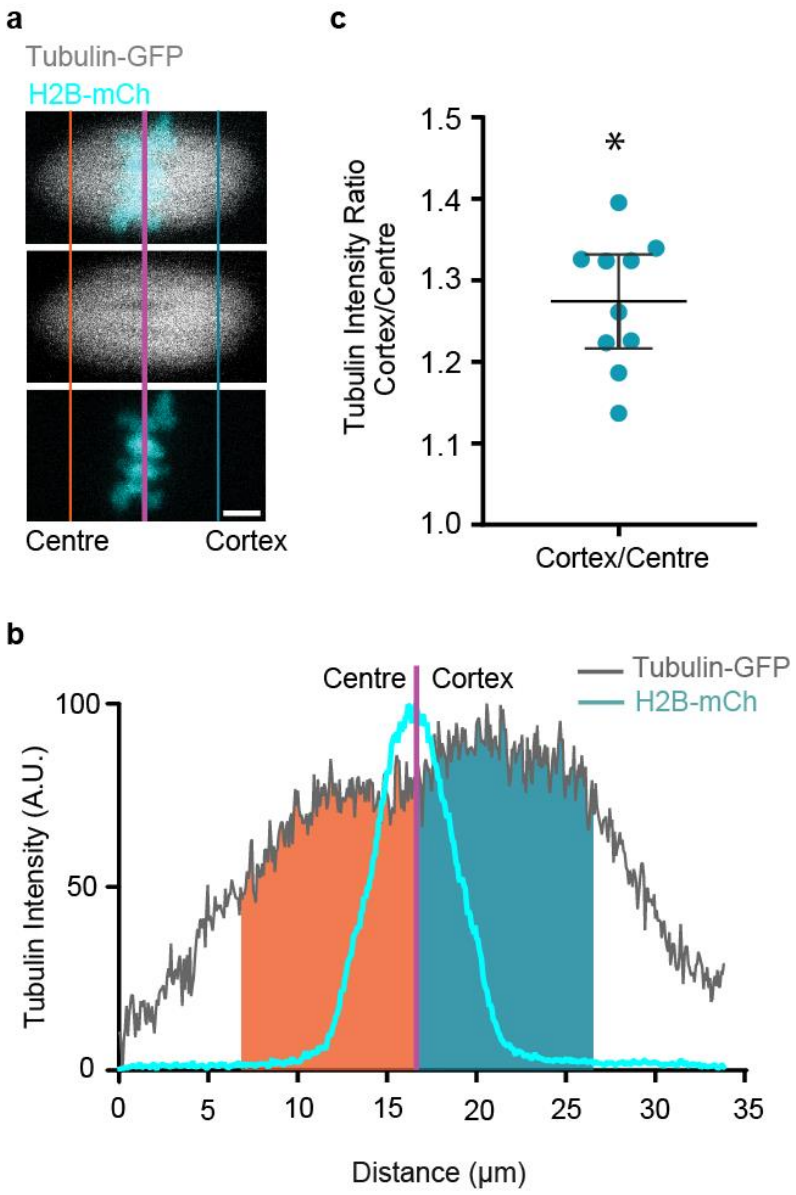

Figure 6.1 Oocyte spindle asymmetry in microtubule tubulin density.

(a) Representative image of microtubules (α-tubulin-GFP, grey) and chromatin (H2B-mCherry, cyan) in an oocyte at 7 h after NEBD. Purple line indicates mean-weighted position of the bivalents in the x axis; blue and orange lines indicate 10 µm distance on the cortical and central side of the bivalents, respectively. Scale bar, 5 µm. **(b)** Representative α-Tubulin intensity profile, in the x-axis, of the spindle (grey) and bivalents (cyan) shown in 'a'. Total α-tubulin intensity within 10 µm of the bivalents on the central (orange) and cortical (blue) spindles halves. **(c)** Cortical/central ratio of α-tubulin fluorescent intensity as shown in 'b' (mean 1.274). *P < 0.05, 95% confidence intervals shown from 1.217 to 1.332 (i.e. >1.0); n = 10 oocytes, combined from two independent experiments.

To follow the movement of acentriolar MTOCs, GV oocytes were microinjected with Cep192-GFP and H2B-mCherry. After two hours arrest for fluorescent protein expression, time-lapse imaging was performed to show the spindle pole formation. MTOCs were localized at the nuclear envelope just before NEBD, and then fragmented concomitant with NEBD. MTOCs were then clustered to form spindle poles by 3 hours after NEBD (Fig. 6.2). To investigate if the two spindle poles were asymmetrical, I measured the intensity of clustered MTOCs (Cep192-GFP) at both spindle poles. With oocyte maturation, the meiotic spindle migrated from centre to cortex at 5-6 hours after NEBD (Chapter 5). According to the spindle migration, spindle poles were defined as cortical pole (close to cortex) and central pole (close to centre) respectively. Spindle poles could not be categorised by this method at prometaphase before spindle migration, however I used time-lapse microscopy to track both spindle poles from NEBD to anaphase and thus could retrospectively assign the poles to central or cortical groups.

The integrated density of MTOCs at both cortical and central poles were compared from 3 hours after NEBD to anaphase, the period during which meiotic drive occurred. The integrated density of cortical MTOCs was much higher than central MTOCs from three hours after NEBD to anaphase (*$P < 0.05$, **$P < 0.01$, ***$P < 0.001$, ****$P < 0.0001$, n=11, paired t-test; Fig. 6.3). According to previous research, the volume of MTOCs is increased during their clustering (Clift and Schuh, 2015). To confirm the asymmetrical MTOCs distribution on meiotic spindle, the volume of two major clusters were also compared during meiosis. Larger MTOCs clusters were observed at cortical spindle poles from three hours after NEBD to anaphase (*$P < 0.05$, **$P < 0.01$, ***$P < 0.001$, ****$P < 0.0001$, n=11, paired t-test; Fig. 6.4), which suggests that more MTOCs are recruited to the cortical side of spindle during meiosis I. All these measurements and comparisons are consistent with asymmetrical microtubule recruitment during spindle formation.

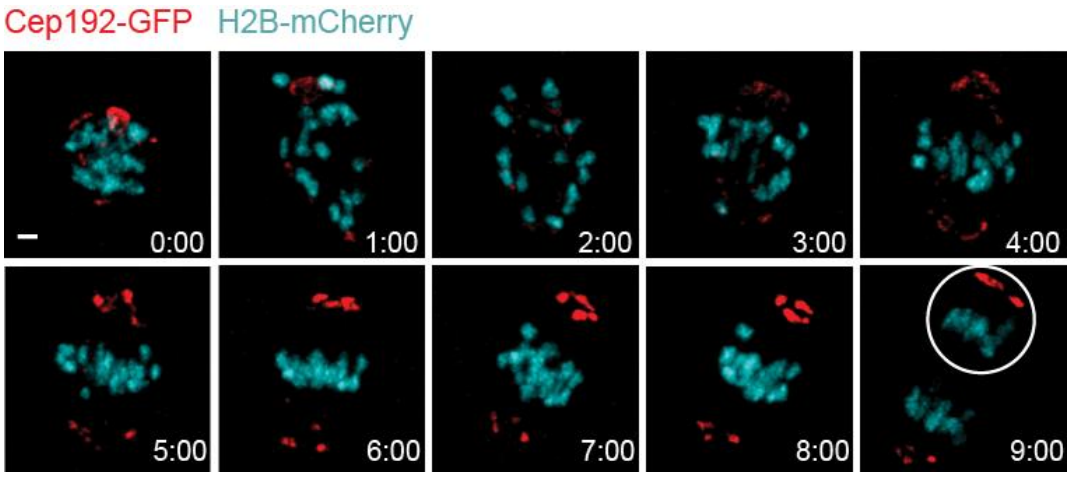

Figure 6.2 Representative time-lapse imaging to show asymmetrical MTOCs recuitment.

MTOCs in oocytes (n = 11, from three independent experiments) were shown by Cep192-GFP (Red) and bivalents were labled by H2B-mCherry (Cyan). Scale bar is 5 μm. Time from NEBD.

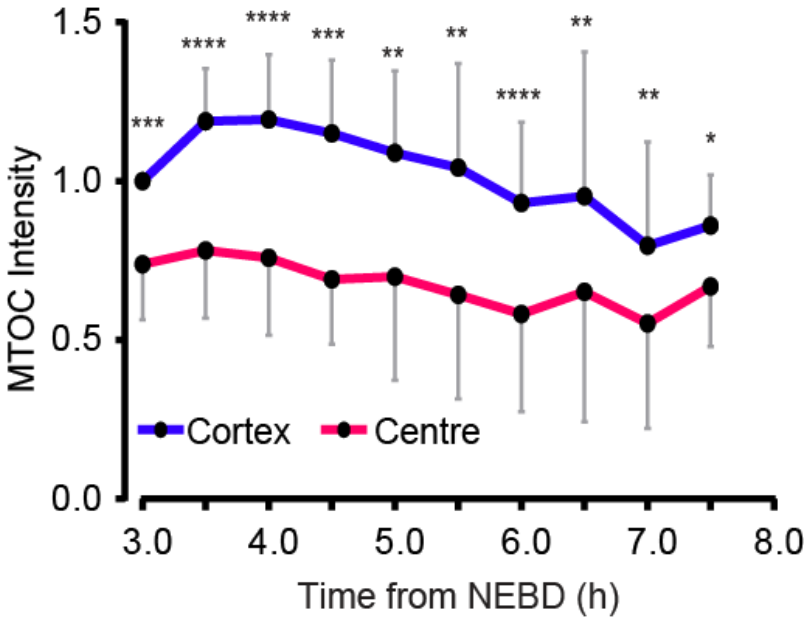

Figure 6.3 Cortical MTOCs fluorescence intensity is higher than central MTOCs.

The MTOC fluorescence intensity at both poles was calculated at 30 min intervals from 3 to 8 hours after NEBD (n = 11 oocytes, from 3 independent experiments). Cortical MTOCs intensity was shown by blue line and central MTOCs intensity was shown by pink line. *P < 0.05; **P < 0.01; ***P < 0.001; ****P < 0.0001, paired t-test, two-tailed; error bars are s.d.

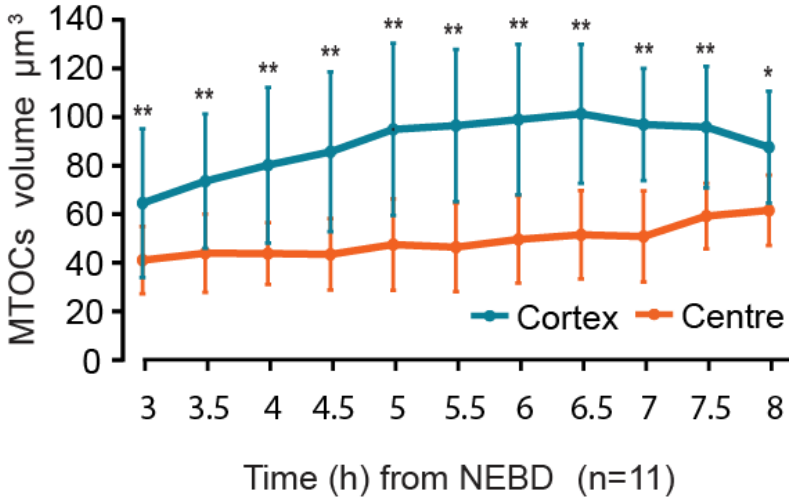

Figure 6.4 The cortical MTOCs volume was larger than central MTOCs.

The volume at both poles was calculated at 30 min intervals from 3 to 8 hours after NEBD (n = 11 oocytes, from 3 independent experiments). Cortical MTOCs volume was shown by blue line and central MTOCs intensity was shown by orange line. *P < 0.05; **P < 0.01; ***P < 0.001; ****P < 0.0001, paired t-test, two-tailed; error bars are s.d.

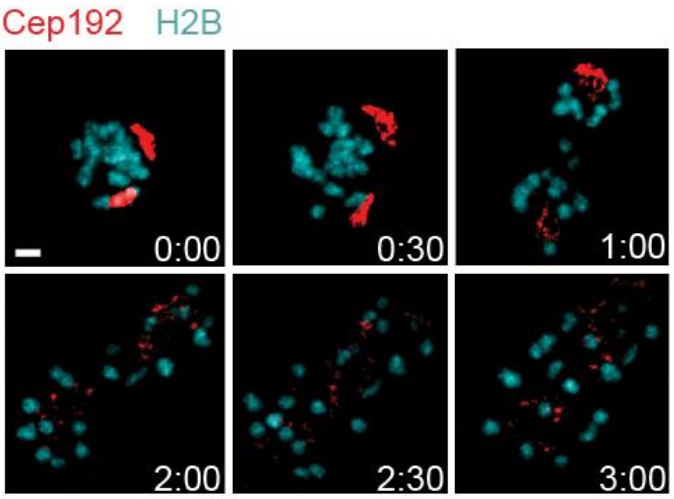

Figure 6.5 Representative time-lapse imaging to show asymmetrical MTOCs recruitment and fragment.

MTOCs in oocytes (n = 9, from 3 independent experiments) were shown by Cep192-GFP (Red) and bivalents were labelled by H2B-mCherry (Cyan). Scale bar is 5 μm. Time from NEBD.

Although the asymmetrical distribution of MTOCs was observed in meiosis I, the origin of this asymmetry was still unclear. To understand the initiation of MTOCs asymmetry, I focused on the localization and fragmentation of MTOCs at the beginning of meiosis I. Previous research showed the MTOCs were fragmented and separated within two hours after NEBD in mouse oocyte (Clift and Schuh, 2015). To show the localization of MTOCs, Cep192-GFP and H2B-mCherry were expressed in oocytes and imaged from NEBD to anaphase. With the same methods, MTOCs were categorised at anaphase (central or cortical) and traced back to NEBD by time-lapse images. Several major MTOCs were recruited to nucleus just before NEBD and separated after NEBD (Fig.6.5).

According to the microscopy results, the asymmetry of MTOCs recruitment and separation were observed from NEBD to three hours after NEBD. Greater MTOCs intensity was observed within two hours after NEBD at what later became the cortical spindle poles (confirmed after spindle migration, *P < 0.05, **P < 0.01, ***P < 0.001, ****P < 0.0001, n=9, paired t-test; Fig.6.5, Fig. 6.6). The volume of MTOCs was also compared between central and cortical poles, larger MTOCs were observed at cortical poles from NEBD to three hours after NEBD (*P < 0.05, **P < 0.01, ***P < 0.001, ****P < 0.0001, n=9, paired t-test; Fig.6.5, Fig. 6.7).

From all these observations it is concluded that asymmetrical MTOCs were formed at the beginning of oocyte maturation and the greater cluster of MTOCs consistently located at cortical spindle poles until anaphase.

To confirm the asymmetry of MTOCs were not induced by Cep192-GFP over-expression, the localization of pericentrin was also tested by immunofluorescence. Oocytes were fixed at 6 hours after NEBD for immunofluorescence. Pericentrin was detected by antibody and chromosomes were stained by Hoechst. To compare the MTOCs intensity, the cortical pericentrin intensity was divided by central pericentrin. The cortical pericentrin intensity was significantly higher than central pericentrin, which is consistent with the live cell imaging results (cortex/centre: 1.32, P= 0.0001, n=12, paired t-test; Fig. 6.8). The volume of pericentrin was also compared in fixed oocytes, larger MTOCs were observed at cortical spindle poles (P= 0.0001, n=10, paired t-test; Fig. 6.9).

According to my results, the meiotic drive and asymmetrical tension on centromere were found at prometaphase (Chapter 4 and 5). Meanwhile, the asymmetrical MTOCs

were observed during the whole meiosis I. I therefore wondered if the asymmetrical microtubule distribution was also established at 4 hours after NEBD. Oocytes were co-expressed with α-Tubulin-GFP and Cep192-mCherry to show microtubules and MTOCs respectively, and chromosomes were labelled with Hoechst. To determine if the consistent asymmetry of microtubules and MTOCs could be observed at prometaphase, oocytes were imaged live at 4 hours after NEBD. The direction of spindle was hard to define because the spindle has not migrated at 4 hours after NEBD. Even if the spindle was in the centre of oocyte, the asymmetrical microtubules were observed consistent with the asymmetry of MTOCs (Fig 6.10a).

To compare the intensity of microtubules, the chromosomes were treated as the centre of spindle and the intensity of α-Tubulin and Cep192 were detected (Fig 6.10b). In the analysis, higher α-Tubulin intensity was found close to the spindle pole with more MTOCs (Fig 6.10b). for quantification, Tubulin intensity on the spindle half with more MTOCs poles was divided by that with less MTOCs, the ratio was shown to be significantly higher than 1 (Tubulin intensity ratio more MTOC/ less MTOC: 1.1; Fig 6.10c, *$P < 0.05$; plots show mean line, n = 12 oocytes, and error bars that are 95% confidence intervals). Therefore, the asymmetrical spindle was established during prometaphase, which is consistent with the timing of meiotic drive (Chapter 3).

After the asymmetrical MTOCs formation was revealed, the recruitment of MTOCs needs further investigation. To understand more details about MTOCs recruitment, Cep192-GFP and H2B-mCherry were expressed in GV stage oocytes for two hours and imaged throughout maturation (Fig 6.11a). Initially, several small MTOCs were observed to localize on the cortex of oocytes at meiosis resumption. With the recruitment initiation, all the primary MTOCs migrated from cortex to the nucleus envelope in two hours (Fig 6.11b).

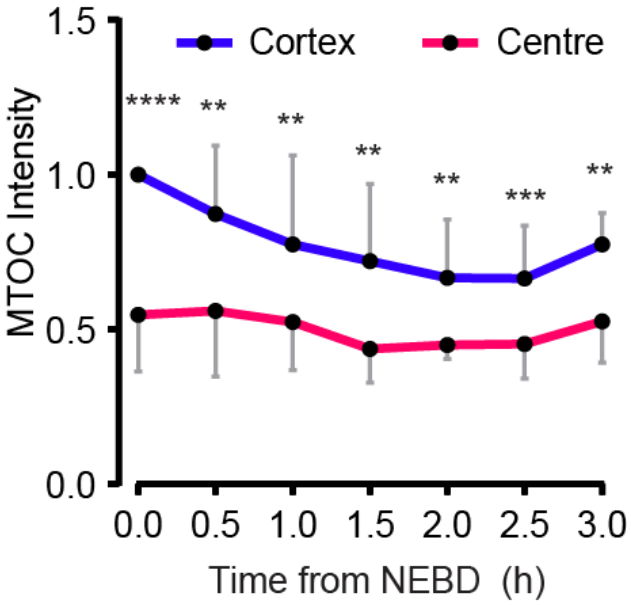

Figure 6.6 The cortical MTOCs fluorescence intensity was higher than central MTOCs in prometaphase.

The MTOC fluorescence intensity at both poles was calculated at 30 min intervals from 0 to 3 hours after NEBD (n = 11 oocytes, from 3 independent experiments). Cortical MTOCs intensity was shown by blue line and central MTOCs intensity was shown by pink line. *P < 0.05; **P < 0.01; ***P < 0.001; ****P < 0.0001, paired t-test, two-tailed; error bars are s.d.

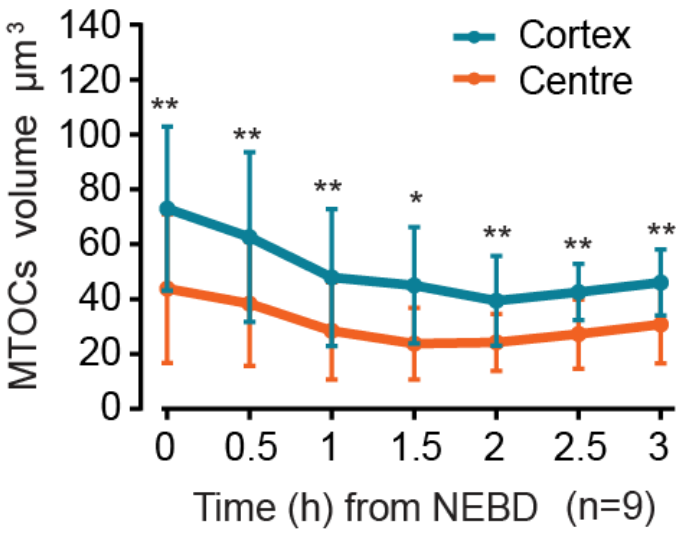

Figure 6.7 The cortical MTOCs volume was larger than central MTOCs in prometaphase.

The volume at both poles was calculated at 30 min intervals from 0 to 3 hours after NEBD (n = 11 oocytes, from 3 independent experiments). Cortical MTOCs volume was shown by blue line and central MTOCs volume was shown by orange line. *P < 0.05; **P < 0.01; ***P < 0.001; ****P < 0.0001, paired t-test, two-tailed; error bars are s.d.

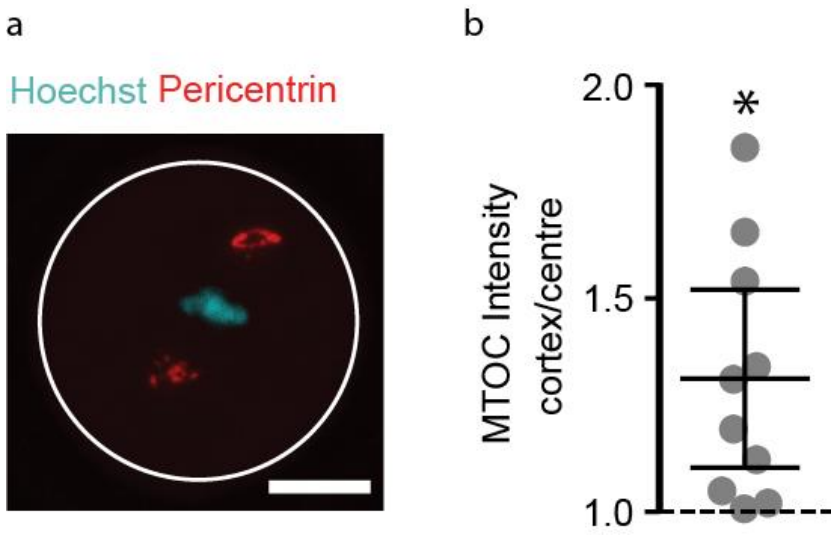

Figure 6.8 Asymmetrical MTOCs shown by pericentrin antibody at 6 hours after NEBD.

(a) Representative z-projection of an oocyte stained for pericentrin (red) and Hoechst (cyan). White circle depicts position of plasma membrane. Scale bar is 20 µm. **(b)** The ratio of cortical and central MTOC intensities at 6 h after NEBD from oocytes in 'a' (10 oocytes from two independent experiments). *P < 0.05; plots show mean line and error bars that are 95% confidence intervals.

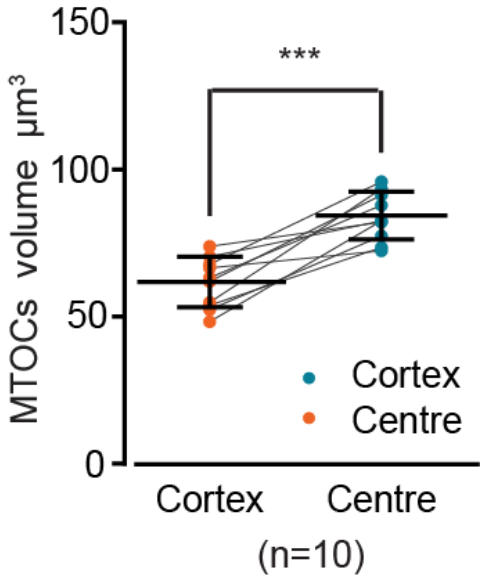

Figure 6.9 The ratio of cortical and central MTOC volume was measured in fixed oocytes at 6 hours after NEBD.

10 oocytes from two independent experiments. Cortical MTOCs volume was shown by blue dots and central MTOCs volume was shown by orange dots. Paired MTOCs clusters were connected by grey line. ***P < 0.001; paired t-test, two-tailed.

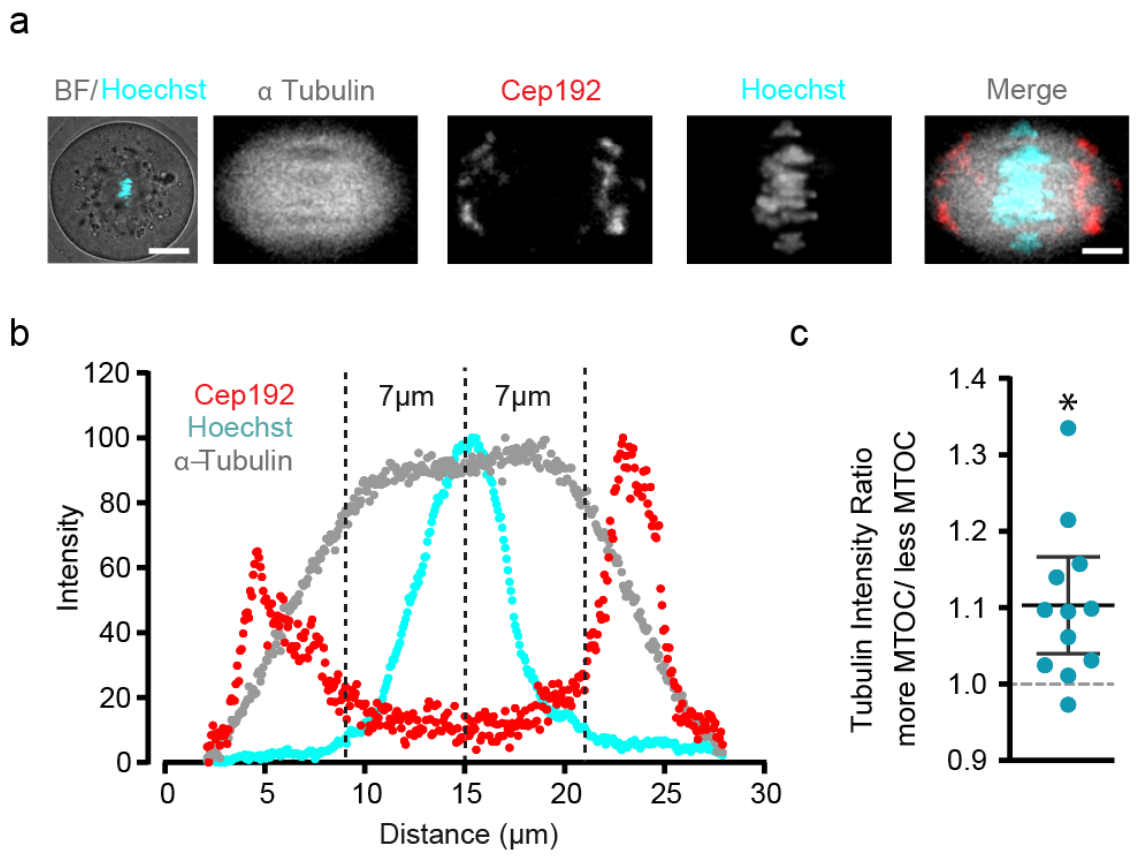

Figure 6.10 Asymmetrical tubulin intensity was consistent with asymmetrical MTOCs at prometaphase.

(a) Representative image of a spindle (α-Tubulin-GFP grey; Cep192-mCherry, red; Hoechst, cyan), at 4h after NEBD, showing its central position within the oocyte. Scale bar: 20 and 5µm. **(b)** Intensity profiles along the long spindle axis of Cep192, Hoechst and α-tubulin from the image in 'a'. Dashed lines show the weighted centre of intensity of the chromatin and 7µm either side. **(c)** Ratio of the tubulin fluorescence in the regions indicated in 'b'; measurements from two independent experiments. The spindle sides are defined by having either more or less MTOCs (Cep192) signal as shown in 'b'. *P < 0.05, plots show mean line (n = 12 oocytes) and error bars that are 95% confidence intervals.

6.3 Discussion

In mammals, the process of mitosis organised by centrosomes is well investigated and understood. However, in mouse oocytes, the centriole is eliminated during early oogenesis and only small acentriolar MTOCs are observed to regulate spindle formation. Following centrosome disassembly, the mechanism of microtubule organization and intracellular architecture formation is still unclear.

In this Chapter, I found the pattern of asymmetrical MTOCs was consistent with the asymmetrical meiotic spindle throughout oocyte maturation. The asymmetrical microtubule distribution is supposed to be formed by asymmetrical MTOCs recruitment because the MTOCs worked as the regulator of microtubules assembly. Therefore, the asymmetrical MTOCs recruitment is assumed as the origin of asymmetrical spindle which in the context of meiotic drive, can distinguish and select the larger or smaller sized centromere.

Apart from meiotic drive, asymmetrical microtubule distribution could also affect the bivalents alignment. The asymmetrical spindle may create more non-aligned bivalents which can induce higher aneuploidy rate during meiosis I.

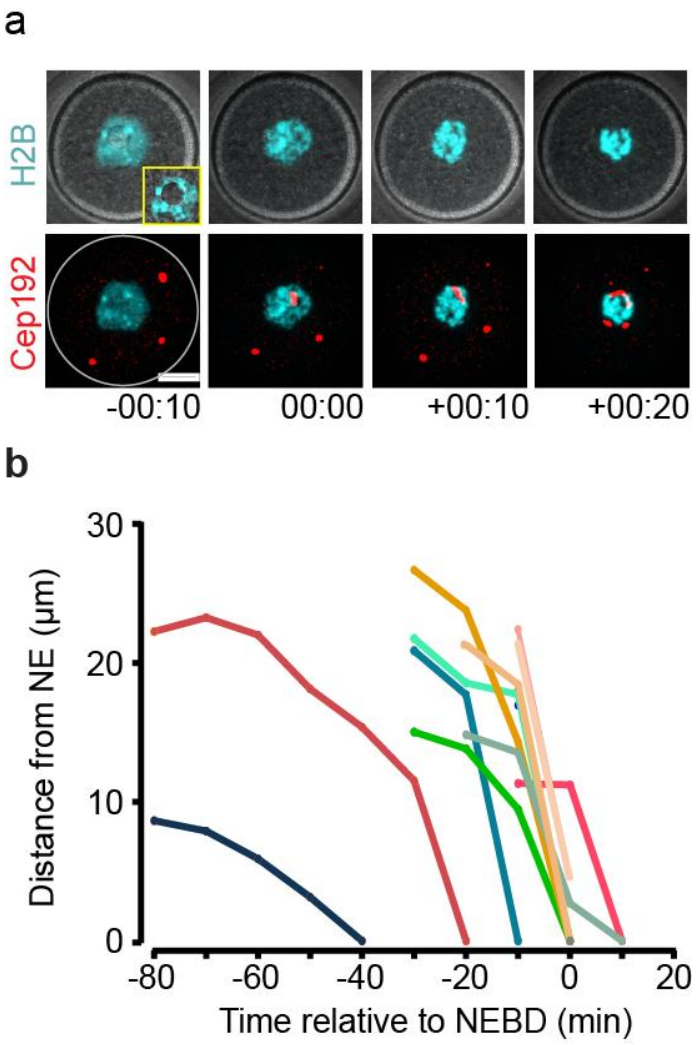

Figure 6.11 MTOCs travel to the nuclear envelope before NEBD.

(a) Representative images (Cep192-GFP, red; H2B-mCherry, cyan) and **(b)** trajectory plots of MTOCs from the oocyte cortex to the centre (n = 9, from two independent experiments). Brightfield inset, shows single z-slice with a 'surrounded nucleolus' (SN) configuration. Time is relative to NEBD (hh:min), and distances are measured relative to the chromatin signal . Scale bar: 20µm.

6.3.1 MTOCs recruitment was observed in oocytes

In previous research, the MTOCs in maturation-competent mouse oocytes were observed on the nuclear envelope and cortical localization of MTOCs were observed in the incompetent oocytes before meiosis I resumption (Clift and Schuh, 2015; Luksza et al., 2013). However, my data indicates that, even in competent mouse oocytes, MTOCs are localized at the cortex and recruited to the nuclear envelope just before NEBD. To confirm the examined oocytes are competent, I used GV stage oocytes that had a surrounded nucleolus (SN) configuration for chromatin (Fig. 6.11a) as these show the greatest potential for embryonic development, and likely represent a more mature state than the alternative non-surrounded nucleolus configuration. In addition to that, polar body extrusion was also observed in all of the tested oocytes. Although the MTOCs recruitment was observed in competent oocytes, the mechanism of MTOCs recruitment was unknown.

According to previous research, the force on MTOCs for stretching and elongation comes from microtubules. With inhibition of dynein by ciliobrevin D, the recruitment and elongation of MTOCs was not disturbed, but their fragmentation was prevented (Clift and Schuh, 2015). Interestingly, after microtubules were depolymerised by nocodazole, the localization of MTOCs on nucleus envelope was impaired. Future research needs to investigate the mechanism of MTOCs recruitment.

6.3.2 More MTOCs might direct the spindle migration in meiosis I

The asymmetrical MTOCs recruitment on nascent spindle poles has been reported in mouse oocytes by different research groups previously (Carabatsos et al., 2000; Michaut et al., 2005). However, the relationship between asymmetrical MTOCs and spindle migration has never been investigated.

It is widely reported that in mouse oocytes spindle migration is actin dependent. The actin chain connection between spindle poles and cortex has been visualized by fluorescent F-actin, which provides a pulling force for spindle migration (Bezanilla and Wadsworth, 2009; Schuh and Ellenberg, 2008). Compared to the mitotic spindle, the number of astral microtubules on the mouse meiotic spindle is decreased. However, a small number of astral microtubules are still present on both spindle poles (Bezanilla

and Wadsworth, 2009). According to one recent investigation, microtubules interact with F-actin during spindle formation in both meiosis I and II (Mogessie and Schuh, 2017). The interaction between microtubules and actin was also suggested by my results (Chapter 5).

In my research, I could always find more MTOCs at the cortical spindle pole, which might associate with the direction of spindle migration. Therefore, combined with my results, a new spindle migration model could be hypothesized. In mouse oocytes, the meiotic spindle is under balanced tension before migration. During MTOCs clustering, the asymmetry of spindle pole is initiated and increased. Hence, the pulling force on asymmetrical MTOCs break the balance. The pole with more astral microtubules may correlate with more actin from the cortex, which provides more pulling force on cortical spindle pole (more MTOCs). The asymmetrical pulling force would be predicted to move the spindle from the centre to the cortex of the oocyte in the direction favouring the pole with most MTOCs.

We can imagine disassembly of the meiotic spindle by a reversible inhibition, for example a cold treatment, that is applied only temporarily, which would allow for the spindle to reform after such a treatment. After the transient cold treatment, the spindle can be assembled asymmetrically again due to the asymmetrical MTOCs distribution. The asymmetrical bivalent can be reoriented during asymmetrical microtubule distribution. Therefore, the meiotic drive should be observed after the spindle reassembly.

Chapter 7: General discussion

7.1 Summary

In my thesis, I discovered a new model for female meiotic drive in mouse oocytes and revealed the possible mechanism of biased chromosome transmission.

An F_1 hybrid mouse model (C57Bl/6×SJL) was created to allow easy recognition of a specific bivalent which had inherited asymmetrical homologous chromosomes from its two parent strains, which contain different sized major satellite DNA, minor satellite DNA, and the kinetochore protein Spc24 (Figures 3.7, 3.8). In the F_1 hybrid mouse oocyte, the preferential orientation of this specific bivalent was observed in meiosis I with high-resolution time-lapse imaging. This led to the discovery of the biased bivalent segregation. The bivalent half containing the larger minor satellite DNA (smaller major satellite DNA) is preferentially retained in the MII oocyte during female meiosis (i.e. it displayed non-Mendelian inheritance). Time-lapse imaging (Figures 4.5, 4.6) showed that this biased chromosome transmission rate correlates with bivalent reorientation in prometaphase I. To understand the mechanism of bivalent reorientation, the role of Aurora kinase was examined in meiotic drive. I demonstrated that the biased reorientation of the asymmetrical bivalents to favour retention in the egg requires Aurora kinase activity (Figure 4.9).

In order for meiotic drive to occur, there must also be an asymmetry within the oocyte to give context to the re-orientation of the bivalent. Therefore, the spindle apparatus was first examined and the intensity of microtubules and MTOCs was measured and compared. This led to the demonstration that the meiotic spindle migrate to cortex at 6 hours after NEBD (Figure 7.1a) and that proper meiotic spindle migration requires both actin and microtubules. With regards to meiotic drive, I found that cortical kinetochores are under greater tension than central kinetochores after chromosome are stretched by spindle microtubules (Figures 5.10, 5.12). I also found that microtubules are assembled asymmetrically across the meiotic spindle in meiosis I (Figure 7.1b). To investigate the microtubule asymmetry, I then looked to the MTOCs. I found that the asymmetrical microtubules may be organized in turn by asymmetrical MTOCs in meiosis I (Figure 6.10).

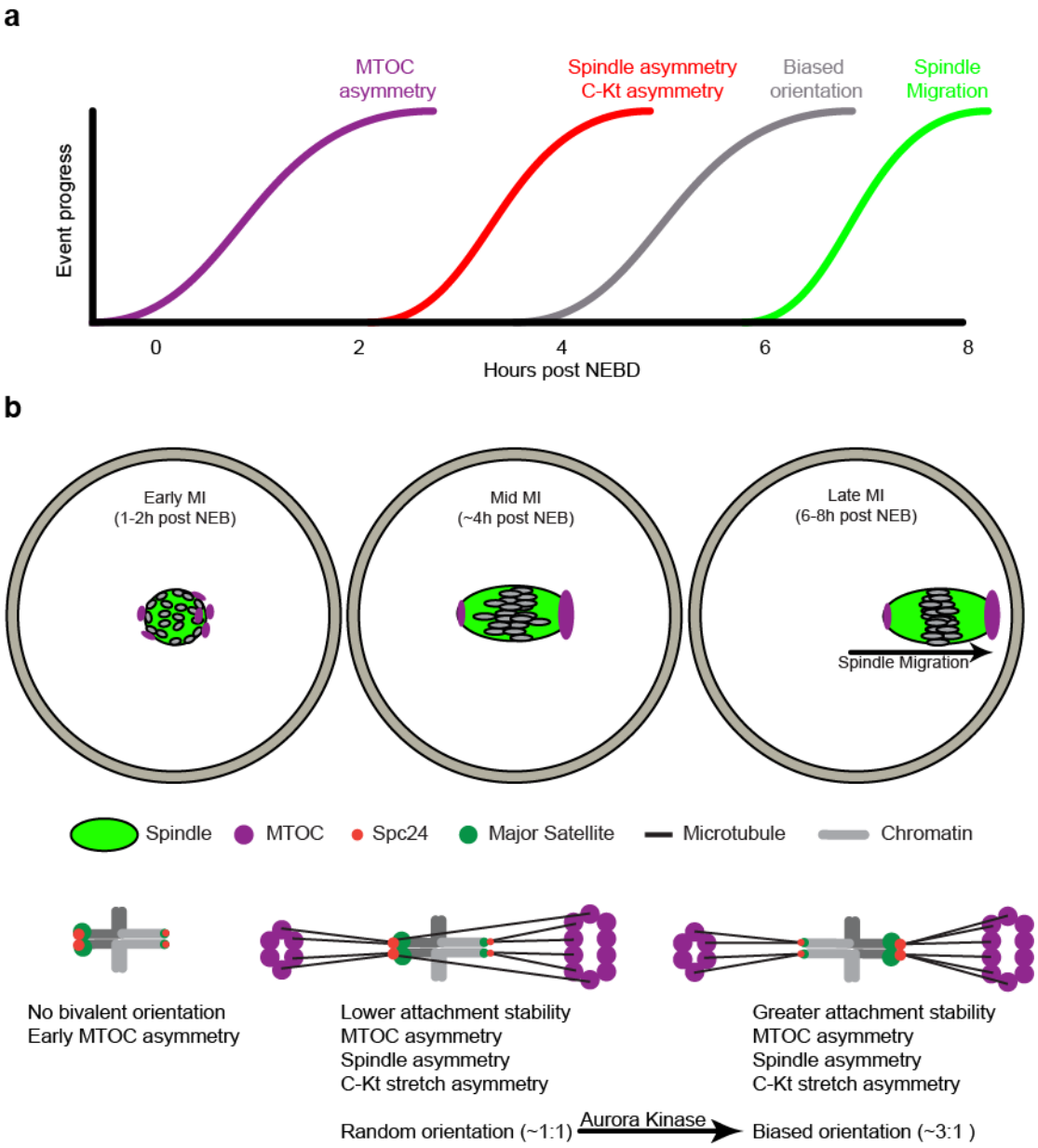

Figure 7.1 Schematic to demonstrate meiotic drive showing the mechanism of asymmetrical bivalent reorientation.

(a) The schematic shows the approximate relative timings of events relating to meiotic drive and spindle migration in times relative to NEBD. **(b)** Cartoons graphically depict the events taking place in early, mid and late MI from left to right, respectively, in the oocyte (top) and at the level of an individual bivalent experiencing meiotic drive (bottom).

In conclusion, according to the above results, I propose the following mechanism of female meiotic drive. The larger major satellite DNA with more kinetochore proteins (SPC24), should contain more binding sites for microtubules than the other bivalent-half. Therefore, when it is facing towards the central pole which contains fewer microtubules (due to fewer MTOCs), it can be reoriented to the cortical pole (more MTOCs) which provides more microtubules for its binding sites. This scenario allows Aurora kinase to destabilise microtubule attachment and bivalent rotation. To achieve a more stable condition, unstable attachments are destabilised by Aurora kinase and reoriented to the opposite direction to form a more stable situation (Figure 7.1b bottom).

7.2 Discussion

7.2.1 The definition of the stronger centromere in the mouse model

In F_1 hybrid mice, some homologue pairs with asymmetrical centromeres are created because they are inherited from inbred parent strains with different sized major and minor satellite repeats. The centromere that recruits more centromeric proteins and kinetochore proteins is termed as the stronger centromere (Chmátal et al., 2014; Iwata-Otsubo et al., 2017). The stronger centromere was observed to be preferentially retained in the MII oocyte and proposed as the selfish element in biased chromosome segregation (Figure 7.2a) (Akera et al., 2017).

Although it was convenient to track and measure the centromere size, because of its large signal, it is the kinetochore that provides the microtubule binding sites and thus the interaction between the spindle and the bivalent. Therefore, the difference in kinetochore size is thought to define the meiotic drive strength of the chromosome and explain the preference for orientation towards the spindle half with higher microtubule density. However, the mechanism of centromeric proteins and kinetochore proteins recruitment on centromeric DNA is still unclear. According to previous research, centromeric DNA (Iwata-Otsubo et al., 2017) and centromeric RNA (Balboula et al., 2017; Ideue et al., 2014; Rošić and Erhardt, 2016; Scott, 2013) affect the recruitment of the centromeric and kinetochore components.

The size of the centromeric DNA repeat regions is thought to determine centromeric protein localization. A recent study in Indian muntjac fibroblast cells showed that larger

centromeres could recruit more kinetochore proteins and in turn attach more microtubules (Drpic et al., 2018). Therefore, it seems possible that both centromeric proteins and kinetochore proteins will be involved in meiotic drive. The study also showed that larger kinetochores were more likely to congress successfully to the metaphase plate, increasing the chances of chromosome segregation correction, but were also more likely to form merotelic attachments, reducing the success rate. It seems likely therefore that there are upper and lower limits on centromere/kinetochore size imposed by the practical constraints of chromosome segregation.

In the case of the fundamental centromeric protein Cenp-A, recruitment appears to be limited by the size of the minor satellite DNA. In a hierarchical fashion, larger minor satellite DNA regions that recruit more Cenp-A can then recruit more kinetochore proteins (Chmátal et al., 2014; Iwata-Otsubo et al., 2017). Surprisingly, at weaker centromeres with smaller minor satellite DNA, major satellite DNA was also noted to be associated with Cenp-A, which indicates that the size of major satellite DNA may also be involoved in Cenp-A localization. Factors relating to the centromeric region, other than the size of the repeat regions, may also be important in determining centromere strength, because the difference between the size of minor satllite DNA is not as extreme as that of Cenp-A (Iwata-Otsubo et al., 2017). Therefore, the epigenetic pathway involved in Cenp-A assembly may also play a role in the asymmetry of centromeres (Black and Cleveland, 2011; Westhorpe and Straight, 2015).

In terms of centromeric RNA, its function in kinetochore proteins localization and stabilization seems more important. Therefore the transcription of centromeric DNA could be another indicator of the centromeric strength. Centromeric RNA that specifically localizes at centromere and chromatin is involved in Cenp-C and Aurora kinase B recruitment (Du et al., 2010; Ideue et al., 2014; Perea-Resa and Blower, 2017; Scott, 2013), and so could be a big contributor to the strength of particular centromeres, assuming that they only act locally at the centromere from which they were transcribed (Figure 7.2b).

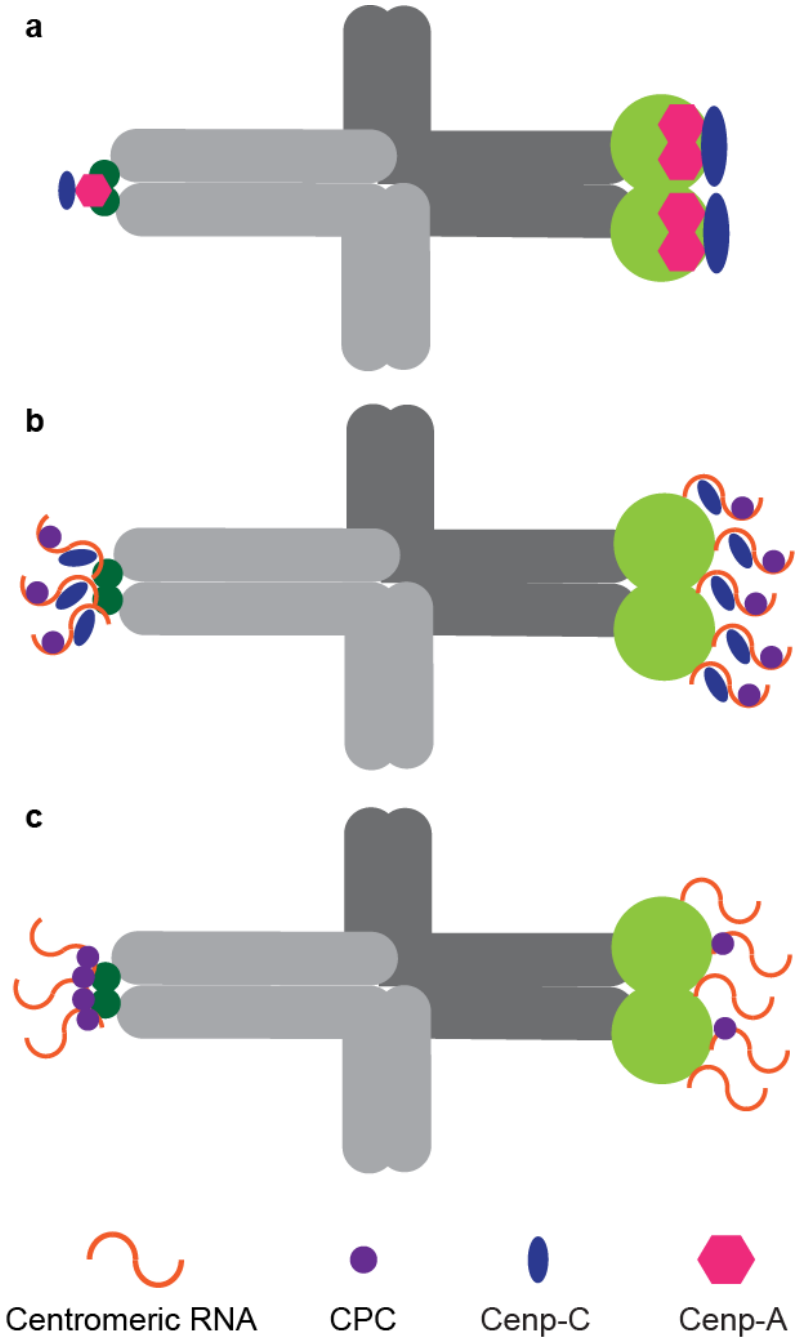

Figure 7.2 Schematic to show the hypothesis of asymmetrical centromeres.

(a) Compared to smaller centromere (dark green), larger centromeres (light green) may provide a bigger platform for centromeric proteins localization. **(b)** The larger centromeres may produce more localized centromeric RNA (orange), so that recruit more Cenp-C (blue) and CPC (purple). **(c)** More centromeric RNA produced by larger centromere may disturb the localization of CPC.

The levels of centromeric RNA are important, as their over-accumulation can impair centromeric function. Accumulation of centromeric RNAs disturb the localization of centromere-associated proteins during mitosis (Bouzinba-Segard et al., 2006; Westhorpe and Straight, 2014). In addition, the chromosome alignment and segregation are impaired by excessive centromeric RNA accumulation (Bouzinba-Segard et al., 2006). It indicates that the over transcription of centromeric DNA is also harmful to Aurora kinase localization. Therefore, the larger centromere that with more centromeric RNA may prevent the recruitment of Aurora kinase on centromere (Figure 7.2c).

Collectively, only an appropriate transcription of centromeric DNA is good enough for related proteins recruitment. In conclusion, I assume that the size of centromeric DNA alone cannot predict centromere strength, however, its transcription and the strength of centromeric transcripts (the capacity of kinetochore protein recruitment) could be more important. Indeed, only the centromeres that are preferentially retained in oocyte should be termed as stronger centromeres.

7.2.2 The asymmetry of first meiotic spindle in mouse model

In meiotic drive, the asymmetry of spindle is necessary for centromere selection and fate determination. The central microtubules differ from cortical microtubules and appear to interact with the stronger centromeres preferentially and keep them in the oocyte after meiosis I. So far, two models have been proposed to explain the asymmetrical spindle in mouse oocytes.

The asymmetrical amount of microtubules and MTOCs

Although the asymmetrical spindle poles were revealed several years ago (see Chapter 1) (Carabatsos et al., 2000; Michaut et al., 2005), however their significance is still unknown. Recently, the asymmetry of spindle poles was observed in relation to asymmetrical microtubules and meiotic drive. The chromosome with the larger kinetochore is preferentially oriented towards the spindle pole with larger MTOCs (at the oocyte cortex) and was extruded into polar bodies at higher than expected frequencies.

To explain this correlation, microtubule distribution was examined through α-tubulin intensity measurement and comparison. It shows the microtubules are assembled

asymmetrically in amount, which provides an opportunity for the competition of asymmetrical homologues centromeres. The larger cortical MTOCs can assemble more microtubules which have more chances to form stable attachments with the larger kinetochores than the smaller ones, e.g. those with more Spc24 (Figure 7.3a) (Wu et al., 2018).

The asymmetrical stability of microtubules

Apart from the physical asymmetry of MTOCs and microtubules, post-translational modifications of the spindle have also been observed in mouse oocytes. The asymmetry of specific post-translational modifications on tubulin were observed on the MI spindle: a recent study showed that α-tubulin tyrosination is enriched on the cortical half of the meiotic spindle, which reduces the stability of the cortical microtubules (Figure 7.3b). This asymmetry was proved to be spindle migration dependent, which suggested that the asymmetry is created by some cortical signal (Akera et al., 2017). The asymmetrical tyrosination requires cell division control protein 42 (CDC42) activity from the cortex, which is established by the RanGTP gradient created by chromatin. A working model is that the more dynamic microtubules on the cortical spindle side were more likely to attach to the weaker centromeres (Kursel and Malik, 2018; Lampson and Black, 2017).

In conclusion, the phenomenon of female meiotic drive is well demonstrated but requires further research to reveal mechanistic details. The real effective meiotic driver and the process of asymmetry of spindle formation are still unclear. In the future, I will focus on centromeric transcripts which seem important in meiotic drive, but its function in meiosis in general is still poorly understood.

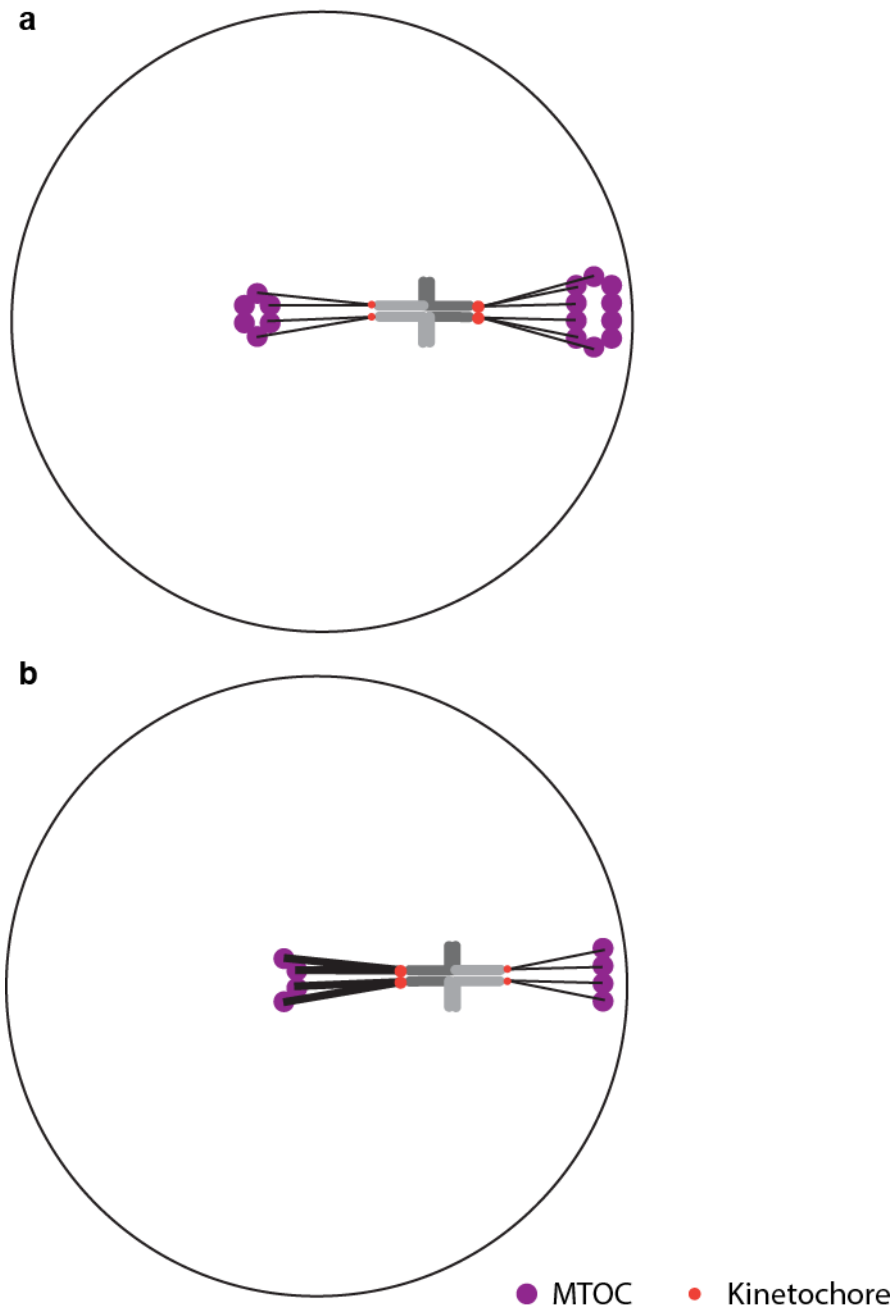

Figure 7.3 Schematic to show a possible effect of asymmetrical microtubule number.

(a) Stable microtubules at the oocyte centre interact with the bivalent-half with the larger kinetochores and so orientating it to remain in the oocyte. **(b)** More microtubules at cortex interact with larger kinetochores and take them into polar bodies. Black: microtubules; Grey: chromosomes.

Appendix A: Published Works Contained in this Thesis

Most of my work presented in this thesis was published in 2018. My contributions to this research article are outlined below.

Wu, T., Lane, S. I. R., Morgan, S. L. and Jones, K. T. (2018). 'Spindle tubulin and MTOC asymmetries may explain meiotic drive in oocytes', Nature Communications, 9(1), 2952.

This research article was published on 27th July 2018. T.W. performed 100% of the laboratory work and statistical analysis for the paper. T.W. also contributed to experiment design and manuscript drafting.

His two supervisors, K.T.J. and S.I.L. devised the study and helped discuss much of the data interpretation and suggested potential experiments. The manuscript was written by K.T.J. and S.I.L. with input from all authors.

Tianyu Wu, Candidate Prof. Keith Jones, Principal Supervisor

Appendix B: M2 Media

Stock solutions were made for quick M2 media preparation. All of them were sterilised using 0.2µm filters and stored in the 4°C fridge.

To make Stock A, the components in Table B.1 were dissolved in 100mL of sterile water and the final volume was measured by a volumetric flask. It was made every 3 months.

To make Stock B and Stock C, the components in B.2 were dissolved into 100mL and 10mL of sterile water respectively. They were made every other week.

To make Stock D and Stock E, the components in B.3 were dissolved into 100mL of sterile water respectively. The pH value of Stock E was adjusted to 7.6 with 1M KOH. They were made every 3 months.

Table B.1 Stock A

Stock A			
Chemical	g/100mL	Chemical	g/100mL
NaCl	5.534	Na Lactate (60%)	4.349
KCl	0.356	Glucose	1.000
KH_2PO_4	0.162	Penicillin G	0.060
$MgSO_4.7H_2O$	0.293	Streptomycin	0.050

Table B.2 Stock B and C

Stock B		Stock C	
Chemical	g/100mL	Chemical	g/10mL
$NaHCO_3$	2.101	Sodium Pyruvate	0.036
Phenol Red	0.010		

Table B.3 Stock D and E

Stock D		Stock E	
Chemical	g/100mL	Chemical	g/100mL
$CaCl_2.2H_2O$	2.520	Hepes	5.958
		Phenol Red	0.010

Finally, M2 was made up of these stock solutions by mixture with extra sterile addition (Table B.4). Bovine serum albumin (BSA) was added after mixture (4mg/mL). M2 was then filtered into a fresh tube and stored in the 4°C fridge.

Table B.4 Making M2 media from stock solutions

M2 Media	
Stock A	5.00 mL
Stock B	0.80 mL
Stock C	0.50 mL
Stock D	0.50 mL
Stock E	4.20 mL
Sterile water	39.0 mL

Appendix C: Image J Macro

The following Image J macro script was installed onto the Image J platform and the functions called using the 's' key for image setup and the 'l' key for running the analysis.

C.1 C-Kt Separation Measurement

The following macro clears the ImageJ results table ready to collect new data

```
macro "Open Analysis [l]" {
        newImage("Untitled", "8-bit White", 400, 400, 1);
        run("Measure");
        close();
        run("Clear Results");
        IJ.renameResults("analysis");
}
```

The following macro records the positions of (and measures the distance between) two points in the images which are 'clicked' by the user.

```
macro "Measure foci distance [s]" {
        getVoxelSize(width, height, depth, unit);
        s=Stack.getPosition(channel, slice, frame);
        run("Duplicate...", "duplicate slices=" + slice-4 + "-"+ slice+4);
        rename("temp");
        run("Split Channels");
        selectWindow("C1-temp");
        run("Foci Picker3D", "background=automatic uniform=1500 automatic=6
        minitype=RelativetoMaximum minisetting=0.50 tolerancesetting=5
        minimum=100 voxelx=1 voxely=1 voxelz=1 contrast=0 useztolerance=No
        ztolerance=5 useshapevalidation=No focishaper=6 computingthread=1");
        selectWindow("FociMask_5.0");
        close();
        if(nResults==0){
                Select Window("C1-temp");
                run("Foci Picker3D", "background=automatic uniform=1500 automatic=6
                minitype=RelativetoMaximum minisetting=0.50 tolerancesetting=2
                minimum=100 voxelx=1 voxely=1 voxelz=1 contrast=0 useztolerance=No
                ztolerance=5 useshapevalidation=No foci shaper=6 computing
                thread=1");
                select Window("FociMask_2.0");
```

```
		close();
	}
	C1X = get Result("CoreX",0);
	print(C1X);
	C1Y = get Result("CoreY",0);
	print(C1Y);
	C1Z = get Result("CoreZ",0);
	print(C1Z);
	run("Clear Results");
	select Window("C1-temp");
	close();
	select Window("C2-temp");
	run("Foci Picker3D", "background=automatic uniform=1500 automatic=6 minitype=Relative to Maximum minisetting=0.50 tolerance setting=5 minimum=100 voxel x=1 voxel y=1 voxel z=1 contrast=0 use z tolerance=No z to lerance=5 use shape validation=No foci shaper=6 computing thread=1");
	select Window("FociMask_5.0");
	close();
	if(nResults==0){
		Select Window("C2-temp");
		run("Foci Picker3D", "background=automatic uniform=1500 automatic=6 minitype=RelativetoMaximum minisetting=0.50 tolerancesetting=2 minimum=100 voxelx=1 voxely=1 voxelz=1 contrast=0 useztolerance=No ztolerance=5 useshapevalidation=No focishaper=6 computingthread=1");
		selectWindow("FociMask_2.0");
		close();
}
C2X = get Result("CoreX",0);
print(C2X);
C2Y = get Result("CoreY",0);
print(C2Y);
C2Z = get Result("CoreZ",0);
print(C2Z);
run("Clear Results");
select Window("C2-temp");
close();
```

```
        d=sqrt(pow((C1X-C2X)*width,2)+pow((C1Y-C2Y)*width,2)+pow((C1Z-
        C2Z)*depth,2));
        get Selection Bounds(x, y, width2, height2);
        cx = x+(width2/2);
        cy = y+(height2/2);
        run("Overlay Options...", "stroke=yellow width=1 fill=yellow set");
        make Oval(cx-2, cy-2, 4, 4);
        run("Add Selection...");
        select Window("analysis");
        IJ.renameResults("Results");
        set Result("MaClX",nResults, (C1X+x)*width);
        setResult("MaClY",nResults-1,(C1Y+y)*width);
        setResult("MaClZ",nResults-1,(C1Z+slice-4)*depth);
        setResult("SpcX",nResults-1, (C2X+x)*width);
        setResult("SpcY",nResults-1,(C2Y+y)*width);
        setResult("SpceZ",nResults-1,(C2Z+slice-4)*depth);
        setResult("distance",nResults-1, d);
        selectWindow("Results");
        IJ.renameResults("analysis");
}
```

C.2 Intensity of Foci Analysis

The following macro measures the intensity and volume of foci within a user-selected region of interest, it utilises the ‘Foci picker 3D’ plugin.

```
macro "Open Analysis [l]" {
        newImage("Untitled", "8-bit White", 400, 400, 1);
        run("Measure");
        close();
        run("Clear Results");
        IJ.renameResults("analysis");
        }
macro "Measure foci distance [s]" {
        getVoxelSize(width, height, depth, unit);
        width = 1/width;
        height = 1/height;
        depth = 1/depth;
```

```
s=Stack.getPosition(channel, slice, frame);
run("Duplicate...", "duplicate slices=" + slice-9 + "-"+ slice+9);
rename("temp");
run("Split Channels");
selectWindow("C2-temp");
close();
selectWindow("C1-temp");
A = 5; B = 5; C = 5; sigma = 2; D = 30;
run("Duplicate...", "duplicate");
rename("Temp");
run("Gaussian Blur 3D...", "x=" + sigma + " y=" + sigma + " z=" + sigma);
run("Foci Picker3D", "background=uniform uniform=" + A + " automatic=6
minitype=Absolute minisetting=" + B + "  tolerancesetting=" + C + " minimum="
+ D + " voxelx=" + width + " voxely=" + height + " voxelz=" + depth + " contrast=0
useztolerance=No ztolerance=5 useshapevalidation=No focishaper=6
computingthread=1");
}
C1X = getResult("CoreX",0);
print(C1X);
C1Y = getResult("CoreY",0);
print(C1Y);
C1Z = getResult("CoreZ",0);
print(C1Z);
selectWindow("C1-temp");
close();
```

C.3 Chromosome Migration Displacement

The following macro measures the position of the chromosomes in each time point within a time-lapse image set and outputs the data to the results window.

```
timepoints =90;
channel = 1;  //channel of interest
run("Set Measurements...", "center redirect=None decimal=3");
    id = getImageID();
    run("Z Project...", "projection=[Sum Slices] all");
    //test
```

```
setAutoThreshold("MaxEntropy dark");
setOption("BlackBackground", false);
run("Make Binary", "method=MaxEntropy background=Dark calculate");
//end test
rename("tempXY");
selectImage(id);
run("Reslice [/]...", "output=1.000 start=Top");
run("Z Project...", "projection=[Sum Slices] all");
//test
setAutoThreshold("MaxEntropy dark");
setOption("BlackBackground", false);
run("Make Binary", "method=MaxEntropy background=Dark calculate");
//end test
rename("tempZ");
for(timepoint = 1; timepoint<timepoints+1 ; timepoint++){
selectWindow("tempZ");
Stack.setPosition(channel, 1, timepoint);
run("Measure");
z = getResult("YM",nResults-1);
selectWindow("tempXY");
Stack.setPosition(channel, 1, timepoint);
run("Measure");
x = getResult("XM",nResults-1);
y = getResult("YM",nResults-1);
print(timepoint, "\t",x,"\t",y,"\t",z);
}
close("tempXY");
close("tempZ");
close("Reslice*");
```

References

Akera, T., Chmátal, L., Trimm, E., Yang, K., Aonbangkhen, C., Chenoweth, D.M., Janke, C., Schultz, R.M., and Lampson, M.A. (2017). Spindle asymmetry drives non-Mendelian chromosome segregation. Science *358*, 668–672.

Almonacid, M., Terret, M.E., and Verlhac, M.H. (2014). Actin-based spindle positioning: new insights from female gametes. J. Cell Sci. *127*, 477–483.

Andersen, J.S., Wilkinson, C.J., Mayor, T., Mortensen, P., Nigg, E.A., and Mann, M. (2003). Proteomic characterization of the human centrosome by protein correlation profiling. Nature *426*, 570–574.

Azoury, J., Verlhac, M.-H., and Dumont, J. (2009). Actin filaments: key players in the control of asymmetric divisions in mouse oocytes. Biol. Cell *101*, 69–76.

Baas, P.W., and Ahmad, F.J. (1992). The plus ends of stable microtubules are the exclusive nucleating structures for microtubules in the axon. J. Cell Biol. *116*, 1231–1241.

Balboula, A.Z., and Schindler, K. (2014). Selective Disruption of Aurora C Kinase Reveals Distinct Functions from Aurora B Kinase during Meiosis in Mouse Oocytes. PLoS Genet. *10(2)*: e1004194.

Balboula, A.Z., Blengini, C.S., Gentilello, A.S., Takahashi, M., and Schindler, K. (2017). Maternal RNA regulates Aurora C kinase during mouse oocyte maturation in a translation-independent fashio. Biol. Reprod. *96*, 1197–1209.

Barisic, M., Silva e Sousa, R., Tripathy, S.K., Magiera, M.M., Zaytsev, A. V., Pereira, A.L., Janke, C., Grishchuk, E.L., and Maiato, H. (2015). Microtubule detyrosination guides chromosomes during mitosis. Science *348*, 799–803.

Barrett, S.L., and Albertini, D.F. (2007). Allocation of Gamma-Tubulin Between Oocyte Cortex and Meiotic Spindle Influences Asymmetric Cytokinesis in the Mouse Oocyte1. Biol. Reprod. *76*, 949–957.

Barros E Silva, A.E., and Guerra, M. (2010). The meaning of DAPI bands observed after C-banding and FISH procedures. Biotech. Histochem. *85*, 115–125.

Baumann, C., Wang, X., Yang, L., and Viveiros, M.M. (2017). Error-prone meiotic division and subfertility in mice with oocyte-conditional knockdown of pericentrin. J. Cell Sci. *130*, 1251–1262.

Bennabi, I., Terret, M.-E., and Verlhac, M.-H. (2016). Meiotic spindle assembly and chromosome segregation in oocytes. J Cell Biol *215*, 611–619.

Bezanilla, M., and Wadsworth, P. (2009). Spindle Positioning: Actin Mediates Pushing and Pulling. Curr. Biol. *19*, R168–R169.

Bischoff, F.R., and Ponstingl, H. (1991). Catalysis of guanine nucleotide exchange on Ran by the mitotic regulator RCC1. Nature *354*, 80–82.

Black, B.E., and Cleveland, D.W. (2011). Epigenetic Centromere Propagation and the Nature of CENP-A Nucleosomes. Cell *144*, 471–479.

Blank, T., Sandaltzopoulos, R., Becker, P., Hyman, A., Heald, R., Karsenti, E., and Tournebize, R. (2003). Self-organization of microtubules into bipolar spindles around artificial chromosomes in Xenopus egg extracts. Nature *382*, 420–425.

Van Blerkom, J. (2006). Microtubule mediation of cytoplasmic and nuclear maturation during the early stages of resumed meiosis in cultured mouse oocytes. Proc. Natl. Acad. Sci. *88*, 5031–5035.

Van Blerkom, J., and Bell, H. (1986). Regulation of development in the fully grown mouse oocyte: chromosome-mediated temporal and spatial differentiation of the cytoplasm and plasma membrane. J. Embryol. Exp. Morphol. *93*, 213–238.

Blower, M.D. (2016). Centromeric Transcription Regulates Aurora-B Localization and Activation. Cell Rep. *15*, 1624–1633.

Bodor, D.L., Mata, J.F., Sergeev, M., David, A.F., Salimian, K.J., Panchenko, T., Cleveland, D.W., Black, B.E., Shah, J. V, and Jansen, L.E. (2014). The quantitative architecture of centromeric chromatin. Elife *3*, e02137.

Bouzinba-Segard, H., Guais, A., and Francastel, C. (2006). Accumulation of small murine minor satellite transcripts leads to impaired centromeric architecture and function. Proc. Natl. Acad. Sci. *103*, 8709–8714.

Bowles, J., and Koopman, P. (2007). Retinoic acid, meiosis and germ cell fate in mammals. Development *134*, 3401–3411.

Bowles, J., Knight, D., Smith, C., Wilhelm, D., Richman, J., Mamiya, S., Yashiro, K., Chawengsaksophak, K., Wilson, M.J., Rossant, J., et al. (2006). Retinoid signaling determines germ cell fate in mice. Science *312*, 596–600.

Brinkley, B.R., and Stubblefield, E. (1966). The fine structure of the kinetochore of a mammalian cell in vitro. Chromosoma *19*, 28–43.

Brunet, S., and Verlhac, M.H. (2011). Positioning to get out of meiosis: The asymmetry of division. Hum. Reprod. Update *17*, 68–75.

Brunet, S., Santa Maria, A., Guillaud, P., Dujardin, D., Kubiak, J.Z., and Maro, B. (1999). Kinetochore fibers are not involved in the formation of the first meiotic spindle in mouse oocytes, but control the exit from the first meiotic M phase. J. Cell Biol. *146*, 1–11.

Budde, P.P., Kumagai, A., Dunphy, W.G., and Heald, R. (2001). Regulation of Op18 during spindle assembly in Xenopus egg extracts. J. Cell Biol. *153*, 149–157.

Burton, A., and Torres-Padilla, M.-E. (2014). Chromatin dynamics in the regulation of cell fate allocation during early embryogenesis. Nat. Rev. Mol. Cell Biol. *15*, 723–735.

Can, A., Semiz, O., and Çinar, O. (2003). Centrosome and microtubule dynamics during early stages of meiosis in mouse oocytes. Mol. Hum. Reprod. *9*, 749–756.

Carabatsos, M.J., Combelles, C.M.H., Messinger, S.M., and Albertini, D.F. (2000). Sorting and reorganization of centrosomes during oocyte maturation in the mouse. Microsc. Res. Tech. *49*, 435–444.

Carmena, M., and Earnshaw, W.C. (2003). The cellular geography of Aurora kinases. Nat. Rev. Mol. Cell Biol. *4*, 842–854.

Carmena, M., Wheelock, M., Funabiki, H., and Earnshaw, W.C. (2012). The chromosomal passenger complex (CPC): From easy rider to the godfather of mitosis. Nat. Rev. Mol. Cell Biol. *13*, 789–803.

Caudron, M., Bunt, G., Bastiaens, P., and Karsenti, E. (2005). Cell Biology: Spatial coordination of spindle assembly by chromosome-mediated signaling gradients. Science *309*, 1373–1376.

Cavrois, M., Fenard, D., Yonezawa, A., Bohuslav, J., Martin, C., Howard, G., Cammack, S., and Givens, R. (2005). The bipolar mitotic kinesin Eg5 moves on both microtubules that it crosslinks. Nature *435*, 114–118.

Chaigne, A., Verlhac, M.H., and Terret, M.E. (2012). Spindle positioning in mammalian oocytes. Exp. Cell Res. *318*, 1442–1447.

Chaigne, A., Terret, M.E., and Verlhac, M.H. (2017). Asymmetries and symmetries in the mouse oocyte and zygote. In Results and Problems in Cell Differentiation. (Springer, Cham), pp. 285–299.

Cheeseman, I.M., Niessen, S., Anderson, S., Hyndman, F., Yates, J.R., Oegema, K., and Desai, A. (2004). A conserved protein network controls assembly of the outer kinetochore and its ability to sustain tension. Genes Dev. *18*, 2255–2268.

Chen, W., and Zhang, D. (2004). Kinetochore fibre dynamics outside the context of the spindle during anaphase. Nat. Cell Biol. *6*, 227–231.

Chen, C.C., Bowers, S., Lipinszki, Z., Palladino, J., Trusiak, S., Bettini, E., Rosin, L., Przewloka, M.R., Glover, D.M., O'Neill, R.J., et al. (2015). Establishment of Centromeric Chromatin by the CENP-A Assembly Factor CAL1 Requires FACT-Mediated Transcription. Dev. Cell *34*, 73–84.

Cherry, L.M., and Johnston, D.A. (1987). Size variation in kinetochores of human chromosomes. Hum. Genet. *75*, 155–158.

Cherry, L.M., Faulkner, A.J., Grossberg, L.A., and Balczon, R. (1989). Kinetochore size variation in mammalian chromosomes: an image analysis study with evolutionary implications. J. Cell Sci. *92*, 281–289.

Chhun, B., Kan, F., Mennella, V., Agard, D.A., McDonald, K.L., Rogers, G.C., Huang, B., and Keszthelyi, B. (2012). Subdiffraction-resolution fluorescence microscopy reveals a domain of the centrosome critical for pericentriolar material organization. Nat. Cell Biol.

14, 1159–1168.

Chmátal, L., Gabriel, S.I., Mitsainas, G.P., Martínez-Vargas, J., Ventura, J., Searle, J.B., Schultz, R.M., and Lampson, M.A. (2014). Centromere strength provides the cell biological basis for meiotic drive and karyotype evolution in mice. Curr. Biol. *24*, 2295–2300.

Choi, T., Aoki, F., Mori, M., and Yamashita, M. (1991). Activation of p34cdc2 protein kinase activity in meiotic and mitotic cell cycles in mouse oocytes and embryos. Development *113*, 789–795.

Choi, Y.K., Liu, P., Sze, S.K., Dai, C., and Qi, R.Z. (2010). CDK5RAP2 stimulates microtubule nucleation by the γ-tubulin ring complex. J. Cell Biol. *191*, 1089–1095.

Ciferri, C., Stukenberg, P.T., Areces, L.B., Mapelli, M., Schneider, T.R., Musacchio, A., Tarricone, C., and Sessa, F. (2005). Mechanism of Aurora B Activation by INCENP and Inhibition by Hesperadin. Mol. Cell *18*, 379–391.

Ciferri, C., Musacchio, A., and Petrovic, A. (2007). The Ndc80 complex: Hub of kinetochore activity. FEBS Lett. *581*, 2862–2869.

Ciferri, C., Pasqualato, S., Screpanti, E., Varetti, G., Santaguida, S., Dos Reis, G., Maiolica, A., Polka, J., De Luca, J.G., De Wulf, P., et al. (2008). Implications for Kinetochore-Microtubule Attachment from the Structure of an Engineered Ndc80 Complex. Cell *133*, 427–439.

Clift, D., and Schuh, M. (2015). A three-step MTOC fragmentation mechanism facilitates bipolar spindle assembly in mouse oocytes. Nat. Commun. *6*, 1–12.

Cochran, J.C., Gatial, J.E., Kapoor, T.M., and Gilbert, S.P. (2005). Monastrol inhibition of the mitotic kinesin Eg5. J. Biol. Chem. *280*, 12658–12667.

Comings, D.E., and Okada, T.A. (1971). Fine structure of kinetochore in Indian muntjac. Exp. Cell Res. *67*, 97–110.

Conduit, P.T., Wainman, A., and Raff, J.W. (2015). Centrosome function and assembly in animal cells. Nat. Rev. Mol. Cell Biol. *16*, 611–624.

Courtois, A., Schuh, M., Ellenberg, J., and Hiiragi, T. (2012). The transition from meiotic to mitotic spindle assembly is gradual during early mammalian development. J. Cell Biol. *198*, 357–370.

Davydenko, O., Schultz, R.M., and Lampson, M.A. (2013). Increased CDK1 activity determines the timing of kinetochore-microtubule attachments in meiosis I. J. Cell Biol. *202*, 221–229.

Dawe, R.K., and Cande, W.Z. (2002). Induction of centromeric activity in maize by suppressor of meiotic drive 1. Proc. Natl. Acad. Sci. *93*, 8512–8517.

Dawicki-McKenna, J.M., Chmátal, L., Lampson, M.A., Schultz, R.M., Falk, S.J., Sullivan, B.A., Black, B.E., Yang, K., Akera, T., and Iwata-Otsubo, A. (2017). Expanded Satellite Repeats Amplify a Discrete CENP-A Nucleosome Assembly Site on Chromosomes that Drive in Female Meiosis. Curr. Biol. *27*, 2365-2373.e8.

Delaval, B., and Doxsey, S.J. (2010). Pericentrin in cellular function and disease. J. Cell Biol. *188*, 181–190.

Drpic, D., Almeida, A.C., Aguiar, P., Renda, F., Damas, J., Lewin, H.A., Larkin, D.M., Khodjakov, A., and Maiato, H. (2018). Chromosome Segregation Is Biased by Kinetochore Size. Curr. Biol. *28*, 1344-1356.e5.

Du, Y., Topp, C.N., and Dawe, R.K. (2010). DNA binding of centromere protein C (CENPC) is stabilized by single-stranded RNA. PLoS Genet. *6(2)*, e1000835.

Dumont, J., and Desai, A. (2012). Acentrosomal spindle assembly and chromosome segregation during oocyte meiosis. Trends Cell Biol. *22*, 241–249.

Dumont, J., Petri, S., Pellegrin, F., Terret, M.E., Bohnsack, M.T., Rassinier, P., Georget, V., Kalab, P., Gruss, O.J., and Verlhac, M.H. (2007a). A centriole- and RanGTP-independent spindle assembly pathway in meiosis I of vertebrate oocytes. J. Cell Biol. *176*, 295–305.

Dumont, J., Million, K., Sunderland, K., Rassinier, P., Lim, H., Leader, B., and Verlhac, M.H. (2007b). Formin-2 is required for spindle migration and for the late steps of cytokinesis in mouse oocytes. Dev. Biol. *301*, 254–265.

Dzhindzhev, N.S., Yu, Q.D., Weiskopf, K., Tzolovsky, G., Cunha-Ferreira, I., Riparbelli, M., Rodrigues-Martins, A., Bettencourt-Dias, M., Callaini, G., and Glover, D.M. (2010). Asterless is a scaffold for the onset of centriole assembly. Nature *467*, 714–718.

Earnshaw, W.C., and Rothfield, N. (1985). Identification of a family of human centromere proteins using autoimmune sera from patients with scleroderma. Chromosoma *91*, 313–321.

Earnshaw, W.C., Ratrie, H., and Stetten, G. (1989). Visualization of centromere proteins CENP-B and CENP-C on a stable dicentric chromosome in cytological spreads. Chromosoma *98*, 1–12.

Fachinetti, D., Han, J.S., McMahon, M.A., Ly, P., Abdullah, A., Wong, A.J., and Cleveland, D.W. (2015). DNA Sequence-Specific Binding of CENP-B Enhances the Fidelity of Human Centromere Function. Dev. Cell *33*, 314–327.

Farache, D., Emorine, L., Haren, L., and Merdes, A. (2018). Assembly and regulation of γ-tubulin complexes. Open Biol. *8(3)*, 170266

De Felici, M., and Barrios, F. (2013). Seeking the origin of female germline stem cells in the mammalian ovary. Reproduction *146*, 125–130.

Ferri, F., Bouzinba-Segard, H., Velasco, G., Hubé, F., and Francastel, C. (2009). Non-coding murine centromeric transcripts associate with and potentiate Aurora B kinase. Nucleic Acids Res. *37*, 5071–5080.

Ferris, S.D., Sage, R.D., and Wilson, A.C. (1982). Evidence from mtDNA sequences that common laboratory strains of inbred mice are descended from a single female. Nature *295*, 163–165.

Fishman, L., and Saunders, A. (2008). Centromere-associated female meiotic drive entails male fitness costs in monkeyflowers. Science *322*, 1559–1562.

Fishman, L., and Willis, J.H. (2005). A novel meiotic drive locus almost completely distorts segregation in Mimulus (monkeyflower) hybrids. Genetics *169*, 347–353.

Franz, A., Basto, R., Raff, J.W., Khodjakov, A., Brunk, K., Vinadogrova, T., and Peel, N. (2008). Centrosome Amplification Can Initiate Tumorigenesis in Flies. Cell *133*, 1032–1042.

Gabriel, S.I., Schultz, R.M., Lampson, M.A., Searle, J.B., Martínez-Vargas, J., Mitsainas, G.P., Ventura, J., and Chmátal, L. (2014). Centromere Strength Provides the Cell Biological Basis for Meiotic Drive and Karyotype Evolution in Mice. Curr. Biol. *24*, 2295–2300.

Garagna, S., Marziliano, N., Zuccotti, M., Searle, J.B., Capanna, E., Redi, C.A., and Lansdorp, P.M. (2001). Pericentromeric organization at the fusion point of mouse Robertsonian translocation chromosomes. Proc. Natl. Acad. Sci. *98*, 171–175.

Gascoigne, K.E., and Cheeseman, I.M. (2011). Kinetochore assembly: if you build it, they will come. Curr. Opin. Cell Biol. *23*, 102–108.

Gavin, a C., Cavadore, J.C., and Schorderet-Slatkine, S. (1994). Histone H1 kinase activity, germinal vesicle breakdown and M phase entry in mouse oocytes. J. Cell Sci. *107(1)*, 275–283.

Gieni, R.S., Chan, G.K.T., and Hendzel, M.J. (2008). Epigenetics regulate centromere formation and kinetochore function. J. Cell. Biochem. *104*, 2027–2039.

Gilchrist, R.B., Ritter, L.J., and Armstrong, D.T. (2001). Mouse Oocyte Mitogenic Activity Is Developmentally Coordinated throughout Folliculogenesis and Meiotic Maturation. Dev. Biol. *240*, 289–298.

Godek, K.M., Kabeche, L., and Compton, D.A. (2015). Regulation of kinetochore-microtubule attachments through homeostatic control during mitosis. Nat. Rev. Mol. Cell Biol. *16*, 57–64.

Gopalan, G., Chan, C.S.M., and Donovan, P.J. (1997). A novel mammalian, mitotic spindle-associated kinase is related to yeast and fly chromosome segregation regulators. J. Cell Biol. *138*, 643–656.

Gruss, O.J., Carazo-Salas, R.E., Schatz, C.A., Guarguaglini, G., Kast, J., Wilm, M., Le Bot, N., Vernos, I., Karsenti, E., and Mattaj, I.W. (2001). Ran induces spindle assembly by reversing the inhibitory effect of importin α on TPX2 activity. Cell *104*, 83–93.

Guenatri, M., Bailly, D., Maison, C., and Almouzni, G. (2004). Mouse centric and pericentric satellite repeats form distinct functional heterochromatin. J. Cell Biol. *166*, 493–505.

Gueth-Hallonet, C., Antony, C., Aghion, J., Santa-Maria, A., Lajoie-Mazenc, I., Wright, M., and Maro, B. (1993). γ-Tubulin is present in acentriolar MTOCs during early mouse development. Cell Sci. *105*, 157–166.

Gui, L., and Homer, H. (2012). Spindle assembly checkpoint signalling is uncoupled from chromosomal position in mouse oocytes. Development *139*, 1941–1946.

Guillaud, P., Maro, B., Rassinier, P., Lefebvre, C., and Verlhac, M.-H. (2002). Asymmetric division in mouse oocytes: with or without Mos. Curr. Biol. *10*, 1303–1306.

Hached, K., Xie, S.Z., Buffin, E., Cladiere, D., Rachez, C., Sacras, M., Sorger, P.K., and Wassmann, K. (2011). Mps1 at kinetochores is essential for female mouse meiosis I. J. Cell Sci. *138*, 2261–2271.

Hall, I.M., Shankaranarayana, G.D., Noma, K. ichi, Ayoub, N., Cohen, A., and Grewal, S.I.S. (2002). Establishment and maintenance of a heterochromatin domain. Science *297*, 2232–2237.

Hall, L.E., Mitchell, S.E., and O'Neill, R.J. (2012). Pericentric and centromeric transcription: A perfect balance required. Chromosom. Res. *20*, 535–546.

Handel, M.A., and Schimenti, J.C. (2010). Genetics of mammalian meiosis: regulation, dynamics and impact on fertility. Nat. Rev. Genet. *11*, 124–136.

Harel, J., Hanania, N., Tapiero, H., and Harel, L. (1968). RNA replication by nuclear satellite DNA in different mouse cells. Biochem. Biophys. Res. Commun. *33*, 696–701.

Hengeveld, R.C.C., Vromans, M.J.M., Vleugel, M., Hadders, M.A., and Lens, S.M.A. (2017).

Inner centromere localization of the CPC maintains centromere cohesion and allows mitotic checkpoint silencing. Nat. Commun. *8*, 15542.

Henikoff, S., and Malik, H.S. (2002). Selfish drivers. Nature *417*, 227.

Henikoff, S., Ahmad, K., and Malik, H.S. (2001). The centromere paradox: Stable inheritance with rapidly evolving DNA. Science *293*, 1098–1102.

Herbert, M., Kalleas, D., Cooney, D., Lamb, M., and Lister, L. (2015). Meiosis and maternal aging: insights from aneuploid oocytes and trisomy births. Cold Spring Harb. Perspect. Biol. *7*, a017970.

Herskowitz Ira (1987). Functional inactivation of genes by dominant negative mutations. Nature *329*, 855–857.

Hertig, A.T. (2004). STUDIES ON THE HUMAN OOCYTE AND ITS FOLLICLE: I. Ultrastructural and Histochemical Observations on the Primordial Follicle Stage. J. Cell Biol. *34*, 647–675.

Hewitt, G.M. (1976). Meiotic drive for B-chromosomes in the primary oocytes of Myrmekotettix maculatus (Orthoptera: Acrididae). Chromosoma *56*, 381–391.

Hodges, C.A., and Hunt, P.A. (2002). Simultaneous analysis of chromosomes and chromosome-associated proteins in mammalian oocytes and embryos. Chromosoma *111*, 165–169.

Holt, J.E., and Jones, K.T. (2009). Control of homologous chromosome division in the mammalian oocyte. Mol. Hum. Reprod. *15*, 139–147.

Holubcová, Z., Blayney, M., Elder, K., and Schuh, M. (2015). Error-prone chromosome-mediated spindle assembly favors chromosome segregation defects in human oocytes. Obstet. Gynecol. Surv. *70*, 572–573.

Van Hooser, A.A., Ouspenski, I.I., Gregson, H.C., Starr, D.A., Yen, T.J., Goldberg, M.L., Yokomori, K., Earnshaw, W.C., Sullivan, K.F., and Brinkley, B.R. (2001). Specification of kinetochore-forming chromatin by the histone H3 variant CENP-A. J. Cell Sci. *114*, 3529–3542.

Huber, H.E., Halczenko, W., Kuo, L.C., Yan, Y., Homnick, C., Xu, B., Buser, C.A., Sardana, V., Hartman, G.D., and Schaber, M. (2003). Inhibition of a Mitotic Motor Protein: Where, How, and Conformational Consequences. J. Mol. Biol. *335*, 547–554.

Ideue, T., Cho, Y., Nishimura, K., and Tani, T. (2014). Involvement of satellite I noncoding RNA in regulation of chromosome segregation. Genes to Cells *19*, 528–538.

Iwata-Otsubo, A., Dawicki-McKenna, J.M., Akera, T., Falk, S.J., Chmátal, L., Yang, K., Sullivan, B.A., Schultz, R.M., Lampson, M.A., and Black, B.E. (2017). Expanded Satellite Repeats Amplify a Discrete CENP-A Nucleosome Assembly Site on Chromosomes that Drive in Female Meiosis. Curr. Biol. *27(15)*, 2365-2373.

Jaffe, L.A., and Egbert, J.R. (2017). Regulation of Mammalian Oocyte Meiosis by Intercellular Communication Within the Ovarian Follicle. Annu. Rev. Physiol. *79*, 237–260.

Jagannathan, M., Cummings, R., and Yamashita, Y.M. (2018). A conserved function for pericentromeric satellite DNA. Elife *7*, 1–19.

Jessberger, R. (2012). Age-related aneuploidy through cohesion exhaustion. EMBO Rep. *13(6)*, 539-546.

Jin, S.-L.C., Richard, F.J., Kuo, W.-P., D'Ercole, A.J., and Conti, M. (2002). Impaired growth and fertility of cAMP-specific phosphodiesterase PDE4D-deficient mice. Proc. Natl. Acad. Sci. *96*, 11998–12003.

Johnson, W.L., Yewdell, W.T., Bell, J.C., McNulty, S.M., Duda, Z., O'Neill, R.J., Sullivan, B.A., and Straight, A.F. (2017). RNA-dependent stabilization of SUV39H1 at constitutive heterochromatin. Elife *6*, e25299.

Jokelainen, P.T. (1967). The ultrastructure and spatial organization of the metaphase kinetochore in mitotic rat cells. J. Ultrasructure Res. *19*, 19–44.

Jones, K.T., and Lane, S.I.R. (2012). Chromosomal, metabolic, environmental, and hormonal origins of aneuploidy in mammalian oocytes. Exp. Cell Res. *318*, 1394–1399.

Jones, K.T., and Lane, S.I.R. (2013). Molecular causes of aneuploidy in mammalian eggs. Development *140*, 3719–3730.

Joseph, A., Mitchell, A.R., and Miller, O.J. (1989). The organization of the mouse satellite DNA at centromeres. Exp. Cell Res. *183(2)*, 494-500.

Kabeche, L., Nguyen, H.D., Buisson, R., and Zou, L. (2018). A mitosis-specific and R loop-driven ATR pathway promotes faithful chromosome segregation. Science *359*, 108–114.

Kapoor, T.M., Lampson, M.A., Hergert, P., Cameron, L., Cimini, D., Salmon, E.D., McEwen, B.F., and Khodjakov, A. (2006). Chromosomes can congress to the metaphase plate before biorientation. Science *311*, 388–391.

Kelly, A.E., and Funabiki, H. (2009). Correcting aberrant kinetochore microtubule attachments: an Aurora B-centric view. Curr. Opin. Cell Biol. *21*, 51–58.

Kirschner, M., and Mitchison, T. (1986). Beyond self-assembly: From microtubules to morphogenesis. Cell *45*, 329–342.

Kitajima, T.S. (2018). Mechanisms of kinetochore-microtubule attachment errors in mammalian oocytes. Dev. Growth Differ. *60*, 33–43.

Kitajima, T.S., Ohsugi, M., and Ellenberg, J. (2011). Complete kinetochore tracking reveals error-prone homologous chromosome biorientation in mammalian oocytes. Cell *146*, 568–581.

Kline, S.L., Cheeseman, I.M., Hori, T., Fukagawa, T., and Desai, A. (2006). The human Mis12 complex is required for kinetochore assembly and proper chromosome segregation. J. Cell Biol. *173*, 9–17.

Knott, G., Strnad, P., Gonczy, P., von Tobel, L., Mikeladze-Dvali, T., Schermelleh, L., and Leonhardt, H. (2012). Analysis of centriole elimination during C. elegans oogenesis. Development *139*, 1670–1679.

Koblížková, A., Neumann, P., Fuková, I., Jedličková, V., Novák, P., Pavlíková, Z., and Macas, J. (2015). Centromeres Off the Hook: Massive Changes in Centromere Size and Structure Following Duplication of CenH3 Gene in Fabeae Species . Mol. Biol. Evol. *32*, 1862–1879.

Kolano, A., Brunet, S., Silk, A.D., Cleveland, D.W., and Verlhac, M.-H. (2012). Error-prone mammalian female meiosis from silencing the spindle assembly checkpoint without normal interkinetochore tension. Proc. Natl. Acad. Sci. *109*, E1858–E1867.

Kollman, J.M., Merdes, A., Mourey, L., and Agard, D.A. (2011). Microtubule nucleation by γ-tubulin complexes. Nat. Rev. Mol. Cell Biol. *12*, 709–721.

Koubova, J., Menke, D.B., Zhou, Q., Capel, B., Griswold, M.D., and Page, D.C. (2006). Retinoic acid regulates sex-specific timing of meiotic initiation in mice. Proc. Natl. Acad. Sci. U. S. A. *103*, 2474–2479.

Kuchnir Fygenson, D., Flyvbjerg, H., Sneppen, K., Libchaber, A., and Leibler, S. (1995). Spontaneous nucleation of microtubules. Phys. Rev. E *51*, 5058–5063.

Kumar, A., Rajendran, V., Sethumadhavan, R., and Purohit, R. (2013). CEP proteins: The knights of centrosome dynasty. Protoplasma *250*, 965–983.

Kursel, L.E., and Malik, H.S. (2018). The cellular mechanisms and consequences of centromere drive. Curr. Opin. Cell Biol. *52*, 58–65.

Kwon, M., Godinho, S.A., Chandhok, N.S., Ganem, N.J., Azioune, A., Thery, M., and Pellman, D. (2008). Mechanisms to suppress multipolar divisions in cancer cells with extra centrosomes. Genes Dev. *22*, 2189–2203.

Lampson, M., and Grishchuk, E. (2017). Mechanisms to Avoid and Correct Erroneous Kinetochore-Microtubule Attachments. Biology *6(1)*, 1.

Lampson, M.A., and Black, B.E. (2017). Cellular and Molecular Mechanisms of Centromere Drive. Cold Spring Harb. Symp. Quant. Biol. *82*, 249–257.

Lampson, M.A., and Cheeseman, I.M. (2011). Sensing centromere tension: Aurora B and the regulation of kinetochore function. Trends Cell Biol. *21*, 133–140.

Lampson, M.A., Renduchitala, K., Khodjakov, A., and Kapoor, T.M. (2004). Correcting improper chromosome–spindle attachments during cell division. Nat. Cell Biol. *6*, 232–237.

Lane, S.I.R., and Jones, K.T. (2017). Chromosome biorientation and APC activity remain uncoupled in oocytes with reduced volume. J. Cell Biol. *216*, 3949–3957.

Lane, S.I.R., Chang, H.Y., Jennings, P.C., and Jones, K.T. (2010). The Aurora kinase inhibitor ZM447439 accelerates first meiosis in mouse oocytes by overriding the spindle assembly checkpoint. Reproduction *140*, 521–530.

Lane, S.I.R., Yun, Y., and Jones, K.T. (2012). Timing of anaphase-promoting complex activation in mouse oocytes is predicted by microtubule-kinetochore attachment but not by bivalent alignment or tension. Development *139*, 1947–1955.

Leader, B., Lim, H., Carabatsos, M.J., Harrington, A., Ecsedy, J., Pellman, D., Maas, R., and Leder, P. (2002). Formin-2, polyploidy, hypofertility and positioning of the meiotic spindle in mouse oocytes. Nat. Cell Biol. *4*, 921–928.

Lee, I.W., Jo, Y.J., Jung, S.M., Wang, H.Y., Kim, N.H., and Namgoong, S. (2018). Distinct roles of Cep192 and Cep152 in acentriolar MTOCs and spindle formation during mouse oocyte maturation. FASEB J. *32*, 625–638.

Lee, S.-C., Yang, K.-T., Tang, T.K., Li, S.-K., Chang, C.-C., Tang, C.-J.C., and Lin, Y.-N. (2010). Aurora-C Kinase Deficiency Causes Cytokinesis Failure in Meiosis I and Production of Large Polyploid Oocytes in Mice. Mol. Biol. Cell *21*, 2371–2383.

Li, R., and Albertini, D.F. (2013). The road to maturation: Somatic cell interaction and self-organization of the mammalian oocyte. Nat. Rev. Mol. Cell Biol. *14*, 141–152.

Li, H., Guo, F., Rubinstein, B., and Li, R. (2008). Actin-driven chromosomal motility leads to symmetry breaking in mammalian meiotic oocytes. Nat. Cell Biol. *10*, 1301–1308.

Li, L., Zheng, P., and Dean, J. (2010). Maternal control of early mouse development. Development *137*, 859–870.

Longo, F.J., and Chen, D.Y. (1985). Development of cortical polarity in mouse eggs: Involvement of the meiotic apparatus. Dev. Biol. *107*, 382–394.

Luksza, M., Queguigner, I., Verlhac, M.H., and Brunet, S. (2013). Rebuilding MTOCs upon centriole loss during mouse oogenesis. Dev. Biol. *382*, 48–56.

Luykx, P. (1965). The structure of the kinetochore in meiosis and mitosis in Urechis eggs. Exp. Cell Res. *39*, 643–657.

Ma, J., Shuda, K., Schultz, R.M., Donovan, P.J., and Schindler, K. (2009). Aurora kinase B modulates chromosome alignment in mouse oocytes. Mol. Reprod. Dev. *76*, 1094–1105.

Ma, W., Baumann, C., and Viveiros, M.M. (2010). NEDD1 is crucial for meiotic spindle stability and accurate chromosome segregation in mammalian oocytes. Dev. Biol. *339*, 439–450.

MacLean-Fletcher, S. (2004). Mechanism of action of cytochalasin B on actin. Cell *20*, 329–341.

MacLennan, M., Crichton, J.H., Playfoot, C.J., and Adams, I.R. (2015). Oocyte development, meiosis and aneuploidy. Semin. Cell Dev. Biol. *45*, 68–76.

Magidson, V., O'Connell, C.B., Lončarek, J., Paul, R., Mogilner, A., and Khodjakov, A. (2011). The spatial arrangement of chromosomes during prometaphase facilitates spindle assembly. Cell *146*, 555–567.

Magidson, V., Paul, R., Yang, N., Ault, J.G., O'Connell, C.B., Tikhonenko, I., Mcewen, B.F., Mogilner, A., and Khodjakov, A. (2015). Adaptive changes in the kinetochore architecture facilitate proper spindle assembly. Nat. Cell Biol. *17*, 1134–1144.

Maison, C., Bailly, D., Peters, A.H.F.M., Quivy, J.P., Roche, D., Taddei, A., Lachner, M., Jenuwein, T., and Almouzni, G. (2002). Higher-order structure in pericentric heterochromatin involves a distinct pattern of histone modification and an RNA component. Nat. Genet. *30*, 329–334.

Maison, C., Bailly, D., Roche, D., de Oca, R.M., Probst, A. V, Vassias, I., Dingli, F., Lombard, B., Loew, D., Quivy, J.-P., et al. (2011). SUMOylation promotes de novo targeting of HP1α to pericentric heterochromatin. Nat. Genet. *43*, 220–227.

Maliga, Z., Kapoor, T.M., and Mitchison, T.J. (2002). Evidence that monastrol is an allosteric inhibitor of the mitotic kinesin Eg5. Chem. Biol. *9*, 989–996.

Malik, H.S., and Henikoff, S. (2009). Major Evolutionary Transitions in Centromere Complexity. Cell *138*, 1067–1082.

Manandhar, G., Schatten, H., and Sutovsky, P. (2004). Centrosome Reduction During Gametogenesis and Its Significance1. Biol. Reprod. *72*, 2–13.

Maraschio, P., Zuffardi, O., Peretti, D., Lambiase, S., and Lo Curto, F. (2004). Indirect immunofluorescence of inactive centromeres as indicator of centromeric function. Hum. Genet. *73*, 12–16.

Masciarelli, S., Horner, K., Liu, C., Park, S.H., Hinckley, M., Hockman, S., Nedachi, T., Jin, C., Conti, M., and Manganiello, V. (2004). Cyclic nucleotide phosphodiesterase 3A-deficient mice as a model of female infertility. J. Clin. Invest. *114*, 196–205.

Masumoto, H., Masukata, H., Muro, Y., Nozaki, N., and Okazaki, T. (1989). A human centromere antigen (CENP-B) interacts with a short specific sequence in alphoid DNA, a human centromeric satellite. J. Cell Biol. *109*, 1963–1973.

Mattson, B.A., and Albertini, D.F. (1990). Oogenesis: Chromatin and microtubule dynamics during meiotic prophase. Mol. Reprod. Dev. *25*, 374–383.

Mayer, T.U., Kapoor, T.M., Haggarty, S.J., King, R.W., Schreiber, S.L., and Mitchison, T.J. (1999). Smart molecule inhibitor of mitotic spindle bipolarity identified in a phenotype-based screen. Science *286*, 971–974.

McIntosh, J.R., Morphew, M.K., Grissom, P.M., Gilbert, S.P., and Hoenger, A. (2009). Lattice Structure of Cytoplasmic Microtubules in a Cultured Mammalian Cell. J. Mol. Biol. *394*, 177–182.

McKay, R.D.G. (1973). The mechanism of G and C banding in mammalian metaphase chromosomes. Chromosoma *44*, 1–14.

McKinley, K.L., and Cheeseman, I.M. (2016). The molecular basis for centromere identity and function. Nat. Rev. Mol. Cell Biol. *17*, 16–29.

McLaren, A. (2003). Primordial germ cells in the mouse. Dev. Biol. *262*, 1–15.

McNulty, S.M., Sullivan, L.L., and Sullivan, B.A. (2017). Human centromeres produce chromosome-specific and array-specific alpha satellite transcripts that are complexed with CENP-A and CENP-C. Dev. Cell *42*, 226–240.

Mehlmann, L.M. (2005). Stops and starts in mammalian oocytes: Recent advances in understanding the regulation of meiotic arrest and oocyte maturation. Reproduction *130(6)*, 791-799.

Mehlmann, L.M., Jones, T.L.Z., and Jaffe, L.A. (2002). Meiotic arrest in the mouse follicle maintained by a G s protein in the oocyte. Science *297*, 1343-1345.

Mennella, V., Agard, D.A., Huang, B., and Pelletier, L. (2014). Amorphous no more: Subdiffraction view of the pericentriolar material architecture. Trends Cell Biol. *24*, 188–197.

Messinger, S.M., and Albertini, D.F. (1991). Centrosome and Microtubule Dynamics During Meiotic Progression in the Mouse Oocyte. J. Cell Sci. *100*, 289–298.

Michaut, M.A., Williams, C.J., and Schultz, R.M. (2005). Phosphorylated MARCKS: A novel centrosome component that also defines a peripheral subdomain of the cortical actin cap in mouse eggs. Dev. Biol. *280*, 26–37.

Mihajlović, A.I., and FitzHarris, G. (2018). Segregating Chromosomes in the Mammalian Oocyte. Curr. Biol. *28*, R895–R907.

Miyanari, Y., Ziegler-Birling, C., and Torres-Padilla, M.E. (2013). Live visualization of chromatin dynamics with fluorescent TALEs. Nat. Struct. Mol. Biol. *20*, 1321–1324.

Mogessie, B., and Schuh, M. (2017). Actin protects mammalian eggs against chromosome segregation errors. Science *357*, eaal1647.

Mogessie, B., Scheffler, K., and Schuh, M. (2018). Assembly and Positioning of the Oocyte Meiotic Spindle. Annu. Rev. Cell Dev. Biol. *34*, 381–403.

Monda, J.K., and Cheeseman, I.M. (2018). The kinetochore–microtubule interface at a glance. J. Cell Sci. *131*, jcs214577.

Moritz, M., Braunfeld, M.B., Guénebaut, V., Heuser, J., and Agard, D.A. (2000). Structure of the γ-tubulin ring complex: A template for microtubule nucleation. Nat. Cell Biol. *2*, 365–370.

Morris, C.A., and Moazed, D. (2007). Centromere assembly and propagation. Cell *128*, 647–650.

Moutinho-Pereira, S., Vandenbeldt, K.J., McEwen, B.F., Maiato, H., Rieder, C.L., Hergert, P.J., and Dong, Y. (2006). The ultrastructure of the kinetochore and kinetochore fiber in Drosophila somatic cells. Chromosoma *115*, 469–480.

Müller, H., Schmidt, D., Steinbrink, S., Mirgorodskaya, E., Lehmann, V., Habermann, K., Dreher, F., Gustavsson, N., Kessler, T., Lehrach, H., et al. (2010). Proteomic and functional analysis of the mitotic Drosophila centrosome. EMBO J. *29*, 3344–3357.

Muro, Y., Masumoto, H., Yoda, K., Nozaki, N., Ohashi, M., and Okazaki, T. (1992). Centromere protein B assembles human centromeric α-satellite DNA at the 17-bp sequence, CENP-B box. J. Cell Biol. *116*, 585–596.

Muroyama, A., Seldin, L., and Lechler, T. (2016). Divergent regulation of functionally distinct γ-tubulin complexes during differentiation. J. Cell Biol. *213*, 679–692.

Musacchio, A., and Desai, A. (2017). A Molecular View of Kinetochore Assembly and Function. Biology. *6(1)*, 5.

Muszynski, M.G., Dawe, R.K., Hiatt, E.N., Reed, L.M., and Yu, H.-G. (2007). A Maize Homolog of Mammalian CENPC Is a Constitutive Component of the Inner Kinetochore. Plant Cell *11*, 1227-1238..

Na, J., Zernicka-Goetz, M., Sharif, B., Lykke-Hartmann, K., Glover, D.M., Laue, E., and McLaughlin, S.H. (2010). The chromosome passenger complex is required for fidelity of chromosome transmission and cytokinesis in meiosis of mouse oocytes. J. Cell Sci. *123*, 4292–4300.

Nguyen, A.L., and Schindler, K. (2017). Specialize and Divide (Twice): Functions of Three Aurora Kinase Homologs in Mammalian Oocyte Meiotic Maturation. Trends Genet. *33*, 349–363.

Nguyen, A.L., Drutovic, D., Vazquez, B.N., El Yakoubi, W., Gentilello, A.S., Malumbres, M., Solc, P., and Schindler, K. (2018). Genetic Interactions between the Aurora Kinases Reveal New Requirements for AURKB and AURKC during Oocyte Meiosis. Curr. Biol. *28*, 3458–3468.

Nicklas, R.B. (1997). How cells get the right chromosomes. Science *275*, 632-637.

Nicolson, G.L., Yanagimachi, R., and Yanagimachi, H. (1975). Ultrastructural localization of lectin-binding sites on the zonae pellucidae and plasma membranes of mammalian eggs. J. Cell Biol. *66*, 263–274.

Niethammer, P., Bastiaens, P., and Karsenti, E. (2004). Stathmin-Tubutin Interaction Gradients in Motile and Mitotic Cells. Science *303*, 1862–1866.

Nigg, E.A., and Raff, J.W. (2009). Centrioles, Centrosomes, and Cilia in Health and Disease. Cell *139*, 663–678.

Nikolic, A., Volarevic, V., Armstrong, L., Lako, M., and Stojkovic, M. (2016). Primordial Germ Cells: Current Knowledge and Perspectives. Stem Cells Int. *2016*, 1741072.

Norris, R.P., Ratzan, W.J., Freudzon, M., Mehlmann, L.M., Krall, J., Movsesian, M.A., Wang, H., Ke, H., Nikolaev, V.O., and Jaffe, L.A. (2009). Cyclic GMP from the surrounding somatic cells regulates cyclic AMP and meiosis in the mouse oocyte. Development *136*, 1869–1878.

Obuse, C., Iwasaki, O., Kiyomitsu, T., Goshima, G., Toyoda, Y., and Yanagida, M. (2004). A conserved Mis12 centromere complex is linked to heterochromatic HP1 and outer kinetochore protein Zwint-1. Nat. Cell Biol. *6*, 1135–1141.

Ottolini, C.S., Newnham, L.J., Capalbo, A., Natesan, S.A., Joshi, H.A., Cimadomo, D., Griffin, D.K., Sage, K., Summers, M.C., Thornhill, A.R., et al. (2015). Genome-wide maps of recombination and chromosome segregation in human oocytes and embryos show selection for maternal recombination rates. Nat. Genet. *47*, 727–735.

Page, S.L., and Hawley, R.S. (2003). Chromosome choreography: The meiotic ballet. Science *301*, 785–789.

Palmer, D.K., O'Day, K., Wener, M.H., Andrews, B.S., and Margolis, R.L. (1987). A 17-kD centromere protein (CENP-A) copurifies with nucleosome core particles and with histones. J. Cell Biol. *104*, 805–815.

Pardo-Manuel De Villena, F., and Sapienza, C. (2001). Nonrandom segregation during meiosis: The unfairness of females. Mamm. Genome *12*, 331–339.

Pardue, M. Lou, and Gall, J.G. (1970). Chromosomal localization of mouse satellite DNA. Science *168*, 1356–1358.

Peacock, W.J., Dennis, E.S., Rhoades, M.M., and Pryor, A.J. (2006). Highly repeated DNA sequence limited to knob heterochromatin in maize. Proc. Natl. Acad. Sci. *78*, 4490–4494.

Pedeutour, F., Irvine, D. V., Choo, K.H.A., Saffery, R., Amor, D.J., Perry, J., and Sirvent, N. (2005). Chromosome size and origin as determinants of the level of CENP-A incorporation into human centromeres. Chromosom. Res. *12*, 805–815.

Perea-Resa, C., and Blower, M.D. (2017). Satellite Transcripts Locally Promote Centromere Formation. Dev. Cell *42*, 201–202.

Perea-Resa, C., and Blower, M.D. (2018). Centromere Biology: Transcription Goes on Stage. Mol. Cell. Biol. *38*, e00263-18.

Petronczki, M., Siomos, M.F., and Nasmyth, K. (2003). The Molecular Biology of Chromosome Segregation in Meiosis Review. Cell *112*, 423–440.

Petrovic, A., Pasqualato, S., Dube, P., Krenn, V., Santaguida, S., Cittaro, D., Monzani, S., Massimiliano, L., Keller, J., Tarricone, A., et al. (2010). The MIS12 complex is a protein interaction hub for outer kinetochore assembly. J. Cell Biol. *190*, 835–852.

Petrovic, A., Mosalaganti, S., Keller, J., Mattiuzzo, M., Overlack, K., Krenn, V., DeAntoni, A., Wohlgemuth, S., Cecatiello, V., Pasqualato, S., et al. (2014). Modular Assembly of RWD Domains on the Mis12 Complex Underlies Outer Kinetochore Organization. Mol. Cell *53*, 591–605.

Petsalaki, E., Akoumianaki, T., Black, E.J., Gillespie, D.A.F., and Zachos, G. (2011). Phosphorylation at serine 331 is required for Aurora B activation. J. Cell Biol. *195*, 449–466.

Pimenta-Marques, A., Bento, I., Lopes, C.A.M., Duarte, P., Jana, S.C., and Bettencourt-Dias, M. (2016). A mechanism for the elimination of the female gamete centrosome in Drosophila melanogaster . Science *353*, aaf4866.

Plohl, M. (2002). Variation in satellite DNA profiles and effects. EMBO J. *21*, 5955–5959.

Plum, L., Giesen, K., Kluge, R., Junger, E., Linnartz, K., Schürmann, A., Becker, W., and Joost, H.G. (2002). Characterisation of the mouse diabetes susceptibilty locus Nidd/SJL: islet cell destruction, interaction with the obesity QTL Nob1, and effect of dietary fat. Diabetologia *45*, 823–830.

Prosser, S.L., and Pelletier, L. (2017). Mitotic spindle assembly in animal cells: A fine balancing act. Nat. Rev. Mol. Cell Biol. *18*, 187–201.

Przewloka, M.R., Venkei, Z., Bolanos-Garcia, V.M., Debski, J., Dadlez, M., and Glover, D.M. (2011). CENP-C is a structural platform for kinetochore assembly. Curr. Biol. *21*, 399–405.

Pummerer, C.L., Luze, K., Grässl, G., Bachmaier, K., Offner, F., Burrell, S.K., Lenz, D.M., Zamborelli, T.J., Penninger, J.M., and Neu, N. (1996). Identification of cardiac myosin peptides capable of inducing autoimmune myocarditis in BALB/c mice. J. Clin. Invest. *97*, 2057–2062.

Quartuccio, S.M., and Schindler, K. (2015). Functions of Aurora kinase C in meiosis and cancer. Front. Cell Dev. Biol. *3*, 50.

Raju, G.A.R., Chavan, R., Deenadayal, M., Gunasheela, D., Gutgutia, R., Haripriya, G., Govindarajan, M., Patel, N.H., and Patki, A.S. (2013). Luteinizing hormone and follicle stimulating hormone synergy: A review of role in controlled ovarian hyper-stimulation. J. Hum. Reprod. Sci. *6(4)*, 227.

Ray, S., Meyhöfer, E., Milligan, R.A., and Howard, J. (1993). Kinesin follows the microtubule's protofilament axis. J. Cell Biol. *121*, 1083–1093.

Reichmann, J., Nijmeijer, B., Hossain, M.J., Eguren, M., Schneider, I., Politi, A.Z., Roberti, M.J., Hufnagel, L., Hiiragi, T., and Ellenberg, J. (2018). Dual-spindle formation in zygotes keeps parental genomes apart in early mammalian embryos. Science *361*, 189–193.

Rhoades, M.M. (1942). Preferential Segregation in Maize. Genetics *27*, 395–407.

Ribeiro, S.A., Salmon, E.D., Earnshaw, W.C., Dong, Y., Vagnarelli, P., Gatlin, J.C., Cameron, L., McEwen, B.F., Joglekar, A., Farr, C.J., et al. (2009). Condensin Regulates the Stiffness of Vertebrate Centromeres. Mol. Biol. Cell *20*, 2371–2380.

Rivera, T., Ghenoiu, C., Rodríguez-Corsino, M., Mochida, S., Funabiki, H., and Losada, A. (2012). Xenopus Shugoshin 2 regulates the spindle assembly pathway mediated by the chromosomal passenger complex. EMBO J. *31*, 1467–1479.

Roberts, A., Paddock, C., Vogel, L., Butler, E., Zaki, S., and Subbarao, K. (2005). Aged BALB / c Mice as a Model for Increased Severity of Severe Acute Respiratory Syndrome in Elderly Humans Aged BALB / c Mice as a Model for Increased Severity of Severe Acute Respiratory Syndrome in Elderly Humans. J. Virol. *79*, 5833–5838.

Romanienko, P.J., and Camerini-Otero, R.D. (2000). The Mouse Spo11 Gene Is Required for Meiotic Chromosome Synapsis. Mol. Cell *6*, 975–987.

Roostalu, J., and Surrey, T. (2017). Microtubule nucleation: Beyond the template. Nat. Rev. Mol. Cell Biol. *18*, 702–710.

Rošić, S., and Erhardt, S. (2016). No longer a nuisance: Long non-coding RNAs join CENP-A in epigenetic centromere regulation. Cell. Mol. Life Sci. *73*, 1387–1398.

Rošić, S., Köhler, F., and Erhardt, S. (2014). Repetitive centromeric satellite RNA is essential for kinetochore formation and cell division. J. Cell Biol. *207*, 335–349.

Rosin, L.F., and Mellone, B.G. (2017). Centromeres Drive a Hard Bargain. Trends Genet. *33*, 101–117.

Royle, S.J., Nixon, F.M., Prior, I.A., Honnor, T.R., Johansen, A.M., Starling, G.P., Clarke, N.I., Brettschneider, J.A., and Beckett, A.J. (2017). Microtubule organization within mitotic spindles revealed by serial block face scanning electron microscopy and image analysis. J. Cell Sci. *130*, 1845–1855.

Ruchaud, S., Carmena, M., and Earnshaw, W.C. (2007). Chromosomal passengers: Conducting cell division. Nat. Rev. Mol. Cell Biol. *8*, 798–812.

Salmon, E.D., and Begg, D.A. (1980). Functional implications of cold-stable microtubules in kinetochore fibers of insect spermatocytes during anaphase. J. Cell Biol. *85*, 853–865.

Salmon, W.C., Heald, R., Nachury, M. V, Waterman-Storer, C.M., Maresca, T.J., and Weis, K. (2004). Importin β Is a Mitotic Target of the Small GTPase Ran in Spindle Assembly. Cell *104*, 95–106.

Sampath, S.C., Leismann, O., Ohi, R., Pozniakovski, A., Funabiki, H., and Salic, A. (2004). The Chromosomal Passenger Complex Is Required for Chromatin-Induced Microtubule Stabilization and Spindle Assembly. Cell *118*, 187–202.

Sanchez, A.D., and Feldman, J.L. (2017). Microtubule-organizing centers: from the centrosome to non-centrosomal sites. Curr. Opin. Cell Biol. *44*, 93–101.

Sanchez, L., Martínez, P., and Goyanes, V. (2011). Analysis of centromere size in human chromosomes 1, 9, 15, and 16 by electron microscopy. Genome *34*, 710–713.

Sanders, J.R., and Jones, K.T. (2018). Regulation of the meiotic divisions of mammalian oocytes and eggs. Biochem. Soc. Trans. *46*, 797–806.

Sandler, L., and Novitski, E. (1957). Meiotic Drive as an Evolutionary Force. Am. Nat. *91*, 105–110.

Santaguida, S., Vernieri, C., Villa, F., Ciliberto, A., and Musacchio, A. (2011). Evidence that Aurora B is implicated in spindle checkpoint signalling independently of error correction. EMBO J. *30*, 1508–1519.

Saskova, A., Solc, P., Baran, V., Kubelka, M., Schultz, R.M., and Motlik, J. (2008). Aurora kinase a controls meiosis I progression in mouse oocytes. Cell Cycle *7*, 2368–2376.

Saunders, W.S., Gharaibeh, B., Petersen, I., Enyenihi, A.H., Huang, X., Gollin, S.M., and Shuster, M. (2002). Chromosomal instability and cytoskeletal defects in oral cancer cells. Proc. Natl. Acad. Sci. *97*, 303–308.

Sawin, K.E., Leguellec, K., Philippe, M., and Mitchison, T.J. (1992). Mitotic spindle organization by a plus-end-directed microtubule motor. Nature *359*, 540–543.

Sawin, K.E., Lourenco, P.C.C., and Snaith, H.A. (2004). Microtubule nucleation at non-spindle pole body microtubule-organizing centers requires fission yeast centrosomin-related protein mod20p. Curr. Biol. *14*, 763–775.

Schatten, H., and Sun, Q.Y. (2011). Centrosome dynamics during mammalian oocyte maturation with a focus on meiotic spindle formation. Mol. Reprod. Dev. *78*, 757–768.

Schindler, K., Davydenko, O., Fram, B., Lampson, M.A., and Schultz, R.M. (2012). Maternally recruited Aurora C kinase is more stable than Aurora B to support mouse oocyte maturation and early development. Proc. Natl. Acad. Sci. *109*, E2215–E2222.

Schmerler, S., and Wessel, G.M. (2011). Polar bodies-more a lack of understanding than a lack of respect. Mol. Reprod. Dev. *78*, 3–8.

Schuh, M. (2011). An actin-dependent mechanism for long-range vesicle transport. Nat. Cell Biol. *13*, 1431–1436.

Schuh, M., and Ellenberg, J. (2007). Self-Organization of MTOCs Replaces Centrosome Function during Acentrosomal Spindle Assembly in Live Mouse Oocytes. Cell *130*, 484–498.

Schuh, M., and Ellenberg, J. (2008). A New Model for Asymmetric Spindle Positioning in Mouse Oocytes. Curr. Biol. *18*, 1986–1992.

Scott, K.C. (2013). Transcription and ncRNAs: At the cent(rome)re of kinetochore assembly and maintenance. Chromosom. Res. *21*, 643–651.

Seong, E., Saunders, T.L., Stewart, C.L., and Burmeister, M. (2004). To knockout in 129 or in C57BL/6 : that is the question. Trends Genet. *20*, 4–7.

Severance, A.L., and Latham, K.E. (2018). Meeting the meiotic challenge: Specializations in mammalian oocyte spindle formation. Mol. Reprod. Dev. *85*, 178–187.

Silk, A.D., Cleveland, D.W., Kolano, A., Verlhac, M.-H., and Brunet, S. (2012). Error-prone mammalian female meiosis from silencing the spindle assembly checkpoint without normal interkinetochore tension. Proc. Natl. Acad. Sci. *109*, E1858–E1867.

Slangy, A., Kress, M., Niggt, E.A., Harper, M., d'Hérin, P., and Lane, H.A. (2004). Phosphorylation by p34cdc2 regulates spindle association of human Eg5, a kinesin-related motor essential for bipolar spindle formation in vivo. Cell *83*, 1159–1169.

Srayko, M., O'Toole, E.T., Hyman, A.A., and Müller-Reichert, T. (2006). Katanin Disrupts the Microtubule Lattice and Increases Polymer Number in C. elegans Meiosis. Curr. Biol. *16*, 1944–1949.

Stearns, T., and Kirschner, M. (1994). In vitro reconstitution of centrosome assembly and function: The central role of γ-tubulin. Cell *76*, 623–637.

Strnad, P., and Gönczy, P. (2008). Mechanisms of procentriole formation. Trends Cell Biol. *18*, 389–396.

Sturtevant, A. (1936). Preferential segregation in triplo-IV females of Drosophila melanogaster. Genetics *21*, 444.

Sturtevant, A.H. (1934). Preferential Segregation of the Fourth Chromosomes in Drosophila melanogaster. Proc. Natl. Acad. Sci. U. S. A. *20*, 515–518.

Sturtevant, A.H. (2006). Preferential Segregation of the Fourth Chromosomes in Drosophila melanogaster. Proc. Natl. Acad. Sci. *20*, 515–518.

Sullivan, L.L., Boivin, C.D., Mravinac, B., Song, I.Y., and Sullivan, B.A. (2011). Genomic size of CENP-A domain is proportional to total alpha satellite array size at human centromeres and expands in cancer cells. Chromosom. Res. *19*, 457–470.

Sun, Q.-Y., Meng, X.-Q., Zhong, Z.-S., Li, Y.-L., Zhang, G., Chen, D.-Y., and Fan, H.-Y. (2004). Localization of γ-Tubulin in Mouse Eggs during Meiotic Maturation, Fertilization, and Early Embryonic Development. J. Reprod. Dev. *50*, 97–105.

Swain, J.E., Ding, J., Wu, J., and Smith, G.D. (2008). Regulation of spindle and chromatin dynamics during early and late stages of oocyte maturation by aurora kinases. Mol. Hum. Reprod. *14*, 291–299.

Swist-Rosowska, K., Engist, B., Jenuwein, T., De La Rosa-Velazquez, I., Shukeir, N., Gamalinda, M., Ching, R., Galan, C., van de Nobelen, S., Karabiber, F., et al. (2017). Major satellite repeat RNA stabilize heterochromatin retention of Suv39h enzymes by RNA-nucleosome association and RNA:DNA hybrid formation. Elife *6*, e25293.

Szollosi, D., Calarco, P., and Donahue, R.P. (1972). Absence of centrioles in the first and second meiotic spindles of mouse oocytes. J. Cell Sci. *11*, 521–541.

Talbert, P.B., and Henikoff, S. (2018). Transcribing Centromeres: Noncoding RNAs and Kinetochore Assembly. Trends Genet. *34*, 587–599.

Tanenbaum, M.E., and Medema, R.H. (2010). Mechanisms of Centrosome Separation and Bipolar Spindle Assembly. Dev. Cell *19*, 797–806.

Tomkiel, J., Cooke, C.A., Saitoh, H., Bernat, R.L., and Earnshaw, W.C. (1994). CENP-C is required for maintaining proper kinetochore size and for a timely transition to anaphase. J. Cell Biol. *125*, 531–545.

Tooley, J.G., Miller, S.A., and Stukenberg, P.T. (2011). The Ndc80 complex uses a tripartite attachment point to couple microtubule depolymerization to chromosome movement. Mol. Biol. Cell *22*, 1217–1226.

Trazzi, S., Bernardoni, R., Diolaiti, D., Politi, V., Earnshaw, W.C., Perini, G., and Della Valle, G. (2002). In vivo functional dissection of human inner kinetochore protein CENP-C. Journal of Structural Biology, *140(1-3)*, 39-48.

Tripathi, A., Prem Kumar, K. V., and Chaube, S.K. (2010). Meiotic cell cycle arrest in mammalian oocytes. J. Cell. Physiol. *223*, 592–600.

Tseng, B.S., Tan, L., Kapoor, T.M., and Funabiki, H. (2010). Dual detection of chromosomes and microtubules by the chromosomal passenger complex drives spindle assembly. Dev. Cell *18*, 903–912.

Tseng, T.-C., CHEN, S.-H., HSU, Y.-P.P., and TANG, T.K. (1998). Protein Kinase Profile of Sperm and Eggs: Cloning and Characterization of Two Novel Testis-Specific Protein Kinases (AIE1, AIE2) Related to Yeast and Fly Chromosome Segregation Regulators. DNA Cell Biol. *17*, 823–833.

Vafa, O., and Sullivan, K.F. (2004). Chromatin containing CENP-A and α-satellite DNA is a major component of the inner kinetochore plate. Curr. Biol. *7*, 897–900.

Vallot, A., Leontiou, I., Cladière, D., El Yakoubi, W., Bolte, S., Buffin, E., and Wassmann, K. (2018). Tension-Induced Error Correction and Not Kinetochore Attachment Status Activates the SAC in an Aurora-B/C-Dependent Manner in Oocytes. Curr. Biol. *28*, 130-139.

Vasquez, R.J., Yvon, A.M., Cassimeris, L., Wadsworth, P., and Howell, B. (2013). Nanomolar concentrations of nocodazole alter microtubule dynamic instability in vivo and in vitro. Mol. Biol. Cell *8*, 973–985.

Verlhac, M.H. (2011). Spindle positioning: Going against the actin flow. Nat. Cell Biol. *13*, 1183–1185.

Vertii, A., Hehnly, H., and Doxsey, S. (2016). The centrosome, a multitalented renaissance organelle. Cold Spring Harb. Perspect. Biol. *8*, a025049.

Volpe, T.A., Kidner, C., Hall, I.M., Teng, G., Grewal, S.I.S., and Martienssen, R.A. (2002). Regulation of heterochromatic silencing and histone H3 lysine-9 methylation by RNAi. Science *297*, 1833–1837.

Voter, W.A., and Erickson, H.P. (1984). The kinetics of microtubule assembly. Evidence for a two-stage nucleation mechanism. J. Biol. Chem. *259*, 10430–10438.

Wang, S., Hassold, T., Hunt, P., White, M.A., Zickler, D., Kleckner, N., and Zhang, L. (2017). Inefficient Crossover Maturation Underlies Elevated Aneuploidy in Human Female Meiosis. Cell *168*, 977–989.

Wang, Z., Wu, T., Shi, L., Zhang, L., Zheng, W., Qu, J.Y., Niu, R., and Qi, R.Z. (2010). Conserved motif of CDK5RAP2 mediates its localization to centrosomes and the Golgi complex. J. Biol. Chem. *285*, 22658–22665.

Warburton, P.E., Cooke, C.A., Bourassa, S., Vafa, O., Sullivan, B.A., Stetten, G., Gimelli, G., Warburton, D., Tyler-Smith, C., Sullivan, K.F., et al. (1997). Immunolocalization of CENP-A suggests a distinct nucleosome structure at the inner kinetochore plate of active centromeres. Curr. Biol. *7*, 901–904.

Wassmann, K., Niault, T., and Maro, B. (2003). Metaphase I arrest upon activation of the Mad2-dependent spindle checkpoint in mouse oocytes. Curr. Biol. *13*, 1596–1608.

Watanabe, Y. (2012). Geometry and force behind kinetochore orientation: Lessons from meiosis. Nat. Rev. Mol. Cell Biol. *13*, 370–382.

Wei, R.R., Sorger, P.K., and Harrison, S.C. (2005). Molecular organization of the Ndc80 complex, an essential kinetochore component. Proc. Natl. Acad. Sci. *102*, 5363–5367.

Wei, R.R., Al-Bassam, J., and Harrison, S.C. (2007). The Ndc80/HEC1 complex is a contact point for kinetochore-microtubule attachment. Nat. Struct. Mol. Biol. *14*, 54–59.

Wendell, K.L., Wilson, L., and Jordan, M.A. (1993). Mitotic block in HeLa cells by vinblastine: ultrastructural changes in kinetochore-microtubule attachment and in centrosomes. J. Cell Sci. *104(2)*, 261–274.

West, J.D., Frels, W.I., and Chapman, V.M. (1978). Mus musculus × Mus caroli hybrids: Mouse mules. J. Hered. *69*, 321–326.

Westhorpe, F.G., and Straight, A.F. (2015). The centromere: Epigenetic control of chromosome segregation during mitosis. Cold Spring Harb. Perspect. Biol. *7*, a015818.

Whittaker, C., and Dean, C. (2017). The FLC Locus: A Platform for Discoveries in Epigenetics and Adaptation Changes may still occur before final publication. Annu. Rev. Cell Dev. Biol *338*, 1–8.

Wieczorek, M., Bechstedt, S., Chaaban, S., and Brouhard, G.J. (2015). Microtubule-associated proteins control the kinetics of microtubule nucleation. Nat. Cell Biol. *17*, 907–916.

Wiese, C., Wilde, A., Moore, M.S., Adam, S.A., Merdes, A., and Zheng, Y. (2001). Role of importin-β in coupling ran to downstream targets in microtubule assembly. Science *291*, 653–656.

Winston, N.J., McGuinness, O., Johnson, M.H., and Maro, B. (1995). The exit of mouse oocytes from meiotic M-phase requires an intact spindle during intracellular calcium release. J. Cell Sci. *108 (1)*, 143–151.

Wittmann, T., Hyman, A., and Desai, A. (2001). The spindle: A dynamic assembly of microtubules and motors. Nat. Cell Biol. *3*, E28–E34.

Wojcik, E.J., Dalrymple, N.A., Alford, S.R., Walker, R.A., and Kim, S. (2004). Disparity in allosteric interactions of monastrol with Eg5 in the presence of ADP and ATP: A difference FT-IR investigation. Biochemistry *43*, 9939–9949.

Wong, A.K.C., Biddle, F.G., and Rattner, J.B. (1990). The chromosomal distribution of the major and minor satellite is not conserved in the genus Mus. Chromosoma *99*, 190–195.

Wong, L.H., Brettingham-Moore, K.H., Chan, L., Quach, J.M., Anderson, M.A., Northrop, E.L., Hannan, R., Saffery, R., Shaw, M.L., Williams, E., et al. (2007). Centromere RNA is a key component for the assembly of nucleoproteins at the nucleolus and centromere. Genome Res. *17*, 1146–1160.

Woo, E.M., Chait, B.T., Funabiki, H., Kelly, A.E., Maniar, T.A., and Sampath, S.C. (2007). Chromosomal Enrichment and Activation of the Aurora B Pathway Are Coupled to Spatially Regulate Spindle Assembly. Dev. Cell *12*, 31–43.

Wu, T., Lane, S.I.R., Morgan, S.L., and Jones, K.T. (2018). Spindle tubulin and MTOC asymmetries may explain meiotic drive in oocytes. Nat. Commun. *9*, 2952.

Yanai, A., Arama, E., Kilfin, G., and Motro, B. (1997). ayk1, a novel mammalian gene related to Drosophila aurora centrosome separation kinase, is specifically expressed during meiosis. Oncogene *14*, 2943–2950.

Yao, L.-J., Zhong, Z.-S., Zhang, L.-S., Chen, D.-Y., Schatten, H., and Sun, Q.-Y. (2004). Aurora-A Is a Critical Regulator of Microtubule Assembly and Nuclear Activity in Mouse Oocytes, Fertilized Eggs, and Early Embryos1. Biol. Reprod. *70*, 1392–1399.

Yen, T.J., McEwen, B.F., Zubrowski, B., Sauer, M.T., Chan, G.K.T., and Savoian, M.S. (2013). CENP-E Is Essential for Reliable Bioriented Spindle Attachment, but Chromosome Alignment Can Be Achieved via Redundant Mechanisms in Mammalian Cells. Mol. Biol. Cell *12*, 2776–2789.

Yi, K., Rubinstein, B., Unruh, J.R., Guo, F., Slaughter, B.D., and Li, R. (2013). Sequential actin-based pushing forces drive meiosis I chromosome migration and symmetry breaking in oocytes. J. Cell Biol. *200*, 567–576.

Yoshida, M.C.C., and Kodama, Y. (1983). C-band patterns of chromosomes in 17 strains of mice. Cytogenet. Genome Res. *35*, 51–56.

Yoshida, S., Kaido, M., and Kitajima, T.S. (2015). Inherent Instability of Correct Kinetochore-Microtubule Attachments during Meiosis I in Oocytes. Dev. Cell *33*, 589–602.

Yu, H.G., and Dawe, R.K. (2000). Functional redundancy in the maize meiotic kinetochore. J. Cell Biol. *151*, 131–141.

Yun, Y., Holt, J.E., Lane, S.I.R., McLaughlin, E.A., Merriman, J.A., and Jones, K.T. (2014). Reduced ability to recover from spindle disruption and loss of kinetochore spindle assembly checkpoint proteins in oocytes from aged mice. Cell Cycle *13*, 1938–1947.

Zheng, Y., Wong, M.L., Alberts, B., and Mitchison, T. (1995). Nucleation of microtubule assembly by a γ-tubulin-containing ring complex. Nature *378*, 578–583.

Zieve, G.W., Turnbull, D., Michael, J., and Mcintosh, J.R. (1980). Production of Large Numbers of Mitotic Mammalian By Use of the Reversible Inhibitor Nocodazole. Exp. Cell Res. *126*, 397–405.